

Radiolabeling of liposomes and polymeric micelles with PET-isotopes

Jensen, Andreas Tue Ingemann; Rasmussen, Palle; Andresen, Thomas Lars

Publication date:
2012

Document Version
Publisher's PDF, also known as Version of record

[Link back to DTU Orbit](#)

Citation (APA):

Jensen, A. T. I., Rasmussen, P., & Andresen, T. L. (2012). Radiolabeling of liposomes and polymeric micelles with PET-isotopes. Technical University of Denmark (DTU).

DTU Library

Technical Information Center of Denmark

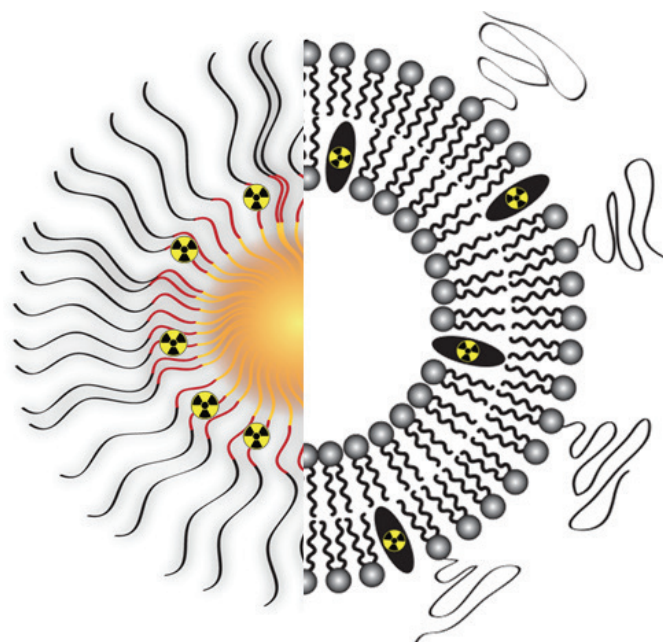
General rights

Copyright and moral rights for the publications made accessible in the public portal are retained by the authors and/or other copyright owners and it is a condition of accessing publications that users recognise and abide by the legal requirements associated with these rights.

- Users may download and print one copy of any publication from the public portal for the purpose of private study or research.
- You may not further distribute the material or use it for any profit-making activity or commercial gain
- You may freely distribute the URL identifying the publication in the public portal

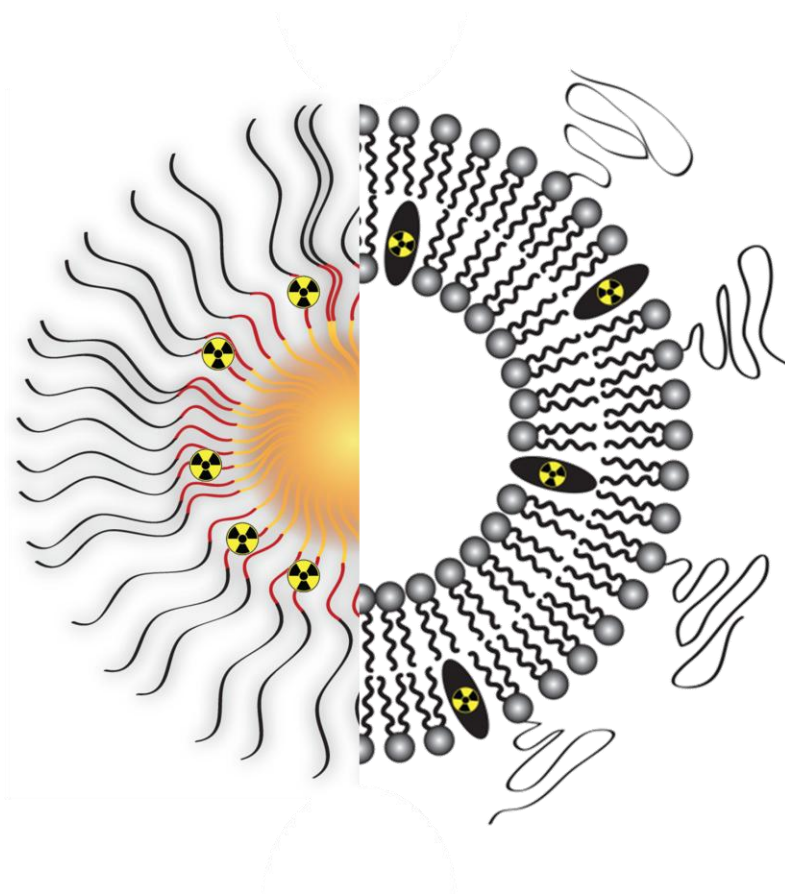
If you believe that this document breaches copyright please contact us providing details, and we will remove access to the work immediately and investigate your claim.

Radiolabeling of liposomes and polymeric micelles with PET-isotopes



Andreas Tue Ingemann Jensen
November 2012

Radiolabeling of liposomes and polymeric micelles with PET-isotopes



PhD Thesis by

Andreas Tue Ingemann Jensen

The Hevesy Laboratory, Center for Nuclear Technologies (DTU)

in collaboration with

The CBIO group, Department of Micro- and Nanotechnology (DTU)

Preface

This thesis is the result of 3 years of graduate work carried out at the Hevesy Laboratory at DTU Nutech as well as in the CBIO (*Colloids & Biological Interfaces*) group at DTU Nanotech. In the project's first year, it was in collaboration with LiPlasome Pharma A/S but continued as a full DTU project from March 1st 2010 due to bankruptcy on the part of LiPlasome Pharma. The main supervisors on the project were Dr. Palle Rasmussen (Head of Program, DTU Nutech) and Dr. Thomas Andresen (Senior Scientist, DTU Nanotech).

During the project, an 8 months stay at the Hebrew University of Jerusalem (Israel) was included. The supervisors on this project were Prof. Yechezkel Barenholz and Dr. Eylon Yavin. This stay was conducted as a leave of absence and for this reason the results obtained are not described in this thesis.

The work is presented in three separate chapters. **Chapter 1** is a general introduction to the field of radiolabeling liposomes and polymeric micelles. **Chapter 2** describes work revolving around the ^{18}F -radiolabeling of liposomes. **Chapter 3** is a description of work concerning the radiolabeling of polymeric micelles. A **general conclusion & perspectives** are given in the end.

Acknowledgements

I am grateful to a number of people that have helped, inspired and in other ways contributed to this project and my personal development. I would especially like to thank my supervisor **Dr. Palle Rasmussen** who has lead my education as a radiochemist and has been a constant support and motivator with an always open door. Special thanks also goes to my co-supervisor **Dr. Thomas Andresen** for being a great source of inspiration, for fruitful scientific discussions, and for setting up my stay in Israel. In addition, the two deserve my deep-felt gratitude for stepping in and taking over the project when the bankruptcy of LiPlasome Pharma would otherwise have ended it.

In addition, I would like to thank the following people;

Dr. Sorin Aburel & Lene Niebuhr for supplying ^{18}F target water rinses, for always being helpful and for keeping a great mood in the lab. **Dr. Dennis Elema, Cristine Sogaard** and **Anette Holst** for supplying ^{64}Cu and for never objecting to my erratic orderings of numerous vials, each containing minuscule amounts of radioactivity. A special thanks goes to Dennis Elema for his patience and his help in teaching me to send my own radioactive formulations to Panum. **Prof. Mikael Jensen** for his great knowledge and fruitful discussions on nuclear physics, PET technology and related subjects that at times have seemed like black magic. **Lasse Hauerberg** and **Henrik Prip** for possessing a practical prowess with which a PhD student may not always be endowed.

Of my fellow PhD students and post docs, special thanks goes to **Dr. Rasmus Jølck, Dr. Anncatrine Petersen, Dr. Simon Andersen, Dr. Thomas Etzerodt, Dr. Kristian Jensen, Dr. Jonas Henriksen, Evgeny Revunov** and **Lise Bjerg**. These individuals have all at some point stepped in and provided much-needed help and great discussions. A very special thanks goes to **Dr. Martin H. F. Pedersen**, who has made my PhD years immensely more enjoyable.

Of my collaborators, I would like to thank **Prof. Andreas Kjær** and **Dr. Tina Binderup** for carrying out our animal studies and for always invaluable input when interpreting the results, **Dr. Pramod Kumar** for synthesizing the unimers described in Chapter 3, and **Bente Mathiesen** for carrying out the bulk of the work in our joint paper. In particular, I would like to thank **Dr. Fedor Zhuravlev** for countless interesting discussions, scientific as well as private, for always being ready to help with chemical questions, and finally, for including me in the $[^{18}\text{F}]\text{HF}$ gas transfer project.

At last, I would like to thank my wife-to-be **Inés Areizaga**, who has somehow managed to accept and support me through my almost 4 years of relentless working hours, 8 months of absence and my infatuation with tiny radioactive particles.

Publications

Andreas T.I. Jensen, Tina Binderup, Thomas L. Andresen, Andreas Kjær, Palle H. Rasmussen.

“PET imaging of liposomes labeled with an [18F]-fluorocholesteryl ether probe prepared by automated radiosynthesis” Journal of Liposome Research, (**Epub ahead of print**). PubMed ID:22803638

Bente Mathiessen, **Andreas T.I. Jensen**, Fedor Zhuravlev.

“Homogeneous Nucleophilic Radiofluorination and Fluorination with Phosphazene Hydrofluorides”
Chemistry – A European Journal, 2011. **17**(28): p. 7796-7805.

Andreas T.I. Jensen, Tina Binderup, Pramod Kumar, Andreas Kjær, Palle H. Rasmussen, Thomas L. Andresen.

“In-vivo comparison of DOTA and CB-TE2A through shell-region ⁶⁴Cu-labeling of core-crosslinked triblock polymeric micelles” Biomaterials (**Submitted**).

Andreas T.I. Jensen, Pramod Kumar, Tina Binderup, Andreas Kjær, Dennis Elema, Thomas L. Andresen, Palle H. Rasmussen.

“The effect of coumarin core-crosslinking on the pharmacokinetics of CB-TE2A conjugated triblock polymeric micelles” (**in preparation**)*.

* Results described in section 3.8.3.

List of abbreviations and acronyms

%CL	Degree of crosslinking
ABC	Accelerated blood clearance
ACN	Acetonitrile
ADME	Absorption distribution metabolism and excretion
ATRP	atom-transfer radical-polymerization
BFC	Bifunctional chelator
CE	Cholesteryl ether
CL	Crosslinked
CMC	Critical micelle concentration
DCM	Dichloromethane
DDS	Drug delivery system
DHG	1,2-di-hexadecyl-glycerol
DLS	Direct light scattering
DMF	Dimethylformamide
DMSO	Dimethylsulphoxide
DSC	Direct scanning calorimetry
DSPC	Di-stearoyl phosphatidylcholine
EC	Electron capture
ECM	Extracellular matrix
EPR	Enhanced permeation and retention
K222	Kryptofix-222
LE	Labeling efficiency
LUV	Large unilamellar vesicle
MLV	Multi-lamellar vesicle
NCA	no-carrier-added
NMRI	Naval Medical Research Institute
NonCL	Non-crosslinked
PAEMA	polyaminomethyl methacrylate
PCMA	polymethacryloyloxyethoxy-4-methylcoumarin
PEG	Polyethylene glycol
PEG	polyethylene glycol
PET	positron emission tomography
HEMA	polyhydroxyethyl methacrylate
PK	Pharmacokinetics

PM	Polymeric micelles
PMMA	polymethyl methacrylate
RCP	Radiochemical purity
RES	Reticuloendotheliam system
RT	Room temperature
SEC	Size-exclusion chromatography
SFC	Supel Flash Cartridge
SPECT	single-photon emission computed chromatography
SUV	Small unilamellar vesicle
T/M ratio	tumor-to-muscle ratio
THF	Tetrahydrofuran
T _m	membrane phase transition temperature
VEGF	Vascular endothelial growth factor

Abstract & Outline

Outline. This thesis is divided into three separate chapters that can be read independently. Chapter 1 is a general introduction, touching upon liposomes and polymeric micelles and radiolabeling with ^{18}F and ^{64}Cu . Chapter 2 and 3 address two separate research projects, each described below. A complete reference list is compiled in the end, immediately after the three chapters. This is followed by the supplementary information, divided into appropriate sections. Finally, the two first-authored manuscripts are attached as appendices.

Chapter 1. The field of nanoparticulate drug delivery has been hailed as a revolution in modern therapeutics, especially in chemotherapy. A major reason is the ability of nanoparticles to accumulate in tumor tissue. Liposomes are the classic nanoparticle, consisting of a lipid membrane with an aqueous core. Polymeric micelles are made from amphiphilic detergent-like copolymers, that self-assemble in water. Therapy with nanoparticles is hampered by often poor tumor accumulation, combined with massive uptake by macrophages in the liver and spleen. For this reason, visualizing nanoparticle pharmacokinetics *in-vivo* is a valuable tool in the on-going research. Such visualization can be done by labeling with radio isotopes. Isotopes that emit positrons (PET-isotopes) can be detected by PET (*positron emission tomography*) technology, an accurate technique that has gained popularity in recent years. PET-isotopes of interest include ^{18}F and ^{64}Cu . In addition to being a research tool, radiolabeled nanoparticles hold promise as a radiopharmaceutical in themselves, as a means of imaging tumor tissue, aiding in diagnosis and surgery.

Chapter 2. A method for labeling liposomes with ^{18}F (97% positron decay, $T_{1/2} = 110$ min) was investigated. ^{18}F is widely available, but is hampered by a short half-life only allowing up to 8 hours scans. ^{18}F must be covalently attached to components of the liposome. By binding to a lipid, it can be stably lodged in the membrane. A glycerolipid and a cholesteryl ether were synthesized with free primary alcohols and a series of their sulphonates (Ms, Ts, Tf) were prepared. [^{18}F]Radiofluorination of these substrates was performed on fully automated equipment using a classic Kryptofix222-mediated procedure in DMSO. Yields were poor, 3-17% depending on conditions. The [^{18}F]fluorinated probes were purified *in-situ* on SEP-Paks. The cholesteryl ether mesylate performed best. This substrate was radiolabeled and formulated in long-circulating liposomes by drying the probe and the lipids together, followed by hydration by magnetic stirring. The liposomes were extruded through 100 nm filter on fully automated equipment. Animal studies were done in tumor-bearing mice, and PET-scans were performed over 8 hours. Clear tumor uptake, as well as hepatic and splenic uptake, was observed, corresponding to expected liposomal pharmacokinetics. Tumor uptake was quantifiable (*tumor-to-muscle ratio* at 8 h: 2.20), showing that the maximum scan duration with ^{18}F is sufficient for visualizing tumor tissue. Because of the low [^{18}F]radiofluorination yields obtained, we investigated ways of labeling lipophilic substrates in nonpolar

solvents. This involved the transfer of [18]HF gas from a solution of concentrated sulphuric acid into a receiving vial containing the substrate in toluene. A phosphazene base was present to bind [18]HF and mediate fluorination. This procedure made it possible to fluorinate highly lipophilic substrates in 71% yields.

Chapter 3. Radiolabeling of polymeric micelles with ^{64}Cu (18% positron decay, $T_{1/2} = 12.7$ h) was investigated. ^{64}Cu allows longer scans (up to 48 hours), which mirrors the duration of nanoparticle pharmacokinetics. It is a metal and must be attached to polymeric micelles by covalently conjugated chelators. DOTA and CB-TE2A are two such chelators, but DOTA is widely believed to be unstable *in-vivo*. DOTA and CB-TE2A were conjugated to *triblock* polymeric micelles in the *shell*-region. Here, they were thought to be shielded by the outer PEG-layer. The micelles were crosslinked in their coumarin-containing cores by exposure to UV light. Subsequently, the micelles were labeled with ^{64}Cu , followed by removal of unspecifically bound ^{64}Cu by EDTA. Good labeling efficiency was achieved with both chelators (40-70%). Some of the prepared micelles were found to exhibit gross instabilities, especially with raised temperature, which prevented their *in-vivo* use. Other micelles were stable and were investigated in xenographted mice. These micelles were 20-45 nm. They showed good tumor uptake (4-5 %ID/g, 48h) and limited uptake in liver (5-7 %ID/g, 48h) and spleen (3-6 %ID/g, 48h). It was concluded that there did not seem to be a significant difference between DOTA and CB-TE2A *in-vivo*. In addition, crosslinked micelles (with ^{64}Cu bound to CB-TE2A) were compared with non-crosslinked micelles. To our surprise, we found that the non-crosslinked micelles exhibited good stability in circulation and obtained a biodistribution very similar to the crosslinked micelles.

Resumé (in Danish)

Kapitel 1. Brugen af nanopartikler til behandling har længe været anset som en revolution, der blot venter på at ske. De ses især som nyttige i kemoterapi mod cancer, da de har en evne til at akkumulere i tumorvæv. Den klassiske nanopartikel er liposomet, der er en fedtmembran, der omkranser en vandholdig kerne. Polymere miceller er en anden type nanopartikel, der består af sæbe-lignende polymerer, der samler sig til veldefinerede partikler i vand. Terapi med nanopartikler hæmmes ofte af lavt tumor-optag kombineret med højt optag i lever og milt. Derfor er det et nyttigt værktøj at kunne følge nanopartiklernes fordeling i organismen. En måde at opnå dette på er ved at mærke dem med radioaktive isotoper. Isotoper der udsender positroner (anti-elektroner) kan detekteres ved hjælp af PET (*positronemissions tomografi*), der er en præcis og relativt ny teknologi. Interessante PET-isotoper inkluderer ^{18}F og ^{64}Cu . Udover at være værktøj i forskningen, har radiomærkede nanopartikler desuden det potentiale at kunne bruges som et radiolægemiddel i sig selv, der kan visualisere tumorvæv og bistå i diagnose og kirurgi i kræftbehandlingen.

Kapitel 2. Vi undersøgte liposomers mærkning med ^{18}F . ^{18}F har en relativt kort halveringstid på 110 min, hvilket kun muliggør PET-scanninger på op til 8 timer. ^{18}F skal bindes kovalent til en bestanddel af liposomet. Ved at binde til et fedtmolekyle kan det indsættes stabilt i membranen. Et glycerolipid og en cholesterylether blev syntetiseret. De havde begge frie primære alkoholer, som blev omdannet til aktiverede sulfunater (Ms, Ts, Tf). Disse substrater blev [^{18}F]radiofluorerede i fuldt automatiseret udstyr ved en klassisk Kryptofix222-medieret procedure i DMSO. Udbyttet var ringe, 3-17% afhængig af reaktionsbetingelser. De [^{18}F]fluorerede prober blev oprenset *in-situ* på SEK-Paks. Mesylatet af cholesteryletheren viste sig at være bedst. Dette substrat blev radiomærket og formuleret i langtids-cirkulerende liposomer ved at tørre proben og lipider sammen, efterfulgt af hydrering ved magnetisk omrøring. Liposomerne blev ekstruderet gennem 100 nm filtre ved en fuldt automatiseret procedure. Undersøgelser i dyr, blev gjort i tumorbærende mus og PET-scanninger blev udført over 8 timer. Klart tumor-optag samt optag i lever og milt kunne ses, hvilket svarer til forventet farmakokinetik for liposomer. Tumoroptyget kunne kvantificeres og en *tumor-til-muskel ratio* på 2,20 fandtes efter 8 timer. Denne værdi giver kontrast nok til at kunne visualisere tumorvæv og viser at de ^{18}F -mærkede liposomer kan bruges til dette. På grund af de lave [^{18}F]radiofluoreringsudbytter der var opnået, undersøgte vi en metode til at radiomærke lipofile substrater i ikke-polære solventer. Dette involverede udvikling af [^{18}F]HF gas fra koncentreret svovlsyre hvorefter det blev ledt ned i en opløsning af substratet i toluen. En phosphazen-base var til stede, som bandt [^{18}F]HF og medierede fluoreringen. Ved denne metode blev udbytter på 71% opnået.

Kapitel 3. Radiomærkning af polymere miceller med ^{64}Cu undersøgt. ^{64}Cu muliggør længere scanningstider (op til 48 hours), i kraft af sin længere halverngstid (12,7 timer). 48 timer svarer godt til det vindue i hvilket nanopartikel-farmakokinetik normalt er interessant. Da ^{64}Cu er et metal skal det bindes til polymere miceller gennem en kovalent bundet chelator. DOTA og CB-TE2A er to sådanne chelatorer, men DOTA menes generelt at være ustabil *in-vivo*. DOTA og CB-TE2A blev begge bundet til triblock polymere miceller i *shell*-regionen, hvor de menes at være beskyttede af det omgivende PEG lag mod interaktion med substanser i blodet. Micellerne kunne krydsbundes idet de i kernen havde polymerer indeholdende coumarin. Coumarin-molekyler krydsbinder når de udsættes for UV-lys. Dernæst blev micellerne mærket med ^{64}Cu og uspecifikt bundet ^{64}Cu blev fjernet med EDTA. God mærkning blev opnået med begge chelatorer (40-70% af den samlede radioaktivitet). Nogle af de fremstillede miceller udviste dog alvorlig ustabilitet, især ved let øgede temperaturer. Dette forhindrede deres brug *in-vivo*. Derimod var andre typer miceller stabile og disse blev undersøgt i tumorbærende mus. Disse miceller havde en størrelsesfordeling mellem 20 og 45 nm. De udviste godt tumor-optag (4-5 %ID/g efter 48 timer) samt begrænset grad af det uønskede optag i lever (5-7 %ID/g) og milt (3-6 %ID/g). Vi konkluderede at vi ikke så nogen signifikant forskel på DOTA og CB-TE2A *in-vivo*. Derudover blev krydsbundne miceller (med ^{64}Cu bundet til CB-TE2A) testet overfor ikke-krydsbundne miceller. Til vores overraskelse fandt vi at de ikke-krydsbundne miceller udviste god stabilitet i blodbanen og faktisk havde samme *in-vivo* distribution som de krydsbundne.

Table of contents

CHAPTER 1 - Introduction to nanoparticulate systemic drug delivery and PET imaging	
1.1 Background	1
1.2 Liposomes	2
1.3 Polymeric micelles	5
1.4 <i>In-vivo</i> pharmacokinetics and accumulation of nanoparticles	9
1.5 Basic radiation theory	12
1.6 Spect & PET – Nuclear tomographic imaging	15
1.7 Important radioisotopes for SPECT and PET	17
1.8 Basic radiochemistry of ^{18}F	18
1.9 Basic radiochemistry and pharmacokinetics of ^{64}Cu and its chelators	20
1.10 Concluding remarks and rationale for nuclear imaging of nanoparticles	24
CHAPTER 2 - Preparation and <i>in-vivo</i> investigation of ^{18}F-labeled liposomes	
2.1 Background	25
2.1.1 Radiolabeling of liposomes with metal isotopes for SPECT-imaging	27
2.1.2 Radiolabeling of liposomes with metal isotopes for PET (^{64}Cu)	29
2.1.3 Radiolabeling by covalent binding (iodine)	30
2.1.4 Summing up radiolabeling methodology	31
2.1.5 Radiolabeling of liposomes with ^{18}F	32
2.1.6 Choice of lipid probe in membrane labeling	33
2.1.7 Double labeling of liposomes	34
2.1.8 Objective	34
2.2 Synthesis of lipophilic sulphonate substrates	35
2.2.1 Synthesis of a di-alkyl glycerol probe substrate	35
2.2.2 Synthesis of a cholesteryl ether probe precursor	39
2.3 Automated synthesis of an ^{18}F -labeled di-hexadecyl glyceride lipid	40
2.3.1 Preparation and drying of the reactor	41
2.3.2 Addition of the substrate	43
2.3.3 Choice of pseudohalide	45
2.3.4 Reaction conditions – Solvent, temperature and duration	46
2.3.5 Formation of impurities	46
2.4 Automated synthesis of an ^{18}F -labeled cholesteryl ether lipid	46
2.5 Purification of the radiolabel	49
2.6 Preparation of radioliposomes	52
2.7 Timeline of radioliposome preparation and locations of activity	55
2.8 <i>In-vivo</i> investigations	55
2.8.1 <i>In-vivo</i> investigation results	56
2.8.2 Discussion of <i>in-vivo</i> results	58
2.9 General discussion and concluding remarks	60
2.10 Fluorination of lipids in nonpolar solvents by [^{18}F]HF transfer to phosphazene bases	62
2.11 Experimental section	64
CHAPTER 3 - ^{64}Cu-labeling and <i>in-vivo</i> investigation of the pharmacokinetics of triblock polymer micelles	
3.1 Background	72
3.1.1 Radiolabeling of polymeric micelles with non-PET isotopes	75
3.1.2 Radiolabeling of polymeric micelles with PET isotopes	75
3.1.3 Photo core-crosslinking by coumarin	76

3.1.4 Objective	77
3.2 Synthesis and functionalization of unimers	78
3.2.1 Synthesis of macroinitiators and monomers	80
3.2.2 Synthesis of PEG-PAEMA-PCMA	80
3.2.3 Synthesis of PEG-PHEMA-PCMA	82
3.2.4 Synthesis of PEG-PHEMA-PMMA	84
3.2.5 Synthesis of PEG-PAEMA-PMMA	84
3.2.6 Purification of unimers by dialysis (procedure A)	84
3.2.7 Determination of CMC	85
3.2.8 Conjugation of chelators to unimers	86
3.2.9 Preparation of micelles (procedure F)	89
3.2.10 Nomenclature used for chelator conjugated micelles	89
3.2.11 Characterization of micelles	90
3.2.12 Formulation of micelles, sizes and zeta potentials	90
3.3 Pilot radiolabeling experiments	92
3.3.1 Initial experiments and unspecific binding of EDTA	93
3.3.2 Unspecific binding of DOTA and capping	94
3.3.3 Unspecific binding of ⁶⁴ Cu and EDTA/DTPA scavenging	96
3.3.4 Labeling of CB-TE2A micelles and precipitation at elevated temperatures	98
3.3.5 Localization of the "high fractions"	100
3.4 Crosslinking	101
3.5 Quantification of micelle material in dispersion	105
3.6 Compilation of labeling results at established conditions	107
3.7 Animal studies with PEG-PAEMA-PCMA micelles – CL versus nonCL	108
3.7.1 What went wrong?	112
3.8 Animal studies with PEG-PHEMA-PCMA micelles – CB-TE2A versus DOTA and the Effect of crosslinking	114
3.8.1 Preparation of the micelles	114
3.8.2 Discussion of <i>in-vivo</i> results – CB-TE2A versus DOTA	116
3.8.3 Discussion of <i>in-vivo</i> results – The effects of crosslinking	119
3.8.4 Thermostability of PEG-PHEMA-PCMA micelles	122
3.9 Concluding remarks	123
3.10 Experimental section	124
 4. GENERAL CONCLUSION & PERSPECTIVES	 129
 5. REFERENCES	 132

SUPPLEMENTARY INFORMATION

APPENDIX 1

"PET imaging of liposomes labeled with an [18F]-fluorocholesteryl ether probe prepared by automated radiosynthesis" (paper)

APPENDIX 2

"In-vivo comparison of DOTA and CB-TE2A through shell-region ⁶⁴Cu-labeling of core-crosslinked triblock polymeric micelles" (manuscript)

Chapter 1

Introduction to nanoparticulate systemic drug delivery and PET imaging

The following chapter is an introduction to the field of drug delivery with nanoparticles and radiolabeling for in-vivo imaging. The chapter will initially focus on systemic administration of liposomes and polymeric micelles in cancer therapy. Then, the concept of nuclear tomographic imaging will be discussed, along with the radioisotopes available for such applications and the radiochemistry of the two isotopes mostly used for PET-imaging, ^{18}F and ^{64}Cu .

1.1 Background

Cancer mortality has been decreasing in recent years [6] but remains a major cause of death. In the United States, one in four deaths are due to cancer [8]. In the European Union, 1,283,101 people, 1 in 500, are estimated to die from cancer in 2012 [6]. In spite of progress, chemotherapeutics remain unspecific and are related to debilitating side effects that can be detrimental to continued treatment, as well as to high rates of tumor recurrence.

In order to achieve the specificity that could significantly decrease systemic side effects, the promises of nanotechnology have been considered. In the early 20th century, Paul Ehrlich envisaged a “magic bullet” that would target only disease causing cells [15]. In recent years, this concept has been applied extensively to nanoparticulate drug delivery. This is because nanoparticles (NPs) have the ability to preferentially target tumor tissue. However, they are still hampered by significant uptake in especially the liver and spleen. The hope is to develop a drug delivery system (DDS) that will target only tumor tissue and prevent attack by the cytotoxic payload on healthy tissues [19]. The radiolabeling of NPs is a valuable tool in the research to discover such systems, as it allows the *in-vivo* tracking of the particles. In addition, radiolabeled NPs could be a radiopharmaceutical in their own right, visualizing tumor tissue and assisting in diagnosis and surgery.

1.2 Liposomes

Liposomes (**fig. 1.1**) were first described in 1964 by Bangham *et al.* [21, 22]. Shortly after their discovery, liposomes were proposed by Gregoriadis *et al.* as potential drug carriers [24]. This laid the foundation for a long and still on-going research effort to develop liposomes into the ideal drug carrier.

Liposomes are lipid vesicles dispersed in aqueous medium. They are largely spherical and can exhibit one or multiple concentric lipid bilayers as well as multivesicularity, that is several smaller vesicles inside the outermost membrane [25]. *Multilamellar*

vesicles (MLVs) with diameters of around 500 nm were what was initially observed by Bangham *et al.* [22]. However, in the field of systemic drug delivery, the overwhelming interest is usually in unilamellar liposomes with hydrodynamic diameters of around 100 nm and smaller. Depending on size, they are termed *small unilamellar vesicles* (SUVs), if smaller than 100 nm in diameter, or *large unilamellar vesicles* (LUVs) if larger. The reasons why smaller sizes are more interesting will be discussed shortly (see **Section 1.4**). The lipid bilayer allows the traversing of relatively lipophilic molecules and prevents the traversing of charged or highly polar structures. Thus, the liposome forms a protective bubble that can carry its cargo through the bloodstream. In this way, liposomal drug delivery can effectively change the pharmacokinetics of a drug molecule, by imparting on it the *in-vivo* behavior of the carrier vehicle.

Liposomes are formed when amphiphilic lipids with the right bilayer-forming capabilities are dispersed in aqueous solution. The most popular way of achieving this is by dissolving the lipids of choice and removing the solvent by either freeze-drying (the solvent often being *tert*-butanol) or by applying a nitrogen stream or rotary evaporation (the solvents often being mixture of chloroform and methanol). The latter method is commonly known as the *film*-method. These methods of preparation have the purpose of mixing the lipids in order to ensure that the formed liposomes are as homogeneous as possible. The drying down of the lipids is followed by a hydration procedure. An aqueous buffer/solution is added and the lipid mixture is agitated above the *membrane phase transition temperature* (T_m) of the membrane (see *below*), often by vortexing or magnetic stirring. This provides MLVs that are converted to unilamellar vesicles by two major methods. The first of these is sonication, where the MLVs are subjected to ultrasound, leaving SUVs of around 25-50 nm

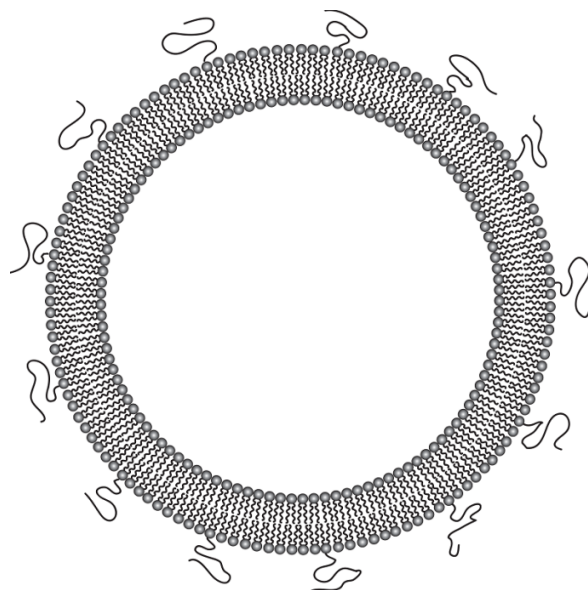


Figure 1.1 – Unilamellar liposome with attached PEG moieties.

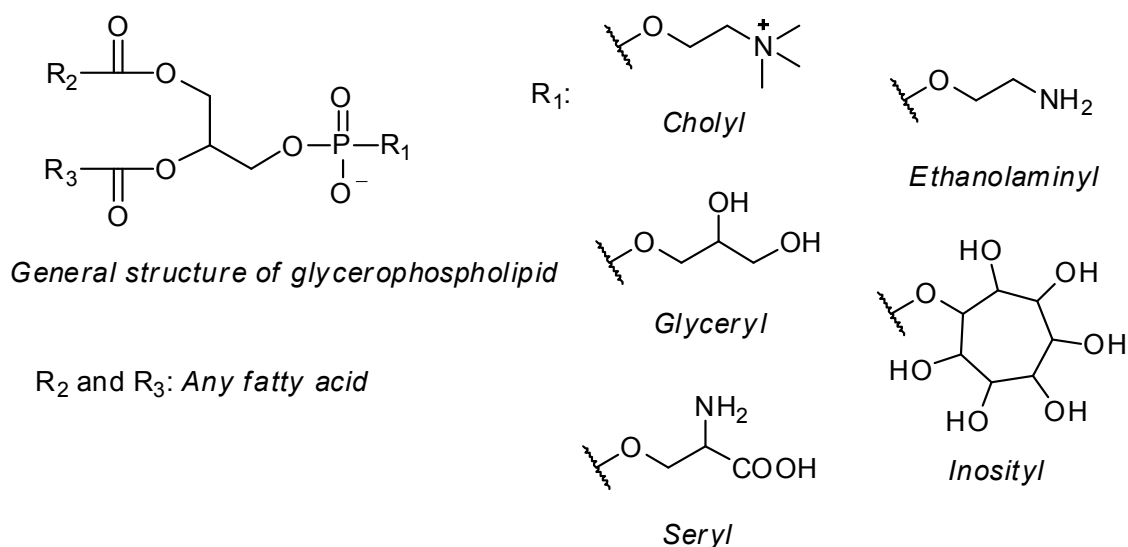


Figure 1.2 – Structures of phospholipids

[40]. The second, and the most widespread, is extrusion (or *French Press*) [42]. In this process, the MLVs are pressed through polycarbonate filters with pore sizes in the desired range. The target range for liposomes prepared by this method is usually 100 nm. Other methods for preparing liposomes exist, notably the ethanol injection method [43-45], the reverse phase evaporation method [46, 47] and the double emulsion method [48], but these are not relevant to this work.

The bilayer of liposomes is mainly constituted of phospholipids, these being among the most abundant biomolecules in nature and the major component of biological membranes. Phospholipids are amphiphiles, consisting of a charged head group and two long aliphatic chains. The term phospholipid derives from the phosphate moiety that constitutes part of the head group. Two major classes of phospholipids exist (fig. 1.2). The first and by far the most commonly used is the glycerophospholipids, where the head group is connected to two fatty acids via a glycerol backbone. The second class is the sphingomyelins. Only glycerophospholipids are of relevance to this work and they will simply be denoted as “phospholipids”. The chemical structure of phospholipids determines the characteristics they will impart on a liposomal membrane in which they are located. Starting with the head group, it determines, along with the phosphate moiety, the charge of the lipid and ultimately the overall charge of the membrane. The most commonly used naturally occurring head groups are phosphatidylcholine (PC), phosphatidylethanolamine (PE), phosphatidylglycerol (PG), phosphatidylinositol (PI) and phosphatidylserine (PS) (fig. 1.2). As the phosphate group is negatively charged at physiological pH ($pK_a \approx 1.1$ [49]), the charge of the head group determines the overall charge of the lipid. Thus, PC and PE give neutrally charged lipids, while PG, PI and PS give negatively charged lipids. Synthetic positively charged phospholipids have been prepared, primarily for nucleic acid delivery [50].

An important characteristic of liposomes is the *lipid chain melting transition* (T_m) of the membrane. This is a phase transition, the temperature of which can be determined by *direct scanning calorimetry* (DSC) [51]. Below the T_m , the lipid fatty acid chains are closely packed and fully extended (“gel phase”), above, they exhibit lateral diffusion and disordered acyl chains (“liquid-crystalline phase”) [40, 52]. The T_m is defined by how closely packed the lipids are and how strong the interactions between them are. The stronger the interactions, the higher the T_m . As straight, saturated lipids are arranged in the bilayer more easily, unsaturated fatty acids decrease T_m . Further, T_m increases with increasing lipid tail length [53]. The T_m is relevant, as all mechanical steps in liposome preparation should be carried out above it. This ensures that the lipids are in the fluid state and therefore mechanically malleable. An interesting phenomenon is that lipid membranes become leaky around the T_m , allowing the passage of drugs [54].

As cholesterol is present in high concentrations (often one third of the total lipid mass [55]) in the plasma membranes of higher organisms, much research has gone into the effect of cholesterol on liposomal membranes. Inclusion of cholesterol in liposome membrane gradually abolishes the separate liquid-crystalline and gel phases and induces a so-called *liquid-ordered phase* [56-58]. A cholesterol mol% of around 40-50% abolishes the main phase transition completely [58, 59]. The liquid aspect of the liquid-ordered phase is that there is rapid diffusion in the plane of the bilayer. However, at the same time, the lipid chains are highly ordered giving the membrane many of the desirable properties of a solid membrane, without actually being crystalline [60]. In modern liposome preparations, cholesterol is usually included because of its ability to make the lipid membrane less permeable [61].

A final major structural element of modern liposomes and perhaps the most important, is the inclusion of a sterically stabilizing polymer-coating. Early generations of liposomes were rapidly cleared from the blood stream, primarily by uptake in macrophages in the liver and spleen (the reticuloendothelial system, or RES) [62, 63]. As we shall see below (section 1.4), long circulation times *in-vivo* are crucial to achieve an appreciable accumulation in the tumor tissue. The advent of *polyethylene glycol* (PEG) coating provided liposomes with reduced RES clearance and allowed them to stay longer in the blood stream [64, 65]. PEG lipids are usually included in the liposome in a 5-10% molar ratio and PEG chains with average molecular weights of 2000 (PEG₂₀₀₀) normally used. The current theory on why PEG-coating provides longer circulation is that it creates a hydrated protective layer around the NP, which prevents binding of serum opsonins, in turn preventing recognition by the RES. However, uptake in healthy tissue, such as liver and spleen, is still relatively high, in spite of PEGylation [66]. There is evidence that this effect is partly the result of the endogenous production of antibodies against PEG lipids [67].

In their modern shape, liposomes are usually around or slightly below 100 nm, PEGylated with a surface charge around neutral and containing cholesterol. In the following, such NPs will be referred to simply as “liposomes”.

1.3 Polymeric micelles

Where liposomes have been around for long, polymeric micelles (PMs, **fig. 1.3**) are a relatively newer addition to the nano arsenal. The first PMs were reported in the late 80s by Kabanov *et al.* [68], and currently, several formulations are undergoing clinical trials [69]. PMs are generally described as self-assembled aggregates, made from amphiphilic polymers. In principle, PMs are similar to regular micelles made from surfactants (such as sodium lauryl sulphate), but very important differences exist.

Generally, PMs are set apart from other NPs by their unique three-dimensional structure. They are assembled in aqueous medium from single *unimers*. A unimer is a long copolymer (for example 10-30 kDa). “Copolymer” refers to a polymer that

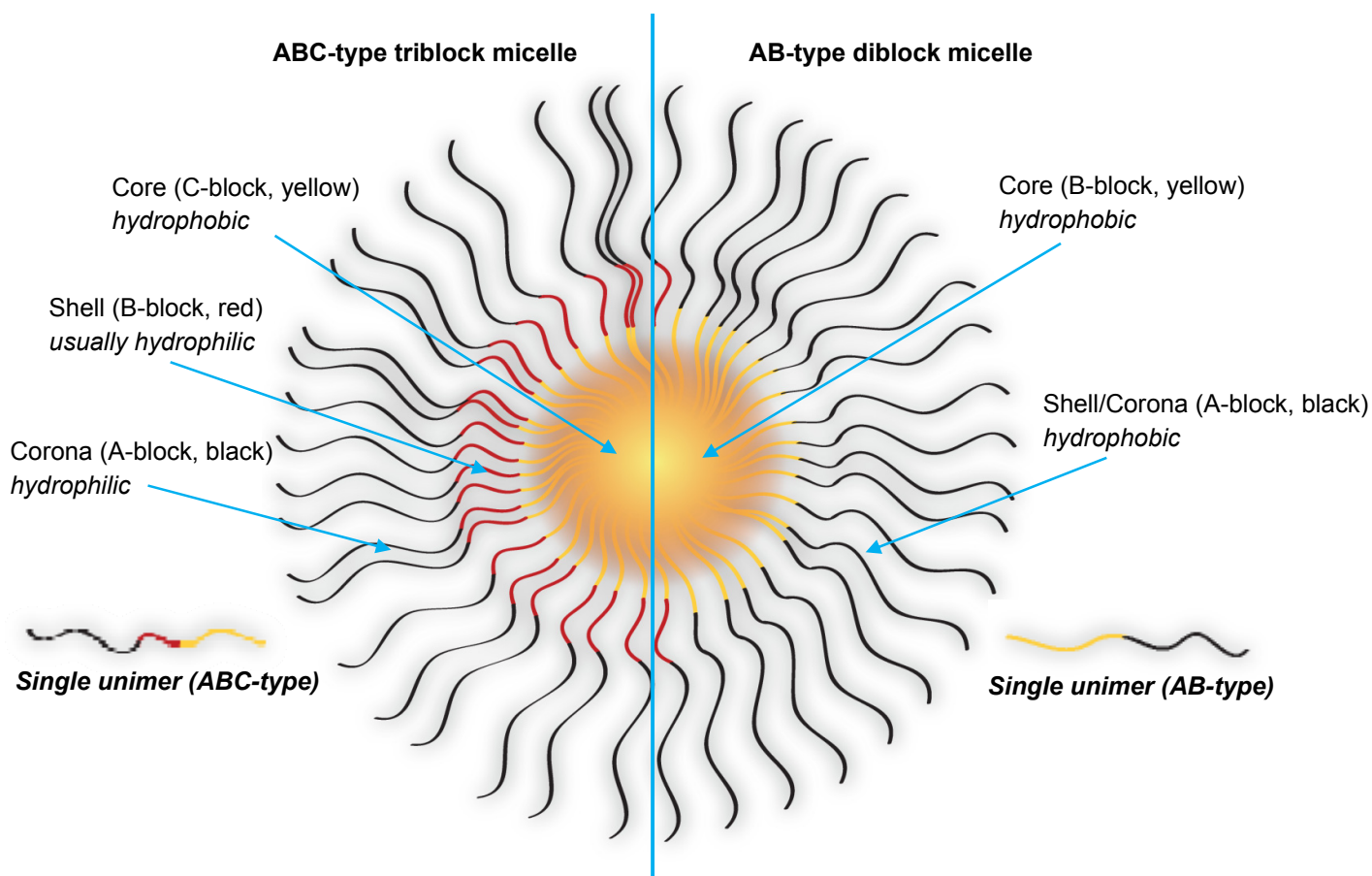


Figure 1.3 – Polymeric micelle split in two parts. On the **right** is shown an AB-type micelle denoted with appropriate nomenclature. Notice that the A-block is a diblock micelle is often termed the “shell” but occasionally the “corona”. On the **left** is shown a typical ABC-type triblock micelle, where the shell-region can be both hydrophilic and hydrophobic.

is made from different polymer types, divided into distinct regions (**fig. 1.3**). Synthesis of unimers will be commented on in **Section 3.2**. A prerequisite for forming micellar aggregates is that one end is hydrophobic and that one end is hydrophilic, as with liposomes, the hydrophilic is usually PEG. This gives the classic *diblock* type of unimer. In aqueous dispersion, the hydrophobic blocks will self-assemble due to the hydrophobic effect [70]. This refers to the entropically driven process of removal of the layer of ordered water molecules around the lipophilic parts of the unimer into the bulk water phase. The inner, hydrophobic part of the PM is called the *core*, while the hydrated hydrophilic layer facing the medium is usually called the *shell*, but sometimes the *corona*. This can be confusing. In diblock PMs, the outer region is usually called the shell, while in triblock PMs it is usually called the corona (**fig 1.3**). The core and the shell normally form two concentric spheres. Most simple PMs form spherical particles but more exotic shapes are possible, such as brushes [71]. If the length of the hydrophilic block is too high, the unimer can exist as single dissolved molecules in water (high CMC, see below) and if the hydrophobic block is too long, the unimers can form structures with non-spherical morphologies [72]. One of the advantages of PMs is the relative freedom in synthesis and design of the NPs. This also gives a highly heterogeneous field, where making generalizations is harder than with liposomes.

As a NP, a number of advantages of PMs are usually presented, especially when compared with liposomes. The most important is probably the size. PMs can be designed with narrow size distributions in the range of 5-100 nm [73]. In recent years much emphasis has been on the size of drug delivery systems (see **Section 1.4**), catapulting PMs and other NPs into the limelight and perhaps taking some attention from liposomes, which cannot be prepared stably in very small sizes. In drug delivery, the main idea of PMs is that they can transport drugs through the blood stream and exhibit typical NP pharmacokinetics (**Section 1.4**). Usually, hydrophobic drugs are transported in the core of the micelles by nonpolar associations, but other manners of loading have been devised, for example complexation [74]. For hydrophobically adhered drugs, the main form of release occurs by diffusion or destabilization of the micelles. A method that utilizes tumor pathophysiology is destabilization by low pH. Tumor interstitial pH is usually slightly lower (around 6.8 [75]) than surrounding tissue, due to poor clearance of metabolic products such as lactic and carbonic acid [75, 76]. In addition, when NPs are taken up by endocytosis they enter endosomes/lysosomes where the pH eventually drops to 5-6. Micelles that become unstable at lowered pH, for example by protonation of histidine residues in the hydrophobic core, have been investigated [77-81]. The protonation increases the hydrophilicity of the core, leading to disruption of the micelles. Furthermore, it is possible to conjugate drugs such as doxorubicin to PMs by acid labile bonds, that hydrolyse at low pH [82]. Another interesting trigger type is by a local increase in temperature, achieved by external heating of the tumor. As diffusion is faster from liquid than from glassy cores, it can be enhanced by increasing the temperature of certain core polymer types [83]. In addition, PMs can be destabilized by irradiation with light [84]. For additional types of release see Oerlemans *et al.* [73].

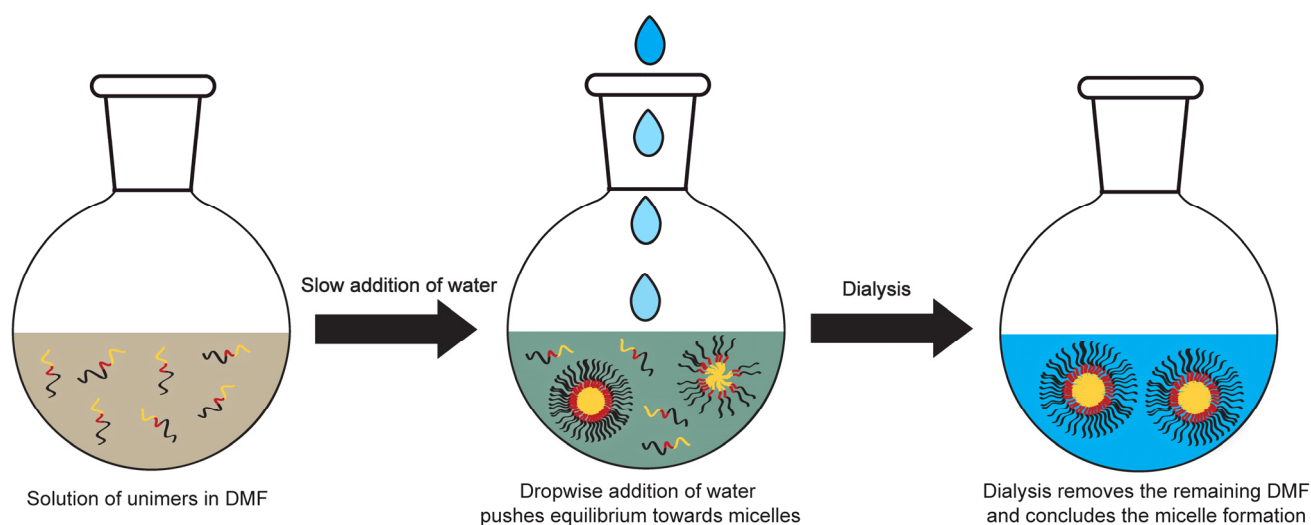


Figure 1.4 – Preparation of PMs by the dialysis method. Unimers are dissolved in DMF followed by dropwise addition of water. This shifts the equilibrium towards micellar aggregates. Dialysis removes the remaining DMF, ensuring virtually complete formation of PMs.

The most common way of preparing polymeric micelles is by the *dialysis method* [85]. This involves dissolving the unimer in an organic solvent that is miscible with water, e.g. DMF. Water is then slowly added and eventually the remaining DMF is removed by dialysis (**fig. 1.4**). As water is a selective solvent for the hydrophilic block, micelles will gradually form. A further way is the *oil-in-water solvent evaporation method*. This involves dissolving the polymer in a water-immiscible organic solvent, creating an emulsion. The organic solvent is then removed by evaporation, leaving micelles [86]. A number of other methods exist. For an overview, see Kedar *et al.* [87].

As micellization is a dynamic process, a key concern is the stability of the aggregate upon dilution. Unimers assemble as micelles only above the *critical micelle concentration* (CMC). If the micelles are diluted to concentrations below this threshold, they can disintegrate into separate unimers. *In-vivo*, a state of sink condition (“infinite dilution”, adhesion to plasma components and general clearance) will soon occur, meaning that unstabilized micelles will be rapidly cleared by glomerular filtration. In general, the CMC of PMs is lower than traditional surfactants. It is possible to prepare PMs with CMC values as low as around 1-10 $\mu\text{g/mL}$, depending on the chemistry of the hydrophobic blocks and their self-interactions [88]. CMC is often determined using the pyrene assay (see **section 3.2.7**) [89]. Thermodynamic stability refers to the potential of micelles to disassemble, while kinetic stability refers to the rate of disassembly, once the concentration falls below the CMC [90]. As such, kinetic stability is paramount for the integrity of PMs in circulation. Kinetic stability can be increased by employing a hydrophobic block that forms a semi-crystalline core [91] and the problem of dissociation can be avoided altogether by *cross-linking* (see below).

While the “classic” PM design and most of the particles reported in the literature are diblock PMs of AB architecture (A being hydrophilic, B being hydrophobic), triblock and graft polymers are gaining prominence [87]. Graft polymers are too complicated for review here, but triblock PMs are quite relevant as **Chapter 3** describes work with such micelles. Copolymer unimers are usually synthesized by coupling the hydrophilic parts, followed by grafting of the hydrophobic parts over the hydrophilic copolymer [87]. Triblock copolymers can be of a number of designs, including ABA [92, 93], ABC [81, 94-97] and BAC [98, 99]. In the ABA design, the B block is hydrophobic and the A blocks identical and hydrophilic, being for example PEG. The BAC design is similar, only with A being hydrophobic and B and C being hydrophilic and different. Often, one hydrophilic block is PEG and the other is functionalized, for example with the capacity of carrying positive charges for gene delivery [99]. In the final design, the ABC-type, A is hydrophilic and C hydrophobic. B can be both, and is often a handle region that can be functionalized. This is the type of PM that will be presented in **Chapter 3**. In ABC-type triblock micelles, the PEG layer (A-block) is usually referred to as the corona, while the B-block is referred to as the shell. ABC and AB-type PMs are shown in **figure 1.3**.

Covalent cross-linking abrogates the issue of the CMC. Such cross-linking can be done in the core of the micelles or in the shell-region in diblock PMs. Methods of *core*-crosslinking include coupling of methacrylate-based functional groups by thermal polymerization [100] or by UV-induced photo-crosslinking, using an initiator [101, 102] or by chemical polymerization [102]. Further, carboxylic acid groups situated in the core can be crosslinked in the presence of suitable carbodiimides (such as EDC) and a diamine [103] or glutaraldehyde [104]. In the *shell*-region, diblock PMs have been cross-linked by UV-initiated radical polymerization [105] or condensation of carboxylic acids with diamines [105]. Reaction of activated carboxylic acids with diamines has also been employed on triblock ABC micelles [81, 106]. The Armes group, a major contributor in the micelle field, published shell-cross-linking of both diblock and triblock PMs by quaternization of tertiary amines with di-iodides (DIEE) [81, 107]. Diblock PMs have also been shell-crosslinked by esterification of polymerized methacrylate residues [107]. Diblock and triblock PMs have both been core-crosslinked by radical polymerization [108]. The group of Wooley has published a large number of papers on *shell-crosslinked knedel-like* (SCK) PMs [11, 109-117]. A number of these have involved radiolabeling and will be commented on further in chapter 3. In addition, a number of reversible strategies for crosslinking have been reported. Li *et al.* shell-crosslinked triblock micelles by the reversible formation of disulfide bonds [118]. Xu *et al.* recently also shell-crosslinking triblock micelles, through terephthalaldehyde (TDA) that formed cleavable imine linkages [119]. Reversible core-crosslinking can also be obtained by UV-irradiation [120]. This concept will be elaborated on further in **Section 3.1.3**.

1.4 *In-vivo* pharmacokinetics and tumor accumulation of nanoparticles

Liposomes were early on recognized as possible carriers of drugs [121]. As the vast majority of especially early research into NPs was carried out on liposomes, much of following passages mention liposomes. Unless otherwise commented on, it is assumed that what applies to liposomes also applies to polymeric micelles. Liposome *pharmacokinetics* (PK), which is mainly based on interaction with the immune system, was reviewed by several authors [122], with the particular case of DOXIL (*a marketed liposomal formulation of the chemotherapeutic doxorubicin*), the composition of which remains the gold standard in liposome research, reviewed by Gabizon *et al.* [123]. A number of liposome formulations in the size range of 90-100 nm have been clinically approved for the delivery of antifungal, antiparasitic, and anticancer agents [123, 124].

The *enhanced permeation and retention* (EPR) effect is one of the pillars of nanoparticulate drug delivery (fig. 1.5). It makes it possible to selectively target tumor tissue. The EPR effect was discovered in 1986 by Matsumura and Maeda [125] and later described in detail by Maeda [126]. Interest in it however, is continuously growing and it has been the subject of a recent review [127]. The EPR effect is exhibited by most tumors, but not in normal tissue. It derives from the fact that a growing tumor needs a continuous supply of blood, nutrients and oxygen in order to survive and grow larger. In order to achieve this, the tumor cells secrete *vascular endothelial growth factor* (VEGF) and other substances which cause angiogenesis [128-130]. Angiogenesis is the recruitment of nearby blood vessels to grow new blood vessel offshoots into the developing tumor tissue. Folkman *et al.* found that angiogenesis started when tumors exceed 0.8-1.0 mm in diameter. These newly constructed blood vessels however display relatively large fenestrations between the endothelial cells, about 200-780 nm, which allow NPs smaller than this cut-off to extravasate preferentially in tumor tissue [131]. To exit normal vasculature, sizes smaller than 1-2 nm are required [132]. In tumors with very small fenestration (~ 200 nm), PMs might be especially useful as the possibility of very small sizes might make extravasation in such tumors easier [133]. In addition to fenestrated endothelium, tumors have poor lymphatic drainage, allowing extravasated particles to stay in the tissue [134]. A key requirement for NPs to take advantage of the EPR effect is that they circulate in the blood stream long enough for extravasation to occur. At least 24 hours is usually desirable. Accumulation by NPs in tumors through the EPR effect is referred to as *passive targeting*, as opposed to active targeting where the NPs have surfaces decorated with targeting moieties [135].

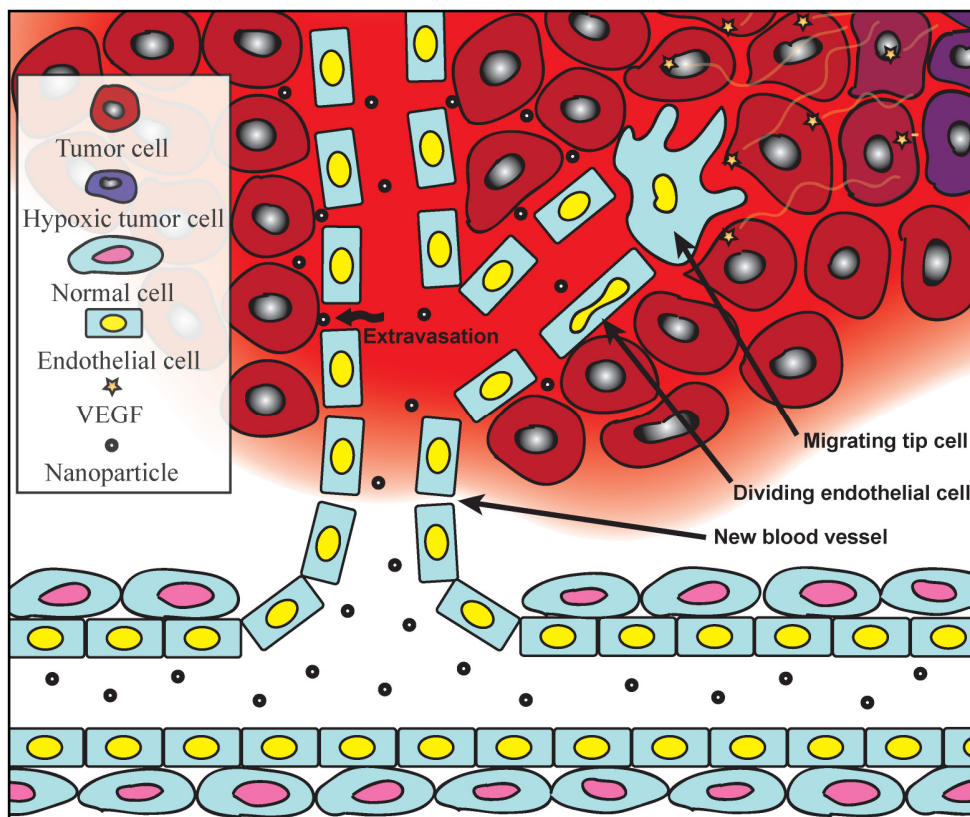


Figure 1.5 – Angiogenesis and the EPR effect. Hypoxic tumor cells excrete VEGF and other growth factors to stimulate angiogenesis. Endothelium in these new blood vessels show fenestrations that allow the extravasation of nanoparticles. In addition, lymphatic drainage is impeded in the tumor tissue.

In spite of the promises held by the EPR effect, a few factors hamper effective accumulation somewhat. This mainly has to do with impaired tumor penetration and has been reviewed by Minchinton and Tannock [136]. To begin with, the interstitial pressure in solid tumors is generally raised [137]. But as the pressure is relatively lower near the edge of the tumor, extravasation can occur here [138]. This causes NPs to deposit in the tumor periphery, and not penetrate deeper into the tumor tissue [127]. Another impediment to tumor accumulation is hypoxic regions with limited blood flow [139]. In larger, late-stage tumors (> 1-2 cm diameter) necrotic and hypovascular areas start to appear in the core of the tumor. This can lead to poorer extravasation and could mean that the relatively small xenografts used in murine models may not adequately mirror the clinical picture [127, 140]. In addition, solid tumors are characterized by a dense *extracellular matrix* (ECM) which impedes deep penetration by NPs [141]. While the EPR effect is well-established and routinely observed, poor tumor penetration remains an issue in nanoparticulate therapy research. In order to reach all cells in a tumor, a chemotherapeutic should be capable of traveling up to 100 μm away from the vasculature and into the tumor tissue [136].

Recent research has shown that NPs smaller than 50 nm, and perhaps smaller still, may have superior tumor accumulation in poorly vascularized tumors, compared to traditional NPs with sizes around 100 nm [142, 143]. These smaller particles may penetrate tumors better, by having easier passage through the openings in the ECM [144]. For these reasons, smaller sized particles could be superior in the treatment of certain tumor types and tumors that are diagnosed at a later stage. This is a primary reason why interest in smaller nanoparticles is currently high.

As mentioned, first generations of liposomes were rapidly cleared from the blood stream. Attaching a protective coat of PEG to the surface of the liposomes provided the defense against opsonization that was needed to ensure long circulation and accumulation in tumor tissue [64, 145]. This prompted a new era in liposome research with the prospect of systemic delivery to tissues other than liver or white blood cells emerging as a possibility and soon led to the development of the first anti-cancer liposomal drug, DOXIL.

However, PEGylated liposomes such as DOXIL have been shown to still activate complement to some degree [122, 146] and to adsorb serum proteins [147]. As such, PEGylation does not appear to fully prevent interaction with serum components, meaning that part of the explanation of the long-circulating nature of PEGylated nanoparticles could be found elsewhere. Moghimi & Szebeni suggested that because of the steric hindrance imposed by the PEG-layer, complement binding occurs in a position that is inaccessible to complement receptors [122]. When PEGylated long-circulating NPs of <150 nm are injected into the blood stream, a significant number is taken up by macrophages in the liver and spleen within the first hour of circulation [122, 148-150]. Very low doses (< 4 µmol/kg) of lipid in the form of stealth liposomes, have been shown to be rapidly cleared, some by liver uptake, but primarily through bladder excretion [148], indicating degradation of liposomes. This rapid clearance is thought to arise from a limited blood pool of opsonins which is capable of removing a certain portions of the particles before being depleted [149, 151]. Therefore, the limited number of these opsonins contributes to the long-circulating nature of PEGylated nanoparticles. Such findings are relevant for radiochemical applications, where trace amounts of radiopharmaceuticals are usually administered. If the amount of NPs is too low, the presence of opsonins may be sufficient to rapidly clear the entire dose. It also shows that PEGylated liposomes, known as “stealth” liposomes, are not as invulnerable to detection as their name might suggest. A challenge with PEGylated liposomes may be that they exhibit heterogeneous surfaces where certain patches have less PEG protection and thus allow opsonization [122, 152].

Opsonization, along with splenic mechanical filtration, leads to uptake of nanoparticles in the liver and spleen. Uptake in these two organs is a hallmark of nanoparticle PK and is usually unwanted. When NPs enter the liver, they pass with the blood through the liver sinusoids before entering the hepatic central vein [153]. The resident macrophages lining the sinusoidal lumen, known as Kupffer cells, are responsible for the uptake of NPs here [154]. In the spleen, blood passes by either closed circulation (“fast pathway”) or open circulation (“slow pathway”) [153, 155]. In closed circulation, the arterial

capillaries empty directly into splenic venous sinusoids, enabling passage of relatively large particulate matter. However, the majority of blood passes through open circulation [153]. Here, blood is emptied into the reticular meshwork of the red pulp, where it passes through tissue rich in macrophages, which will clear opsonized or otherwise recognizable particles. Eventually it enters the sinuses, but upon doing so the blood is filtered through the fenestrated endothelium in the sinusoid walls [156]. Particles larger than 150-200 nm in diameter, that are too rigid to undergo deformation will be cleared from circulation by this mechanism, thus setting an upper limit for the size of systemically administered NPs [157].

Renal clearance is a further concern in systemic delivery of NPs, which sets a lower limit for NP size. With “classic” systems, such as liposomes, with relatively large sizes, this is not an issue, but as focus is shifting towards smaller DDS, such as polymeric micelles, it becomes important. Choi *et al.* showed that quantum dots with hydrodynamic diameters lower than about 5.5 nm can be expected to undergo glomerular filtration [158]. Generally, caution should be exercised with particles with hydrodynamic diameters below 10 nm [132, 159]. Size cut-offs are affected by flexibility of the NPs [160], and for non-spherical NPs, shape also plays a role [161].

PEGylated nanoparticles of the right size may have circulation half-lives between 2 to 24 hours in mice and rats and can be as high as 45 hours in humans [122].

A final aspect of Stealth liposome PK is the *accelerated blood clearance* (ABC) effect. A second dose of liposomes administered several days after a first dose is cleared more rapidly than the first dose [162-164]. The ABC effect has been shown to be mediated by anti-PEG IgM [165]. The antibodies are produced in response to the first injection. PMs have been shown to also cause generation of IgM by one study [166] although the effect was less than that seen with liposomes. The ABC effect is usually a concern with repeated injections (e.g. chemotherapy) of nanoparticles and not in single injections for example with the purpose of imaging cancer.

1.5 Basic radiation theory

Generally, unstable nuclei decay in a number of different ways in order to reach a stable state. The most important modes of decay are summarized here.

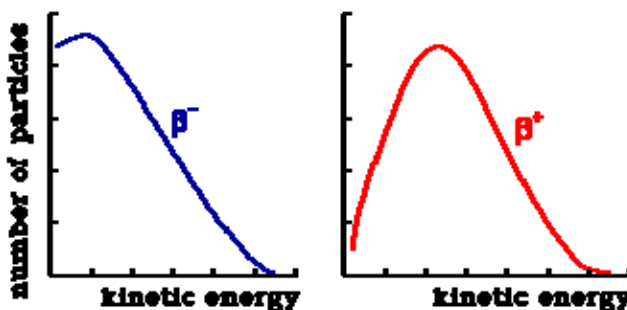


Figure 1.6 - Examples of energy spectra for β^- and β^+ decays.
From <http://physics-database.group.shef.ac.uk>

Alpha decay is the emission of an alpha particle from a nucleus. Alpha-particles are almost exclusively emitted from heavy nuclei (the atomic number Z being above 83). An alpha-particle is identical to a helium nucleus and exits the decaying nucleus with a certain amount of kinetic energy. This energy is deposited in surrounding matter. Alpha decay can be seen as a way for the nucleus to lose both mass and charge. Emissions of alpha particles are all of the same energy, making alpha radiation monoenergetic. Generally, alpha radiation is short-range and deposits high levels of energy. It is thus useful in localized *radiation therapy* where tissue destruction is desired [167]. Alpha-emission is not relevant to this work and will not be commented on further.

β^- radiation is one of the two forms of beta radiation, the other being β^+ or *positron* radiation. β^- radiation is essentially the emission of electrons (sometimes referred to as *negatrons*). It can be seen as a way for the nucleus to lose a charge (in essence, convert a neutron to a proton) but remain at the same mass. Interestingly, β^- radiation is not monoenergetic, meaning that the emitted electrons have a spectrum of different energies (see **fig. 1.6**). This is explained by the emission of another particle, an antineutrino, which can carry a bigger or a smaller portion of the released energy. The distribution of energy between electron and antineutrino thus varies from decay to decay. Compared to alpha radiation (short range), β^- radiation is of medium range. β^- is generally useful in nuclear therapy due to its ionizing effects [167].

Positron (β^+) emission is used in PET imaging and is basically the opposite of β^- radiation (**fig. 1.7**). Accordingly, the emitted particle is an antielectron/positron. Positron emission occurs in nuclei which are neutron deficient, the net effect being that a proton is converted to a neutron. As in β^- decay, positrons are emitted as a spectrum of different energies, slightly skewed to the right when compared to a β^- spectrum (see **fig. 1.6**). The difference in shape is due to repulsion of the positron by the positively charged nucleus. The energy is divided between the positron and a neutrino. The positron is emitted with an energy between 0 and a maximal energy (E_{max}) as well as an average energy. The maximal and average energies are determined by the PET isotope in question. After emission, it will gradually lose its kinetic energy through impacts with atoms in the surrounding matter. When it runs out of energy, it will annihilate with an electron. Therefore, its initial energy determines the length of the path it will travel before annihilation. This has traditionally been thought to negatively influence the resolution of PET images, but as the distance travelled is in a zigzag manner close to the point of origin, it has relatively little practical relevance [168]. When annihilation takes place, the positron and the negatron are converted to energy, which results in the emission of two anti-parallel photons of 511 keV each. As the mass energy of the positron and the electron is constant, 511 keV is always the energy of each photon of this *annihilation radiation*, regardless of isotope. An alternative to positron emission, which has the same net effect on the nucleus, is electron capture (EC). Here, an orbital electron is captured by the nucleus and combined with a proton to form a neutron. Lighter nuclei (such as ^{18}F) tend to “prefer” positron emission over EC as the orbital electrons are further from the nucleus. EC results in an excess of energy on the atomic level (due to electronic reconfiguration), which is released as Auger electrons

(emission of low energy electrons) or X-rays. The energy thus released is usually only a few keV and does not affect general tissue dose much.

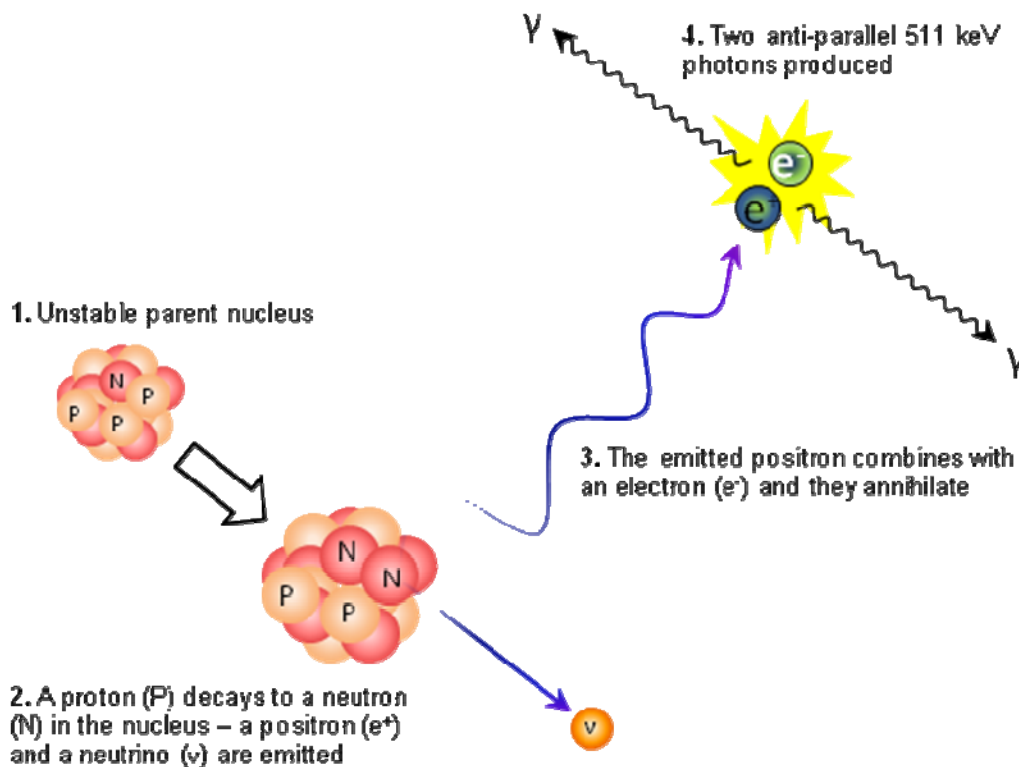


Figure 1.7 - Simplified representation of positron decay and annihilation. An unstable parent nucleus decays by converting a proton to a neutron, which emits a neutrino and a positron. The positron travels some distance from the nucleus and annihilates with an electron, emitting two anti-parallel gamma photons of 511 keV each. *Adapted from Kristian Jensen – Adamanzanes, 2009 (PhD thesis).*

A nucleus can exist in an excited state, meaning that it is unstable due to an excess of energy. This usually occurs following another type of decay, such as alpha or beta. The excess energy can be emitted in the form of a gamma-photon. This is used in SPECT imaging (see **Section 1.6**). Gamma emission is monoenergetic. An important type of gamma-emitters are metastable nuclei or so-called *nuclear isomers*. These have relatively long half-lives and are thus well-suited for medical purposes. Such nuclei are said to decay by *isomeric transition*. An important example is ^{99m}Tc , the “m” referring to the metastability. An alternative to isomeric transition is internal conversion (IC). In this mode of decay, the excess energy is transferred to an orbital electron that is then emitted as radiation instead of the gamma-ray.

1.6 SPECT and PET – Nuclear tomographic imaging

Generally, two very broad areas of diagnostic imaging exist. One modality is *anatomical imaging*, which provides information of the structures of the body. To this area belongs the CT scans, where X-rays provide 3D representations of the anatomy [169]. The other modality is *functional imaging* where tracers exhibit ADME according to their chemical, and in the case of NPs, also their three-dimensional structure. The latter is also often referred to as *molecular imaging*, but for NPs this is somewhat misleading. To the area of functional imaging belong *single-photon emission computed chromatography* (SPECT) and *positron emission tomography* (PET). As SPECT and PET do not give anatomical information, they are often used in connection with CT to ease the quantification of radiotracer uptake in a given tissue or organ.

SPECT technology is not the main point of this work, but the basic principles are discussed here as knowledge of SPECT is necessary to understand the wider field of NP imaging. For new and exciting principles and techniques in SPECT, please

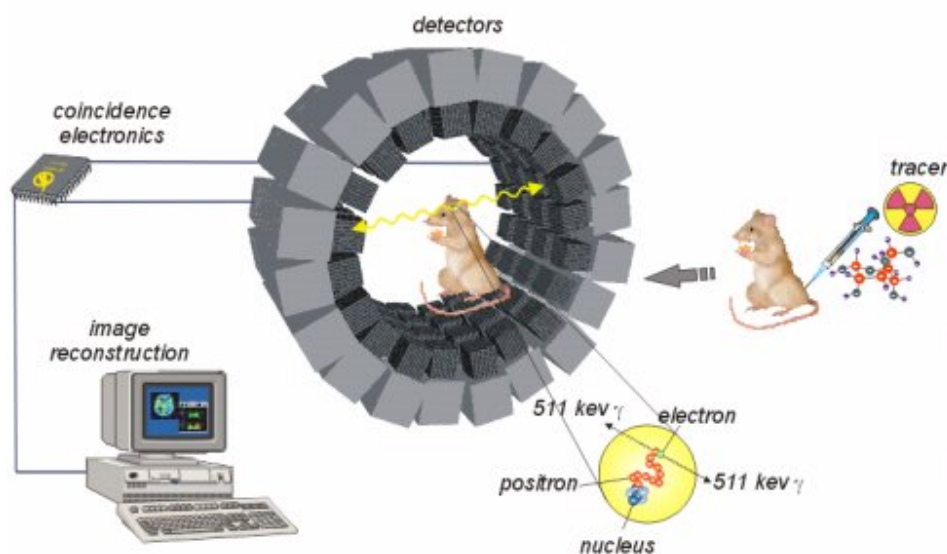


Figure 1.8 – Schematic representation of small animal PET imaging. The animal is injected with the tracer and placed (prostrate) in the PET detector. The coincidence detections are processed in a computer.

Figure adapted from <http://www2.fz-juelich.de/zel/index.php?index=136>

see Rahmin & Zaidi [170]. SPECT can be used to detect the *in-vivo* location of isotopes emitting gamma rays (SPECT isotopes). In SPECT imaging, a series of gamma cameras is mounted around the patient or object of interest. These are set

in many, equally spaced, angular intervals. Collimators are used to define the angle of the gamma rays that reach the detecting unit of the gamma camera. A collimator is in essence a lead plate that contains a large number of holes. As much radiation is filtered off by the collimators and not detected, the geometric efficiency (percentage of detected to emitted photons) in SPECT imaging is relatively low, on the order of 0.01% [170]. Generally, it is desirable that the energy of the emitted photons is between 100-300 keV. If the energy is too low, too much radiation is absorbed in tissue, if it is too high, the collimators cannot efficiently shield unwanted photons. An advantage of SPECT over PET is that different isotopes can be distinguished in the same scan. The reason is that gamma photons have different energies, whereas annihilation radiation is always 511 keV. This allows techniques such as *double labeling* of nanoparticles, which is commented on **section 2.1.7**. Another advantage is that SPECT isotopes with half-lives longer than PET isotopes are widely available, making longer scans possible. However, with NPs scan, periods of maximum 2-3 days are usually not necessary, meaning that PET isotopes such as ^{64}Cu are generally sufficient. When longer scans are desired, PET isotopes such as ^{124}I , ^{86}Y [171] and especially ^{89}Zr [172, 173] are currently gaining prominence.

Positron emission tomography (PET) is a nuclear imaging method that uses radiopharmaceuticals labeled with positron emitting radioisotopes (PET isotopes). The radiopharmaceutical is usually injected intravenously into the subject where it is allowed to distribute according to regular ADME processes. Its location is then monitored externally by suitable equipment. The underlying imaging principle is based on the simultaneous detection of the two photons that are released as annihilation radiation after the emitted positron comes to a halt and encounters an electron. A PET detector consists of a ring of scintillation detectors, placed in a ring around the subject, that records coincidence signals (i.e. records both perpendicular annihilation photons at the same time) from various planes simultaneously and processes the data into a 3-dimensional image (see **fig. 1.8**).

By the PET technique, concentrations of the radiotracer can be measured quantitatively in target organs. PET is at least 10-fold more sensitive than SPECT, being in the range of 10^{-11} - 10^{-12} M [170, 174, 175]. The reason for this improved sensitivity is that, in SPECT, it is necessary that the collimators only let in photons of a certain angle, in order to improve resolution. Photons arriving from a slightly skewed angle are filtered off. In PET, the possibility of coincidence detection abrogates the need for physical collimators. Instead the collimation is done electronically. This allows PET to detect about 1% of all positron emissions [170]. The improved sensitivity results in improved image quality and the possibility of performing shorter scans [170]. Further, PET has a much better spatial resolution [170, 175, 176]. These factors, make small lesions easy to miss in SPECT [176, 177] and in the clinic, PET provides improved image quality over SPECT [178]. A factor that influences the possible maximum resolution of PET imaging is the emission of non-perpendicular annihilation photons. This happens when the kinetic energy of the positron has not reached zero upon annihilation. In that case, the remaining momentum will be transferred to the photons and the angle between them will not be 180° .

1.7 Important radioisotopes for SPECT and PET

Here is presented the physical properties of a series of the most widespread and/or interesting SPECT and PET isotopes (table 1.1). These are all isotopes that have previously been used to label NPs or that have potential as such.

For the SPECT isotopes, technetium-99m (^{99m}Tc) is the most common. Its photon energy of 140 keV is generally considered

Table 1.1 – Overview of relevant isotopes for radiolabeling of nanoparticles. All energies are given as mean energies.

SPECT isotope	Half-life	γ -emissions, keV	Other relevant emission	Comments
^{67}Ga	3.26 d	93.3 (39%) 185 (21%) 300 (17%) 394 (5%)	X-ray (8.6 keV, 50%)	High-energy photon emission. Requires thick septa for collimation.
^{99m}Tc	6.01 h	140 (87%)	IC (12%, 140 keV)	Very commonly used. Eluted from a generator. Good photon energy.
^{111}In	2.80 d	171 (91%) 245 (94%)	X-ray (23 keV, 69%) X-ray (26 keV, 11%)	-
^{123}I	13.2 h	179 (83%)	IC (14%, 127 keV)	-
PET isotope	Half-life	B^+ , keV	Other relevant emissions	Comments
^{18}F	110 min	249.8 (97%)	EC (3%)	Good positron energy, high resolution.
^{64}Cu	12.7 h	278.1 (18%)	β^- (579 keV, 39%) EC (43%)	Commonly used PET isotope. Good positron energy. Suitable for <i>theranostics</i> .
^{124}I	4.18 d	820 keV (23%)	EC (77%) γ (603 keV, 63% + others)	High positron energy (poor resolution). Many high-energy γ -photons. Interesting due to long half-life [1].
^{89}Zr	3.27 days	396 keV (23%)	EC (77%) γ (909 keV, 99%)	Acceptable positron energy (mean range ~ 1 mm). Long half-life. Not yet used with NPs.

Data from: Phillips [2], Gomme [4], NUDAT (<http://www.nndc.bnl.gov/nudat2/>).

close to optimal. However, the main advantage of ^{99m}Tc is that it can be eluted from a so-called technetium-generator. This generator contains ^{99}Mo that decays to ^{99m}Tc that is eluted. Thus, a cyclotron is not needed on-site, greatly reducing costs. ^{67}Ga has photon emission of high energy that requires the use of thick lead collimators in order to prevent

decreased resolution. ^{111}In has somewhat lower energy photon emissions lowering the need for thick collimators. ^{123}I is a popular SPECT-isotope due to its low photon energy and chemical properties as a halogen. This allows covalent binding to nanoparticle constituents, a feature that is not possible with the other three SPECT isotopes listed here. The PET isotopes listed in **table 1.1** are all of a half-life long enough to justify imaging of nanoparticles. Other popular, but very short-lived, PET isotopes include ^{11}C , ^{15}O and ^{68}Ga . Iodine-124 is currently not widely used for PET imaging, mainly as the large positron range and disturbing photon emissions diminish resolution. Due to its desirable long half-life some authors have however suggested ways to overcome the limitations of ^{124}I [171]. ^{89}Zr is another long-lived PET isotope that is currently gaining in popularity. As it allows longer scans than ^{64}Cu , it may very well have future applications in NP research [172, 173]. To the knowledge of the author, only dextran NPs have been labeled with ^{89}Zr thus far [179].

1.8 Basic radiochemistry of ^{18}F

^{18}F is the most popular PET isotope today. An example of its widespread use is in the cancer diagnosing radiopharmaceutical [^{18}F]2-fluoro-2-deoxy-glucose ([^{18}F]FDG, colloquially *FDG*) that is a radiotracer for glucose utilization [180]. Here, the [^{18}F]fluoride atom isosterically takes the place of a secondary alcohol. About 90% of all current (2012) clinical PET scans are performed with [^{18}F]FDG [181]. ^{18}F ($T_{1/2}$ 109.8 min) is very attractive for labeling tracers that do not require a very long radioactive half-life. It decays almost exclusively by positron decay (97%), emitting a relatively low energy positron (E_{max} 0.635 MeV) that travels ≤ 2 mm in water [182]. This path length is similar to the highest resolution possible with modern PET cameras [182].

[^{18}F]fluoride is usually produced on a cyclotron, through irradiation of ^{18}O -enriched water with protons. This will prompt the nuclear reaction $^{18}\text{O}(p,n)^{18}\text{F}$ [183]. Here, the *p* refers to a proton entering the nucleus, and the *n* to a neutron leaving. This gives an atom with an unchanged nominal mass but with an added charge, converting the ^{18}O to the radioactive ^{18}F . This reaction is high yielding at relatively low cyclotron energies (< 16 MeV) [182] and provides the [^{18}F]fluoride anion no-carrier-added (NCA), as a solution in water.

At an estimated free energy of hydration of - 104 kcal/mol, [^{18}F]fluoride in water is nucleophilically inert [184]. Hydration means that nucleophilic substitution with [^{18}F]fluoride in organic solvents must take place under anhydrous conditions [185]. If water is present, it will coordinate to the fluoride, with up to 15 water molecules, making it unreactive [186]. In order to separate the [^{18}F]fluoride from the bulk water, two steps are usually taken. The first is to lead the solution through a small anion-exchange column (SEP-PAK) containing a quarternary amine stationary phase (a QMA column) [187]. This catches the [^{18}F]fluoride and, as a bonus, makes it possible to recover the expensive ^{18}O -water. A further

advantage of employing the QMA column is that impurities in the [^{18}F]fluoride solution such as metal ions can be washed away. The activity is then eluted with a small volume of usually a water-acetonitrile mixture containing a weak, non-nucleophilic base, such as potassium carbonate. Besides eluting the fluoride, the carbonate will serve as base in the ensuing substitution reaction. In addition, as [^{18}F]HF is volatile [188], it is important to keep the [^{18}F]fluoride deprotonated. The water is then removed by two or three successive azeotropic evaporations with acetonitrile. It is believed that completely “naked” fluoride is never obtained, as each successive removal of a water molecules becomes increasingly difficult [182]. In difficult procedures such as $\text{S}_{\text{N}}\text{Ar}$ reactions, very dry [^{18}F]fluoride appears necessary, whereas it is less essential in aliphatic substitution [182]. There is even evidence that *adding* small amounts of water might serve to decrease adsorption of [^{18}F]fluoride to the vessel without decreasing reactivity [182]. This effect is particularly pronounced in Pyrex vessels [189]. To the reaction mixture is furthermore added a phase transfer catalyst, to separate the charge of [^{18}F]fluoride anion from the present cations, usually K^+ . A common choice is Kryptofix-222 (K_{222}), which chelates the potassium ions, effectively turning them from small hard ions into soft ions with a large surface [190]. This decreases their affinity for the [^{18}F]fluoride, thus rendering it more reactive. Besides K_{222} , large cations such as tBu_4N^+ can also be used, serving the same purpose.

As [^{18}F]fluoride adheres strongly to certain materials, the reactor vessel material is an important consideration in nucleophilic fluorinations with [^{18}F]fluoride [189]. Generally, adsorption decreases for vessel materials in the order of Pyrex > glassy carbon > platinum [182].

A further concern is the purity of the substrate. In order to obtain optimal yields, it is important that the substrate is of the utmost purity and does not contain entities that can associate with or otherwise decrease the reactivity of the [^{18}F]fluoride.

In aliphatic nucleophilic substitution with [^{18}F]fluoride, yields may vary substantially, but can be expected to be decent, at times quantitative [182]. Generally, the chemistry follows the line of non-radioactive $\text{S}_{\text{N}}2$ and leaving groups can be sulphonates (Ts, Ms, Tf) or halides. As reactions are often carried out at high temperature (to achieve a faster reaction with less decay of the radioisotope), elimination side reactions can cause problems [191]. This can be expected to be less pronounced with primary (pseudo)halides. Solvents employed are almost exclusively aprotic polar solvents as they improve reactivity in $\text{S}_{\text{N}}2$ reactions, with acetonitrile, DMSO and DMF being especially popular. Acetonitrile has the advantage of being easier to remove but cannot go as high in temperatures as the other two.

1.9 Basic radiochemistry and pharmacokinetics of ^{64}Cu and its chelators

In recent years ^{64}Cu has garnered significant interest as a PET isotope. In comparison with ^{18}F , ^{64}Cu has the significant advantage of its much longer half-life of 12.7 hours. As PET scans are usually conducted for about four half-lives, this makes it possible to track longer-circulating radioactive entities *in-vivo* for about 48 hours (some researchers have scanned up to 72 hours [192]). This has made ^{64}Cu especially interesting in the radiolabeling of antibodies [193] and NPs [194]. Longer half-life also makes transport from cyclotron to hospital over considerably longer distances possible.

^{64}Cu emits positrons (18%) at a max energy of 653 keV and has a substantial β^- decay (37%) with max energy of 578 keV. This makes it a useful PET isotope as well as a potential theranostic isotope (i.e. an isotope suitable for both therapy and diagnosis [195, 196]). However, at the same time, the β^- decay gives it a slight disadvantage in imaging as the emitted electrons will impart a certain radiation dose in tissues of accumulation. Especially liver and spleen, in the case of nanoparticles.

^{64}Cu is usually produced on a cyclotron, by the $^{64}\text{Ni}(p,n)^{64}\text{Cu}$ nuclear reaction [197], which involves the irradiation of ^{64}Ni by a proton beam. Absorption of a proton leads to emission of a neutron, leading to an unchanged nominal mass of the

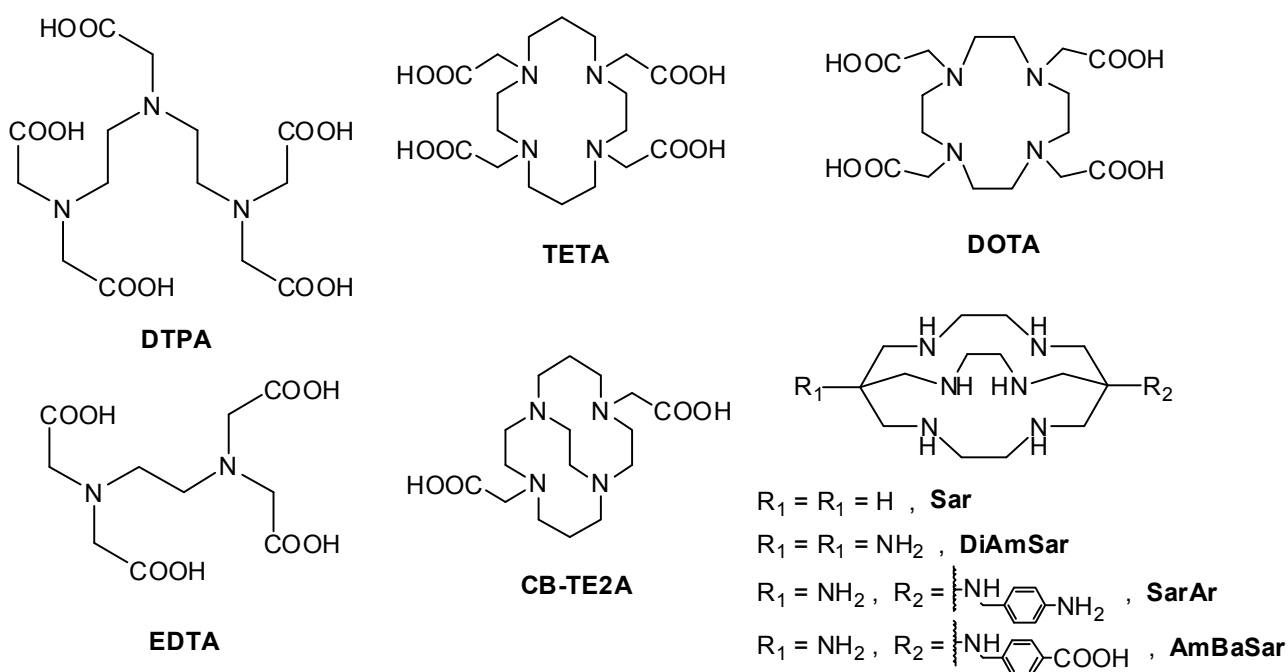


Figure 1.9 – Common chelators of Cu^{2+}

nucleus, but an extra charge. This reaction is essentially similar to what was described above for the production of ^{18}F . The $^{64}\text{Cu}^{2+}$ is then purified on an ion-exchange column and eluted as CuCl_2 in aqueous HCl [198]. Evaporation of the water/HCl leaves CuCl_2 .

In aqueous solution, Cu can exist in three oxidation states (I-III), but due to the superior stability of Cu^{2+} this form is used in the vast majority of cases. Being a transition metal, ^{64}Cu is coupled to molecules of interest by chelation. Several chelators have been developed that can attach $^{64}\text{Cu}^{2+}$ to biological molecules and nanoparticles. The most widely used are macrocyclic chelators, containing electron-pair donating amines and charge-compensating side-arms such as carboxylic acids [199]. These trap $^{64}\text{Cu}^{2+}$ in locked three-dimensional cages, conveying high stability (known as the *macrocyclic effect* [200]). Polyaminocarboxylates such as DOTA and TETA (see **figure 1.9**) have been the subject of countless studies, due to their high availability as bifunctional chelators (BFCs), exhibiting functionalized arms, such as activated NHS-esters, for easy conjugation. Both DOTA and TETA can be labeled with $^{64}\text{Cu}^{2+}$ at room temperature for a relatively short time of 30-45 minutes [201, 202]. During labeling, the pH is slightly lowered (5.5-6.5) to deprotonate the amines and prevent precipitation of ^{64}Cu -hydroxide.

It is however well-established that both DOTA and TETA have some instability *in-vivo* [198, 199]. This has been attributed to poor kinetic stability, which may have little relation to the excellent thermodynamic stability (logK) of both chelators (DOTA: 22.2-22.7, TETA: 20.5-21.9) [198]. In order to improve on this, stronger binding chelators such as the sarcophagine cages and *cross-bridged TE2A* (CB-TE2A) have been developed.

In order to understand the seemingly compromised kinetic stability of certain chelators, it is necessary to take a look at the *in-vivo* trafficking of Cu^{2+} . Copper is an essential trace element, present in numerous cuproenzymes [203], but as free Cu^{2+} is toxic it is not generally present in living systems [203]. Instead it is sequestered by copper-binding proteins. These include, superoxide dismutase (SOD), ceruloplasmin, transcuprein and albumin. When free Cu^{2+} enters the blood stream it initially binds to transcuprein [204]. From here it can shift to albumin and these two make up an exchangeable blood pool [205]. However, it relatively quickly finds its way to the liver, possibly transported by transcuprein [205], where it is taken up by hepatocytes [206]. Some copper also enters the kidneys, from where it appears to be rapidly cleared [207]. From the liver, the copper is either **1**) eliminated, the majority being through biliary excretion [203] with a certain degree of enterohepatic circulation or **2**) reshuttled back into the blood stream, bound to the copper transporting protein ceruloplasmin, that is synthesized in the hepatocytes. Within 24 hours, 6-8% of copper taken up into the liver reappears, bound to ceruloplasmin [206]. Ceruloplasmin transports copper to other tissues and it is important to note, that copper does not spontaneously exchange from it [203]. More than 99% of this bound copper is excreted and reabsorbed in the kidneys [206], meaning that excretion in the urine is not a major pathway of elimination.

Bass et al. demonstrated that $^{64}\text{Cu}^{2+}$ escapes from TETA through transchelation in the liver to superoxide dismutase (SOD) [208]. SOD is an enzyme that is present in the cytosol of eukaryotic cells, especially in liver, kidney, adrenal and red blood cells [208]. This was done by injecting rats with [^{64}Cu]TETA-octreotide, followed by homogenization and analysis of the liver 20 h postinjection. 69% of the ^{64}Cu in the liver eluted with SOD. Injection of ^{64}Cu -acetate also resulted in formation of $^{64}\text{CuSOD}$ in the liver. It appears that in order for uptake in SOD to occur, it is necessary that the ^{64}Cu -containing entities are either taken up by liver cells (whether hepatocytes or Kupffer cells is unclear) or that they lose their copper in the blood stream, which is then transported to the cytoplasm of hepatocytes.

Boswell et al. conducted an interesting study making several important points [209]. They injected four chelators, including DOTA, TETA and CB-TE2A labeled with ^{64}Cu into rats. They showed that all the chelators were as good as cleared from all tissues after 24 hours with all *percent injected dose per gram* (%ID/g) values being lower than $0.6 \pm 0.2\%$ except ^{64}Cu -DOTA in liver, which was at $1.06 \pm 0.16\%$. Specifically for the chelator CB-TE2A, they showed that the chelated copper was as good as cleared from the circulation (by renal excretion) 2 hours after injection. It seems reasonable to assume that this applies to all the chelators. This finding is consistent with Petersen *et al.*, who reported that ^{64}Cu -DOTA was removed rapidly from circulation (after 24 hours all ID%/g were below 1%) and did not show significant tissue retention. This reaction is high yielding at relatively low energies (< 16 MeV) [210]. In the organism, Boswell *et al.* investigated liver and blood. In blood, the results suggested that activity might have been transferred to ceruloplasmin. For DOTA and TETA, the activity in blood was almost exclusively protein bound after 4 hours. For CB-TE2A after 20 hours, two thirds was protein bound (very little activity remained in the blood for CB-TE2A). These results suggest that TETA and DOTA do lose Cu^{2+} activity to hepatocytes, hinting at less than ideal stability in the blood stream. However, as the chelators themselves are rapidly cleared, the authors do not conclude if it would be significant for a DOTA-containing macromolecule or nanoparticle that is long-circulating. As DOTA-containing radiopharmaceuticals are currently in clinical use and providing good, clean images, such as DOTATATE [177], this may not be the case. Transchelation in the liver was assessed by homogenizing the tissue and measuring percentage of protein (primarily superoxide dismutase) associated ^{64}Cu and chelator associated ^{64}Cu . It was found that almost complete transchelation from DOTA occurred after just one hour and from TETA after about 4 hours. From CB-TE2A about a third of ^{64}Cu was protein-associated after 20 hours. This again hints at improved kinetic stability for CB-TE2A. However, when nanoparticles are taken up into liver tissue they are metabolized regardless, making subsequent transchelation irrelevant. Thus, an important question is whether the copper is lost by transchelation following uptake in the liver or, the worst case scenario, lost in the blood stream and then transported to the liver. *In-vivo*, TETA appeared more stable than DOTA [209].

McQuade *et al.* compared a DOTA-conjugated peptide labeled with both ^{64}Cu and ^{86}Y . They found substantially higher liver and other non-target uptake for the ^{64}Cu -labeled peptide. They attributed this to chemical differences between the ^{64}Cu -DOTA chelate and the ^{86}Y -chelate, which could lead to either loss of ^{64}Cu in the blood and subsequent liver uptake, or

increased uptake in the liver of the ^{64}Cu -containing compound itself [211]. Rogers et al. compared different ^{64}Cu chelators and showed that TETA was actually the most stable in liver. After *in-vivo* injection of ^{64}Cu -TETA conjugated antibodies in rats, liver was homogenized and analyzed after 1 and 5 days, showing 8% ^{64}Cu -SOD (>90% intact mAb) and 41% ^{64}Cu -SOD (43% intact antibody), respectively. It appeared here that the antibodies may be taken up in liver and then the ^{64}Cu is transchelated to SOD [212]. Wu et al. found that a DOTA conjugated tracer (RGD peptide) was degraded much more rapidly in liver than in other organs [213]. Whether the ^{64}Cu was lost to proteins or very hydrophilic fractions (hydrolysis of the tracer) remains unclear.

The sarcophagine cage was developed in the late 70s and early 80s by Sargeson *et al.* [214, 215]. This group synthesized the DiAmSar form in 1984 [214]. They later functionalized DiAmSar into SarAr, containing a primary amine primarily for coupling to carboxylic acid residues [207, 216]. AmBaSar, with a carboxylic acid, for coupling to nucleophilic residues, such as amines, was subsequently prepared by Cai *et al.* [217, 218]. The Sar cage forms a highly stable chelate with $^{64}\text{Cu}^{2+}$ under *in-vivo* conditions. Sar chelators have been shown to give less liver accumulation than DOTA and TETA [219]. Liver uptake of ^{64}Cu from injection of a Sar functionalized antibody was half of what was observed with DOTA functionalized antibody by Wu *et al.* [220] and Cai *et al.* [192]. In general, the Sar cages incorporate $^{64}\text{Cu}^{2+}$ under mild conditions. An AmBaSar coupled peptide was labeled with $^{64}\text{Cu}^{2+}$ at room temperature and pH 5.0 (0.1 M NH_4OAc -buffer) in 1 h with a yield of $\geq 80\%$ [217]. Evidence suggests that placing a linker, such as those used in SarAr and AmBaSar, between one of the primary amines of Diamsar and the subject as desirable [221]. The Sar complexes have been shown to form very stable chelates with Cu^{2+} *in-vivo* [216, 222].

Labeling of CB-TE2A with $^{64}\text{Cu}^{2+}$ requires relatively harsh conditions, such as 1-2 h at 95 °C (pH = 8) for labeling yields of $\geq 95\%$ [201, 223] or 1 h at 85 °C (pH = 5.5) for labeling of 96% [39]. This is detrimental when labeling proteins, liposomes or other structures labile to high temperatures. But for substrates able to withstand the high temperature, CB-TE2A provides a remarkably stable chelate with $^{64}\text{Cu}^{2+}$. It has been shown that CB-TE2A forms a chelate with Cu^{2+} that is significantly more stable both *in-vitro* and *in-vivo* than does DOTA and TETA [209, 224, 225]. With CB-TE2A, both pendant arms are used in forming a hexadentate complex with Cu^{2+} . This means that when one of these arms is used for conjugation, there is a potential loss in stability. However, studies with CB-TE2A conjugated to a somastatin analogue [226] and to bombesin [225], confirmed that it retained its stability.

In spite of excellent reported properties, DiAmSar has not yet gained widespread use. This could be because of the relatively cumbersome synthetic procedure of functionalizing the two primary amines [207, 217]. The same is true for CB-TE2A, presumably due to harsh labeling conditions, and inavailability as a *bifunctional chelator* (BFC). A sound argument for the continued use of DOTA is that the methodology and toxicology are well-known [199]. In addition, it is widely available as a BCF.

1.10 Concluding remarks and rationale for nuclear imaging of nanoparticles

As has been demonstrated, the field of nanoparticle research is still very much in development. While the design of the particles themselves is relatively advanced, researchers still battle with undesirable pharmacokinetics such as poor tumor uptake and widespread uptake in undesired tissues such as liver and spleen. Not until better *in-vivo* control of the nanoparticles is achieved, can they provide the therapeutic revolution they have been expected to. To better understand how changes in design affect the *in-vivo* pharmacokinetics of nanoparticles, efficient and sensitive imaging modalities are needed. As we have seen, PET imaging is very well suited for this purpose. Thus, radiolabeling of nanoparticles has become a quite intensely researched field.

An offshoot of radiolabeling of nanoparticles for improved understanding is the idea to use them as a tool for imaging and diagnosing tumors and metastases. This springs from the tumor accumulation of nanoparticles which, although modest, is sufficient to achieve appreciable contrast between tumor and surrounding tissue (T/M-ratio), usually in about 8 hours. These ideas will be discussed further in the following two chapters. An obvious drawback of nanoparticle tumor imaging is that liver metastases can easily go unnoticed. Other realms of nanoparticle radiolabeling is loading of nanoparticles with therapeutic (α , β^- or even Auger-emitters) isotopes with the intent of causing tissue damage in targets of interest, usually tumors. From here springs the idea of *theranostics*, where the same particles are loaded with both therapeutic and diagnostic isotope, for a dual-modality approach [195].

Chapter 2

Preparation and *in-vivo* investigation of ^{18}F -labeled liposomes

*Described in this chapter is the development of methodology for conducting fully automated [^{18}F]radiofluorination of lipid probes and the subsequent insertion of these into the bilayer membranes of liposomes. Also described are in-vivo studies with such liposomes. The discussion of the results obtained here address ^{18}F -labeled liposomes as a diagnostic tool for cancer as well as a tool in liposome research. Also included **section 2.10** is a short discussion of radiofluorination in non-polar organic solvents. The chapter starts with a review of historical and current techniques for radiolabeling liposomes. The results presented here were published in the Journal of Liposome Research and in Chemistry – a European Journal.*

2.1 Background

Early on and still today, liposomes are labeled with beta-emitting classics such as ^3H (*tritium*) [227] and ^{14}C [228-230]. These isotopes are attached covalently to a lipophilic compound of choice. This provides for very stable labeling as the probe can be expected to stay in the membrane. A prerequisite for such labeling is that the lipid is not metabolized or exchange with serum components such as lipoproteins [231, 232]. This type of liposome labeling will in the following be referred to as *membrane labeling* (**fig. 2.1**) and will be commented on further in **section 2.1.3**. An immediate advantage is that it is not necessary to change the liposome formulation by incorporating alien molecules, as lipids already present in the membrane can have hydrogens or carbons exchanged for their respective radioisotopes. Nonetheless, there are major drawbacks when using ^3H and ^{14}C ; (1) isotopes must be covalently bound through laborious radiochemical synthesis, (2) due to the short traveling distances of the beta particles, quantification can only be done by excision of organs/xenographs and (3) the necessary use of scintillation methodology, which includes time-consuming sample preparation.

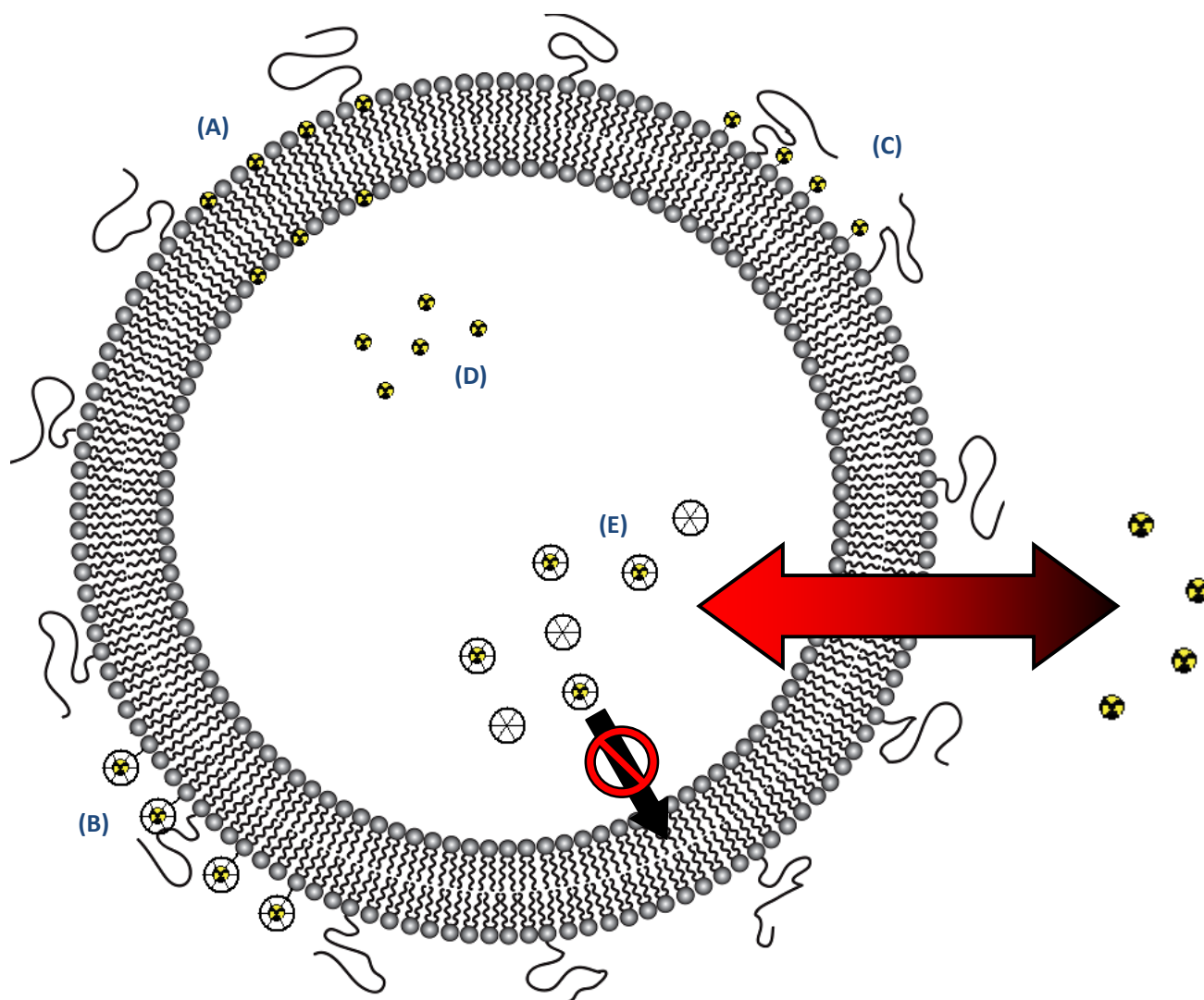


Figure 2.1 – Liposome (PEGylated) with presentation of different labeling methods. (A) *Membrane labeling*. The radioisotope is covalently attached to a lipid molecule that is inserted into the membrane. (B) *Surface chelation*. The membrane includes lipids with covalently attached chelators, that can bind metal radioisotopes. (C) *Surface labeling*. The radiolabel attached to the surfaces of preformed liposomes through a chemical reaction. Only reported for $^{99\text{m}}\text{Tc}$. (D) *Passive loading*. Radioisotopes passively enter the liposome lumen during preparation. (E) *After-loading*. Radioisotopes outside of preformed liposome cross the membrane by conversion to a lipophilic species, that is in equilibrium across the membrane. Inside the liposome the isotopes are bound by a stronger, hydrophilic agent, which prevents them from escaping.

In order to achieve easier quantification of activity in organs and ultimately non-invasive imaging by SPECT and PET, short-lived gamma-emitting isotopes have been introduced. These have a further advantage beyond the quantification by

gamma-counting of organs (*ex-vivo* studies) and SPECT or PET imaging (both considered *in-vivo* studies); this being the issue of avoiding contamination of equipment, glassware and people with long-lived radioisotopes such as tritium and ^{14}C . Ideally, liposomes should be preformed and labeled immediately prior to use or alternatively, the liposomes should be prepared with the radiolabel already in the lipid mixture and used immediately. The reasons are; (1) as most diagnostic SPECT/PET isotopes have relatively short half-lives, a short time between preparation of the isotope and administration is preferable, (2) as radiolysis [233] of any compound is always a hazard, exposure to radiation should be as short as possible, (3) as non-radioactive metallic impurities in the radioisotope accumulate in respect to the radioactive isotopes as the sample decays, these can theoretically saturate the binding sites, when chelators are used for labeling.

2.1.1 Radiolabeling of liposomes with metal isotopes for SPECT-imaging

As SPECT isotopes are commonly metals, covalently linking these to liposomes is not feasible. Furthermore, the short half-lives prevent time-consuming methodology. For these reasons, a series on ingenious methods for liposome labeling has been developed.

Technetium-99m ($^{99\text{m}}\text{Tc}$)

Early on, Richardson *et al.* attempted to label liposomes by reducing radioactive sodium pertechnetate ($[\text{}^{99\text{m}}\text{Tc}]\text{NaTcO}_4$) to the chemically reactive $^{99\text{m}}\text{Tc(IV)}$ in the presence of SnCl_2 and preformed liposomes [5, 234-236]. They reported an excellent labeling efficiency (LE) of >90% with less than 2% free pertechnetate after labeling. In their method, the reduced $^{99\text{m}}\text{Tc(IV)}$ associates with the liposome, providing a *surface labeling* (fig. 2.1). The method was later employed by Love *et al.* [20, 230, 237] They found evidence of the radiolabel leaching from the surface in all but negatively charged liposomes [20]. However, instability for negative liposomes was reported by another group [229]. Surface labeling in general can present problems, as the metal ions are in direct contact with blood stream components, often with unpredictable effects. Other reports have given contradictory results with regards to the stability of $^{99\text{m}}\text{Tc}$ on the surface of liposomes and there is general evidence that liposomes labeled in this way are prone to rapid release of the radiolabel [14, 238].

Ahkong and Tilcock tried to label liposomes with $^{99\text{m}}\text{Tc}$ by attaching DTPA to the surface of the liposomes (*surface chelation*, fig 2.1). This was found to enhance the stability of the binding [229]. Hnatowich *et al.* used a similar method [14]. They achieved about 90% LE and found relatively good stability. However after 2h incubation in plasma only 67% activity remained with the liposomes. Goto *et al.* used the same method [239]. Espinola *et al.* entrapped $^{99\text{m}}\text{Tc}$ -DTPA inside liposomes by *passive loading* (fig. 2.1) [240]. In passive loading, liposomes are formed in a solution containing the species to be loaded. They found some leakage of the $^{99\text{m}}\text{Tc}$ -DTPA complex. Oku *et al.* also used passive loading for labeling

liposomes with $^{99\text{m}}\text{Tc}$ obtaining LEs of 5-10% [26]. In conclusion, none of these early reported methods for $^{99\text{m}}\text{Tc}$ labeling of liposomes appear to have furnished solid labeling procedures with excellent *in-vivo* stability.

A breakthrough in $^{99\text{m}}\text{Tc}$ labeling was achieved in 1992, when *after-loading* (figure 2.1) was introduced by Phillips *et al.* [23]. After-loading (or *remote-loading* or *active loading*) denotes a procedure where a radioisotope (or alternatively, a drug molecule) is rendered lipophilic, allowing it to travel across the lipophilic membrane. Once inside the liposome, it is trapped in various ways, usually by converting it to a charged species. Phillips *et al.* reconstituted the commercially available chelator hexamethylpropyleneamine oxime (HMPAO) with $^{99\text{m}}\text{TcO}_4$ and incubated the resulting lipophilic complex with preformed glutathione-containing liposomes. The complex crossed the membrane and was reduced by the glutathione [241] to its hydrophilic form. Phillips *et al.* reported excellent LEs (>90%) and good *in-vivo* stability [23]. The method was used by the group of Corstens to conduct both animal [29] and human [28] *in-vivo* scans, obtaining LEs of 60-70% and 60-85% respectively. Such relatively low LEs made a purification step by *size-exclusion chromatography* (SEC) necessary, in order to remove activity not associated with the liposomes. PEGylation has not been found to interfere with labeling by after-loading [242]. In 1999, the same group adapted the use of hydrazinonicotinic acid (HYNIC) [243] for complexing $^{99\text{m}}\text{Tc}$ to the surface of liposomes [31]. This can be regarded as the first reported case of surface chelation where an *in-vivo* stable conjugate and excellent LE (>95%) were achieved.

A recently reported after-loading method for $^{99\text{m}}\text{Tc}$ involved the thiol-containing chelating agent BMEDA [32]. This compound coordinates to $^{99\text{m}}\text{Tc}$ and carries it across the membrane to interact with encapsulated glutathione. An advantage is that it can also label liposomes with the β^- -emitting therapeutic radionuclides rhenium-186 (^{186}Re) and rhenium-188 (^{188}Re) [244-246], providing a double labeling. Further, it can directly label DOXIL by sharing the cross-membrane pH gradient [247]. Loading of liposomes with both therapeutic nuclides and $^{99\text{m}}\text{Tc}$ using BMEDA remains in use to this day [248-250].

Gallium-67 (^{67}Ga) and Indium-111 (^{111}In)

As ^{67}Ga and ^{111}In share main group and both form trivalent ions without the need for reduction, similar labeling methods exist for the two. Liposomes labeled with ^{67}Ga and ^{111}In appeared around 1980. Espinola *et al.* were among the first to incorporate ^{111}In -oxine into the membrane of liposomes, by a method resembling passive loading [240]. The oxine complex is mixed into the lipid film and during hydration, the complex gets trapped in the membrane. This is however, a relatively unstable labeling method *in-vivo*. Hnatowich *et al.* labeled liposomes with ^{67}Ga by inserting a DTPA-conjugated lipid into the liposome membrane followed by a labeling step [14]. They achieved LEs of >90% and concluded relatively good stability in plasma. However, their liposomes only showed 71% retention of activity after 6 hours incubation in 50% plasma.

Hwang et al. were among the first to report after-loading methodology for these radioisotopes. They developed a method where ^{111}In and ^{67}Ga are complexed to oxine, giving a lipophilic complex. The complex was then incubated with liposomes encapsulating nitriloacetic acid (NTA). After crossing the lipid membrane, the oxine would transfer the metal ion to the stronger-binding NTA [7, 251]. The labeling could be performed at 37 °C and was shown to be stable *in-vivo* [251]. At around the same time, Mauk & Gamble published a similar method for In^{111} , but using the ionophore A23817 [9]. A disadvantage of their method however, was that temperatures above T_m (60-80 °C) were needed for loading. This can disrupt the liposomal membrane and lead to leakage of potential contents. Beaumier & Hwang loaded acetylacetone complexed ^{111}In into NTA-loaded liposomes [252]. Gabizon et al. investigated deferoxamine (DF) with ^{67}Ga [18]. DF is a stronger chelator than NTA, giving the general advantage of diminishing transfer of the chelated metal to transferrin once the liposomes disintegrate. Instead the chelator bound radiolabel is filtered in the kidneys. This interferes less with the imaging [238]. Later on, Ogiwara et al. entrapped ^{67}Ga in liposomes by the oxine/NTA after-loading method [253, 254]. After-loading of ^{111}In with encapsulated DTPA was achieved by Corvo et al. and Laverman et al. [30, 255, 256].

2.1.2 Radiolabeling of liposomes with metal isotopes for PET (^{64}Cu)

The use of liposomes in PET imaging has recently been reviewed by Silindir et al. [257]. With the advent of PET in combination with CT (PET/CT), it has gained increasing prominence in the field of liposome imaging. However, the only metal PET-isotope which has so far been used with liposomes is ^{64}Cu . Seo *et al.* recently published a number of papers concerning the labeling of liposomes with ^{64}Cu [38, 39, 258]. In his group, they have consistently used methodology for surface chelation. Initially, they employed a classic procedure by preparing the liposomes with the chelator-conjugated lipid [38]. However, this presents the common problem that the radioisotope (^{64}Cu) has to be attached to the chelator while the liposome is formed, meaning that harsh conditions for labeling are not possible. They later developed a method where a disulfide compound conjugated with CB-TE2A would be labeled with ^{64}Cu . This compound would then be converted to the thiol and conjugated to the surface or to the distal PEG-end of maleimide functionalized preformed liposomes [39, 258]. This enabled the use of the strong chelator CB-TE2A (see chapter 1, section 1.8) for which the harsh labeling conditions necessary are usually incompatible with liposomes. However, the images presented by Seo et al. have in all cases been of relatively poor resolution, making it problematic to assess the feasibility of the labeling methods they have employed.

Promising progress in efficient liposome labeling with ^{64}Cu was made when a method was developed for active loading of ^{64}Cu into DOTA-containing liposomes [210, 259]. This method is a “classic” after-loading procedure where 2-hydroxyquinoline is used. Liposomes are loaded at relatively mild conditions of 20-50 °C for labeling efficiencies of >95%

with good retention of the encapsulated DOTA- ^{64}Cu complex. Excellent stability of the prepared radioliposomes was reported and images of good resolution were obtained.

2.1.3 Radiolabeling by covalent binding (iodine)

As mentioned above, initial investigations with covalently bound radioisotopes were done with tritium and deuterium. However, for SPECT and PET isotopes, covalent binding has also been investigated. Two general methods have been used for the association of non-metal isotopes with liposomes. These being, (1) encapsulation (either passive or active) of a compound to which the isotope is covalently bound or (2) binding the radioisotope to a lipid which is then inserted into the bilayer membrane (*membrane labeling*).

Iodine (all isotopes)

As the iodine isotopes exhibit such great variety in function of each isotope, from the weak beta-minus emitter ^{125}I to the potentially useful PET-isotope ^{124}I [260], there has been a natural desire to develop efficient methods for labeling liposomes with iodine. Early experiments with iodine were done by Hardy *et al.* in 1980 who labeled liposomes with sodium iodide by passive encapsulation [261]. Recently, a method was reported for active-loading of radioiodine into liposomes using the *Bolton-Hunter* (BH) reagent [33, 34], achieving 62% encapsulation in PEGylated liposomes. The BH reagent contains an activated NHS ester as well as a *para*-phenol moiety, which can be iodinated in the *ortho*-position. The compound then travels across the membrane to react with the amine of encapsulated arginine to provide a trapped, charged compound [34].

Other methods have included Arrowsmith *et al.* who prepared ^{131}I iodine monochloride and let it react with egg lecithin. The resulting labeled lipids were then incorporated into the membrane of liposomes [17]. The method was later reproduced [20]. Schroit prepared a non-exchangable ^{125}I labeled lipid (*phosphatidylethanolamine, PE*) derivative, that was incorporated into the membrane of liposomes [262].

A rather successful methodology for iodination is the Iodogen method described in 1978 by Fraker *et al.* in their heavily cited paper [263]. Iodogen (a mild organic oxidant) is used to oxidize iodide to the reactive species I^+ . This method has been employed on liposomes to label protein that was later passively encapsulated [30].

Table 2.1 – Chronological overview of SPECT/PET radiolabeling methods for liposomes, including year of first publication. PET isotopes are highlighted in light grey.

Year	Isotope	First author	Method	Details	LE	Ref.
1977	$^{99\text{m}}\text{Tc}$	Richardson	Surface labeling	SnCl_2 reduction	> 90%	[5]
1978	^{111}In	Hwang	After-loading	oxine/NTA	~68%	[7]
1979	^{111}In	Mauk	After-loading	A23817/NTA	>90%	[9]
1981	^{67}Ga	Hnatowich	Surface chelation	DTPA	>90%	[14]
1984	^{131}I	Arrowsmith	Membrane labeling	Oxidation	RCY: 77%	[17]
1988	^{67}Ga	Gabizon	After-loading	oxine/DF	57-88%	[18]
1989	$^{99\text{m}}\text{Tc}$	Love	Surface labeling	SnCl_2 reduction	50-60%	[20]
1992	$^{99\text{m}}\text{Tc}$	Phillips	After-loading	HMPAO	> 90%	[23]
1993	$^{99\text{m}}\text{Tc}$	Oku	Passive loading	DTPA	5-10%	[26]
1995	^{18}F	Oku	Passive loading	^{18}F FDG	10-15%	[27]
1996	$^{99\text{m}}\text{Tc}$	Corstens	After-loading	HMPAO	60-85%	[28, 29]
1999	^{111}In	Corvo	After-loading	oxine/DTPA	>85%	[30]
1999	$^{99\text{m}}\text{Tc}$	Laverman	Surface chelation	HYNIC	> 95%	[31]
2003	$^{99\text{m}}\text{Tc}$	Bao	After-loading	BMEDA	>85%	[32]
2006	Iodine	Mougin-Degraef	After-loading	Bolton-Hunter	>62%	[33, 34]
2007	^{18}F	Urakami	Membrane labeling	Preformed liposomes	46.4±4.8%,	[35, 36]
2007	^{18}F	Marik	Membrane labeling	^{18}F FDP	RCY: 43%	[37]
2008	^{64}Cu	Seo	Surface chelation	BAT	> 83%	[38]
2010	^{64}Cu	Seo	Surface chelation	CB-TE2A	> 95%	[39]
2011	^{64}Cu	Petersen	After-loading	2-hydroxyquinoline/DOTA	> 95%	[41]

2.1.4 Summing up labeling methodology

A summary of labeling methods is provided in **table 2.1**. In general, after-loading methods have been the most successful labeling methodology for metal isotopes, with the highest *in-vivo* stability [2]. Typically, after-loading provides stable loading with LEs of 50-100%. The non-encapsulated activity is commonly removed by SEC. If the loading efficiency is close to 100%, a SEC step can in some cases be omitted, greatly simplifying the procedure. If developed adequately, with highly hydrophilic complexes entrapped in the liposomes, after-loading methodology will effectively prevent leaching of the radioisotopes from the vesicles. As a further advantage, the surface of the liposome, and especially its charge density and distribution, will remain unaltered. Leaching can be problematic with surface chelation, unless very strong chelators, such as CB-TE2A, are used. After-loading can, in principle, label preformed liposomes, meaning that radioisotope and liposome

can be prepared at different locations. However, these liposomes have to be prepared with the entrapment agent already in the liposome, meaning that commercially available formulations cannot be labeled right off the shelf. Another, relatively theoretical, issue with after-loading is the possibility that the ionophore or carrier accumulates in the membrane and leads to alteration of its characteristics. This will be abrogated with dilution, however, as the carrier will readily displace to the aqueous bulk phase. A further disadvantage is that as soon as the liposomes disintegrate, the water-soluble radiolabeled species can enter the blood stream and potentially accumulate in secondary locations, thus disturbing the imaging. These issues will be addressed further in **section 2.8**.

For non-metal radioisotopes the picture is somewhat different, as after-loading for such isotopes requires special chemical reactions to occur inside the liposome, such as with the BH reagent for the iodine isotopes. For the other major non-metal radioisotope ^{18}F , no after-loading method has been developed to date. However, covalent linkage of the isotope to a lipid molecule also provides an attractive labeling methodology.

2.1.5 Radiolabeling of liposomes with ^{18}F

In 1995, Oku *et al.* were the first to label liposomes with ^{18}F , by passively encapsulating [^{18}F]fluorodeoxyglucose ([^{18}F]FDG) [27, 264]. As with all classic passive accumulation methodologies, this resulted in relatively poor encapsulation efficiencies of about 10-15%. Nonetheless, they found the liposomes to be stable *in-vivo* and suitable for imaging. However, the imaging pictures presented by Oku *et al.* were of poor quality [27] and correspondence with the authors has not resulted in obtaining better quality images. For this reason the results are hard to assess. Further, Oku *et al.* only measured for two hours, which is somewhat short for achieving proper tumor accumulation and *tumor-to-muscle* (T/M)-ratios.

Marik *et al.* developed [^{18}F]fluorodipalmitin as a lipid probe that was incorporated into the lipid membrane during hydration of the lipid film [37]. The probe developed consisted of a *dipalmitoyl glycerol* lipid with the alcohol exchanged for an [^{18}F]fluoride in the 3-position. The probe was labeled by standard K222 nucleophilic fluorination in ACN, mixed with the lipids and hydrated. The MLVs were then sonicated and extruded (200 nm followed by 100 nm filters) to provide relatively small SUVs of 45 ± 18 nm. Sonication is known to give liposomes that are relatively small [265]. *In-vivo* PET scans were then carried out in non-xenografted mice for 90 minutes. It is not known why Marik *et al.* opted to sonicate the MLVs as most commercial and research liposomes are around 100 nm. Furthermore, in spite of nice results, kinetics and PET-images, the lack of xenografts and consequently sufficient scanning time for tumor accumulation, makes it difficult to assess the feasibility of these liposomes in cancer diagnosis.

To label preformed liposomes, which is generally highly problematic when using ^{18}F -fluorinated lipid probes, Urakami *et al.* developed the SophT method [35, 36]. In this method, incorporation of an amphiphilic ^{18}F -labeled probe is achieved by incubation of the dried probe with a liposome dispersion, around the phase transition temperature of the lipids. Doing this, Urakami *et al.* achieved an impressive labeling efficiency of $46 \pm 5\%$. Urakami *et al.* concluded that liposomal labeling with their probe of choice was stable in serum. However, the reported PET scans showed what appears to be considerable bladder accumulation over the course of 1 hour, especially for the 90 nm liposomes [35]. This seems to indicate that the issue of leaching from *in-vivo* sink conditions has not yet been adequately addressed.

2.1.6 Choice of lipid probe in membrane labeling

When carrying out membrane labeling of liposomes, the choice of the lipid molecule to be labeled is crucial. The objective is a compound that will stay in the membrane in *in-vivo* conditions and that will not suffer chemical or enzymatic degradation.

Chemical and enzymatic stability can be attained by not including bonds that are readily hydrolyzed in the pH range of 5 (*can occur in tumors* [266] and *lysosomes* [267]) to 7.4 (*physiological pH*) or degraded by endogenous enzymes, usually the main concern being esterases [268] or amidases [269]. The stability of common chemical bonds towards both hydrolysis and enzymatic degradation can be given as *ester* < *amide* < *ether*. Thus, ether bonds are usually preferable.

Obtaining a probe that will be stably lodged in the membrane usually depends on two factors, the first being the lipophilicity of the compound. If a compound is sufficiently insoluble in water and has a 3-dimensional structure that fits in the membrane, it can be expected to stay there, even faced with bloodstream sink conditions. The second is resistance to inter-membrane lipid transfer by blood stream enzymes. It has been shown that cholesterol, cholesteryl esters, phospholipids and triglycerides all exchange between lipid membranes *in-vivo*. These phenomena have been reviewed, with especially the review by Bell being very comprehensive [270-272].

Cholesteryl ethers, usually as the ^3H - or ^{14}C -labeled hexadecyl ether, have long been used as liposome membrane probes, based on their favorable *in-vivo* characteristics [273-275]. Cholesteryl ethers are metabolically inert, highly lipophilic and non-exchangable [227].

2.1.7 Double labeling of liposomes

By combining the methodologies described above, several groups have prepared liposomes labeled with two different radioisotopes. This is known as double- or dual labeling. It has usually involved a membrane or surface label combined with a labeling of the aqueous core. This concept will not be dealt with in detail here, but a few interesting examples are presented. Mougin-Degraef et al. combined the BH reagent loading of ^{125}I with surface labeling with ^{111}In through a DTPA-conjugated DSPE phospholipid [34]. Their results showed gross discrepancy between the two labels in both PEGylated and conventional liposomes, with the ^{125}I -BH label generally excreted in the urine and the ^{111}In -lipid label accumulating in liver and spleen. Awasthi et al. carried out a double active-loading procedure by combining the HMPAO procedure and the oxine procedure for $^{99\text{m}}\text{Tc}$ and ^{111}In respectively [276]. Here was also observed distinct differences between the two radiolabels, with for example $^{99\text{m}}\text{Tc}$ eliminated much more readily through the kidneys. From these studies, the conclusion must be that great caution should be taken when assuming that the long-term (> 4h) pharmacokinetics of the radiolabel correspond with those of the liposomes.

2.1.8 Objective

In light of the methodology addressed above, and in particular the studies involving ^{18}F -labeling, we decided to prepare **^{18}F membrane labeled liposomes**. We synthesized a novel cholesteryl ether lipid probe and in order to conduct the radiosynthesis and liposome preparation, fully automated procedures were investigated and developed. The liposomes would be investigated *in-vivo* in tumor xenografted mice by 8 hour PET scans. The objective was to investigate whether ^{18}F -labeled liposomes were feasible as a short term diagnostic instrument as well as a research tool for PET imaging of the lipid part of liposomes in studies of up to 8 hours.

The developed probe would furthermore be a lipophilic PET-probe, meaning that it could be useful in double-labeling, combined with another hydrophilic probe associated with the liposome by active-loading.

2.2 Synthesis of lipophilic sulphonate substrates

It was decided to prepare two probes, one 1,2-di-hexadecyl-glycerol (**DHG**) and one cholesteryl ether (**CE**). These and their resemblance to endogenous lipids are depicted in **fig. 2.1**. In general, it was desired to obtain the sulphonate substrates in a very high degree of purity, as even low levels of impurities might interact with the minuscule amounts of ^{18}F and disturb the radiolabeling. For this reason, most compounds were routinely purified by flash chromatography, even when the procedures afforded products that were pure by TLC after work-up.

2.2.1 Synthesis of a di-alkyl glycerol probe substrate (**1**)

As the corresponding alcohol **2** was commercially available, it was initially purchased and mesylated/tosylated/triflated to give **3**, **4** and **5** (**scheme 2.1**). Eventually, the mesylate (**3**) was chosen as the candidate for ^{18}F fluorination, meaning that this was the only compound that was fully characterized and the only one to be purified by flash chromatography. In turn, the tosylate (**4**) was purified by recrystallization, which proved possible in spite of the lipidic nature of the compound. The

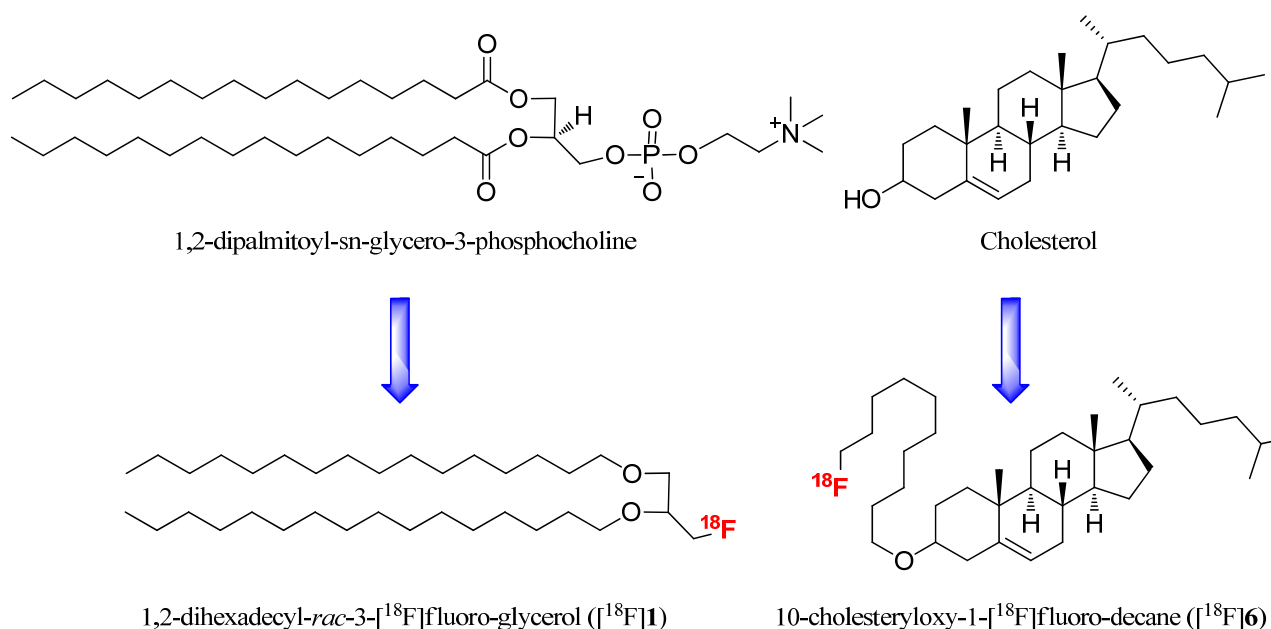
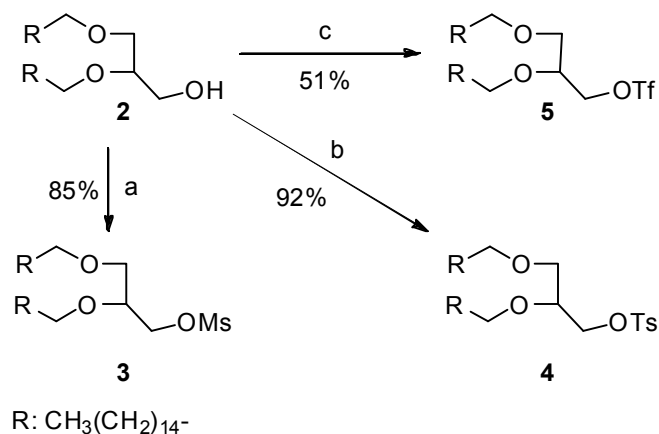


Figure 2.1 – Target lipid probes. ^{18}F **1** was meant as an analogue to a phospholipid, whereas ^{18}F **6** was a derivative of cholesterol

Scheme 2.1: Pseudohalogenation of 1,2-dihexadecyl-*rac*-glycerol

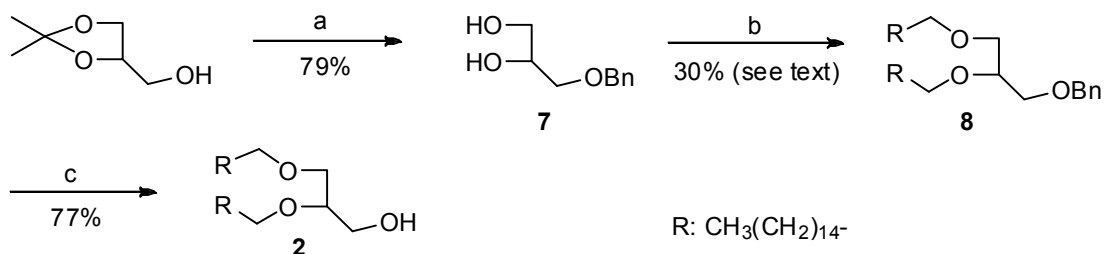


Reagents and conditions: (a) MsCl , pyridine, DCM, RT, 4h, (b) TsCl , pyridine, DCM, RT, overnight, (c) Tf_2O , DCM, 1h.

triflate (**5**) was impossible to purify on silica due to decomposition. Instead, during workup, it was dissolved in heptane and washed with methanol, in order to remove any polar impurities. This afforded a compound that was pure by ^1H -NMR, but only in fair yield.

Due to a high price of the alcohol, it was desired to synthesize it from cheaper starting materials (**scheme 2.2**). In order to achieve this, DL-1,2-isopropylidene-*rac*-glycerol was used as a precursor. This compound is well-suited when specific modification of the 3-position is required [277]. If necessary, it can be prepared optically pure in large scale from D-mannitol [278] and can also be purchased as such. Benzylation proceeded without difficulty. Deprotection of the acetal was conveniently carried out by adding the acidic AmberLite IR120 H^+ resin. This afforded the crude product as a red oil – the color most likely being due to the beads losing some of their red color to the solution. The final purified **7** was colorless. The alcohols on **7** were etherified using classic Williamson ether synthesis [279] with hexadecylbromide as substrate and NaH as base to yield **8**. Purification of the crude compound by flash chromatography was problematic and one impurity was difficult to remove from all product-containing fractions. For this reason, the fractions containing this impurity were pooled and the pure fractions were pooled. The amount or nature of the impurity was not determined. The pure fractions were used in the further synthesis. It was attempted to remove the benzyl group by catalytic hydrogenation. This, however, turned out to be an unusually sluggish process, with even week-long hydrogenation not resulting in a completed reaction. It is contemplated that this may have been caused by a partially oxidized Pd/C catalyst. In future attempts to synthesize **2** by this method, it may be advisable to use a hydrogen pressure of more than one atmosphere.

Scheme 2.2: Synthesis of 1,2-dihexadecyl-*rac*-glycerol

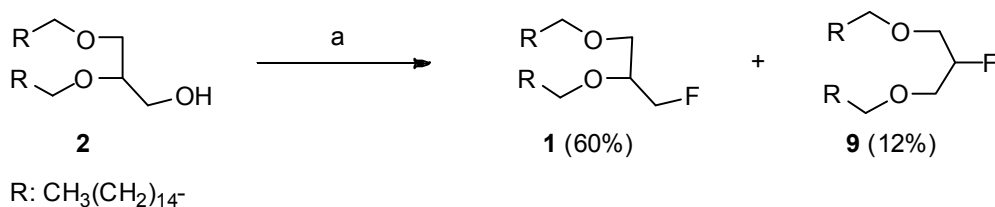


Reagents and conditions: (a) I: NaH, BnBr, DMF, 0 °C \Rightarrow RT, overnight; II: AmberLite IR120 H+, RT, overnight, (b) NaH, $\text{Br}(\text{CH}_2)_{15}\text{CH}_3$, DMF, -78 °C \Rightarrow RT \Rightarrow 140 °C, 6.5 h, (c) H_2 (g, 1 atm), DCM, RT, 2 weeks.

2 was converted to sulphonates as shown in **scheme 2.1**.

In order to assess the authenticity of the ^{18}F -fluorinated product (^{18}F **1**), a non-radioactive (“cold”) reference compound (**1**) was needed. A convenient way of preparing such a compound was using the DAST reagent [**280**] for converting the alcohol **2** to the fluoride **1** (**scheme 2.3**). DAST is a highly reactive diaminosulfur trifluoride which reacts under mild conditions, the main drawback being formation of HF. In the course of the reaction of **2** with DAST a byproduct was formed. This was isolated and identified by NMR as 1,3-O-dihexadecyl-2-fluoro-*rac*-glycerol (**9**). The proposed mechanism for its formation is shown in **figure 2.2**. Attack of the alcohol on the sulfur leads to elimination of first HF, then a further fluoride, which leads to the formation of the sulfoximine intermediate. This intermediate can then undergo an $\text{S}_{\text{N}}2$ reaction [**281**, **282**] or the formation of a carbocation [**282**]. However, as the alcohol here is primary, it appears that $\text{S}_{\text{N}}2$ is more likely. Attack by the fluoride will then lead to the formation of **1**, whereas attack by the ether oxygen will lead to the formation of the epoxide, which in turn can be attacked by fluoride in either the 2- or 3-position, leading to the formation

Scheme 2.3: Fluorination of 1,2-O-dihexadecyl-*rac*-glycerol



Reagents and conditions: (a) DAST, DCM, -78 °C (2h) \Rightarrow 0 °C (1h)

of **9** or **1**, respectively. In the first synthesis of **1**, the temperature was initially $-78\text{ }^{\circ}\text{C}$ but was quickly raised to $0\text{ }^{\circ}\text{C}$, followed by reaction for 1 hour. This led to yields of **1** (52%) and **9** (13%). In order to improve the yield of **1**, the reaction was allowed to proceed for 2 hours at $-78\text{ }^{\circ}\text{C}$ and then 1 hour at $0\text{ }^{\circ}\text{C}$, as the reaction was not observed to have gone to completion during the first 2 hours. This provided yields of 60% and 12% respectively. The difference may be due to normal variation. Both reactions were carried out on the same small scale (23-25 mg **2**), which may have resulted in slightly lower yields than what could normally be expected as well as some uncertainty on the exact yields. In recent years, reagent milder than DAST, such as PBSF and TBAT have gained prominence [283]. Such reagents may be able to improve the yield of **1** in comparison to **9**, as would an extra carbon atom between the alcohol and the glycerol backbone, which would effectively prevent attack by the oxygen.

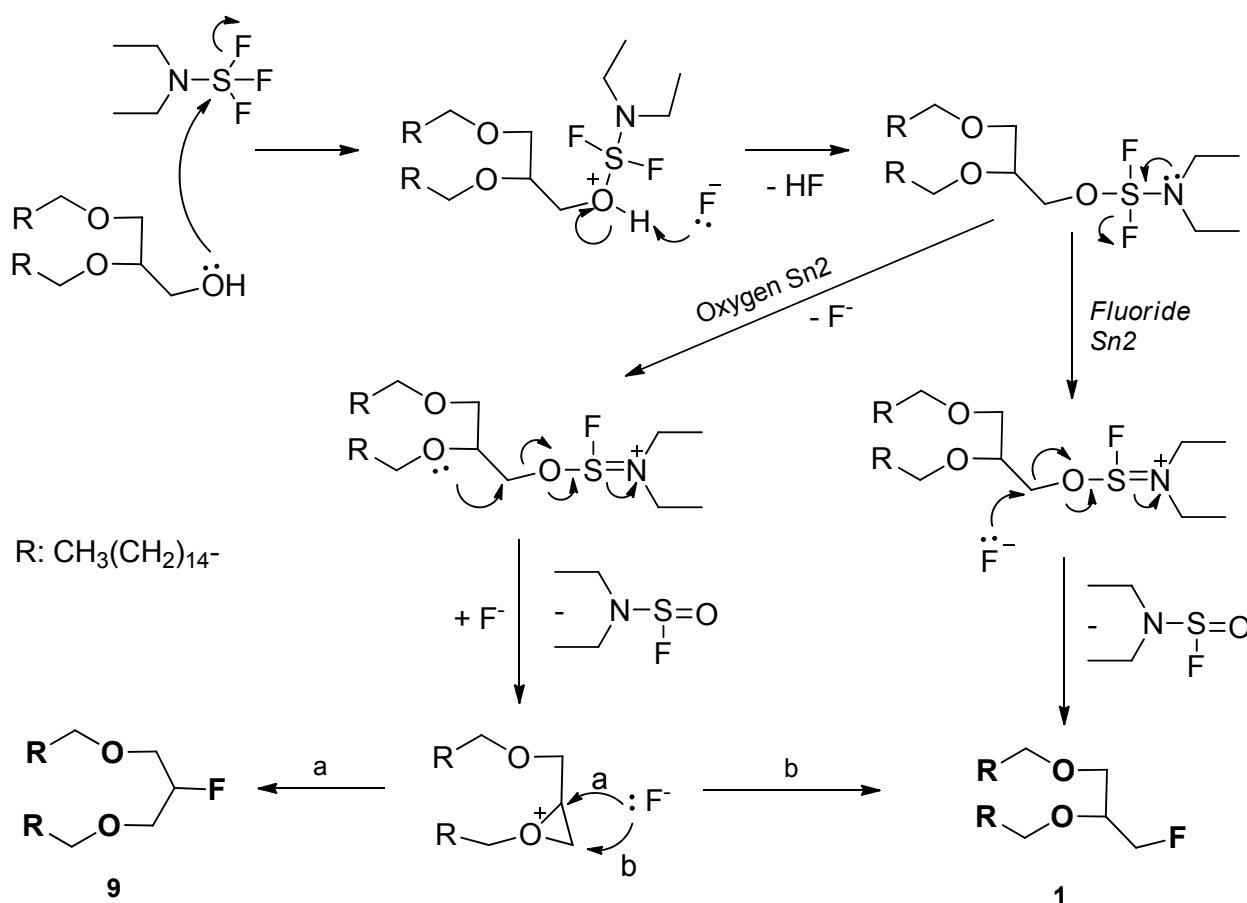


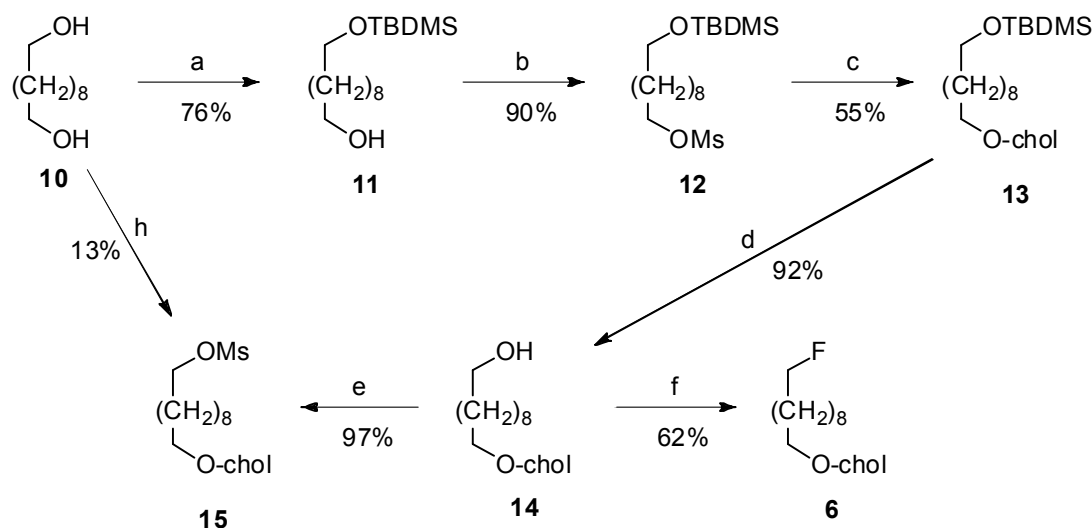
Figure 2.2 - Mechanism of formation of 1,2-O-hexadecyl-3-fluoro-*rac*-glycerol (**1**) and 1,3-O-hexadecyl-2-fluoro-*rac*-glycerol (**9**).

2.2.2 Synthesis of a cholesteryl ether probe precursor

As no commercially available cholesteryl ether with a terminal alcohol could be found, this precursor was synthesized from cholesterol (**scheme 2.4**). 1,10-decanediol (**10**) was used to convert the cholesterol to a cholesteryl ether. It was contemplated that the length of the alkyl chain was not critical, but a chain of some length was desired in order to impart a certain degree of lipophilicity on the probe. Hexadecyl chains are a common choice [227], but 1,16-hexadecanediol was not found to be commercially available at a reasonable price.

Initially, the diol was silyl ether mono-protected using TBDMSCl. By dropwise addition of TBDMSCl to **10**, with **10** in a molar excess of 3:1, followed by addition of imidazole. Calculations carried out in ROOT, assuming same probability of reaction at all alcohols, showed the maximum theoretical yield of **11** to be 83%. The achieved yield of 76% is thus an effective yield of $76/83 = 92\%$. This was followed by mesylation of the remaining alcohol. These steps were followed by classic Williamson ether synthesis, initiated by formation of the sodium cholesteryl salt and followed by reaction with **11** to form **12**. Previous experiments had been conducted where a bromide was used instead of a mesylate, but due to no or very low yields, the mesylate was employed instead. This reaction was conducted in toluene in the presence of DMF,

Scheme 2.4: Synthesis of a cholesteryl ether lipid probe



Reagents and conditions: (a) TBDMSCl, imidazole, DMF, rt, 20 h, (b) MsCl, pyridine, DCM, rt, 5 h, (c) i: cholesterol, NaH (60%), toluene, 80 °C, 1 h, ii: (addition of **12**), DMF, 80 °C, 16 h, (d) TBAF, THF, rt, 6 h, (e) MsCl, pyridine, DCM, rt, 5 h, (f) DAST, DCM, - 78 °C \Rightarrow rt, 2 h, (h) i: MsCl, pyridine, DCM, rt, 2.5 h, ii: cholesterol, NaH, THF, 60 °C, 30 min, iii: (addition of dimesylate to cholesteryl salt), 65 °C (6.5 h) \Rightarrow rt (3 days).

where the role of the polar, aprotic DMF is to stabilize the charged $\text{S}_{\text{N}}2$ intermediate [284]. Toluene is added to ensure proper dissolution of the lipidic compounds. The TBDMS-group was easily removed by treatment with TBAF, where the affinity of the fluoride to the silicium of the silyl ether provides mild cleavage [285]. In spite of the lipidic nature and at times waxy appearance of the prepared cholesteryl ethers, it was possible to recrystallize **14** from hexane. This was combined with flash chromatography to afford a high degree of purity.

From the alcohol **14** the mesylate **15** was prepared. Other pseudohalides of the cholesteryl ether were not prepared, since experiences with probe **1** had revealed mesylates as the best option (see section 2.3). As in those syntheses, a fluoride analogue **6** was prepared from **14** by reaction with DAST. This synthesis turned out with only fair yields, which may again be caused by the low scale. No specific side reactions were observed.

Another convenient method for preparing terminal alcohol cholesteryl ethers has been reported by a number of groups. This method involves conversion of the alcohol of the cholesterol into a suitable leaving group by tosylation [286-288]. This is followed by reacting it with a suitable diol, usually through prolonged refluxing in dioxane. A cholesteryl ether from 1,10-decanediol has been synthesized in this way [289]. In partial inspiration from this method, a methodology for a semi one-pot synthesis of **15** was devised (pathway h, scheme 2.4). This involved di-mesylation of the diol and the subsequent crude purification of the di-mesylate through a silica plug, which would remove polar impurities such as pyridinium chloride as well as unreacted MsCl . Solvents were removed *in vacuo*. The dimesylate was then reacted with the sodium cholesterolate salt prepared using NaH . Adding the sodium cholesterolate to the dimesylate is thought to be crucial in order to minimize formation of cholesteryl di-ether. Even in spite of the poor yield (13%), this procedure redeems itself by the low number of operations, cheap starting materials and the direct furnishing of the desired mesylate.

2.3 Automated synthesis of an ^{18}F -labeled di-hexadecyl glyceride lipid

With the sulphonate substrates in hand, nucleophilic [^{18}F]fluorination was the next step. This was to be carried out on a custom-built fully-automated synthesis constructed and programmed (LabView) at the Hevesy Laboratory (Nutech, DTU) (figure 2.3). The mechanics of this machinery are described further in **Supplementary Information I**. In this section the focus is on the chemistry of the radiofluorination.

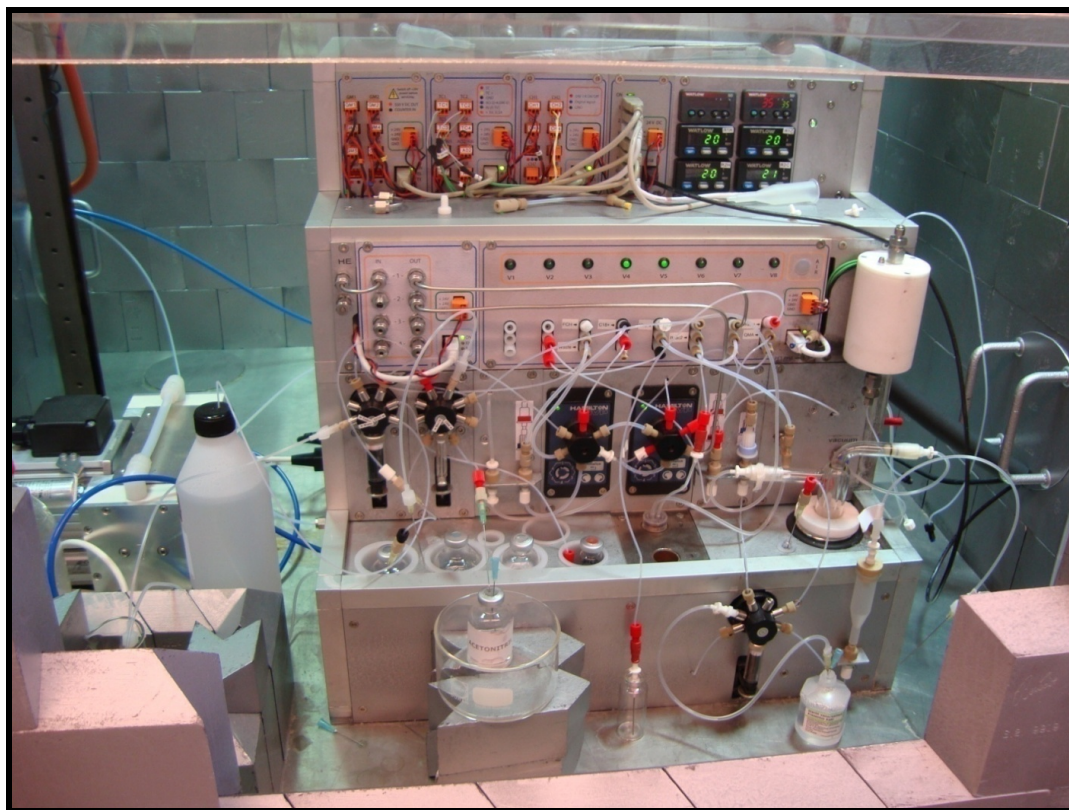


Figure 2.3 – The synthesis robot

2.3.1 Preparation and drying of the reactor

During investigation of the fluorination, the activity (^{18}F) was received in a glass vial, in a solution that was obtained by rinsing excess activity off the target with Milli-Q water. The counter cation of the [^{18}F]fluoride in NCA fluorination is generally considered unknown, and is a mixture of various metals. This solution was lead through a K_2CO_3 preconditioned QMA SEP-PAK column [290], which would consistently quantitatively capture the fluoride. The eluate was discarded. Leading a solution of Kryptofix222 (K222) and K_2CO_3 in acetonitrile-water (1:1, 0.6 mL) through the QMA eluted the activity, with very small amounts still present on the SEP-PAK (see **table 2.6**). The resulting solution containing the [^{18}F]K(K222)F complex was then transferred to the glass reactor, where the reaction itself would take place. Here, an initial evaporation cycle removed water and acetonitrile. The evaporation cycle was conducted as a combination between lowered pressure (achieved by a connected membrane pump) and a helium stream. In addition, the temperature of the socket in which the reactor was placed could be raised and lowered actively (through a stream of liquid nitrogen).

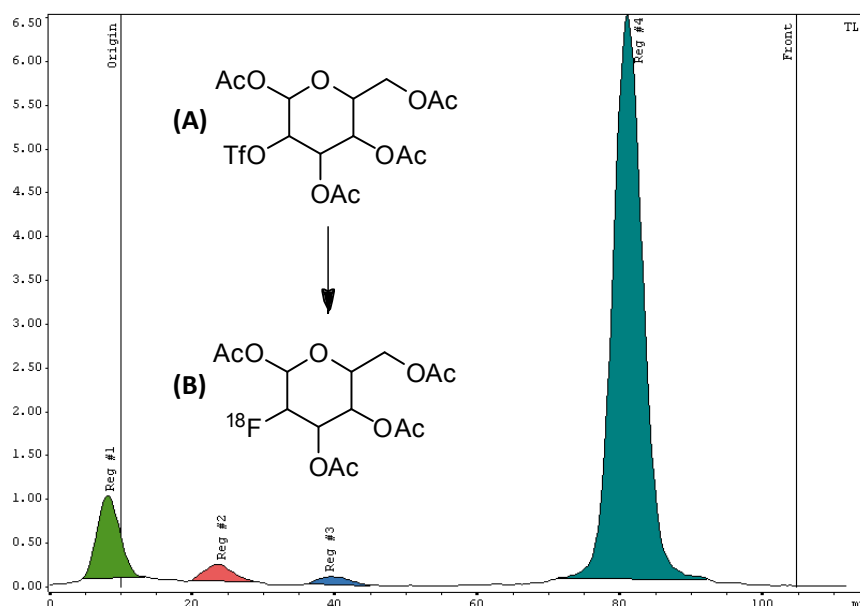


Figure 2.4 – Test radiofluorination of FDG-precursor (A). The green peak at the starting line is unincorporated ^{18}F while the large turquoise peak on the right is the $[\text{}^{18}\text{F}]$ -fluorinated species (B) – the desired product. The red and blue peaks are unknown, minor impurities.

The initial evaporation usually left a little liquid still visible in the reactor. As exposing the reagents to high temperatures might cause the $[\text{}^{18}\text{F}]$ fluoride to adhere to the glass, the temperature of the initial evaporation was kept relatively low and some residual water was left. This water was then removed by three successive azeotropic evaporations with 0.3 mL acetonitrile each, leaving a dry reactor containing $[\text{}^{18}\text{F}]\text{K}(\text{K}222)\text{F}$, $\text{K}(\text{K}222)\text{KCO}_3$ and K_2CO_3 . During the initial optimization phase, the water contents in the dried vial were assessed by adding dry acetonitrile and measuring the water content by Karl Fischer titration. In the optimized settings it was generally found that about 0.5 μL water was left in the reactor (before the evaporation of toluene – see [section 2.3.2](#)). However, as is seen below ([section 2.3.2](#)) this did not impede radiofluorination of an FDG precursor substrate. This should also be seen in the light, that the pre-packaged acetonitrile used in FDG-production has traces of water (about 2000 ppm) and that it is generally accepted that traces of water in radiofluorination may not be detrimental to, but may actually aid the reaction by providing better solubilization of $[\text{}^{18}\text{F}]\text{K}(\text{K}222)\text{F}$ (see [Chapter 1 – section 1.7](#)).

2.3.2 Addition of the substrate

Before, the pseudohalide precursors were used, the system was tested with the regular precursor used in the production of FDG for clinical use (**Figure 2.4**). The substrate was dissolved in 2 mL acetonitrile, added to the dried reagents and heated for 20 minutes at 80 °C. The mixture was then analyzed by radio-TLC (H_2O -acetonitrile, 5:95) to show a very high degree of conversion to the desired [^{18}F]-fluorinated product. This indicated that the drying stages and the system itself was working satisfactorily for radiofluorination.

Table 2.2 – Selected [^{18}F]-labeling results – Labeling of the di-hexadecyl-glyceride substrates (mesylate: **3**, tosylate: **4**, triflate: **5**). All values are decay-corrected.

Entry	Substrate	Added in	Solvent (mL)	Time (min)	Temp. (°C)	CF [†]	Impurities
1	4 (5 mg)	CHCl_3	DMSO (1)	20	150	none	A
2	3 (5 mg)	CHCl_3	DMSO (1)	20	150	none	No obs.
3	3 (5 mg)	Toluene	DMSO (1)	20	100	2.76%	A
4	3 (5 mg)	Toluene	DMSO (1)	30	100	2.60%	No obs.
5	3 (5 mg)	Toluene	DMSO (1)	20	165	2.79%	No obs.
6	3 (5 mg)	DMF (1 mL)*	DMSO (1)	30	100	none	Numerous
7	5 (3 mg)	Toluene	DMSO (1)	20	165	1.52%	A, B
8	5 (5 mg)	Toluene	DMSO (1)	30	100	1.39%	A, B
9	3 (5 mg)	Toluene	DMSO (1)	30	100	2.17%	A, B
10	3 (5 mg)	Toluene	DMSO (1)	30	100	2.18%	A, B
11	3 (5 mg)	Toluene	DMSO (1)	30	100	1.75%	A, B
12	3 (5 mg)	CHCl_3	DMSO (1)	30	80	0.92%	A, B
13	3 (5 mg)	CHCl_3	ACN (3)	30	80	1.90%	A, B
14	3 (5 mg)	Toluene	ACN (3)	20	80	1.27%	B
15	3 (5 mg)	Toluene	ACN (3)	20	80	1.37%	A, B
16	3 (5 mg)	Toluene	ACN (3)	20	80	1.80%	A, B
17	3 (2.5 mg)	Toluene	ACN (3)	20	80	0.31%	None
18	3 (2.5 mg)	THF (250 μL)**	ACN (2.75)	20	80	0.33%	None
19	3 (2.5 mg)	Toluene	ACN (3)	20	80	0.66%	None
20	3 (2.5 mg)	Toluene	Dioxane (3)	30	80	2.70%	A, B
21	3 (2.5 mg)	Toluene	Dioxane (3)	30	80	0.79%	B
22	3 (2.5 mg)	Toluene	Dioxane (3)	30	80	0.56%	None
23	3 (2.5 mg)	Toluene	DMSO (2)	20	165	1.88%	A

* Added as a supersaturated solution in DMF. ** Added as a solution in THF. [†] Conversion factor - see text.

Addition of the lipid substrates presented certain challenges however. The main one being that it was not possible to dissolve them at room temperature in any potential polar aprotic reaction solvent, such as acetonitrile, DMF or DMSO. Usually substrates are dissolved in such solvents [182] and this solution is added directly to the dried reagents and heated for the reaction to take place. Marik *et al.* had a similar issue and overcame it by dissolving the ^{18}F fluorination reagents (^{18}F]KFK₂₂₂, (K(K222))₂CO₃ and K₂CO₃) in acetonitrile and transferring the solution to a *suspension* of the substrate in acetonitrile [37]. This however, was not possible in our setup. It was possible to prepare supersaturated solutions of **3** in DMF (table 2.2 – entry 6) and of **15** (table 2.3 – entry 4+7) in DMSO, both by slight heating. These solutions would be stable upon standing at room temperature, but adding them to the reactor and heating yielded no or extremely little product. This was puzzling, and it is speculated that the mesylates may have precipitated from the solutions as a result of the agitation caused by the passage of the syringes and tubes on their way to the reactor. In addition, it was attempted to dissolve and react substrates in chloroform, chloroform-acetonitrile (1:1) and tetrahydrofuran, but all attempts gave little or extremely little of the desired product (scheme 2.5).

For these reasons, after drying the reagents, the substrate was added as a solution in an apolar organic solvent. Initially, this was done in chloroform but the evaporation of this solvent proved too violent, which led to loss of activity (and probably also substrate) to the cooling trap. This was likely to be because of the relatively high volatility of the chloroform and for this reason, toluene was chosen instead. With toluene, it was possible to achieve a very well-controlled evaporation with almost no bubbling.

Generally, the assessment of the radiofluorinations was based upon calculation of a **conversion factor** (CF). This was measured by performing radio-TLC on the extracted reaction mixture at the end of the synthesis. The reaction vessel was then rinsed with chloroform upon which radio-TLC was also performed. The conversion factor was then calculated by finding the ratio of product to activity in the reaction and rinsing mixtures and multiplying it by the ratio of activity in the reaction mixture to the entire activity from the start of the synthesis. Thus, the CF is the un-isolated radiochemical yield with regards to all the activity in the vial arriving from the cyclotron rinse, even the activity that was not transferred to the machine and that which was not transferred to the reaction mixture. Generally the amount of product to unincorporated ^{18}F fluoride was higher in the chloroform rinse, although the total activity

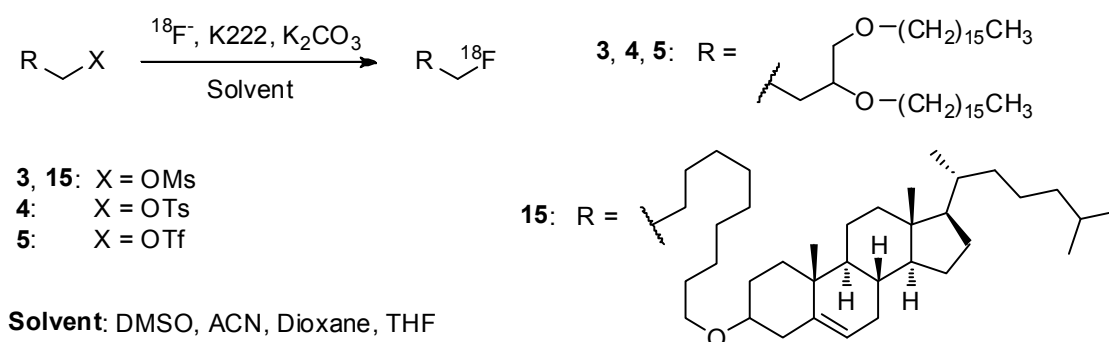
Textbox 2.1 – Example of a conversion factor (CF) calculation (table 2.3 – entry 9)

Total activity at start of synthesis: **1540 MBq**. Activity in DMSO (reac. mix.) extraction: **763.1 MBq** (5.85% **15**). Activity in the CHCl₃ rinses (7+2 mL): **161.5 MBq** (8.60% **15**).

$$\text{CF} = (763.1/1540) \cdot 5.85\% + (161.5/1540) \cdot 8.60\% = 2.9\% + 0.9\% = \mathbf{3.8\%}$$

was lower than in the reaction mixture. A substantial amount stayed behind in the reaction vessel – likely ^{18}F fluoride adhered to the glass walls (see **table 2.6**). An example of a CF calculation is given in **textbox 2.1**.

Scheme 2.5: ^{18}F -radiofluorination.



2.3.3 Choice of pseudohalide

Initially, the tosylate **4** of the di-hexadecyl-glyceride lipid was prepared and labeling was attempted. Formation of the desired fluoride was observed, but in negligible CFs. A further factor speaking against the tosylate **4** was that it is significantly less polar than the mesylate **3** and therefore runs further on silica. As the corresponding fluoride **1** is even less polar it runs further than the two pseudohalides. This would mean that on silica, it would be harder to separate **4** from **1** than **3** from **1**, where the chromatographic separation is greater. For those two reasons, it was decided to proceed with the mesylate **3**. As the mesylate was subsequently found to also give low CFs, the triflate **5** was prepared and tested (**table 2.2 – entry 7+8**). However, it did not give substantially better yields than the mesylate and furthermore was somewhat more difficult to purify and handle (due to the higher reactivity of the triflate). In addition, when using the triflate an impurity was formed that ran very similar to **1** on silica, meaning that purification would be problematic. It is speculated that this impurity may have been the elimination product. It was not seen when using the mesylate or the tosylate. For these reasons it was decided to continue with only the mesylate **3**.

2.3.4 Reaction conditions – Solvent, temperature and duration

Reaction conditions for the fluorinations were generally chosen based on standard literature procedures. Nucleophilic radiofluorination is usually conducted in either ACN [37, 291, 292] or DMSO [293-296]. Typical temperatures range from 80-100 °C for ACN (closed vessel) and 120-165 °C for DMSO. Reaction times may vary but are usually shorter than 30 minutes, in order to avoid substantial decay of the ^{18}F . ACN is usually desired for its ease of removal while DMSO is essential if higher temperatures/shorter reaction times are required. Other polar aprotic solvents that are commonly employed include DMF, THF, nitrobenzene, dichlorobenzene, dichloromethane or sulfolane [182]. The chemistry of radiofluorination is addressed in greater detail in **chapter 1, section 1.8**. For the di-hexadecyl ether glyceride probe it was found that DMSO gave the most reliable and highest CFs (see **table 2.2**), for which reason DMSO was eventually chosen as the solvent of choice. A high reaction temperature was found to give reliable, relatively high CFs, while reaction time was not varied substantially. The experiences regarding solvent (DMSO) and reaction temperature (165 °C) were applied to the cholesteryl ether.

2.3.5 Formation of impurities

During the investigation of the di-alkyl ether glyceride, impurities were seen to form during the radiofluorination. In general two different impurities were formed. On the TLC plates used for analysis, one impurity was slightly above the spot for **1**. This was termed *Impurity A*. The other impurity was termed *Impurity B* and was found below the spot for **1**. The three spots had the following retention factors in heptane:EtOAc (97-3): *Impurity A*: 0.83, **1**: 0.76, *Impurity B*: 0.46. In general the impurities formed in very small amounts and spotting relatively large amounts of the reaction mixtures was necessary to see them on TLC by KMnO_4 development. Impurities in the final radiolabel is perceived as a problem as they could potentially insert themselves into the lipid membrane and either alter the physicochemical properties of the membrane or change its interactions with the biological environment. These impurities will be commented on further in the following sections.

2.4 Automated synthesis of an ^{18}F -labeled cholesteryl ether lipid

The systems and ideas for drying the reactor and adding substrate mentioned in sections 2.3.1. and 2.3.2. were applied to the cholesteryl ether lipid as well. Selected labeling results are presented in **Table 2.3**. The standard way of adding the substrate **15** was as a solution in toluene. It was possible to prepare a solution in DMSO that was stable at RT but, as was observed with the preparation of **1**, addition of this solution did not result in any of the desired product (*entries 4+7*).

Reaction in ACN was tried in a few instances (*entry 11 shown, table 2.3*), but did not result in a significantly higher yield than the reaction in DMSO. A few experiments (*entries 1 and 12*) were carried out with 2 mL DMSO instead of 1. Although *entry 1* seemed to provide a higher yield than a similar reaction with 1 mL, this was not found to be a general trend and there was no statistical grounds on which to claim that this was actually the case. *Entry 12* was observed to give a similar yield to reactions with 1 mL DMSO. As no real difference was found, and because purification was perceived to be easier with less DMSO (see section 2.5), it was opted to use 1 mL.

Table 2.3 – Selected [¹⁸F]-labeling results – Labeling of the cholesteryl ether substrate (**15**). All values are decay-corrected. CFs in **bold** are SEP-PAK isolated radiochemical yields (RCY). CFs in **bold*** with asterisk are RCYs from the Supel Flash Cartridge. CFs in **bold and italics** (entries 19+20) denote both RCY of probe and final yield in liposomes. These were both high activity syntheses. † denotes entries 4+7 where supersaturated solution of **15** in DMSO were added. Both resulted in zero conversion.

Entry	Amount of 15 (mg)	Added in	Solvent (mL)	Time (min)	Temp. (°C)	CF/RCY	Impurities
1	2.7 mg	Toluene	DMSO (2)	20	165	4.04%	No obs.
2	2.5 mg	Toluene	DMSO (1)	20	165	3.12%	No obs.
3	2.5 mg	Toluene	DMSO (1)	20	165	1.59%	“A”
4	2.5 mg	DMSO (1 mL)†	DMSO (1)*	20	165	None	A
5	2.5 mg	Toluene	DMSO (1)	20	165	3.14%	A
6	2.5 mg	Toluene	DMSO (1)	20	165	1.33%	NA
7	5.0 mg	DMSO (1 mL)†	DMSO (1)*	20	165	None	A
8	2.5 mg	Toluene	DMSO (1)	10	165	4.4%	A
9	2.5 mg	Toluene	DMSO (1)	5	165	3.8%	A
10	2.5 mg	Toluene	DMSO (1)	10	165	1.68	A
11	2.5 mg	Toluene	ACN (2)	20	80	2.4%	A
12	2.5 mg	Toluene	DMSO (2)	10	165	1.8%	NA
13	2.5 mg	Toluene	DMSO (1)	10	165	0.74%*	NA
14	2.5 mg	Toluene	DMSO (1)	10	165	0.48%*	NA
15	2.5 mg	Toluene	DMSO (1)	10	165	0.20%*	NA
16	2.5 mg	Toluene	DMSO (1)	10	165	0.47%*	NA
17	2.5 mg	Toluene	DMSO (1)	10	165	1.86%	“A”
18	2.5 mg	Toluene	DMSO (1)	10	165	1.50%	“A”
19	2.5 mg	Toluene	DMSO (1)	10	165	2.75% (0.79%)	“A”
20	2.5 mg	Toluene	DMSO (1)	10	165	1.76% (0.28%)	“A”

Comments to entries: 7 – Presence of MsCE was found in the reaction mixture. 4 – Impurity even in absence of product. 3,17,18,19,20 – The removal of impurity A was abandoned. 8+9 – short reaction time seems to give higher conversion – and less impurity A. 11 – More impurity A than usually.

As time is a crucial factor with ^{18}F -labeling, due to the short half-life, shorter reaction times of 5 and 10 minutes were investigated. It was generally observed that shorter reaction times did not lower the conversion, but may even have raised it a bit (*entries 8+9*). Due to difficulty in sampling the reaction mixture and thereby monitoring the reaction, the exact optimal reaction time was not found. As 10 minutes was found to give the highest conversion (*entry 8*) this reaction time was chosen. That short reaction times gave similar or even higher CFs while unreacted substrate and ^{18}F fluoride was still present in the mixture at longer reaction times of 20 minutes may indicate that degradation of the product was competing with its formation – and indeed that the formation of product is very slow compared to general reaction times when radiofluorinating mesylates.

As was seen for the 1,2-dihexadecyl glyceride probe, an impurity slightly above the radio-TLC spot for the fluoride **6** was observed. This impurity was also designated as “**impurity A**” (see section 2.3.5). By TLC analysis it was found to be different to the one observed for the hexadecyl glyceride probe. However, as the TLC retention factor relationship between both labeled probes **1** and **6** and their corresponding impurity were very similar, they were thought to arise from a similar side reaction and both termed *impurity A*. As with the 1,2-dihexadecyl glyceride probe, the impurity arose regardless of reaction solvent, indicating that it does not originate from the apparatus, but is related to the substrate. This also ruled out DMSO-mediated Swern oxidation [297, 298]. The impurities generally arose in very low amounts and were only visible on TLC through repeatedly spotting the mixture in the same lane. For this reason, identification of the impurities was difficult (*see below*). As the impurity proved extremely difficult to remove chromatographically (section 2.5) it was eventually assessed that the very small amount in which it was present (<0.1 mg) was negligible and the idea of removing it was abandoned. No “*impurity B*” was observed for the cholesteryl ether probe.

Table 2.4 – ^{18}F -labeling results – with base-to-substrate ratios above 1. All values are decay-corrected. Substrate **15** was added in toluene. The reaction was run for 30 minutes at 120 °C in 2 mL DMSO. “Base” denotes $\mu\text{mol K}_2\text{CO}_3$

Entry	Type	Substrate (S)	Base (B)	SB ratio	K_{222}	CF
1	Low scale	5.1 mg (8.21 μmol)	7.24 μmol	1.1	13.3 μmol	3.64%
2	High scale	35 mg (56.4 μmol)	50.8 μmol	1.1	58.5 μmol	17.3%
3	Standard	2.5 mg (4.03 μmol)	50.8 μmol	0.08	58.5 μmol	3.1 – 4.4%
4	Marik et al. [37]	5.5 mg (7.61 μmol)	7.24 μmol	1.05	13.3 μmol	-
5	FDG	52.5 μmol	50.8 μmol	1.03	58.5 μmol	-

It has been reported that the ratio of the precursor to the base (K_2CO_3) are crucial to the degree of labeling in nucleophilic fluorination [37, 191, 299]. If the substrate-to-base (SB) ratio is too low, yields will be greatly reduced due to an elimination side-reaction. It is thought that this is a major factor contributing to the low CFs and RCYs reported here. Experiments were done with SB-ratios above one (Table 2.4). It was found, that it was possible to substantially increase

the conversion (17.3% was obtained, *entry 2*) by running the reaction with 35 mg of the cholesteryl ether mesylate **3** in an SB-ratio of 1.1 (*reaction solvent*: 2 mL DMSO). At these concentrations however, significant amounts (13 mg) of *impurity A* was formed, which was difficult to remove by chromatography (see **Section 2.5**). Therefore, it was opted to use a lower amount of the mesylate (2.5 mg), where the presence of *impurity A* was deemed negligible. From the large scale 1.1 SB-ratio experiment mentioned above, the cholesteryl ether *impurity A* was isolated (13 mg) and analyzed. The resulting ^1H -NMR spectrum was compared with that of the mesylate (**3**) and besides the disappearance of the mesyl methyl group, only the two protons next to the mesyl group were identified upfield (shift 4.25 \rightarrow 3.53). This suggests substitution or other modifications of the mesyl group. The mass was measured on MALDI-TOF (Na-spiked) and found to be 685.3, suggesting a possible mass of $685.3 - \text{Na}^+ = 662.3$. It has so far not been possible to deduce the identity of *impurity A* (see **Supplementary Information II**).

The presence of such impurities stresses the importance of a universal visualization/detection method. It was attempted to employ an SB-ratio >1 at lower substrate concentrations (see **table 2.4**, *entry 1*) but this did not increase the conversion in our system (solvent: 2 mL DMSO). Therefore, it can be concluded that not only SB-ratio, but also concentration plays a role in yield. In order to achieve high yields but low levels of impurities one would therefore need a concentrated reaction mixture containing a low total amount of precursor. This would mean that reaction in a small volume would be desirable. It can be speculated that a fully automated fluorination setup employing reaction vessels that allow concentrated reactions in small solvent volumes, such as microfluidic systems [300], could satisfy these standards.

2.5 Purification of the radiolabel

After reaction, the labeled probe was initially purified by leading the reaction mixture (DMSO) through two serially connected C18 SEP-PAKS, with the eluate being discarded (**figure 2.5**). This was done in order to capture the highly lipophilic cholesteryl ether probe [^{18}F]**6** on the columns. This was one of the reasons 1 mL DMSO reaction mixtures were preferred. It was feared that 2 mL was able to elute some of the probe causing desired radioactive product to be lost through the eluate. With 1 mL DMSO mixtures, it was repeatedly shown that the discarded eluant did not contain any [^{18}F]**16**. In fact, much activity was caught on the C18s, even polar activity that did not run on silica. This was generally thought to be free [^{18}F] F^- but could also have been polar active byproducts from the reaction. That this activity was retained could indicate that the C18 plus SEP-PAKS have highly polar sites where charged species in trace amounts can be retained. This step was followed by three washes of the entire system with water (3 + 4 + 5 mL). Each successive wash had an increase in volume in order to ensure an optimal washing procedure, where residues left from the previous wash would be caught by the subsequent one. The water washes were led through the C18 plus SEP PAKS and discarded along

with the initial DMSO reaction solvent. These washes were carried out in order to effectively remove DMSO from the system as it might have disturbed the chromatographic purification to follow and would be difficult to remove by evaporation during the subsequent liposome preparation. Even the three water washes did not remove all activity from the C18s, as they retained about 10% of the total activity (**table 2.6**).

Table 2.5 – Elution of activity caught on the Supel Flash Cartridges. All elutions were done with 15 mL of the stated eluant followed by 15 mL of air. The acetonitrile eluted 51.8% of the retained activity with 97% in the form of the labeled probe [^{18}F]**16**.

	Eluant	Activity	Percentage
Before rinses	-	16,11	100%
1. Rinse	Chloroform	0,192	1,19%
2. Rinse	Acetonitrile	8,35 (97% [^{18}F] 16)	51,8%
3. Rinse	Water	3,62	22,5%
After rinses	-	4,45	27,6%
Total			103%

After capture of the [^{18}F]-labeled probe on the C18s, the entire system was washed thrice with heptane (6 + 6 + 7 mL). The heptane was first led into the reactor, dissolving and carrying with it any labeled probe left behind. Notice that the first heptane wash volume (6 mL) is higher than the volume of the last water wash (5 mL), in order to extract all the lipid material that might have been displaced upwards by the water. These heptane washes were then led through either three serially connected Silica PLUS SEP-PAKs or a Supel Flash Cartridge (SFC) (**figure 2.7**). As **2** dissolves easily in heptane but does not run on silica, this method was chosen to apply the labeled probe to the silica column, thus preparing it for chromatographic purification. Initially, three serially connected Silica Plus Sep-PAK were used, but separation of the labeled probe from *impurity A* was not satisfactory. This was speculated to may have been because of the free solvent volume between each SEP-PAK (**figure 2.5**). For this reason, the SFCs were tried, as this represented a continuous silica column. Separation was indeed improved on the SFC cartridge but a different problem occurred in that most of the activity did not elute from the cartridge, but instead appeared stuck on it. It was possible to elute the lost labeled probe by leading polar solvents such as ACN through the cartridge (**table 2.5**). This could again indicate that the stationary phase of the cartridge is not entirely uniform and contains trace amounts of sites to which radioactive compounds can associate strongly. **Table 2.3 entries 13-16** show the decreased yields when using the SFC.

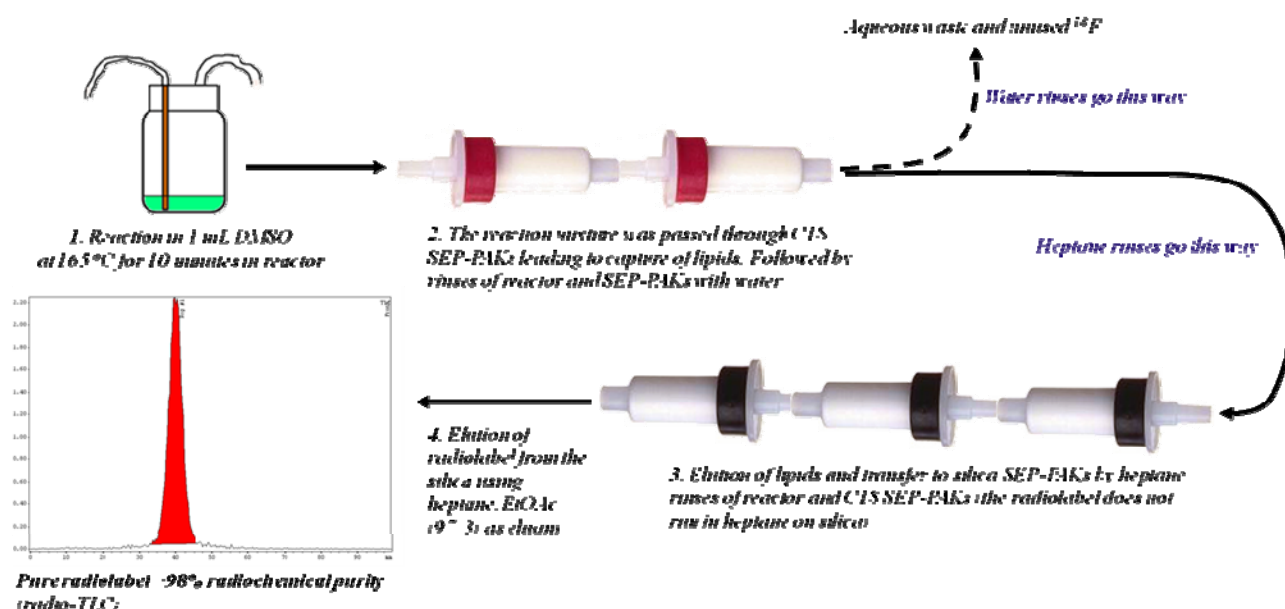


Figure 2.5 – Schematic representation of chromatographic purification of the radiolabel. Silica SEP-PAKs (not FLUKA cartridge) is shown.

^{18}F 6 was then eluted from the silica by either heptane-toluene (1:1, $R_f = 0.31$) or heptane-EtOAc (97:3, $R_f = 0.24$). Heptane-EtOAc (97:3) was used in the final preparations as ^{18}F 6 was eluted in a smaller volume of about 4 mL eluant, which was more easily evaporated in the following liposome preparation. Generally, removal of impurity A proved difficult and eventually the idea of preparing liposomes without this impurity was abandoned. It was attempted to quantify (by weighing) how much of the impurity was present in each preparation but as so little was formed it proved impossible (< 0.1 mg). For this reason it was assessed that the presence of the impurity was negligible. The total amount of lipid used to prepare the liposomes was about 13 mg (see section 2.6), meaning that the impurity would make up less than 1%. As the impurity appeared to be derived from the substrate it was of a lipidic nature and could be hypothesized to insert itself into the membrane in the same manner as regular cholesterol. The very small amount present was thought not to disturb the integrity of the membrane. Another aspect of the presence of impurities is whether they would augment complement activation [301]. That such small amounts of impurities could for example increase charge density seems unlikely.

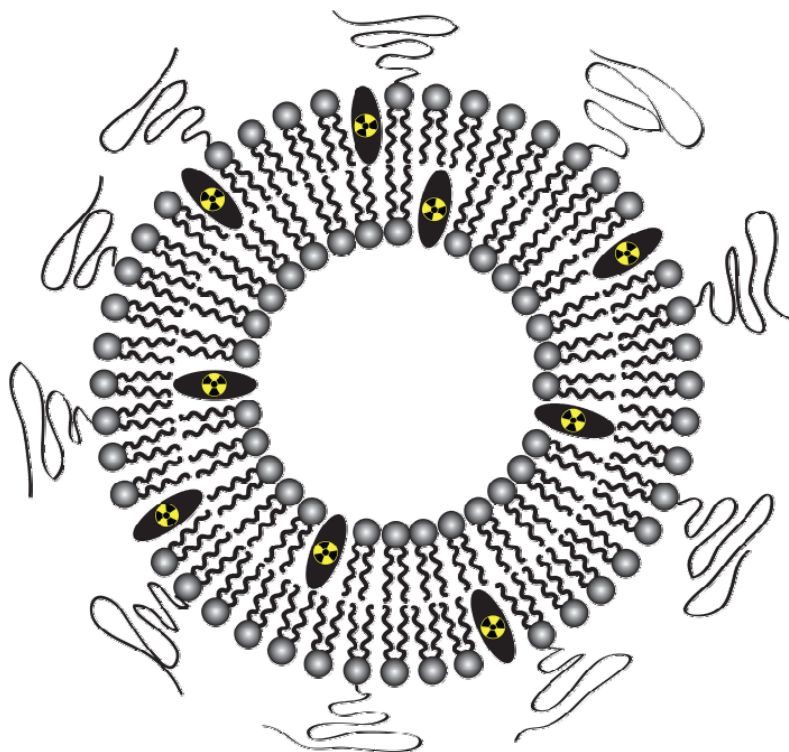


Figure 2.6 – Cartoon of ^{18}F -labeled liposome (*membrane not drawn to scale*).

2.6 Preparation of radioliposomes

The purified radiolabel emerged from the synthesis robot as a solution in 4 mL eluant which was transferred to a 10 mL pear-shaped flask. This flask was fitted with a septum through which a needle was fitted to function as an air inlet. Through the septum was also fitted a needle through which vacuum was applied and the flask was placed in a 115 °C oil bath. The combination of the vacuum, the air stream coming in through the air inlet and the heating bath evaporated the 4 mL solvent in less than 5 minutes. To the flask was then added 0.5 mL of a lipid solution in CHCl_3 . The lipid mixture was

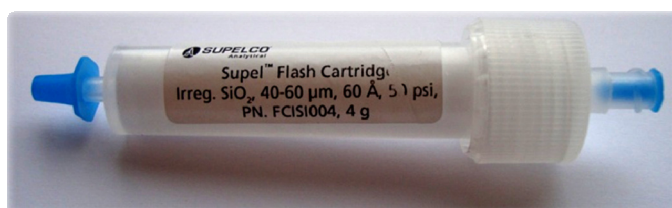


Figure 2.7 – Supel Flash Cartridge, 4 g silica (SFC)

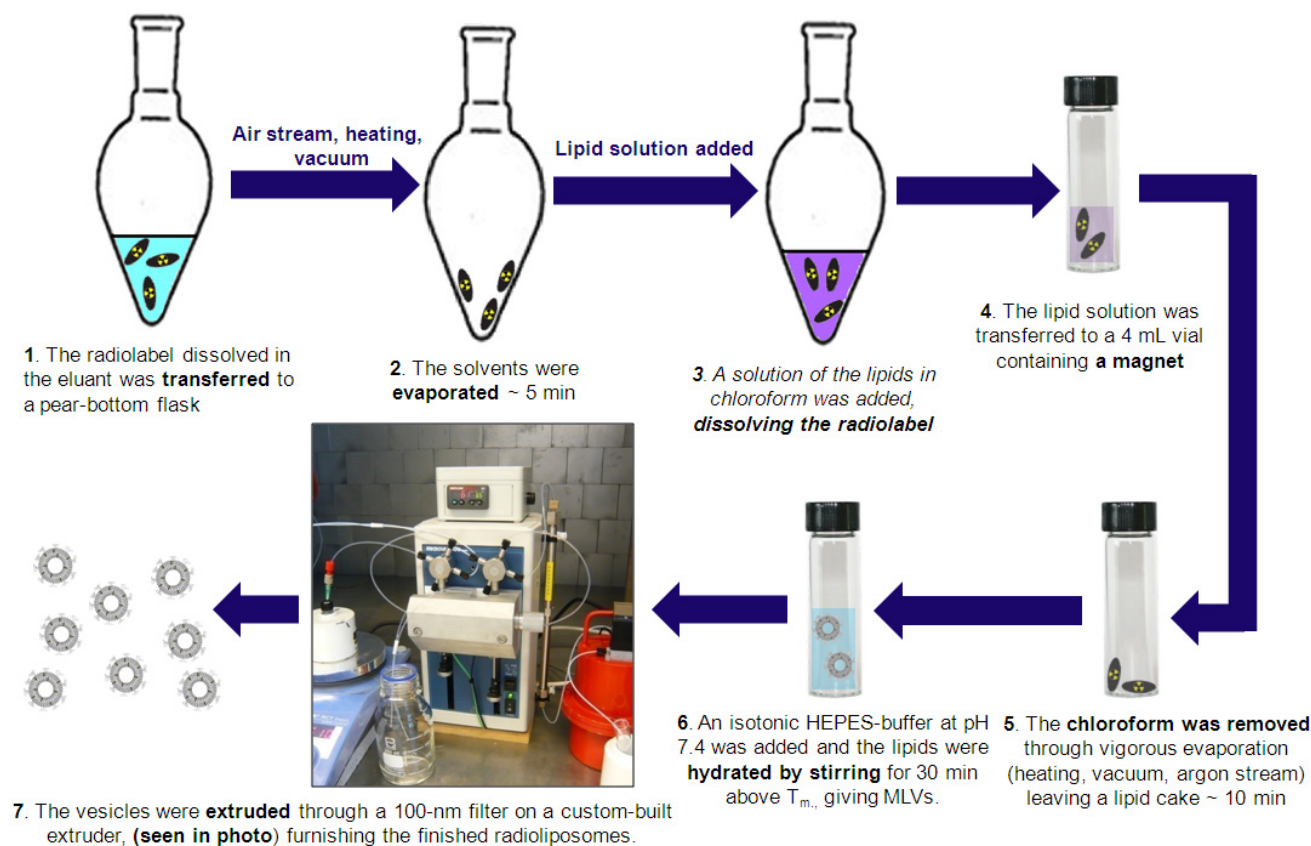


Figure 2.8 – Schematic overview of radioliposome preparation.

of a nature and molar ratios mimicking those of DOXIL [302] – DPPC 7.5 mg (9.5 mmol) DSPC, 3.0 mg cholesterol (7.8 mmol), 2.7 mg DSPE-PEG₂₀₀₀ (1 mmol); in molar ratios of 0.52;0.43;0.05. The CHCl_3 was then transferred by syringe to a 4 mL vial containing a magnet. This vial was placed in a custom-made lead block that was heated to 70 °C. Through a septum had been fitted vacuum and an argon stream. This setup was able to remove the CHCl_3 in about 3-3½ minutes. The argon flow had the double function of both evaporating the CHCl_3 faster and preventing it from boiling. This step was repeated, in that the pear-shaped flask was washed once more with 0.5 mL CHCl_3 and this was transferred to the 4 mL vial and evaporated. Through this procedure, more than 95% of the activity was transferred to the vial and a nice lipid cake was formed. In order to thoroughly remove traces of CHCl_3 this main evaporation cycle was followed by a period of high vacuum and elevated temperature. This was achieved by removing the argon inlet so that only the vacuum inlet was inserted through the septum. Vacuum was achieved by a membrane pump and the vial temperature was started at 70 °C but allowed to drop to 60 °C (the temperature for hydration) during the process. This was done for 5 minutes. In order to hydrate the lipid film and prepare multi-lamellar vesicles (MLVs) 0.7 mL isotonic (NaCl 140 mM) hepes buffer (hepes 10 mM) at pH 7.4 was added. This would give a final lipid concentration of about 26 mM. The mixture was then stirred at high

speed at a temperature of 60 °C for 30 minutes. Although it is not a standard method of preparation (the usual method being manual vortexing), in our hands it appeared to work nicely. The stirring temperature of 60 °C was chosen as it represents a temperature of 18 °C above the phase transition temperature (T_m) of DPPC. Although cholesterol abrogates the distinct phase transition temperature of the lipid [303], it is standard methodology to agitate at elevated temperature to properly disperse the lipids. The stirring time of 30 minutes was chosen by visual inspection of the vial. When lipid films were stirred in buffer at 60 °C it was observed that after 10 minutes, the suspension was very turbid, milky and foamy. After 20 minutes, the appearance was similar, although less foamy. After 30 minutes, the mixture had not changed further and did not change upon continued stirring. It is understood that longer stirring could potentially give smaller MLVs and thus ease the following extrusion, but since time is a crucial factor in ^{18}F -labeling a stirring time that was as short as possible was desired.

After stirring, the mixture was extruded on a custom-built extrusion device (this device was also used in **Chapter 3, section 3.3.1.** for gel permeation chromatography, **figure 2.8**). Of the 0.7 mL MLV suspension, 0.5 mL was extracted for extrusion. A filter size of 100 nm was used to achieve liposomes in this size range. Although repeated extrusion through a single-size filter is occasionally used for SUV/LUV preparation [210], it is common to extrude through progressively smaller filter sizes [304]. This relieves some of the force necessary for extrusion of fairly large MLVs through small filter pores and prevents the filter membrane from rupturing. Especially for higher lipid concentrations (above around 50 mM) it is often necessary to change filters in this way. However, due to the high radioactivity employed in the liposome preparations presented here, such filters changes were impossible. For this reason the above-mentioned relatively low lipid concentration of 26 mM was used and the filter membranes were never observed to rupture. The suspension was passed through the filter 31 times which gave liposomes of around 121 nm (number weighted, PDI: 0.072). In general however, it was observed that some parts of the extrusion device were not sealed tightly enough, which led to leakage of lipid suspension as a results of the large pressure build-ups during extrusion. This was a major drawback with regards to just being able to use one filter size and resulted in considerable loss of activity.

The final preparation of ^{18}F -labeled liposomes yielded 0.5 mL suspension with an activity of 156.1 MBq. In order to assess the radiochemical purity (RCP) of the product the remaining 0.2 mL that was not extruded was mixed with tetrahydrofuran to give a clear solution. This solution was analyzed by radio-TLC to show an excellent RCP of > 98% (see **Figure 2.5**).

2.7 Timeline of radioliposome preparation and locations of activity

Here is presented the entire process of the radioliposome preparation (**table 2.6**) in chronological order with location of the radioactivity (decay-corrected) along with the time of each step started.

Table 2.6 – Chronological procedure and approximate remaining activity after each step. Values shown are typical and indicative. (n between 3 and 7). Time values are for a 10 minute reaction. All percentages are decay-corrected.

Step	Location of activity	Time after start	Location of activity	Comments
1	<i>In cyclotron vial</i>	0	100%	<i>About 10% stayed in the cyclotron vial</i>
2	<i>On QMA column</i>	0-3 min	90%	
3	<i>In reaction vessel total</i>	3-35 min	85-90%	
	<i>Adhered to glass</i>		18 ± 7%	
	<i>In DMSO reac. mixture</i>		50 ± 5%	
	<i>In CHCl_3 rinse (pooled)</i>		9.5 ± 1%	
4	<i>As labeled probe (CF)</i>	-	4.1 ± 0.3%	
5	<i>Application to C18s</i>	35-37 min		
	<i>Water rinses (pooled)</i>		48 ± 7.6%	<i>With water/heptane rinses, glass adherence was lower, at 8.5%</i>
	<i>Heptane rinses (pooled)</i>		0.5 ± 0.7%	
	<i>Adhered to glass</i>		8.5 ± 1.4%	
	<i>Chromatography</i>	37-60 min		
	<i>C18 SEP-PAKs</i>		9.3 ± 1.5%	
	<i>Silica SEP-PAKs</i>		6.9 ± 2.7%	
6	<i>RCY as purified probe (SEP-PAKs)</i>	60 min	2.12 ± 0.5%	<i>Significant loss was observed during extrusion</i>
9	<i>As hydrated MLVs</i>	110 min	2.0 ± 0.8%	
10	<i>After extrusion – finished radioliposomes</i>	130 min	0.53 ± 0.4%	

2.8 In-vivo investigations

For *in-vivo* studies in mice, an ^{18}F activity of 10 MBq per mouse is generally required. This is usually administered in 0.2 mL, but if the radioactivity concentration is higher than 50 MBq/mL, smaller volumes are given. With a half-life as short as for ^{18}F (110 min), this can also mean that different volumes are injected, depending on when the active product is administered to a given mouse. In general, it can be argued that with radioliposomes, both for diagnostic and therapeutic purposes, the specific activity (activity/lipids) should be as high as possible, meaning that the administered amount of lipid matter is as low as possible. Liposomes do not suffer from CMC (*critical micelle concentration*) related problems of dilution

to nearly the same extend as do for example polymeric micelles, so very low concentrations are possible. Such low concentrations can help to prevent classic liposome-related side effects, such as pseudoallergic shock [301].

In the *in-vivo* studies carried out with these liposomes four mice were used. These were of the NMRI (Naval Medical Research Institute) type, which is used for general purpose applications. Seven tumors were implanted, with one mouse carrying only one tumor. These were of the type human lung carcinoid (NCI-H727, 2 tumors), small cell lung cancer (NCI-H69, 3 tumors) and glioblastoma (U87MG, 2 tumors).

2.8.1 In-vivo investigation results

In-vivo studies were performed in tumor-bearing mice over the course of eight hours, with scans performed at 0 hours, 2 hours and 8 hours. In **table 2.7** is seen the sizes of the tumors on the day of the *in-vivo* studies.

Table 2.7 – Tumor sizes (all data in mm, with volumes in mm^3)

Mouse	Right tumor					Left tumor				
	length	width	mean	radius	volume	length	width	mean	radius	volume
1	6	6	6	3	113	6	6	6	3	113
2	9	9	9	4.5	382	-	-	-	-	-
3	6	6	6	3	113	8	8	8	4	268
4	9	9	9	4.5	382	13	10	11.5	5.75	796

The biodistribution of the ^{18}F -liposomes was determined by encircling so-called *regions-of-interest* (ROIs) on the scan images and quantifying the presence of radioactivity. These data, in organs relevant to liposome pharmacokinetics as described in **Chapter 1 – section 1.4**, are seen in **table 2.8** and depicted graphically in **figure 2.9** and **figure 3.0**.

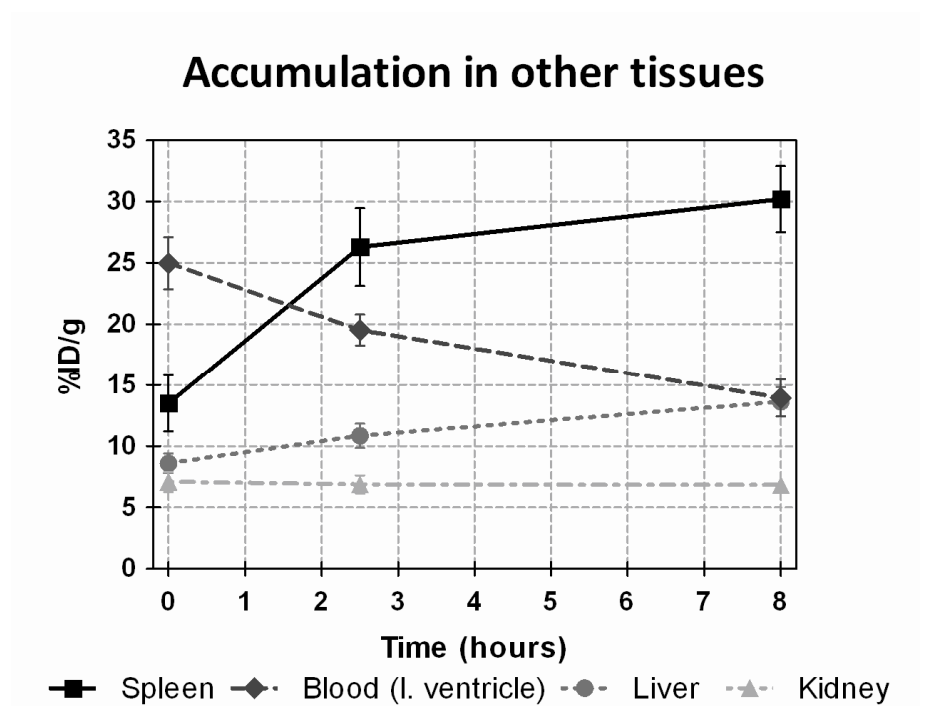


Figure 2.9. *Accumulation in other relevant tissues.* Average percent injected dose per gram for all mice, plotted for spleen, blood, liver and kidney (values are decay corrected).

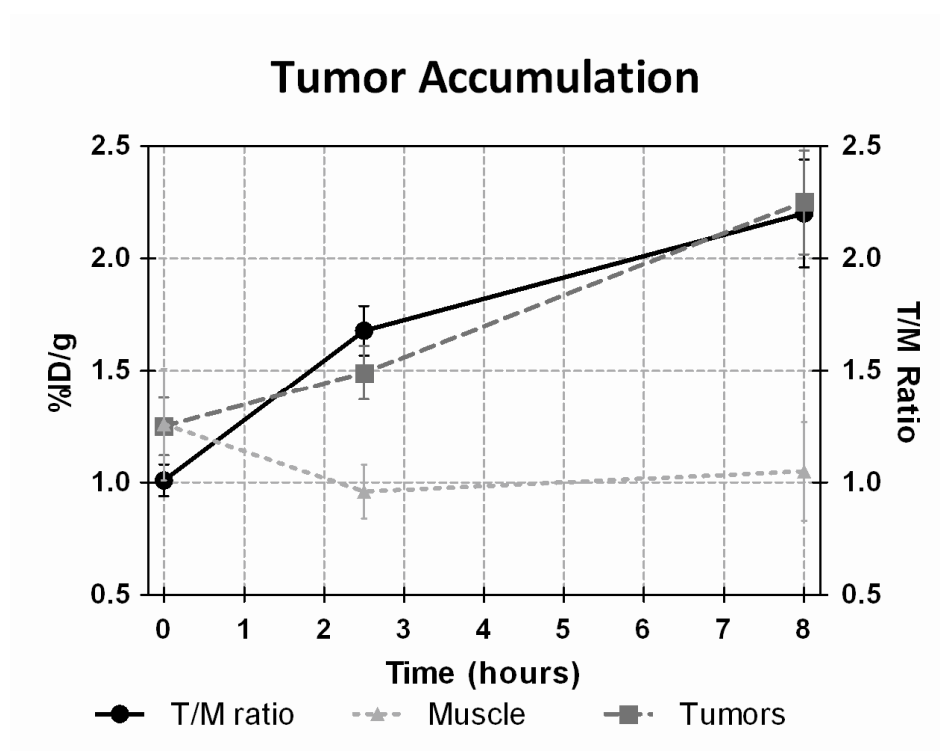


Figure 2.10. *Tumor accumulation.* Percent injected dose per gram is shown as averages for muscle and tumors (left and right) in all mice. The average T/M ratio for the tumors is plotted on the right y-axis (values are decay corrected).

Relative accumulation in organs of interest is often given as ratios, with tumor accumulation given as the *tumor-to-muscle* (T/M) ratio. This ratio is important when it comes to the feasibility of a given radiopharmaceutical as a diagnostic agent, where the T/M-ratio implies the contrast of the imaging. T/M-ratio as a function of time is plotted in **figure 2.10**.

Table 2.8 – Biodistribution based on PET

	0 h		2.5 h		8 h	
	%ID (n=4)	%ID/g (n=4)	%ID (n=4)	%ID/g (n=4)	%ID (n=4)	%ID/g (n=4)
blood	0.39 ± 0.04	24.97 ± 2.15	0.37 ± 0.01	19.51 ± 1.28	0.19 ± 0.03	13.94 ± 1.50
liver	10.01 ± 0.68	8.60 ± 0.79	13.52 ± 0.96	10.84 ± 1.00	15.62 ± 1.20	13.63 ± 1.18
spleen	0.80 ± 0.06	13.50 ± 2.31	3.11 ± 0.27	26.29 ± 3.19	3.53 ± 0.43	30.19 ± 2.70
kidney	1.93 ± 0.29	7.06 ± 0.81	1.84 ± 0.10	6.87 ± 0.73	1.83 ± 0.21	6.82 ± 0.48
tumors	0.31 ± 0.09	1.25 ± 0.13	0.34 ± 0.80	1.49 ± 0.12	0.49 ± 0.11	2.25 ± 0.23
muscle	0.04 ± 0.01	1.26 ± 0.25	0.06 ± 0.01	0.96 ± 0.14	0.07 ± 0.02	1.05 ± 0.22

In **figure 2.11** and **figure 2.12** are shown images from the PET scans. In **figure 2.12** the PET image is fused with a CT images, and tumor accumulation is clearly seen.

2.8.2 Discussion of in-vivo results

In the muscle tissue the activity stayed on a relatively stable and low level, although a slight drop was seen, which is in agreement with the decreased availability of the tracer due to clearance from the blood. In the tumors, *percent injected dose per gram* (%ID/g) increased from 1.25 ± 0.13 (0 h) to 2.25 ± 0.23 (8 h) over the course of the measurement. This indicates that liposomes are accumulating in the tumor and that it is quantifiable within an eight hour time frame. The accumulation is reflected in the *tumor-to-muscle* ratio (T/M-ratio, **figure 2.10**) indicating that, despite the moderate accumulation in the tumors over the 8 hour time frame, the signal-to-noise ratio is good with a T/M-ratio above 2 after eight hours. These results show that tumor accumulation can indeed be shown in the course of the 8-hour study that is possible with ^{18}F -labeled liposomes.

In the spleen, accumulation of liposomes is relatively fast with no significant difference in tracer uptake for the 2.5 h and 8 h scans. It is known that liposomes larger than 200 nm are caught in the red pulp tissue of the spleen [154]. Therefore, some of what is observed might be a relatively rapid removal of the larger liposomes. Furthermore, as was described in **Chapter 1 – section 1.4**, a significant fraction of liposomes is known to be taken up by hepatic and splenic macrophages during the first hour after injection [122]. This effect is also likely to contribute to the initial increase of activity in the spleen. In absolute terms this accounts for $3.53 \pm 0.43\%$ of the entire injected activity (ID%) at 8 hours (**table 2.8**).

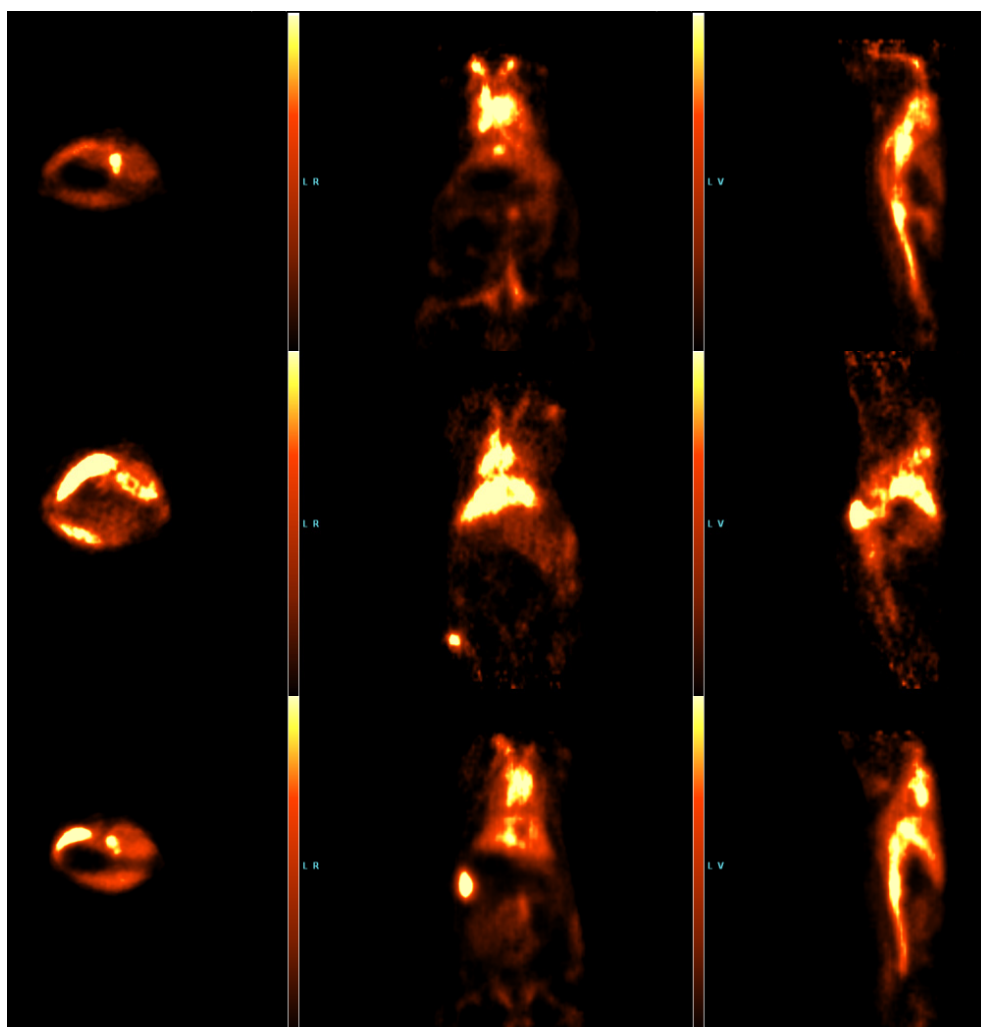


Figure 2.11. Representative PET images showing the ^{18}F CE biodistribution at 0h (top panel), 2.5h (middle panel) and 8h (lower panel) post-injection of ^{18}F CE in the NCI-H727 bearing mouse. The accumulation in the spleen is evident from the axial view (left column), the heart and liver accumulation is evident from the coronal view (middle column) whereas the accumulation in heart, liver and vena cava is evident from the sagittal view (right column).

Accumulation in the liver is also seen, however at a steadier pace. Petersen *et al.* concluded that hepatic accumulation reaches its zenith 4 hour after administration and thereafter reaches a plateau [210]. Seo et al. also found a relatively stable concentration of activity in the liver throughout the 48 h scan period [38]. Hepatic accumulation at 8 hours accounts for 13.6 ± 1.2 %ID/g. The activity in the blood dropped, as could be expected from the hepatic and splenic elimination from the bloodstream. The activity in the kidney stayed at a stable and relatively low level with no increase in

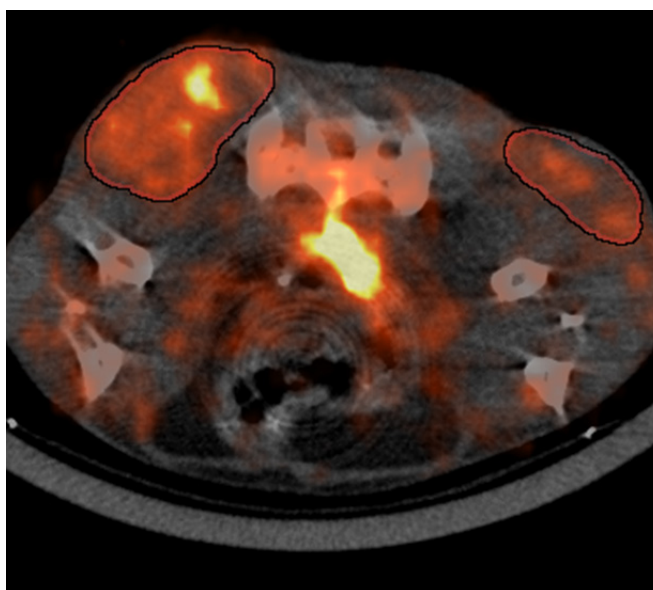


Figure 2.12 - *In vivo* visualization of the ^{18}F FCE accumulation in xenografted tumors by co-registered microPET/CT. Tumors (NCI-H727) are marked by rings on the image of the tumor-bearing nude mouse (axial view). The PET/CT image is acquired 8h post injection of ^{18}F FCE

accumulation over time indicating that renal excretion is limited, as could also be expected with liposome-based tracers. Measuring activity in the kidney however, can often be misleading as the activity is transferred from the kidney to the bladder, where accumulation can be seen. From here, it is excreted through the urine. In our scans, we did not observe any activity in the bladder. Overall, the pharmacokinetic tendencies observed here correspond fairly well with what is generally known about long-circulating, PEGylated liposomes [38, 41, 305, 306].

2.9 General discussion and concluding remarks

While ^{64}Cu -labeled liposomes provide excellent pharmacokinetic data for long-term *in-vivo* monitoring [259], ^{18}F offers some conceivable advantages. The short half-life of ^{18}F makes only studies up to 8 hours feasible, but as we have shown here, this is enough to show tumor accumulation. With current liposome technology, tumor accumulation typically peaks between 24-48 hours [123, 307]. In the future however, with for example improved targeting, it is conceivable that accumulation may be faster, warranting the use of shorter lived radioisotopes, where patient radiation dose will be smaller. Furthermore, targeting methodology other than systemic targeting of tumors may have faster pharmacokinetics. This includes the deliberate targeting of RES components [308]. In addition, the cholesteryl ether lipid probe (2) can be used with other lipidic nanosystems, such as polymeric micelles [309] or solid lipid nanospheres [310]. As a general

consideration, the short half-life of ^{18}F and the higher abundance of positron decays, as compared to ^{64}Cu , results in a lower radiation dose to the patient. However, if only an 8-eight hour scan is required, the initial activity needed for ^{64}Cu is considerably lower than for ^{18}F . Thus, the question of tissue dose becomes relatively complicated. As a non-metal, ^{18}F can be covalently linked to membrane lipids, providing a very stable linkage in a non-water soluble probe. In the event of breakdown of the liposomes, for example by uptake and lysis in cells, this prevents the marker from entering the blood stream and potentially accumulate in secondary locations or otherwise exhibit behavior different to that of liposomes. It has been shown that with co-encapsulation of different radioactive hydrophilic species ($^{99\text{m}}\text{Tc}$ -HMPAO and ^{111}In -DF), that they exhibited significantly different pharmacokinetic after around 24 hours after administration [276]. This suggests that liposomes are degraded over time, allowing water-soluble contents to escape. This should be an important consideration whenever markers for the aqueous core of liposomes are employed. A further potential concern, one that is rarely addressed, is whether blood stream complement membrane attack complexes are capable of causing partial liposome lysis and allowing water soluble contents to escape and exhibit independent pharmacokinetics [311]. ^{64}Cu suffers from substantial liver uptake due to copper metabolism in the liver, if the copper is released from the liposomes [39, 312, 313]. Complexed copper such as ^{64}Cu -DOTA does not show this however [210]. It is also important to keep in mind, that ^{18}F is readily available to nuclear medicine facilities worldwide, while the access to e.g. ^{64}Cu is much more limited and therefore only available near highly specialized facilities. The possible transport range for ^{64}Cu is much larger though, and a single facility would in theory be able to supply an area the size of Europe with ^{64}Cu -tracers. This would increase transportation costs considerably, however. Generally, the cost of ^{64}Cu -labeled tracers is higher than ^{18}F -labeled tracers and this may limit their clinical implementation.

Labeling of liposomes during preparation has its drawbacks. The main one being that liposomes and radioisotope must be prepared at the same facility. Furthermore, the liposomes are prepared during exposure to potentially large doses of radiation. This problem becomes more pressing in potential studies in larger animals or humans where more activity is needed. We addressed this issue by employing (1) formation of a lipid film by evaporation from heated vials under vacuum and argon/air streams, (2) hydration of the lipid film by magnetic stirring and (3) fully automated extrusion. By inserting the labeled probe into a preformed liposome a major advantage would be that commercially available formulations could be readily labeled. This would require however, that the labeling could be performed at a lower, ideally ambient, temperature [314], in order not to cause leakage from the liposomes or to damage labile biomolecules, and that the labeling was stable *in-vivo*.

The feasibility of using cholesteryl ethers derives from the ether bond being non-hydrolyzable, the probe being non-metabolizable and the high lipophilicity preventing the probe from leaving the liposome. The main disadvantages of using the probe presented here is first of all the fact that it is not commercially available, making it necessary to synthesize it. The second being the relatively low yield obtained. As already discussed however, this is not thought to derive from the nature of the probe.

To summarize, in the sections above were described a method with which to prepare ^{18}F -labeled liposomes, with the nucleophilic radiofluorination and the extrusion of the liposomes carried out by fully automated means.

2.10 Fluorination of lipids in non-polar solvents by $[^{18}\text{F}]\text{HF}$ transfer to phosphazene bases

In the work described in the above, the yields of the radiofluorination were very low. Part of this was speculated to be because of low solubility of the highly lipidic substrates in the polar solvents that are traditionally used in radiofluorination. In addition, as was mentioned in **Chapter 1 – section 1.8**, it is generally thought that absence of water is beneficial in some radiofluorination reactions. For these reasons, we devised a system which would transfer dry $[^{18}\text{F}]\text{HF}$ to a solution of a phosphazene base, which would conduct the fluorination. The work described in this section was carried

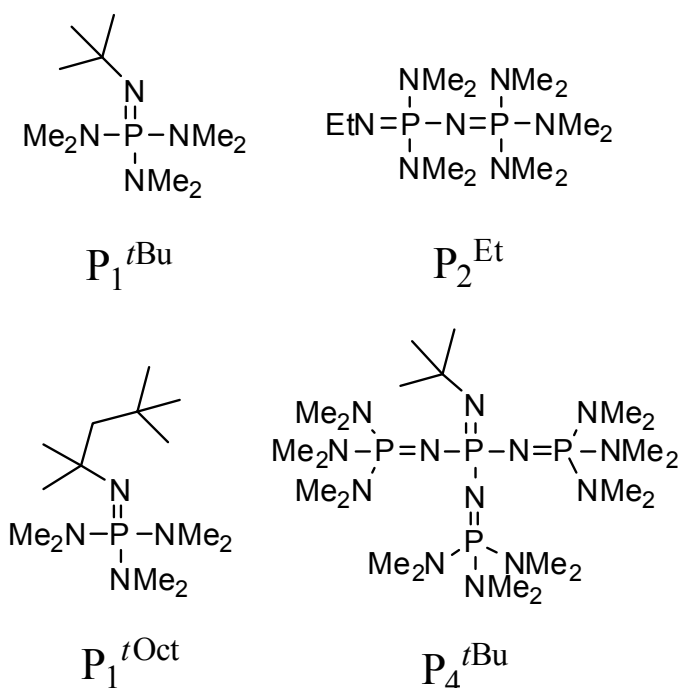


Figure 2.13 – Schwesinger's phosphazene bases used in this study

out in corporation with Dr. Fedor Zhuravlev and Bente Mathiesen, with Bente Mathiesen conducting the bulk of the fluorination experiments. It is described in Chemistry – A European Journal (*see paper 2 of this thesis*).

$[^{18}\text{F}]\text{HF}$ gas was generated by dissolving the $^{18}\text{F}^-$ in concentrated (98%) sulphuric acid. The pKa of hydrofluoric acid being 3.17, this protonates the $[^{18}\text{F}]\text{fluoride}$ and generates $[^{18}\text{F}]\text{HF}$ (g). The gas was caused to leave the mixture by heating it to 80 °C for 30 minutes, under irradiation in an ultrasound bath at 35 kHz. The $[^{18}\text{F}]\text{HF}$ was carried off by a stream of dry argon gas that was bubbled through the reaction mixture, which was kept in a receiving vessel. The $[^{18}\text{F}]\text{HF}$ transfer yield was 16–82%.

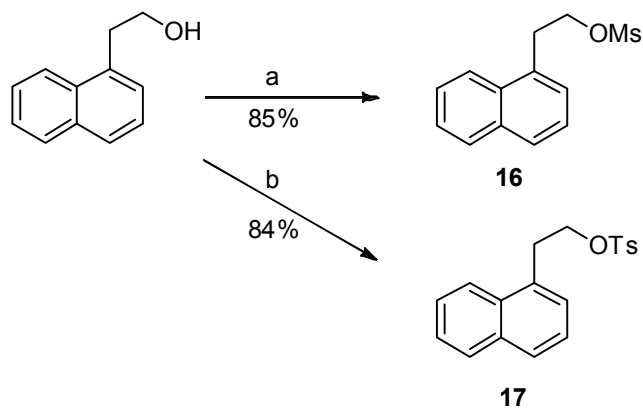
In the receiving vessel (made from glassy carbon) was contained a solution of one of Schwesinger's phosphazene bases [315] (**fig. 2.13**). These are strong, non-nucleophilic organic bases where protonation takes place at a double bonded nitrogen atom. We proposed that such compounds would diminish the dissociation of HF from the base that can occur with weaker bases, thus keeping more on the BH^+F^- form, giving a more reactive $[^{18}\text{F}]\text{fluoride}$. In addition, we believed

that their bulk and nonpolar domains would increase solubility and induce a cation-anion mismatch that could increase the nucleophilicity of the [^{18}F]fluoride. A few reaction solvents and mixtures were used, but for the lipophilic substrates that are relevant to this work, toluene proved practical and well-suited. As it turned out, P_2^{Et} and P_4^{tBu} furnished superior fluorination results, so these were chosen for the subsequent experiments.

In order to test the system, lipophilic pseudohalides were synthesized and tested. From the work already described, compound **3** (scheme 2.1, page 36) was tested and in addition, **16** and **17** (Scheme 2.6) were


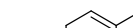
synthesized. Radiofluorination of these substrates gave the results shown in **Table 2.9**. A general procedure for the full [^{18}F]HF transfer and radiofluorination can be found in the **Supplementary Information VIII**. Radiochemical yields (RCY) at the chosen conditions were generally good to excellent, confirming that we had developed a functional system that

Scheme 2.6: Pseudohalogenation of 1-naphtaleneethanol



Reagents and condition: (a) MsCl, pyridine, DCM, 0°C => RT, 3h, (b) TsCl, pyridine, DCM, 13h.

Table 2.9 – Radiofluorination of lipophilic substrates with phosphazene bases and [^{18}F]HF.

Substrate	Phosphazene base	Solvent	RCY (%)	Product
3 (10 mg)	P ₄ ^{tBu} (10 μL)	Toluene (2 mL)	71 ± 6	$\begin{array}{c} \text{H}_3\text{C}(\text{H}_2\text{C})_{15}\text{O} \\ \text{H}_3\text{C}(\text{H}_2\text{C})_{15}\text{O} \end{array} \text{---} \text{CH}_2\text{CH}_2\text{---}^{18}\text{F}$
16 (1.1 mg)	P ₂ ^{Et} (1 μL)	Toluene (1 mL)	91 ± 4	
17 (10 mg)	P ₂ ^{Et} (10 μL)	Toluene (2 mL)	82 ± 6	

Conditions: 120 °C for 30 minutes. Radiochemical yields were determined by Radio-TLC (n = 3) after purification by passing the reaction mixture through a silica SEP-PAK.

significantly outperformed the traditional [^{18}F]KFK222 system when labeling highly lipophilic substrates such as **3** (compare the yields obtained in **table 2.4, page 48**).

2.11 Experimental section

All reagents and solvents were purchased from Sigma-Aldrich (DK). Solvents were purchased in purum quality or better and were not further purified. Solvents for anhydrous syntheses were dried over molecular sieves (3Å, Sigma Aldrich) to water concentrations of <100 ppm (DMF) and <50 ppm (all others). Glassware was oven-dried overnight or heatgun-dried under a stream of dry argon prior to use. Reactions were conducted in an argon atmosphere. Chromatography was done using Merck silica purchased from VWR (DK); flash chromatography in Silica gel 60, 0.040-0.063, TLC on Silica gel 60 F₂₅₄. All visualization was done by UV light as well as KMnO₄-staining w. heating. SEP-PAKs (C18 Plus, Silica Plus and QMA Light) were purchased from Waters (USA). Chromacol 6 mL flat-bottom fluorination vials and ^{18}O -enriched water were purchased from Rotem Industries Ltd. (Israel).

NMR-analyses were recorded in CDCl₃ on a Bruker Ultrashield 500 MHz or a Bruker/Spectrospin 250 MHz. The residual solvent peak (CHCl₃) was used as reference peak in both ^1H - and ^{13}C -NMR spectra. Mass spectrometry was done on either an **1**) Agilent 6410 Triple Quadrupole Electrospray Mass Spectrometer coupled to an Agilent 1200 HPLC system (ESI/HPLC-MS) using a linear gradient of water/acetonitrile/TFA (A: 95/5/0.1 and B: 5/95/0.086) with a flow rate of 1 mL/min. **2**) Bruker Esquire 4000 iontrap (IT) equipped with an electrospray ionization (ESI) interface. **3**) Bruker Daltonics REFLEX IV MALDI-TOF mass spectrometer.

^{18}F -fluoride anion was produced on a GE PETtrace Cyclotron. Radio-TLC was performed on a Raytest MiniGita Star.

The radio-synthesis, including purification, and the extrusion were performed on two separate fully automated, LabView-operated systems, custom-built in our group.

2.9.1 Synthesis

1,2-O-hexadecyl-3-fluoro-rac-glycerol (1)

Compound **2** (25 mg, 45 μmol) was dissolved in CH₂Cl₂ (3 mL). After cooling to – 78 °C, DAST (17 μL, 129 μmol) was added. The flask was stirred cold for 2 hours and then allowed to attain RT over the course of 2 hours. The reaction was quenched by the addition of 5% aq. Na₂CO₃ (4 mL). The CH₂Cl₂ layer was separated and the water phase was extracted with CH₂Cl₂ (3x3 mL). The organic phases were pooled and the solvent was removed *in vacuo*. Purification by flash chromatography in heptane-toluene (7:3) yielded **15 mg (60%)** of **1** as a white solid and **3 mg (12%)** of **9** as a white solid. *Analysis of 1*: ^1H NMR (250 MHz, CDCl₃) δ 4.65 – 4.32 (m, 2H), 3.72 – 3.42 (m, 7H), 1.65 – 1.47 (m, 4H), 1.26 (br s, 52H), 0.88 (t, J = 6.6 Hz, 6H). m/z (MALDI-TOF, DHB-matrix - Na⁺-spiked, LP25%, 200 shots); Found: 565.57 (M+Na⁺), calculated: 542.54 + 22.99 =

565.53. Analysis of **9**: ¹H NMR (250 MHz, CDCl₃) δ 4.72 (dt, *J* = 48.4, 4.8 Hz, 1H), 3.63 (dd, *J* = 22.6, 4.7 Hz, 4H), 3.47 (t, *J* = 6.7 Hz, 4H), 1.65 – 1.48 (m, 4H), 1.25 (br s, 52H), 0.87 (t, *J* = 6.6 Hz, 6H).

1,2-O-hexadecyl-rac-glycerol (2)

Compound **8** (3.39 g, 5.38 mmol), was dissolved in CH₂Cl₂ (15 mL) and Pd/C (10%, 210 mg) was added. An H₂ atmosphere of 1 atm was established and the mixture was stirred at RT. After 2 weeks the reaction was terminated, even though it had not gone to completion (*see text, section 2.2.1*). The mixture was filtered and the solvent removed *in vacuo*. Purification by flash chromatography in toluene-EtOAc (95:5) yielded **2.253 g (77%)** of **2** as a white solid. Compared with original sample for authenticity. ¹H NMR (500 MHz, CDCl₃) δ 3.75 – 3.69 (m, 1H), 3.65 – 3.58 (m, 2H), 3.56 – 3.40 (m, 6H), 2.17 (br s, 1H), 1.61 – 1.51 (m, 8H), 1.36 – 1.20 (m, 48H), 0.88 (t, *J* = 7.0 Hz, 6H).

1,2-di-O-hexadecyl-3-O-mesyl-rac-glycerol (3)

Compound **2** (103 mg, 0.190 mmol) was dissolved in CH₂Cl₂ (9 mL) and pyridine (6 mL). MsCl (59 μL) was added and the mixture was allowed to react for 4 hours at RT. The mixture was transferred to a separating funnel containing CH₂Cl₂ (40 mL) and brine (30 mL). The organic phase was separated and washed with brine (2x40 mL). The combined aqueous phases were extracted once with CH₂Cl₂. The combined organic phases were rotary evaporated and the crude product was purified by flash chromatography in toluene-EtOAc (49:1), yielding **100 mg (85%)** of **3** as a white solid. *R_f* = 0.34 (toluene:EtOAc – 49:1). ¹H-NMR (500 MHz, CDCl₃): δ 4.38 (dd, *J* = 10.3, 3.6; 1H), 4.25 (dd, *J* = 10.9, 5.8; 1H), 3.67 (m, 1H), 3.57 (t, *J* = 6.6; 2H), 3.48 (m, 4H), 3.04 (s, 3H), 1.56 (m, 4H), 1.36-1.20 (m, 52H), 0.89 (t, *J* = 6.9; 6H). ¹³C-NMR (125 MHz, CDCl₃): δ 76.4, 71.9, 70.8, 69.7, 69.1, 37.4, 31.9-26.0 (*aliphatic*, 31.9 (2C), 29.9 (2C), 29.68 (2C), 29.67 (2C), 29.65 (2C), 29.64 (2C), 29.61 (2C), 29.59 (2C), 29.5 (2C), 29.4 (2C), 29.3 (2C), 26.1 (2C), 26.0 (2C)), 22.7 (2C), 14.1 (2C). *m/z* (MALDI-TOF, DHB-matrix - Na⁺-spiked, LP25%, 200 shots); Found: 641.38 (M+Na⁺), calculated: 618.53 + 22.99 = 641.92.

1,2-di-O-hexadecyl-3-O-tosyl-rac-glycerol (4)

Compound **2** (28 mg, 52 μmol) was dissolved in CH₂Cl₂-pyridine (2:3, 5 mL). TsCl (115 mg, 603 μmol) was added and the mixture was stirred overnight (18 h). The solvents were removed *in vacuo* and the residue was partitioned between heptane (20 mL) and methanol-water (9:1, 20 mL). The heptane phase was washed twice with methanol-water (9:1, 2x20 mL). The polar phase was extracted once with heptane (10 mL). The organic phases were pooled and the solvents removed *in vacuo*. The residue was recrystallized from methanol giving **33 mg (92%)** of **4** as a white solid. *R_f* = 0.45 (heptane:EtOAc – 4:1). ¹H NMR (250 MHz, CDCl₃) δ 7.80 (d, *J* = 8.3 Hz, 2H), 7.33 (d, *J* = 8.0 Hz, 2H), 4.15 (dd, *J* = 10.3, 4.2 Hz, 1H), 4.02 (dd, *J* = 10.3, 5.8 Hz, 1H), 3.66 – 3.53 (m, 1H), 3.50 – 3.30 (m, 6H), 2.44 (s, 3H), 1.53 – 1.39 (m, 4H), 1.25 (br s, 52H), 0.88 (t, *J* = 6.6 Hz, 6H).

1,2-di-O-hexadecyl-3-O-trifluorosulphonyl-rac-glycerol (5)

Compound **2** (63 mg, 0.12 mmol) was dissolved in CH_2Cl_2 (5 mL) and pyridine (50 μL , 0.618 mmol). The mixture was placed in a water bath (RT) and 1M triflic anhydride in CH_2Cl_2 (140 μL , 0.140 mmol) was added slowly. After stirring for 1 hour, the mixture was reduced *in vacuo* to about 0.5 mL and partitioned between heptane (20 mL) and methanol (20 mL). The heptane phase was washed twice with methanol (2x10 mL) and evaporated to dryness *in vacuo* giving **40 mg (51%)** of **5** as a white solid. $R_f = 0.49$ (heptane:EtOAc – 9:1). ^1H NMR (250 MHz, CDCl_3) δ 4.64 (dd, $J = 10.5, 3.4$ Hz, 1H), 4.52 (dd, $J = 10.5, 5.9$ Hz, 1H), 3.76 – 3.63 (m, 1H), 3.59 – 3.50 (m, 3H), 3.48 – 3.39 (m, 3H), 1.62 – 1.48 (m, 4H), 1.25 (br s, 52H), 0.88 (t, $J = 6.6$ Hz, 6H).

3-O-benzyl-rac-glycerol (7)

Sodium hydride (0.70 g, 29 mmol) was placed in a flask under an argon atmosphere. DMF (30 mL) was added and the mixture was cooled to 0 °C. Isopropylidene glycerol (**6**, 2.82 mL, 22.7 mmol) was added and the mixture was stirred for 10 minutes. Benzyl bromide (3.24 mL, 27.2 mmol) was added and the mixture was allowed to attain RT and stirred overnight. The reaction was quenched with water (1 mL) and the solvents were removed *in vacuo*. The resulting viscous, turbid liquid was dissolved in methanol (*not anhydrous*, 30 mL). 7 heaped spoonfuls AmberLite IR120 H+ resin was added and the mixture was stirred overnight at RT. The resin was removed by filtration and the solvent was removed *in vacuo*, leaving a red oil. The product was purified by flash chromatography in a gradient of CH_2Cl_2 -EtOAc (1:1) \rightarrow EtOAc (neat), leaving **3.26 g (79%)** of **7** as a viscous, turbid oil. $R_f = 0.28$ (EtOAc). ^1H NMR (250 MHz, CDCl_3) δ 7.32 – 7.18 (m, 5H), 4.46 (s, 2H), 3.86 – 3.75 (m, 1H), 3.69 – 3.13 (m, 6H). ^{13}C NMR (63 MHz, CDCl_3) δ 137.84, 128.53 (2C), 127.91, 127.86 (2C), 73.59, 71.74, 70.91, 64.06.

1,2-O-hexadecyl-3-O-benzyl-rac-glycerol (8)

Sodium hydride (1.08 g, 45 mmol), was added to an RB flask. DMF (30 mL) was added and the mixture was cooled to -78 °C. Compound **7** (3.26 g, 17.9 mmol) was added as a solution in DMF (30 mL) under heavy evolution of gas (H_2). The flask was allowed to attain RT under stirring. The hydrogen gas was removed by flushing with argon. Hexadecylbromide (13.11 mL, 42.9 mmol) was added and the mixture was heated to 140 °C. After 6.5 hours the precursor **7** was observed by TLC to have been consumed. Water (5 mL) was added to quench the reaction. The solvents were removed *in vacuo*. The residue was dissolved in CHCl_3 , filtered and the solvent was removed *in vacuo*. Flash chromatography was carried out by subsequent elutions in heptane (neat) \rightarrow toluene (neat) \rightarrow heptane-EtOAc (8:2). This gave **8** as a waxy semisolid. Pure fractions, pooled: **3.39 g (30%)**, slightly impure fractions, pooled: **2.47 g (22%)**. $R_f = 0.24$ (toluene). ^1H -NMR (250 MHz, CDCl_3) 7.40-7.26 (m, 5H), 4.56 (s, 2H), 3.62-3.40 (m, 9H), 1.62-1.50 (m, 8H), 1.45-1.15 (br.s, 48H), 0.88 (t, $J = 6.4, 6\text{H}$). ^{13}C -NMR (62.5 MHz, CDCl_3) 138.67, 128.46 (2C), 127.73 (2C), 127.64, 78.14, 73.54, 71.84, 70.96, 70.79, 70.55, 32.09 (2C), *aliphatic* (30.29, 29.86, 29.81, 29.67), 29.52, 22.84, 14.25. m/z (MALDI-TOF, DHBmatrix- K^+ -spiked, LP15%, 200 shots); Found: 669.64 ($\text{M}+\text{K}^+$), calculated: 630.60 + 38.96 = 669.56.

10-O-TBDMS-1-decanol (11)

1,10-decanediol (2.02 g, 11.6 mmol) was dissolved in DMF (35 mL). TBDMSCl (1.17 g, 3.90 mmol) was dissolved in DMF (10 mL) and added dropwise. Imidazole (530 mg, 7.78 mmol) was added in DMF (10 mL). The reaction was stirred for 20 hours at RT. The mixture was partitioned between toluene (120 mL) and water (100 mL). The organic phase was washed with water (2x50 mL) and the solvent was removed *in vacuo*. Purification by column chromatography in heptane:EtOAc (80:20) gave **847 mg (76%)** of **11** as a clear colorless oil. $R_f = 0.31$ (Heptane:EtOAc – 80:20). $^1\text{H-NMR}$ (500 MHz, CDCl_3): δ 3.65 (br.t., $J = 5,8$ Hz, 2H), 3.60 (t, $J = 6.8$ Hz, 2H), 1.55 (m, 4H), 1.38-1.30 (m, 13H), 0.91 (s, 9H), 0.06 (s, 6H). $^{13}\text{C-NMR}$ (62.5 MHz, CDCl_3) 63.3, 63.1, 32.9, 32.9, 29.6, 29.6, 29.4, 26.0, 25.9, 25.8, 18.4, -5.3. ESI- MS^+ (m/z) 1 : Found: 289.20 ($\text{M}+\text{H}^+$), calculated: $288.3 + 1.0 = 289.3$.

1-O-Ms-10-O-TBDMS-decane-diol (12)

Compound **11** (759 mg, 2.76 mmol) was dissolved in CH_2Cl_2 (30 mL). Pyridine was added (2.2 mL, 27.3 mmol). The flask was placed in an ice bath and MsCl (650 μL , 8.40 mmol) was added. The reaction was stirred for 5 h at RT. The mixture was partitioned between water (100 mL) and toluene (100 mL). The organic phase was washed with water (2x50 mL) and the solvent was removed *in vacuo*. Purification by column chromatography in toluene:EtOAc (95:5) gave **876 mg (90%)** of **12** as a clear, colorless oil. $R_f = 0.42$ (toluene:EtOAc – 95:5). $^1\text{H-NMR}$ (250 MHz, CDCl_3): δ 4.22 (triplet, $J = 6.6$ Hz, 2H), 3.60 (t, $J = 6.5$ Hz, 2H), 3.00 (s, 3H), 1.74 (m, 2H), 1.5 (m, 2H), 1.43-1.29 (m, 12H), 0.90 (s, 9H), 0.05 (s, 6H). $^{13}\text{C-NMR}$ (62.5 MHz, CDCl_3) 70.0, 63.2, 37.4, 32.8, 29.4, 29.27, 29.25, 29.1, 18.4, 25.9, 25.7, 25.4, 28.2, -5.4. ESI- MS^+ (m/z) 1 : Found: 367.20 ($\text{M}+\text{H}^+$), calculated: $366.23 + 1.00 = 367.23$.

10-cholesteryloxy-1-O-TBDMS-decanol (13)

Cholesterol (505 mg, 1.31 mmol) was dissolved in toluene (10 mL) and NaH 60% in mineral oil (78 mg, 1.95 mmol) was added. The mixture was heated to 80 $^\circ\text{C}$ and after 1 hour compound **12** (450 mg, 1.23 mmol) was added as a solution in toluene (1 mL). DMF (3 mL) was added. The mixture was stirred for 16 h at 80 $^\circ\text{C}$. The reaction mixture was filtered, mixed with toluene (50 mL) and the organic phase was washed with brine (3x50 mL). The combined aqueous phases were extracted once with heptane (20 mL). The combined organic phases were dried over Na_2SO_4 , filtered and the solvents were removed *in vacuo*. The crude product was purified by column chromatography in a gradient of heptane:toluene: 9:1 (50 mL) followed by 1:1 (140 mL) and finally toluene (50 mL). The fractions containing only **13** were rotary evaporated yielding **444 mg (55%)** of **13** as a clear, very viscous semi-solid. $R_f = 0.5$ (heptane:toluene – 1:1). $^1\text{H-NMR}$ (500 MHz, CDCl_3): δ 5.36 (m, 1H), 3.61 (t, $J = 6.6$ Hz, 2H), 3.46 (m, 2H), 3.14 (m, 1H), 2.38 (m, 1H), 2.21 (m, 1H), 2.01 (m, 2H), 1.87 (m, 3H), 1.62-1.43 (m, 11H), 1.40-1.24 (m, 16H), 1.20-0.97 (m, 12H), 0.95-0.88 (m, 19H), 0.70 (s, 3H), 0.07 (s, 6H). $^{13}\text{C-NMR}$ (125 MHz, CDCl_3): δ 141.2, 121.4, 79.0, 68.2, 63.3, 56.8, 56.2, 50.3, 42.4, 39.8, 39.5, 39.3, 37.3, 36.9, 36.2, 35.8, 32.9, 32.0, 31.9,

30.2, 29.57, 29.55, 29.49, 29.42, 28.5, 28.2, 28.0, 26.2, 26.0, 25.8, 24.3, 23.8, 22.8, 22.6, 21.1, 19.4, 18.7, 18.4, 11.9, -5.3. m/z (MALDI-TOF, DHB-matrix - Na^+ -spiked, LP30%, 200 shots); Found: 679.3 ($\text{M}+\text{Na}^+$), calculated: $656.59 + 22.99 = 679.58$.

10-cholesteryloxy-1-decanol (14)

13 (722 mg, 1.10 mmol) was dissolved in THF (25 mL). TBAF trihydrate (720 mg, 2.28 mmol) was added and the mixture was stirred at RT for 6 hours. The mixture was concentrated under reduced pressure and partitioned between hexane (100 mL) and water (80 mL). The hexane phase was washed with water (2x60 mL) and the solvent was removed *in vacuo*. Purification by column chromatography in heptane:EtOAc (82:18) gave **582 mg (98%)** of **14** as a white solid. The product was dissolved in boiling hexane and recrystallized at 0 °C with no change in yield. $R_f = 0.23$ (heptane:EtOAc 85:15). ^1H -NMR (250 MHz, CDCl_3): δ 5.35 (m, 1H), 3.65 (doublet of triplets, $J = 6.1$ Hz (t), 5.2 Hz (d); 2H), 3.45 (t, $J = 6.8$ Hz 2H), 3.13 (m, 1H), 2.36 (m, 1H), 2.20 (m, 1H), 2.06-1.77 (m, 5H), 1.58-0.86 (m, 49H), 0.69 (s, 3H). ^{13}C -NMR (125 MHz, CDCl_3): δ 141.2, 121.4, 79.0, 68.2, 63.1, 56.8, 56.2, 50.3, 42.4, 39.8, 39.5, 39.3, 37.3, 36.9, 36.2, 35.8, 32.8, 32.0, 31.9, 30.2, 29.52, 29.50, 29.47, 29.4, 28.5, 28.2, 28.0, 26.2, 25.7, 24.3, 23.8, 22.8, 22.6, 21.1, 19.4, 18.7, 11.9. ESI- MS^+ (m/z)²: Found: 565.6 ($\text{M}+\text{Na}^+$), calculated: $542.9 + 22.99 = 565.9$.

10-cholesteryloxy-1-O-Ms-decanol (15). **14** (199 mg, 0.366 mmol) was dissolved in CH_2Cl_2 (15 mL) and pyridine (1.00 mL, 12.4 mmol). MsCl (100 μL , 1.29 mmol) was added and the mixture was stirred for 5 hours at RT. The mixture was concentrated under reduced pressure and partitioned between toluene (50 mL) and water (50 mL). The organic phase was washed with water (2x50 mL) and the combined aqueous phases were extracted once with hexane (30 mL). The combined organic phases were dried over Na_2SO_4 , filtered and the solvents were removed *in vacuo*. Purification by column chromatography in toluene:EtOAc (98:2) gave **221 mg (97%)** of **15** as a white solid. $R_f = 0.40$ (toluene:EtOAc – 95:5) ^1H -NMR (500 MHz, CDCl_3): δ 5.36 (m, 1H), 4.24 (t, $J = 6.6$ Hz, 2H), 3.46 (m, 2H), 3.14 (m, 1H), 3.02 (s, 3H), 2.37 (m, 1H), 2.20 (m, 1H), 2.05-1.96 (m, 2H), 1.93-1.81 (m, 3H), 1.76 (m, 2H), 1.62-1.24 (m, 28H), 1.20-0.88 (m, 22H). ^{13}C -NMR (125 MHz, CDCl_3) 141.2, 121.4, 79.0, 70.2, 68.1, 56.8, 56.2, 50.2, 42.3, 39.8, 39.5, 39.2, 37.4, 37.3, 36.9, 36.2, 35.8, 32.0, 31.9, 30.2, 29.4, 29.3, 29.1, 29.0, 28.5, 28.2, 28.0, 26.2, 25.4, 24.2, 23.8, 22.8, 22.6, 21.1, 19.4, 18.7, 11.9. ESI- MS^+ (m/z)²: Found: 643.5 ($\text{M}+\text{Na}^+$), calculated: $620.48 + 22.99 = 643.47$.

10-cholesteryloxy-1-O-Ms-decanol (15) - Alternative direct synthesis

1,10-decanediol (1.00 g, 5.74 mmol) was dissolved in CH_2Cl_2 (50 mL) and pyridine (27 mL, 335 mmol). MsCl (2.00 mL, 25.8 mmol) was added and the mixture was stirred for 2.5 hours at RT. The solvents were removed *in vacuo* and the resulting solids were redissolved in toluene:EtOAc (1:1). Solids that did not dissolve were discarded. The mixture was passed through 20 g silica and the solvents were removed *in vacuo* giving 1.706 g (105%) of the crude dimesylate. In a different flask, NaH 60% (206 mg, 5.15 mmol) was suspended in THF (5 mL) and placed in an ice-bath. Cholesterol (1.79 g, 4.63 mmol) was added as a solution in THF (10 mL). The mixture was heated to 60 °C for 30 minutes allowing sodium

cholesterolate to form. The crude dimesylate was dissolved in DMF (45 mL) and the cholesterolate was added by cannulation. The mixture was allowed to react at 65 °C for 6.5 hours. As this was insufficient time, it was allowed to stir at RT for 3 days, leading to completion. The mixture was partitioned between water (100 mL) and hexane (100 mL). The polar phase was washed with hexane (2x100 mL). The organic phases were combined and the solvents were removed *in vacuo*. Purified by column chromatography in a gradient of neat toluene followed by toluene:EtOAc (98:2). The fractions containing only **5** were rotary evaporated yielding **371 mg (13%)** of **5** as a white solid. *See above for characterization.*

10-cholesteryloxy-1-fluoro-decane (6). **4** (29 mg, 53.4 µmol) was dissolved in CH₂Cl₂ (2 mL) in a -78 °C bath. DAST (40 µL, 410 µmol) was added and the mixture was allowed to attain RT. After two hours, 0.5 M K₂CO₃ (2 mL) was added and the mixture was partitioned between heptane (15 mL) and brine (15 mL). The organic phase was washed with brine (2x10 mL), dried over Na₂SO₄ and the solvents were removed *in vacuo*. Purification by flash chromatography in heptane:toluene (1:1) gave **18 mg (62%)** of **6** as a white solid. *R_f* = 0.31 (heptane:toluene – 1:1) ¹H-NMR (500 MHz, CDCl₃): δ 5.36 (m, 1H) 4.44 (doublet of triplets, *J* = 50 Hz (d), 6.3 Hz (t); 2H), 3.45 (m, 2H), 3.13 (m, 1H), 2.36 (m, 1H), 2.20 (m, 1H), 2.00 (m, 2H), 1.86 (m, 3H), 1.69 (m, 2H), 1.62-0.82 (m, 47H), 0.69 (s, 3H). ¹³C-NMR (125 MHz, CDCl₃) 141.2, 121.4, 83.59 (d, *J* = 162 Hz, 1C), 79.0, 68.1, 56.8, 56.2, 50.2, 42.3, 39.8, 39.5, 39.2, 37.3, 36.9, 36.2, 35.8, 32.0, 31.9, 30.4 (d, *J* = 19.1 Hz, 1C), 30.2, 29.46 (d, *J* = 4.5 Hz), 29.45, 29.2, 28.5, 28.2, 28.0, 26.2, 25.2, 24.3, 23.8, 22.8, 22.6, 21.1, 19.4, 18.7, 11.9. *m/z* (MALDI-TOF, DHB-matrix - Na⁺-spiked, LP28%, 200 shots); Found: 567.5 (M+Na⁺), calculated: 544.50 + 22.99 = 567.49.

1-O-Ms-2-(naphthalen-1-yl)ethanol (16). 1-naphthaleneethanol (888 mg, 5.23 mmol) was dissolved in anhydrous CH₂Cl₂ (40 mL) and anhydrous pyridine (6 mL) under an argon atmosphere and cooled to 0 °C on an ice-bath. MsCl (1.0 mL, 2.5 eq) was added and the mixture was allowed to react at RT for 3 hours. The mixture was reduced by rotary evaporation and partitioned between 100 mL water and 100 mL hexane. The organic phase was separated and washed with 2 x 100 mL water. The organic phase was reduced and the crude product was purified by flash chromatography in toluene:EtOAc (95:5), *R_f* = 0.26, yielding **1.092 g (85%)** of the title compound as a white solid. **1H-NMR** (500 MHz, CDCl₃): δ 8.03 (dd, *J* = 8.7, 0.8; 1H), 7.89 (m, 1H), 7.80 (m, 1H), 7.55 (m, 2H), 7.43 (m, 2H), 4.56 (t, *J* = 7.3; 2H), 3.56 (t, *J* = 7.3; 2H), 2.81 (s, 3H). **13C-NMR** (125 MHz, CDCl₃): δ 133.89, 132.07, 131.76, 128.99, 127.97, 127.46, 126.51, 125.84, 125.49, 123.09, 69.54, 37.37, 32.81.

1-O-Ts-2-(naphthalen-1-yl)ethanol (17). 1-naphthaleneethanol (535 mg, 5.23 mmol) was dissolved in anhydrous CH₂Cl₂ (30 mL) and anhydrous pyridine (5 mL) under an argon atmosphere. TsCl (3118 mg, 5.3 eq) was added and the mixture was allowed to react at RT for 13 hours (overnight). The mixture was reduced by rotary evaporation and partitioned between 100 mL water and 100 mL hexane. The organic phase was separated and washed with 2 x 100 mL water. The organic

phase was reduced and the crude product was purified by flash chromatography in toluene, R_f = 0.28, yielding **892 mg (84%)** of the title compound as a white solid. **¹H-NMR** (250 MHz, CDCl₃): δ 7.84 (m, 2H), 7.75 (d, *J* = 8.1; 1H), 7.62 (m, 2H), 7.48 (m, 2H), 7.32 (m, 2H), 7.18 (m, 2H), 4.35 (t, *J* = 7.3; 2H), 3.44 (t, *J* = 7.3; 2H), 2.39 (s, 3H). **¹³C-NMR** (62.5 MHz, CDCl₃): δ 144.43, 133.95, 133.17, 132.07, 131.76, 129.61, 128.85, 127.75, 127.70, 127.36, 126.25, 125.64, 125.43, 123.04, 69.81, 32.59, 21.47.

2.9.2 Radiofluorination

[¹⁸F]fluoride was captured from ¹⁸O-enriched water on a QMA light Sep-Pak SPE cartridge preconditioned with K₂CO₃. The activity was eluted with 50% acetonitrile in water (0.6 mL) containing K₂CO₃ (7.0 mg, 50.8 μmol) and Kryptofix 222 (22.0 mg, 58.5 μmol). The eluate was transferred to a 6 mL Chromacol vial and the solvent was evaporated in 7 minutes through a series of increases in temperature under vacuum (≈ 60 mBar) and a helium stream (100 mL/min followed by 200 mL/min). Residual water was removed by azeotropic evaporation with acetonitrile (3x0.3 mL). **3**, **4**, **5** or **15** (2.5 – 35 mg) was added in toluene, chloroform, DMF, THF or DMSO (0.5-1 mL) and either **1**) the solvent was evaporated and dry DMSO (1-2 mL), dioxane (3 mL) or acetonitrile (2-3 mL) was added as reaction solvent or **2**) the reaction was conducted in that solution. The mixture was allowed to react for 5-20 minutes at 80-165 °C. After reaction, the mixture was either **1**) extracted for CF determination, followed by a double wash of the reactor with chloroform or **2**) passed through two C18 Sep-Pak Plus cartridges, previously treated with acetonitrile (15 mL) and water (15 mL) with the intent of chromatographic purification. If chromatographic purification was carried out, the following applies. The reactor was washed three times with water (3, 4 and 5 mL). This water was lead through the C18 Sep-Pak cartridges. The reactor was then washed three times with heptane (2x6 mL plus 1x7 mL). This was passed through the C18s and subsequently through three Silica Sep-Pak Plus cartridges, previously treated with heptane (20 mL), applying the lipid product to the Silica Sep-Pak cartridges. The product was eluted in heptane-toluene (1-1) or heptane:EtOAc (97:3) giving **1** or **2** in RCPs of >95% and RCYs of <2.75%. Identified against a cold reference compounds (**1** or **6**) by radio-TLC and KMnO₄-staining.

2.9.3 Preparation of radioliposomes

The eluent (4 mL) containing **7** was transferred to a 10 mL pear-shaped flask and the solvent was removed in 5 minutes at 115 °C under a slight vacuum and a stream of air. Lipids (7.5 mg DSPC, 3.0 mg cholesterol, 2.7 mg DSPE-PEG2000; in molar ratios of 0.52;0.43;0.05) were added in chloroform (0.5 mL) to dissolve **7**. The resulting chloroform solution was transferred to a 4 mL vial containing a magnet and the solvent was removed in 5 minutes at 70 °C under a stream of argon. To transfer remaining lipids and activity, the 10 mL flask was rinsed with chloroform (0.5 mL), which was also

transferred to the 4 mL vial and evaporated for 5 minutes under the same conditions. In order to remove residual chloroform, the vial was subjected to high vacuum and an argon stream for a further 5 minutes at 70 °C. To the resulting lipid cake was added 0.7 mL isotonic HEPES buffer at pH 7.4 (150 mM NaCl, 10 mM HEPES) and the lipids were hydrated by magnetic stirring at 1200 rpm for 30 minutes at 60 °C. 0.5 mL of the lipid dispersion was extruded using an automated, custom-built extruder where the MLVs were passed through 100 nm polycarbonate filters 31 times.

Chapter 3

^{64}Cu -labeling and *in-vivo* investigation of the pharmacokinetics of triblock polymer micelles

*Presented in this chapter are our efforts to develop solid methodology for labeling triblock polymeric micelles (PMs) with ^{64}Cu . These micelles were stabilized by coumarin-mediated photo core-crosslinking. Radiolabelled micelles were tested *in-vivo* in mouse models. We investigated the influence of crosslinking as well as the type of chelator (DOTA vs. CB-TE2A) on the *in-vivo* imaging and pharmacokinetics of the particles. This chapter is divided into three major parts. First, an introduction to radiolabeling of PMs, then a description of the development work undertaken to successfully label triblock PMs and finally a description of the testing of these systems *in-vivo*. Part of this work (CB-TE2A vs. DOTA as conjugated to PEG-PHEMA-PCMA micelles, **section 3.8**), has been submitted to Biomaterials. In addition, a paper concerning the impact of crosslinking on coumarin-core micelles (**section 3.8.3**) is in preparation.*

3.1 Background

Polymeric micelles (PMs) are a relatively new type of nanoparticles and research into their radiolabeling has not been as widespread as for liposomes. Most published papers concern PET isotopes and especially ^{64}Cu . When labeling PMs, the possibilities are more limited than with liposomes. Very generally, methodology can be divided into five different areas (**fig. 3.1**), these being **1**) General *covalent labeling*. This method is only for non-metal such as ^{18}F , and β^- emitters such as ^3H and ^{14}C [**316, 317**]. When a radioisotope is covalently linked, it is usually unimportant where on the unimer it is located. **2**) *Distal end chelation*. Here, the chelator is placed on the distal, water-facing end of the unimer, likely attached to a terminal amine. **3**) Diblock shell/corona chelation. To avoid confusion, this method will in the following be referred to as *corona chelation*. What this denotes is the conjugation of chelators along the length of the shell/corona in diblock micelles. This of course requires a corona made from functionalizable monomers. **4**) *Shell chelation*. This is a method reserved for ABC type triblock polymers. The chelator is conjugated to the functionalizable B region. In theory, this method allows relative screening from the surroundings by the A-region (PEG layer) and it is thus conceivable that it has certain advantages. Use of *shell chelation* will be presented in this work. **5**) Finally, *lipid anchored chelators* can be added to the micelles [**318, 319**]. These are embedded into the lipophilic core and present the chelator to the aqueous phase for

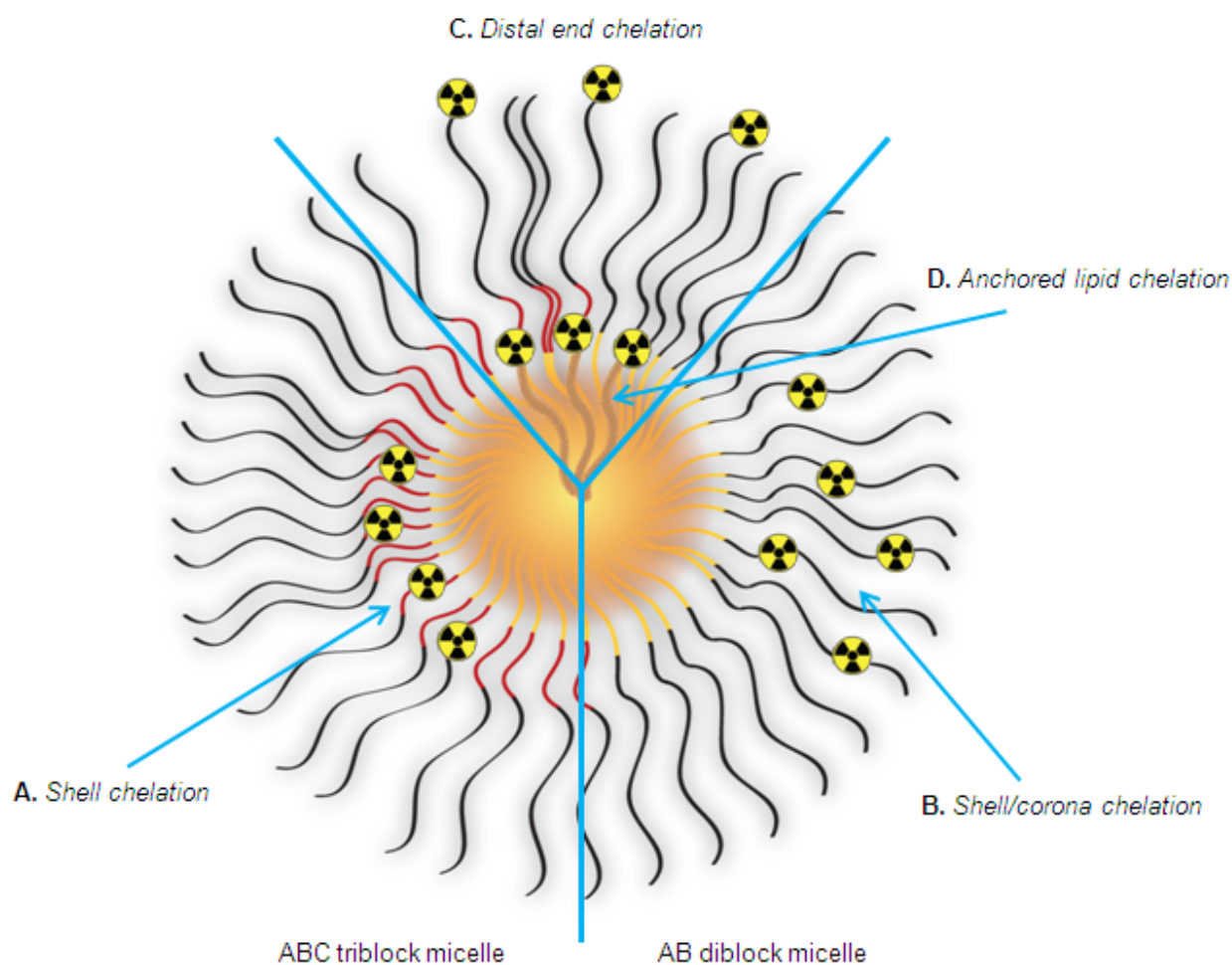


Figure 3.1 – Methods of labeling polymeric micelles. The micelle depicted is divided into an ABC triblock micelle (left) and an AB diblock micelle (right). **A** is only applicable to ABC-type micelles, while **B** is only applicable to AB-type micelles. **C** and **D** are possible on both types.

radiolabeling. An obvious disadvantage is that the chelator is not covalently attached, meaning that sink conditions could readily displace it from the nanoparticle. An advantage is that such a method could allow labeling of preformed and thus commercial micelle formulations.

A recurring theme in the different labeling methodologies for PMs is the degree to which the chelator is located on the surface versus deeper inside the particle. When the chelator is located deeper inside the particle, three things may happen; **1)** Interactions of the chelator with the surroundings may be limited, possibly diminishing immune responses, uptake and complement activation, **2)** The effect of sink conditions may be lessened, preventing loss of chelated metals, **3)** Labeling may be more difficult, due to a harder path of diffusion to the chelator. Little research has been done on these

Table 3.1 – Selected published pharmacokinetic data for radiolabeled PMs. All results are from mice and from recent publications.

Ref.	Tumor (%ID/g)			Liver (%ID/g)			Spleen (ID%/g)			T _½ **	Size	Comments
	1 h	24 h	48 h	1 h	24 h	48 h	1 h	24 h	48 h			
[3]	-	-	4	-	-	32	-	-	15 [†]	25h	60 nm	¹¹¹ In, distal ^Δ , nonCL
[3]	-	-	2	-	-	8	-	-	1.5 [†]	9 h	60 nm	¹¹¹ In, DOTA, distal, nonCL
[3]	-	-	0.5	-	-	6	-	-	1 [†]	26 h	15 nm	¹¹¹ In, Bn, distal ^Δ , nonCL
[10]	-	-	9	-	-	13	-	-	22	29 h	58 nm	¹¹¹ In, distal, nonCL
[11]	3	6	-	35	27	-	8	5	-	NA	20 nm	SCK, ⁶⁴ Cu, TETA, shell, CL
[12]	3*	2	-	13*	8	-	-	2	-	NA	65 nm	NOTA, distal, ⁶⁴ Cu, nonCL
[13]	-	-	5	-	-	7	-	-	11	46 h	24 nm	Distal, DTPA, ¹¹¹ In, CL
[16]	-	9	9	-	5	6	-	5	7	37 h	24 nm	Distal, DTPA, ¹¹¹ In, CL

* Recorded at 4 h. [†] Spleen and pancreas values pooled. ** The secondary (long) half-life of biphasic clearance. Some systems displayed steady, low blood concentration (NA), possibly as a result of very short half-life. ^Δ Results seemingly pooled for both DOTA and DTPA. nonCL: non-crosslinked, CL: crosslinked.

issues, but a few studies are worth mentioning. Seo *et al.* obtained results that showed a lower liver accumulation from liposomes where the chelator was placed near the surface, than from liposomes where it was placed at the distal PEG end [39]. Fonge *et al.* recently carried out a study with ¹¹¹In-labeled liposomes, where they concluded that the chelator used for complexation has significant effects on nanoparticle pharmacokinetics, beyond that which can be explained by complexation stability [3]. They used particles where the chelators were placed on the distal ends of PEG-chains. A few studies have also compared the influence of various chelators on biomacromolecules. Tolmachev *et al.* labeled protein constructs with ¹¹¹In using both DOTA and DTPA and found that DTPA provided better tumor uptake and better tumor-to-organ ratios [320]. Ekblad *et al.* labeled so-called affibodies with ^{99m}Tc and concluded that the position of the chelator influenced the *in-vivo* stability of the radiolabel [321]. Sabbah *et al.* compared the biodistribution and tumor targeting of antibodies labeled with ¹¹¹In through conjugation of both DOTA and DTPA [322]. They found significant difference in organ uptake between the two chelators, specifically tumor uptake was two-fold higher for the DTPA conjugate. This research indicates that *different chelators affect the pharmacokinetics of nanoparticles/biomacromolecules and that their location may be important*. Thus, it may be argued that chelators should not be placed on the surface of nanoparticles, and that when it is desired to compare the *in-vivo* stability of two different chelators, they should be placed below the PEG-layer. This should negate the biochemical interactions of the chelators with the surroundings and make it possible to only assess their stability.

3.1.1 Radiolabeling of polymeric micelles with non-PET isotopes

A number of groups have labeled PMs with ^{111}In . Recently, Fonge *et al.* labeled diblock non-crosslinked PMs with ^{111}In using DTPA or DOTA conjugated to the distal ends of PEG chains [3, 323]. *In-situ* radiolabeled unimers were incorporated into PMs during preparation. As mentioned above, they observed differences between the two chelators. Selected *in-vivo* data from this and other studies is seen in **table 3.1**. Interestingly, they found that the insertion of a benzyl (Bn) group between the chelator and the PEG chain led to significantly improved tumor accumulation in all cases. They attributed this to lipophilic adherence to blood proteins, prolonging circulation time. Generally, at 48 hours tumor uptake (%ID/g) values of <2% were obtained, except in one case, for 60 nm micelles, with a Bn group included (4-5 %ID/g). Hoang *et al.* [10] labeled PMs (58 nm) with DTPA through distal chelation. They obtained relatively impressive tumor accumulation at about 9 %ID/g at 48 h (**table 3.1**). Liver and spleen accumulation differed markedly from that observed by Fonge *et al.* for similar micelles of similar size. Zhao *et al.* presented core-crosslinked (through silica clusters) PMs (24 nm) that were labeled with ^{111}In through distal chelation with DTPA [16]. They showed an impressive tumor accumulation of 8.5 %ID/g (at both 24h and 48h). Hepatic and splenic uptake were relatively modest at respectively; 5.0 (24h) and 6.1 (48h) and 5.1 (24h) and 6.8 %ID/g (48h). Non-CL PMs of about 55-60 nm have been labeled with ^{125}I by Park *et al.* [324], but his group did not use xenografted mice. In addition, labeling of PMs with tritium continues to be in use [325].

3.1.2 Radiolabeling of polymeric micelles with PET isotopes

A number of studies concerning labeling of PMs with ^{64}Cu have been published. The Wooley/Welch has championed research in what they have termed *shell-crosslinked knedel-like* (SCK) nanoparticles [11, 109-117]. A number of their papers have concerned radiolabeling of these particles [11, 115, 326, 327]. An SCK micelle is in essence a diblock micelle where the hydrophilic shell region exhibits multiple carboxylic acid groups [328, 329]. These can be crosslinked through diamines and functionalized in various ways. Rossin *et al.* [11] labeled SCK micelles with ^{64}Cu using TETA. The TETA moieties are thought to have been placed on or near the surface of the particles in a type of *corona chelation*. Targeted and non-targeted micelles were compared. The targeted micelles showed lower tumor accumulation than nontargeted, which attained 5.6 ± 0.9 %ID/g after 24 h. Liver accumulation was large for both targeted (21.5 %ID/g) and untargeted (26.9 %ID/g). This could be due to the large number of negative charges on the surface, ^{64}Cu loss from TETA, TETA interaction with surroundings, or all of these. Spleen accumulation was modest (4.5-4.7 %ID/g). Sun *et al.* published results using a similar method [115, 326]. SCK micelles were labeled with ^{64}Cu through DOTA [326]. As opposed to their previous studies, the particles now used were PEGylated by conjugation to the acid-groups in the shell-region, thus providing a pseudo-

triblock, shell-labeled and shell-crosslinked (20% *degree of crosslinking*, %CL) micelle. The particles were tested in healthy rats and can therefore not be compared with our study. Very recently, the Wooley/Welch groups reported the labeling of SCK micelles with ^{64}Cu through click chemistry post-preparation conjugation of chelators [327].

Pressly *et al.* [330] labeled triblock PMs in the hydrophobic core by attaching DOTA. Admittedly, this is a method not included in **fig. 3.1** and it could be considered rather unorthodox. The PMs were incubated with ^{64}Cu for 1 hour at 80 °C. No labeling efficiency was reported, but it was suggested that it could be difficult for $^{64}\text{Cu}^{2+}$ to penetrate into the core. They showed that PMs with longer PEG chains (5k) has significantly prolonged circulation times in rats compared to PEG₂₀₀₀ and PEG₁₀₀₀, and could circulate for up to 48 hours and beyond. Xiao *et al.* labeled unimolecular (non-disintegrating) polymeric micelles (65 nm) with ^{64}Cu by conjugating NOTA to the distal ends of attached PEG chains [12]. A tumor-to-muscle (T/M) ratio of 7.5 ± 1.5 ($n = 3$) was achieved after 24 hours. Curiously, the blood concentrations remained low at around 2 %ID/g throughout the 24 hour scan.

Few PMs have been labeled with PET isotopes in protected regions of the particles, such as the shell-region. Fukukawa *et al.* [331] conjugated DOTA to core-shell star copolymers in a region that corresponds to the shell-region in triblock micelles. Labeling with ^{64}Cu was done for 1 h at 80 °C, but no labeling efficiency was reported and *in-vivo* studies were done in healthy rats. Dong *et al.* recently labeled a new type of micelles with ^{64}Cu by conjugating the BAT chelator [38] to a helical peptide, which functioned as the B block in a pseudo ABC PM of 15 nm. The micelles were not crosslinked and were tested in healthy mice and showed modest liver and spleen accumulation (about 5 %ID/g after 48 h in both cases) and good circulation in blood, with a calculated (biphasic fit) half-life of 29.5 hours.

3.1.3 Photo core-crosslinking by coumarin

The concept of photo core-crosslinking (PCCL) was touched upon briefly in the introduction. PMs are crosslinked to prevent their disintegration *in-vivo*. The main idea of using UV light irradiation to core-crosslink PMs is to avoid the use of chemical reagents. Chemical crosslinking (such as shell-crosslinking by diamines [103]) usually requires a purification step to remove the added reagents following the crosslinking. In addition, it is usually more time-consuming than PCCL. Several strategies for PCCL of PMs have been reported. Some of these employed a photoinitiator to set off crosslinking reactions in the core [101, 102, 332-334]. A photoinitiator is a compound that decomposes to radicals under the influence of UV light. Incorporation of coumarin moieties in the core provides a way of crosslinking by UV irradiation, without the need for adding reagents or initiators [120, 335]. The chemical properties of coumarin as a reversibly dimerizable compound were excellently reviewed in 2004 by Trenor *et al.* [336]. Coumarin undergoes 2+2 photodimerization to a cyclobutane ring (**fig. 3.2**) when exposed to UV light of $\lambda > 310$ nm. If irradiated at $\lambda < 260$ nm, the ring is cleaved, refurnishing the two coumarin

moieties as separate molecules [120]. The coumarin mediated cross-linking is thus reversible. As the carbon-carbon double bond of coumarin absorbs light around 320 nm, the degree of crosslinking can be assessed by measuring the drop in absorbance at this wavelength [120, 336, 337]. An important thing to note is that coumarin can dimerize, albeit slowly, in sunlight [337]. It has been shown that two coumarin double bonds need to be less than 4.2 Å apart in order to dimerize [338]. Coumarin can dimerize with four different configurations. These are anti head-to-head, anti head-to-tail, syn head-to-head, and syn head-to-tail types [339]. As coumarin with a methyl group in the 4-position exhibits faster dimerization rates than other coumarin derivatives [339], it is usually employed in micelle crosslinking [120, 335], including the work at hand. In addition to coumarin, thymine [340] and cinnamyl [341] have been used in PCCL.

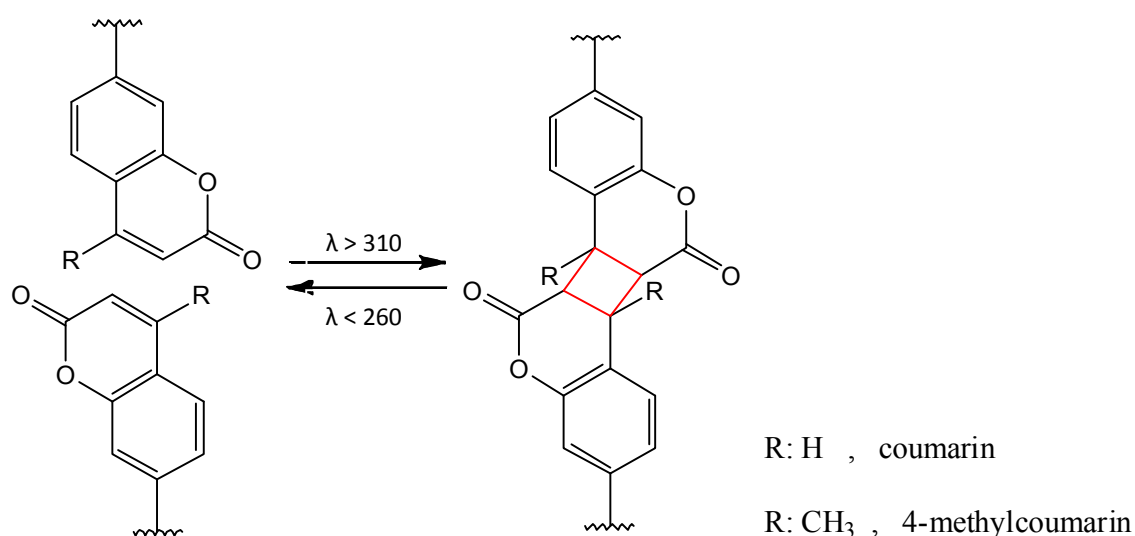


Figure 3.2 – Photo core-crosslinking of coumarin derivatives.

3.1.4 Objective

In the work presented in this chapter, we desired to label triblock ABC-type micelles with ^{64}Cu using the chelators, DOTA and CB-TE2A. The chelators would be conjugated to a functionalizable B-region. Such labeling would, in theory, protect the chelators from interacting with components of the *in-vivo* environment, especially the immune system, and perhaps prolong circulation and tumor accumulation, while diminishing liver and spleen accumulation. In addition, the micelles would be photo-corecrosslinked through coumarin. Using such a system we wanted to **1)** Investigate the difference in *in-vivo* stability between DOTA and CB-TE2A and **2)** investigate the difference in *in-vivo* pharmacokinetics and biodistribution between crosslinked and noncrosslinked micelles.

3.2 Synthesis and functionalization of unimers

The basic unimers (seen in **figure 3.3**) were prepared and characterized by Dr. Pramod Kumar at DTU Nanotech (Lyngby, DK), while functionalizations and formulations were carried out by the author. Four types of unimers were synthesized. PEG-PAEMA-PMMA and PEG-PHEMA-PMMA were only used in initial pilot experiments as they cannot be crosslinked by PCCL. For this reason, their synthesis is only very briefly described here. The other two, PEG-PAEMA-PCMA and PEG-PHEMA-PCMA were investigated extensively, including in *in-vivo* experiments. Their synthesis is described in full detail,

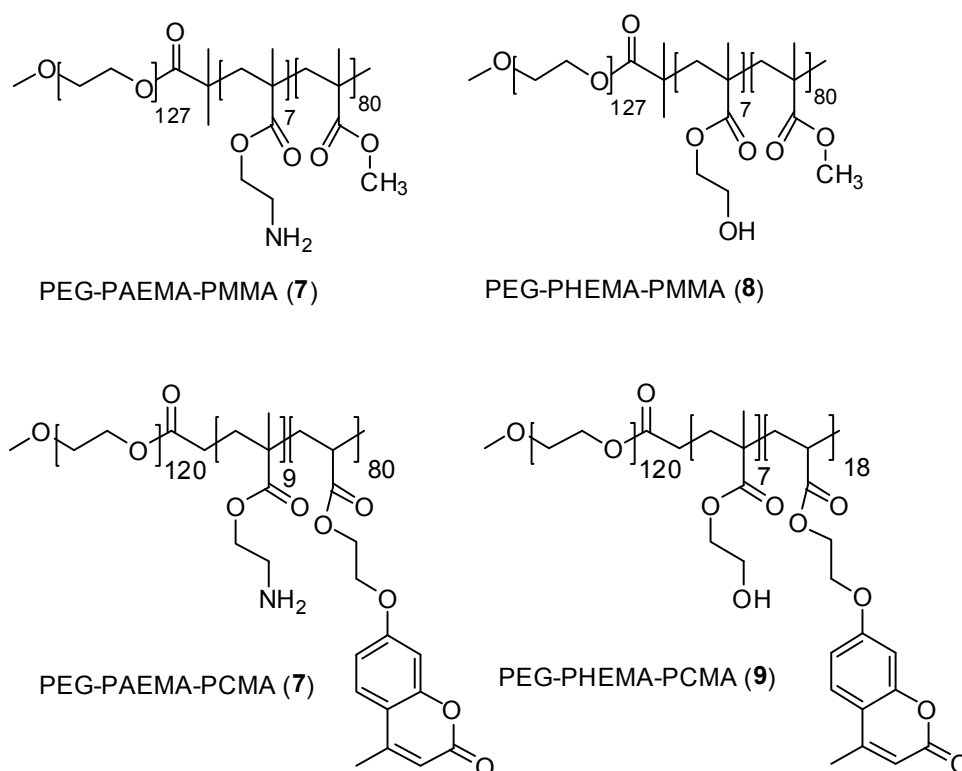
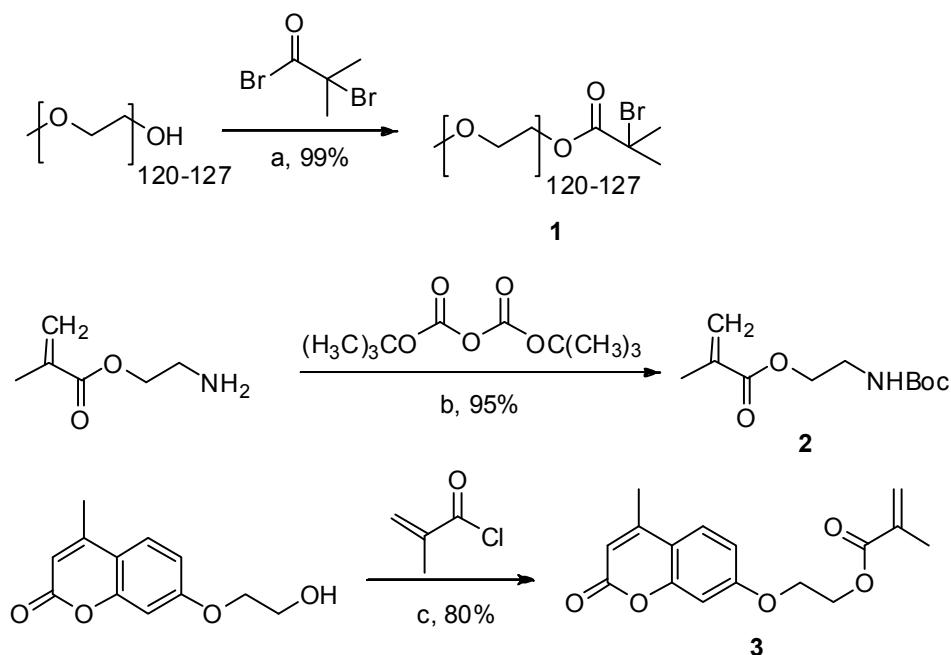


Figure 3.3 – Structures of triblock copolymers used as unimers. Note that the PEG block is identical in all unimers, PAEMA is amino-functionalized, PHEMA is alcohol functionalized, PMMA is a non-crosslinkable core, while PCMA is a photo-crosslinkable core, containing 4-methyl coumarin.

below and elsewhere (see **Supplementary Information III**). The unimers used were constructed from five different blocks, these being PEG: *polyethylene glycol*, PAEMA: *polyaminomethyl methacrylate*, PHEMA: *polyhydroxyethyl methacrylate*, PMMA: *polymethyl methacrylate*, PCMA: *polymethacryloyloxyethoxy-4-methylcoumarin* (**fig. 3.3**).

All polymers used in this study were prepared by the *atom-transfer radical-polymerization* (ATRP) method [342, 343]. The method was extensively reviewed by Matyjaszewski & Xia [344]. ATRP is a so-called *living* polymerization method, where polymerization proceeds in the absence of irreversible chain transfer or chain termination and where the product polymer after finished polymerization can be grafted with a different type of monomer, forming block copolymers [345]. The polymerizable system is composed of the monomer, an initiator with a transferable (pseudo)halogen and a catalyst, usually a transition metal such as Cu [344]. In a typical ATRP polymerization, as the ones described below, the initiator, a chloride or other halide, is in the presence of copper(I), complexed with for example bipyridine (bpy). The reaction starts when a halogen is transferred to the CuCl/bpy complex, forming CuCl₂/bpy. The resulting radical then proceeds to react with the double bond of the monomer. The halogen atom can then be reversibly transferred back to the growing polymer chain, regenerating the CuCl/bpy complex. This transfer of the halogen prevents the chain from terminating, and the propagation can proceed by repeating the process [346]. A defining characteristic of ATRP is the possibility of obtaining

Scheme 3.1: Synthesis of macroinitiators and monomers



Reagents and conditions: (a) TEA, 40 °C, 2 days, (b) TEA, 0 \Rightarrow RT, 24h, (c) TEA, benzene, RT, 1h.

highly monodisperse unimer populations [347]. This is relevant when preparing polymeric micelles, where one is generally interested in particles of as well-defined sizes as possible, as size, as we saw in **chapter 1 section 1.4**, affects the PK of nanoparticles. ATRP reactions are usually not allowed to proceed until full monomer conversion. As reaction rates slow towards full consumption of monomer, reaction time gets excessively long, leading to higher tendency towards side reactions that could result in end-group loss. For this reason, reaction are often not allowed to proceed above 95% monomer conversion [344]. All the described polymerization reactions were carried out in oxygen-free conditions.

3.2.1 Synthesis of macroinitiators and monomers

To use as initiator for all the unimers was synthesized PEG₅₀₀₀-Br (**1**). This was done by a slightly modified literature procedure [81]. An end-methylated PEG₅₀₀₀ chain, CH₃(OCH₂CH₂)₁₂₀₋₁₂₇OH, was reacted with 2-bromoisobutyryl bromide in anhydrous toluene, in the presence of TEA, furnishing the desired PEG ester bromide in quantitative (99%) yield (**Scheme 3.1**). This PEG polymer constituted the A-block in the finished ABC-type unimers.

The Boc-protected amino-functionalized B-block, 2-[N-(t-butoxycarbonyl)amino]ethyl methacrylate (AEMA(Boc), (**2**) was synthesized by a slightly modified literature procedure [348]. Aminoethyl methacrylate HCl was dissolved in dry DCM and boc-protected by reaction with bis(t-butyl) dicarbonate in the presence of TEA (**Scheme 3.1**), furnishing the desired product in excellent yield (95%).

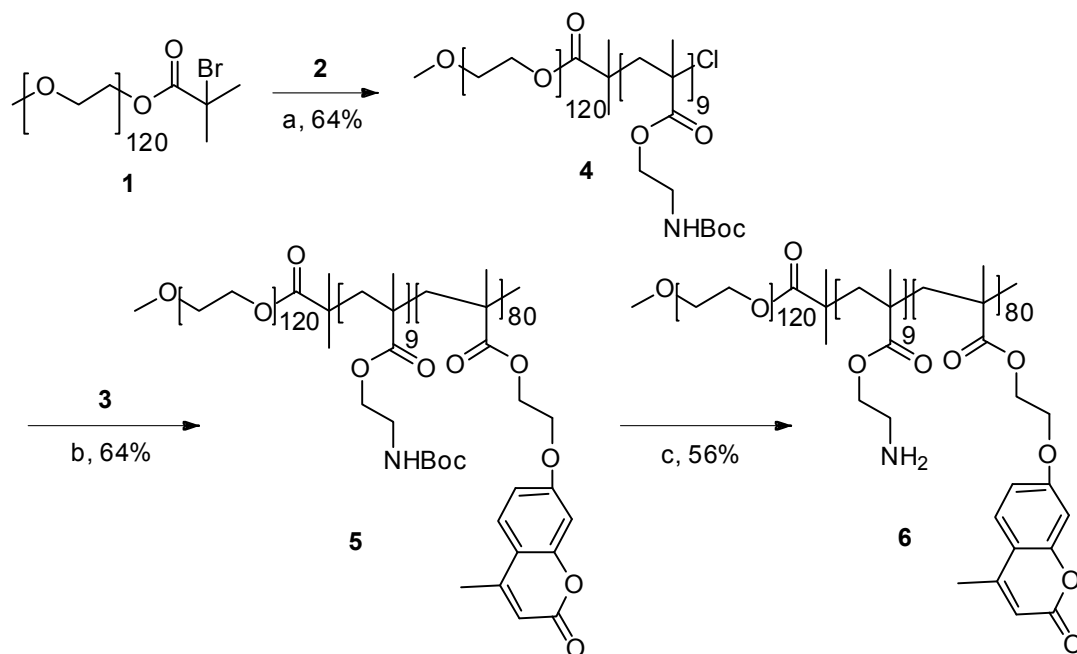
The unimer to make up the C-block in coumarin core micelles, 7-(2-methacryloyloxyethoxy)-4-methylcoumarin (CMA), was synthesized according to a literature procedure [349]. It should be noted that in this reference, coumarin, not 4-methylcoumarin, is used. 7-(2-hydroxyethoxy)-4-methylcoumarin was dissolved in benzene and reacted with methacryloyl chloride in the presence of TEA, to give **3** in very good yield (80%), (**Scheme 3.1**).

3.2.2 Synthesis of PEG-PAEMA-PCMA

The synthesis was conducted in three major steps. **1** was used as template unto which the other two blocks, **2** and **3**, were successively grafted (**Scheme 3.2**).

For the first polymerization step (grafting of the B-block), **1** was polymerized with AEMA(Boc) (12 equiv) in methanol for 15 h at 40 °C under oxygen-free conditions, in the presence of CuCl (1 equiv) and bpy (2 equiv). After ending the reaction

Scheme 3.2: Synthesis of PEG-PAEMA-PCMA



Reagents and conditions: (a) CuCl/bpy , MeOH , $40\text{ }^{\circ}\text{C}$, 15h, (b) CuCl/PMDETA , CuCl_2 , DMF , $80\text{ }^{\circ}\text{C}$, 24h, (c) TFA/DCM (1:1), RT, 24h.

by exposure to air, the product was worked up and ultimately precipitated from ether, giving **4** in a 64% yield. At this point, the number of added AEMA(Boc) monomers was determined by NMR.

The C-block (PCMA) was grafted onto the PEG-PAEMA(Boc)-Cl by dissolving it in DMF, along with the CMA monomer (82 equiv), CuCl_2 (0.8 equiv), PMDETA (3 equiv) and CuCl (1 equiv). PMDETA is an organic tridentate ligand, serving in the role as the complexing agent, that has been shown to provide higher polymerization rates for certain monomers [350]. CuCl_2 was added in order to lower the concentration of radicals, thus giving better control of the polymerization and preventing side reactions [351]. The reaction was allowed to proceed for 24 h at $80\text{ }^{\circ}\text{C}$ under oxygen-free conditions. The finished crude PEG-PAEMA(Boc)-PCMA (**5**) was precipitated from methanol and characterized. The reason for characterization at this point was that GPC would be problematic with deprotected charged amines.

Molecular weights of PEG_n-PAEMA(Boc)_m-PCMA_p.

M _n [a]	M _w [a]	M _w /M _n [a]	M _n [b]	n[c]	m[c]	p[c]
22100	26800	1.21	30390	120	9	80

[a] Determined by GPC, [b] Determined by NMR, [c] Number of repeating units of PEG block (n), PAEMA(Boc) block (m) and PCMA block (p). n, m and p were determined by NMR.

The crude product was deprotected in TFA-DCM (1:1), precipitated from ether and purified by dialysis (**procedure A**, all procedures can be found in the **Experimentals** section in the back of this chapter). NMR showed the disappearance of the Boc-signal at 1.39 ppm (CDCl₃). Accordingly, the deprotected unimer can be expected to have molecular mass of 9 * 100 = 900 less than the protected unimer. Assuming that the NMR derived molecular weight is the most accurate, the MW of the unimer is thus **21 kDa**. An NMR spectrum of the deprotected unimer can be seen in **Supplementary info IV**. A detailed report of the synthesis procedure can be found in **Supplementary info III**.

3.2.3 Synthesis of PEG-PHEMA-PCMA

The macroinitiator **1** was dissolved in MeOH and HEMA (10 equiv.) was grafted on at 25 °C for 24 hours under oxygen-free conditions, in the presence of CuCl (1.1 equiv) and bpy (2.1 equiv.). After reaction, copper was removed by passing through a silica column. The mixture was reduced *in vacuo* and precipitated from diethylether. Drying furnished the desired product in a 82% yield (**Scheme 3.3**). The number of grafted monomers was determined by NMR.

The coumarin monomers were grafted on by dissolving **7** in DMF, along with the CMA monomer **3** (80 equiv.), CuCl₂ (0.9 equiv), PMDETA (7 equiv) and CuCl (1 equiv). The reaction was allowed to proceed for 24 h at 80 °C under oxygen-free conditions. The crude PEG-PHEMA-PCMA was precipitated from methanol, filtered and dried, re-dissolved in DMF and dialyzed against Milli-Q water (**Procedure A**). Subsequently, the unimer was characterized by IR, GPC and H-NMR (for a full synthetic description and analysis results, see **Supplementary info III & IV**).

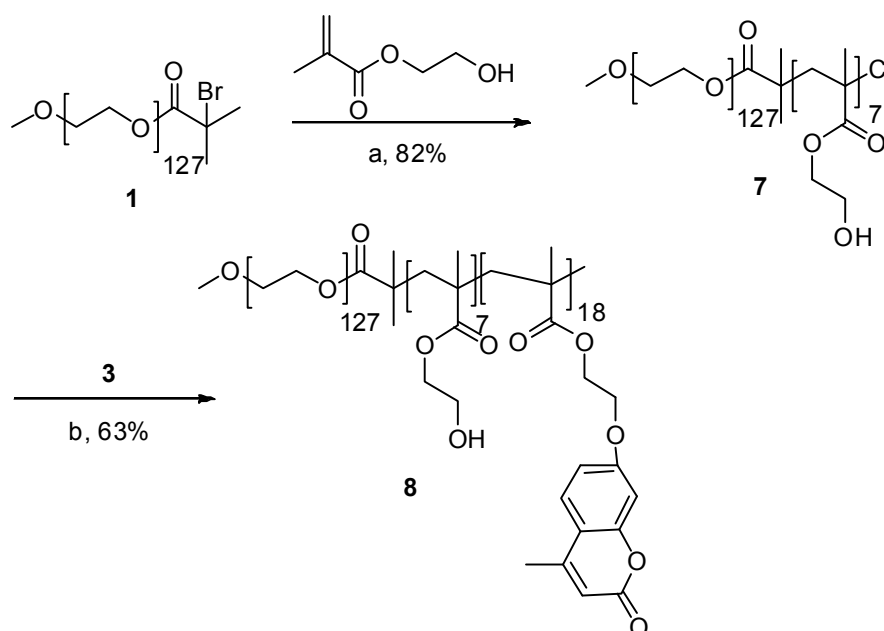
Molecular weights of PEG_n-PHEMA_m-PCMA_p.

M _n [a]	M _w [a]	M _w /M _n [a]	M _n [b]	n[c]	m[c]	p[c]
12400	9550	1.35	11814	127	7	18

[a] Determined by GPC, [b] Determined by NMR, [c] Number of repeating units of PEG block (n), PHEMA block (m) and PCMA block (p). n, m and p were determined by NMR.

It should be noted that in spite of reaction conditions being very similar to those for the preparation of PEG-PAEMA-PCMA, the polymerization of CMA unto PEG-PHEMA-Cl appeared much more sluggish than unto PEG-PAEMA-Cl, resulting in a significantly shorter coumarin block and consequently smaller micelles (*see later sections*).

Scheme 3.3: Synthesis of PEG-PHEMA-PCMA



Reagents and conditions: (a) CuCl/bpy, MeOH, 25 °C, 24h, (b) CuCl/PMDETA, CuCl₂, DMF, 80°C, 24h

3.2.4 Synthesis of PEG-PHEMA-PMMA

The unimer synthesis was initiated by dissolving **1** in MeOH along with the HEMA unimer (see **Scheme 3.3**) (10 equiv), bpy (2.1 equiv) and CuCl (1.1 equiv). Polymerization proceeded for 24 h at 25 °C. The crude product was precipitated from diethylether and isolated (82% yield). This was followed by the grafting on of the PMMA block. The PEG-PHEMA-Cl was dissolved in DMF along with MMA (methyl methacrylate, 85 equiv), CuCl₂ (0.8 equiv), PMDETA (3.3 equiv) and, after establishing oxygen-free conditions, CuCl (1 equiv). Polymerization was allowed to proceed for 25 h at 35 °C after which the crude product was concentrated and precipitated from petroleum ether, from which it was extracted with water (63% yield).

3.2.5 Synthesis of PEG-PAEMA-PMMA

The PEG-PAEMA-PMMA unimer synthesis was started from the macroinitiator **1**. The diblock copolymer PEG-PAEMA-Cl was synthesized as described above for PEG-PAEMA-PCMA. Further, the PMMA block was grafted on as described above for PEG-PHEMA-PMMA.

3.2.6 Purification of unimers by dialysis (procedure A)

After synthesis, the crude unimers were dissolved in DMF and water was added dropwise. Usually resulting in a 1:2 (DMF:water) ratio. The concentration of micelle material in the resulting DMF:water mixture was around 5 mg/mL, which was a general concentration used in most of the prepared formulations. The mixture was subsequently dialyzed against Milli-Q water for three days, with daily changing of the medium. The pore cut-off size of the dialysis tubing was MW = 12.400. The volume of the dispersion before and after dialysis was not seen to change much. After dialysis, the dispersion could be freeze-dried directly to provide the pure unimer. Generally, dialysis resulted in a loss of about 20% of the crude dry weight.

Dialysis was used in order to remove small molecular impurities, as well as the residual copper from the polymerization reactions (the crude unimers were slightly green). Especially the copper was a major concern, as even trace amounts could occupy the chelator binding sites in the following chelator conjugations. For this reason, the unimer purification was initially done with EDTA added to the dialysis medium. This however gave serious problems during radiolabeling because of a carry-over of trace amounts of EDTA (elaborated on in **section 3.3.2**) and was abandoned. Instead, the dialysis was

conducted with Milli-Q water that was pH-corrected with HCl to about 5. At pH values lower than 7, Cu^{2+} exists in the form of a soluble hydrate that can be dialyzed off. At pH values above ~ 7 the Cu^{2+} precipitates as the hydroxide, making removal by dialysis problematic.

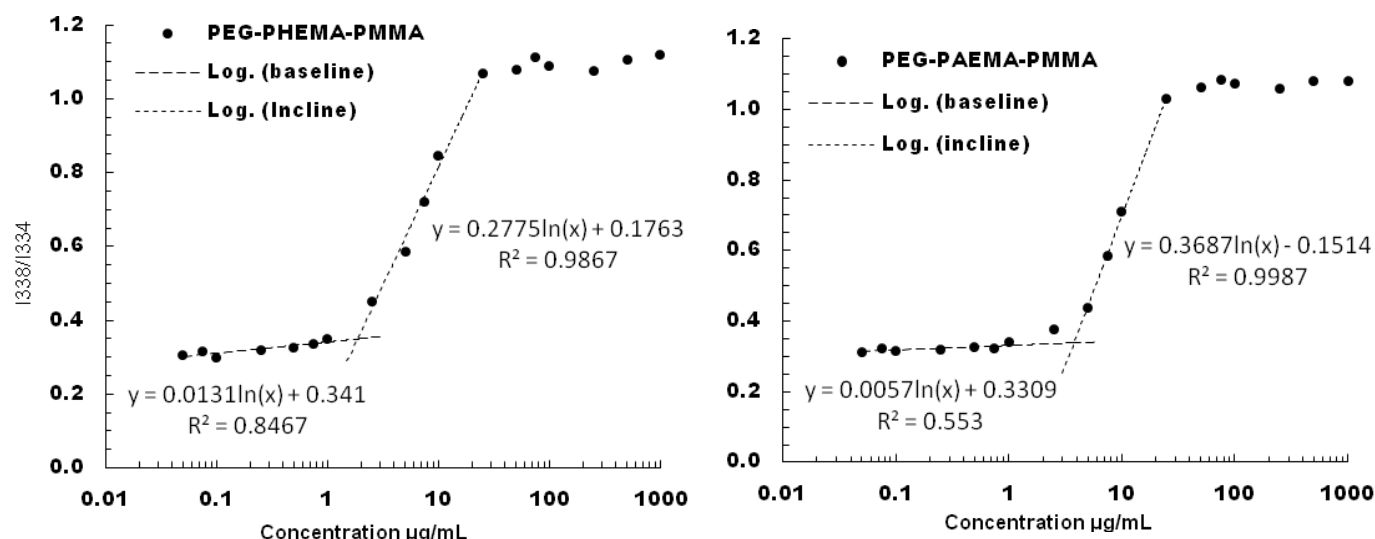


Figure 3.4 – Determination of CMC by the pyrene assay. *Left*: CMC determination for PEG-PHEMA-PMMA. The CMC was calculated by finding the intersection of the two graphs for baseline and incline to be: 2 $\mu\text{g/mL}$. *Right*: CMC determination for PEG-PAEMA-PMMA. The CMC was determined in the same manner to be 4 $\mu\text{g/mL}$.

3.2.7 Determination of CMC

In order to determine the critical micelle concentration (CMC) of the micelles, the pyrene assay [89] was used (**procedure B**). Pyrene is a polycyclic aromatic hydrocarbon consisting of four fused benzene rings, resulting in a flat aromatic system. Pyrene is a fluorophore and exhibits a redshift in its excitation spectrum when partitioning into a nonpolar environment. This causes a change in the ratio of emission intensities between 338 and 334 nm (I_{338}/I_{334}) when micelles are formed and incorporate pyrene into their hydrophobic cores. Therefore, the appearance of micelles in a solution containing pyrene should cause a sharp increase in the I_{338}/I_{334} ratio, indicating the CMC. It was contemplated that the method would be a useful way of showing successful crosslinking for micelles, in that, after crosslinking, there would be no sharp rise in I_{338}/I_{334} but rather a flat curve following the concentration of the micelle material.

It was initially desired to use this method to assess the CMC of the PCMA-core micelles. However, as this core types was a conjugated system, it was found to interfere with the light irradiation and emission and the idea was abandoned. The method was successfully used to determine the CMC of both PEG-PAEMA-PMMA and PEG-PHEMA-PMMA (**fig. 3.4**). As can be seen on the graphs, by drawing lines over the initial baseline region (before the rise), and on the incline slope, the CMC can be determined at the intersection of these two lines. The CMC values for the two unimers were calculated to be 4 µg/mL for PEG-PAEMA-PMMA and 2 µg/mL for PEG-PHEMA-PMMA.

3.2.8 Conjugation of chelators to unimers

The functionalization of the unimers consisted in conjugating the two macrocyclic chelators, DOTA and CB-TE2A to the primary amines on the PEG-PAEMA-PCMA and PEG-PAEMA-PMMA polymers, as well as to the primary alcohols of the PEG-PHEMA-PCMA and PEG-PHEMA-PMMA polymers (**scheme. 3.4**).

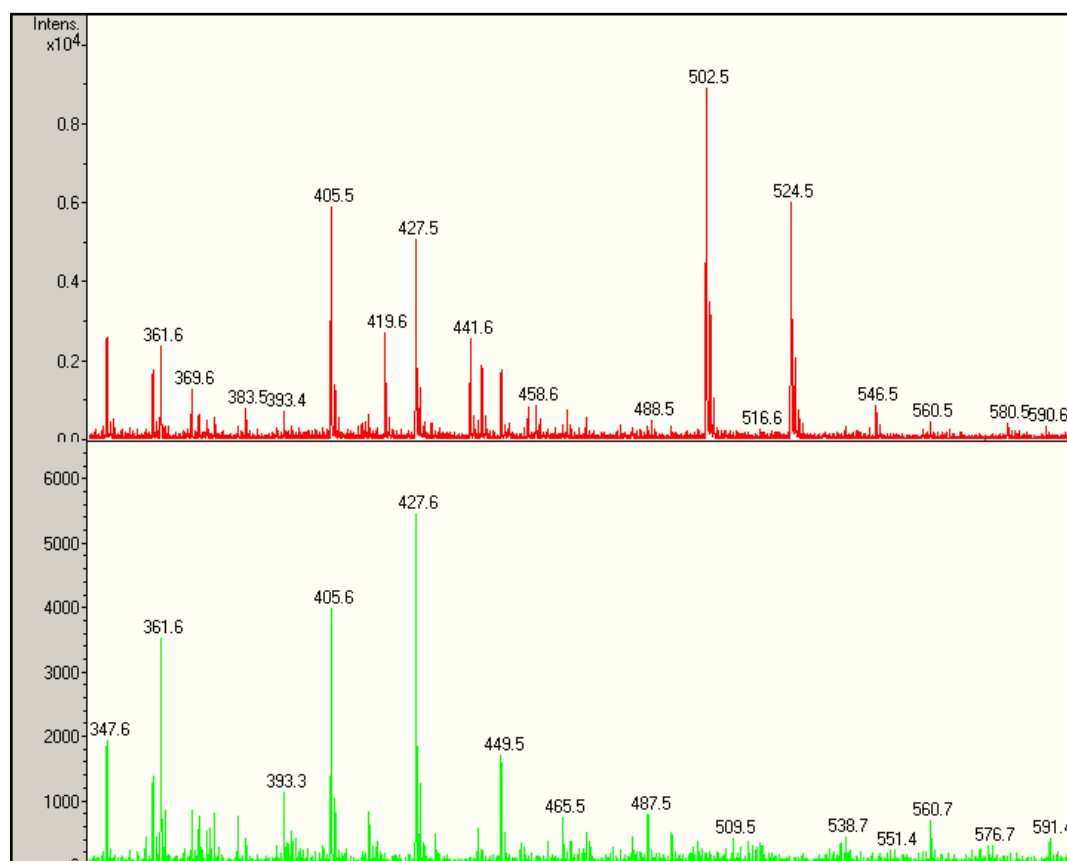


Figure 3.5 – Monitoring of DOTA conjugation to PEG-PAEMA-PCMA. 502.5: DOTA-NHS, 524.5: DOTA-NHS + Na, 405.5: DOTA, 427.5: DOTA + Na.

Conjugation of DOTA (procedure C)

Conjugation of DOTA was somewhat simple, in that the activated ester DOTA-NHS is commercially available. As a standard procedure, the purified unimers were dissolved in anhydrous DMF with a base added. The base was usually TEA but DIPEA was used in a few cases. Notably, DMAP was employed as base in the DOTA-conjugation of PEG-PHEMA-PCMA. Which base was used is not expected to influence the reaction significantly. After addition of DOTA-NHS and base, the mixture was allowed to stir overnight. This was followed by dialysis against Milli-Q water (cut off size MW: 12400) in order to remove small molecular byproducts. The reactions in which DOTA was coupled to the amines of PEG-PAEMA-PMMA were monitored by Maldi-TOF (**fig. 3.5**). It was observed that the reaction went to completion (i.e. that DOTA-NHS was consumed after standing overnight). However, some free DOTA was observed, indicating that the commercial product either had a slight impurity of non-activated DOTA or that some hydrolysis had occurred. It was later observed (see **section 3.3.2**) that when DOTA was conjugated to amine-containing unimers, trace amounts would stay behind, even after dialysis. This was solved by capping the remaining amines (see **procedure C**).

DOTA was initially conjugated to PAEMA unimers in a 1:1 ratio, the rationale being that 1 part PAEMA-type unimer, each unimer with one DOTA attached would be mixed with 9 parts un-functionalized PHEMA-type unimers. This would give an overall DOTA presence of one chelator per ten unimers. Later on in the project, it was found to not be possible to synthesize PEG-PHEMA-PCMA to match the available PEG-PAEMA-PCMA in size (~ 40 nm). For this reason it was opted to conjugate DOTA in a 1:10 ratio.

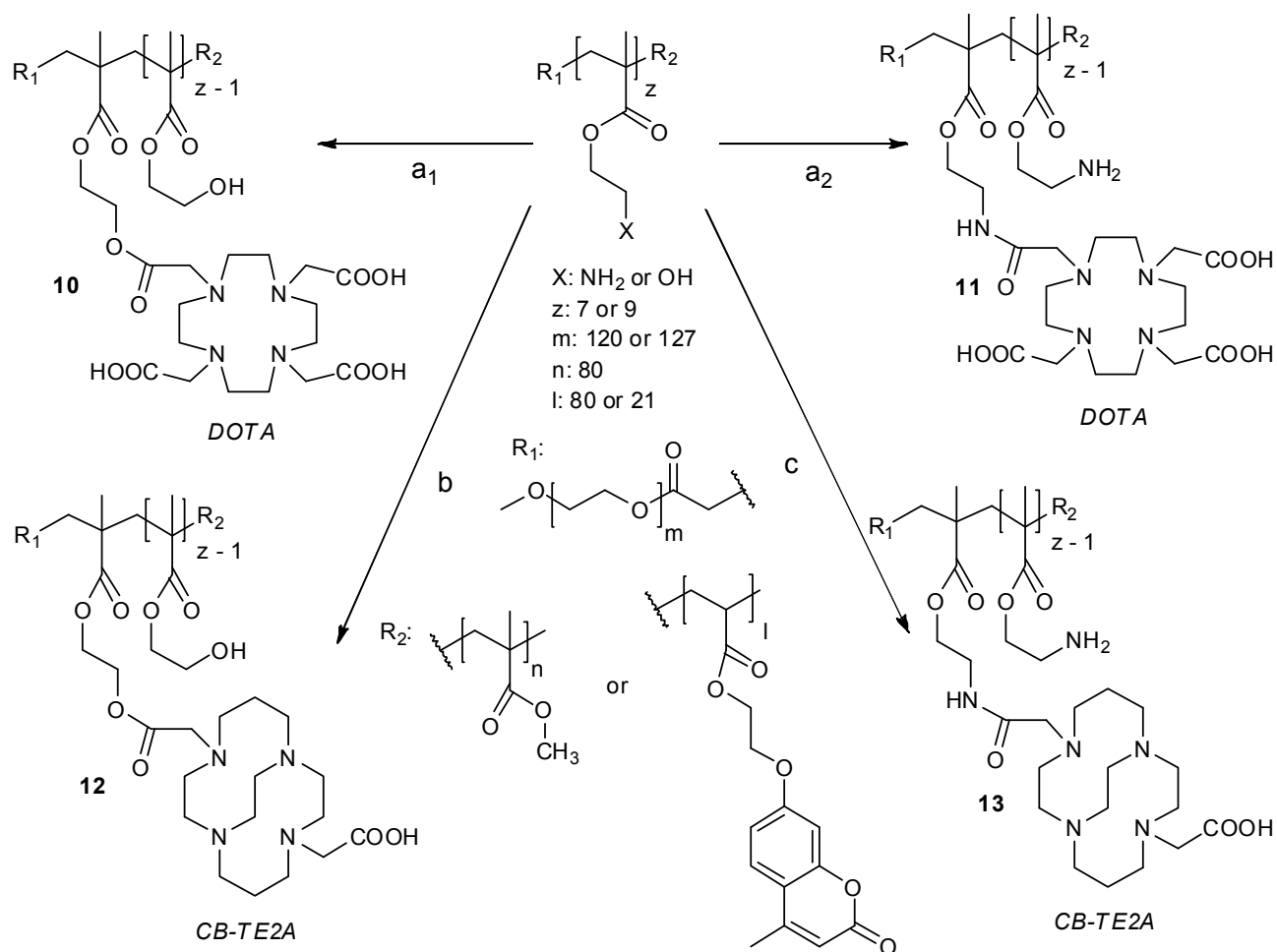
When DOTA was coupled to PEG-PHEMA-PCMA the same thoughts as above were applied, except that DOTA was conjugated in a 1:1 ratio and DMAP was used as base (**procedure C**).

Conjugation of CB-TE2A (procedure D and E)

Conjugation of CB-TE2A was not as easy but still relatively straightforward. Monitoring this reaction by MALDI-TOF was not possible, as CB-TE2A was added in excess. CB-TE2A has two free carboxylic acids, one of which is usually used for conjugation to macromolecules or nanoparticles. EDC.HCl was chosen as the coupling agent, as the water-soluble urea reaction product would not precipitate during the subsequent dialysis. Initially the coupling was done in the presence of an excess of NHS (**procedure D**) but later, with DMAP as catalyst (**procedure E**). The main idea of the conjugation was to dissolve the unimer in question (be it PAEMA or PHEMA) along with an excess of CB-TE2A (3 eq). Coupling reagent (EDC.HCl) would then be added in 1 equivalent. CB-TE2A exhibits two carboxylic acid arms, meaning that in this case there would be six available carboxylic acids with which the EDC could react. This would mean that a large excess of the CB-TE2A would be mono-activated, while a little would be di-activated. Normally when using carbodiimides as limiting reagents, this leads to reaction with a further acid, which forms an acid anhydride. If an excess of NHS was present, along with an excess of base, it would then react with the acid anhydride and furnish an NHS ester which would proceed to react with

the unimer. The final product would be the unimer conjugated with CB-TE2A in slightly less than a 1:1 ratio. The initial idea behind using NHS was that the conjugation of the activated CB-TE2A and the unimer, being a large molecule, would be relatively slow. By first preparing an NHS-ester, this compound would be more stable than the EDC conjugate, to for example hydrolysis from trace water (the available CB-TE2A was the dihydrate), and better suited for a long reaction. If DMAP was present as catalyst, it would react with the acid anhydride and the product would proceed to react with the unimer. As DMAP was only used with a PHEMA polymer, no excess of base was added. It is important to note that CB-TE2A (dihydrate) is not soluble in DMF unless a base is added.

Scheme 3.4 - Conjugation of chelators to unimers



Reagents and conditions: (a), DOTA-NHS, TEA (a_2), DMAP (a_1), DMF, RT, overnight, (b) CB-TE2A, EDC.HCl, DMAP, DMF, RT, overnight, (c) CB-TE2A, EDC.HCl, NHS, TEA, DMF, RT, overnight.

Determining the yield of chelator conjugation to PEG-PHEMA-PCMA

The yields of the chelator conjugation to the PEG-PHEMA-PCMA micelles were estimated by incubating the micelles (200 μL , 1 equiv) with non-radioactive Cu^{2+} , twice the maximum molarity of chelator present (2 equiv), spiked with ^{64}Cu . After incubation of 4 h at 80 $^{\circ}\text{C}$ (CB-TE2A) or 3 h at room temperature (DOTA), unincorporated copper was scavenged (30 min) by adding EDTA in excess (400 equiv). Conjugation yield was estimated as the ratio of the non-eluting peak (micelles) towards the EDTA-peak. The conjugations were found to be low yielding (estimated yields: DOTA: 4%, CB-TE2A: 5%). However, this fitted well with our desire to put few chelators in the shell-region. A large number of chelators would occupy significant space in the shell-region and possibly affect the micelles in undesirable ways (due to extra free charges and the likely compromising of size and integrity), while not contributing with increased ^{64}Cu -binding capacity (due to the trace molarity of radioactive ^{64}Cu). Accordingly, approx. 5% of the unimers in the PEG-PHEMA-PCMA micelles hold a chelator. Generally, good radiolabeling was observed with these micelles (*see later section*), indicating that the degree of chelator conjugation was adequate. In addition, size and zeta-potential were not seen to change after chelator conjugation, indicating that a low degree of degree conjugation is desirable (*see section 3.8*). The only aspect which seemed affected by chelator conjugation was the thermostability (*section 3.8.3*). Here, CB-TE2A conjugated micelles aggregated after 61 h at 80 $^{\circ}\text{C}$, while the DOTA conjugated micelles did not.

3.2.9 Preparation of micelles (procedure F)

After the chelators had been conjugated, micelles were prepared. This was usually done by slow addition (drop-wise) of Milli-Q water directly to the reaction mixture. Water was added until the ratio between DMF and water was between 1:1 and 1:2. Then the mixture was dialyzed against Milli-Q water for three days, with daily changes of the medium. Thus, fresh medium would be added a total of three times. As long as there was not an excess of air present in the dialysis tube when dialysis was started, the volume was not observed to change significantly during dialysis. Generally, the target concentration of micelle material in the finished dispersions was 4-5 mg/mL.

3.2.10 Nomenclature used for chelator conjugated micelles

In addition to the already mentioned unimer-based nomenclature, (PEG, PAEMA, PHEMA, PCMA and PMMA), special designations were used for chelator-conjugated unimers and micelles. Whenever a unimer was conjugated with a chelator in a fashion where each unimer would in average be conjugated to one chelator molecule, such unimers were said to be conjugated 100% (i.e. 100% of unimers hold a chelator). Whenever a unimer was conjugated to a chelator so that, on

average one in ten unimer would have a chelator conjugated, such unimers were said to be conjugated at 10%. Such conjugations were done on the micelles that were eventually used in the *in-vivo* studies with PEG-PAEMA-PCMA type micelles. The same type of nomenclature was used for mixed micelles. Whenever a 100% conjugated unimer (PAEMA-type) was mixed with an un-conjugated unimer (PHEMA-type) in a 1:9 ratio, the resulting mixed micelle was said to be conjugated in a 10% fashion.

3.2.11 Characterization of micelles

The PMs were characterized by *direct light scattering* (DLS), providing hydrodynamic diameters and zeta-potential. The micelle dispersion (~4-5 mg/mL) was diluted in 10 mM HEPES buffer (no NaCl added, pH = 7.4) to about 0.15 mg/mL, which usually gave adequate count rates of 200 - 500 kcps. Size was measured three times *on the same sample*, each with 5 runs, and the resulting average with standard deviation is reported. Size was consistently reported as the *number weighted median* and (when specified) as the *intensity weighted median*. Zeta-potential was measured by running 20 runs of 10 scans. In **table 3.3** is seen characterization data from selected micelle formulations.

3.2.12 Formulations of micelles, sizes and zeta potentials

At the outset of the project, the primary idea was to conjugate DOTA or CB-TE2A to a PAEMA polymer in a 100% fashion. Subsequently, it would be mixed with a corresponding unimer of PHEMA type in a 1:9 (PAEMA:PHEMA) ratio. This would result in micelles conjugated with chelator at 10%. For this reason a series of micelles were conjugated with chelator at 100% and characterized. In the PMMA series, these were mixed with PEG-PHEMA-PMMA in a 1:9 ratio (10% chelator) and characterized (**table 3.3, entry 5 + 6**). When working with the PCMA series, which eventually became the series to be tested *in-vivo* (see **section 3.7 + 3.8**), it became apparent that PEG-PHEMA-PCMA could not be synthesized in a size that matched the PEG-PAEMA-PCMA at hand. The PEG-PAEMA-PCMA was ~40 nm (80 coumarin repeats), whereas the PEG-PHEMA-PCMA could not be synthesized in a size higher than ~20 nm (18 coumarin repeats), despite numerous attempts. Because of this difference in size, it was decided not to mix these two unimer types for *in-vivo* use. However, in order to see if the mixed micelle was viable, it was prepared (**entry: 11**) and subsequently radiolabeled (see **section 3.3.4**).

In **Table 3.3** the sizes and zeta potentials of selected prepared micelle formulations can be seen. In general, it was observed that conjugation of chelators, even in 100%, did not change the size of the micelles markedly (compare **entry 1** with **entry 3**, **entry 7** with **entry 8** and **9**, and **entry 10** with **entry 12** and **13**). For one type however (PMMA), conjugation of 100% DOTA to PEG-PAEMA-PMMA, an increase in size was observed (compare **entries 1** and **2**). It is possible that the increase may be attributed to general disturbances and uncertainty during DLS measurement, but as the increase was

observed over four different preparations, it may be significant. No size changes were observed for PCMA micelles. There was a slight size difference between PEG-PAEMA-PMMA and PEG-PHEMA-PMMA (**1** and **4**) of about 10 nm. For the mixed micelles prepared from these two unimers (**5** and **6**), sizes were between the two unimers in one case (**5**) and close to the size of the 90% unimer PEG-PHEMA-PMMA in the other (**6**). Accordingly, it seems that the majority unimer determines the hydrodynamic diameter. This is also observed when comparing **9**, **10** and **11**, where the mixed micelle (**11**) is closer in size to the majority PHMEA type (**10**). The zeta-potential of the micelles were generally observed to be relatively close to neutral. The free-amine, unmodified PAEMA-type micelles displayed positive zeta-potential in the area of 7.5 mV (**1** and **7**). When chelators were attached to these micelles (without capping the remaining amines, see **section 3.3.2**), the zeta potential dropped to 1-3 mV (**2** and **3**). This is understandable as the chelators take up a free amine on each unimer and introduce free carboxylic acids. When chelators were attached along with capping of the amines, the zeta potential dropped even further to the range of -3 to -1 mV (**8** and **9**). It is also interesting to note that **entry 6**, which contained 10% un-capped PAEMA unimer (with 100% CB-TE2A) had a zeta-potential around 0 mV. In general, good correlation between availability of charged groups on the micelles and zeta potential is observed. A slightly negative contribution to the zeta-potential is usually expected from the PEG-chains alone [**210**].

TABLE 3.3 – Sizes and surface charges of chelator conjugated and, mixed and capped micelles.

Entry	Unimer**	Chelator*	Capping†	Size (nm)	PDI	Zeta-pot. (mV)
1	P-PA-PM	None	None	32 ± 1 (n = 3)	0.18 ± 0.03 (n = 3)	7.5 ± 0.1 (n = 2)
2	P-PA-PM	DOTA (100%)	None	44 ± 4 (n = 16)	0.11 ± 0.01 (n = 3)	1.3 ± 0.7 (n = 8)
3	P-PA-PM	CB-TE2A (100%)	None	30 ± 1 (n = 4)	0.08 ± 0.01 (n = 3)	3.0 ± 1.0 (n = 4)
4	P-PH-PM	None	None	20 ± 1 (n = 3)	0.28 ± 0.01 (n = 3)	-3.2 ± 0.4 (n = 2)
5	P-PA-PM/ P-PH-PM (1:9)	DOTA (10%)	None	26 ± 4 (n = 3)	0.15 ± 0.05 (n = 3)	-2.9 ± 1.0 (n = 3)
6	P-PA-PM/ P-PH-PM (1:9)	CB-TE2A (10%)	None	21 ± 1 (n = 4)	0.10 ± 0.14 (n = 3)	-0.8 ± 1.0 (n = 4)
7	P-PA-PC	None	None	38 ± 3 (n = 6)	0.05 ± 0.02 (n = 6)	7.3 ± 0.2 (n = 2)
8	P-PA-PC	DOTA (10%)	Yes	39 ± 3 (n = 12)	0.11 ± 0.03 (n = 12)	- 3.0 ± 1.0 (n = 4)
9	P-PA-PC	CB-TE2A (100%)	Yes	37 ± 4 (n = 6)	0.11 ± 0.02 (n = 3)	- 2.5 ± 1.7 (n = 1)
10	P-PH-PC	None	NA	19 ± 1 (n = 3)	0.33 ± 0.00 (n = 3)	-4.1 ± 0.4 (n = 2)
11	P-PA-PC/ P-PH-PC (1:9)	CB-TE2A (10%)	Yes	25 ± 2 (n = 3)	0.18 ± 0.02 (n = 3)	-3.39 ± 0.68 (n = 1)
12	P-PH-PC	CB-TE2A (5%)	NA	21 ± 1 (n = 3)	0.17 ± 0.02 (n = 3)	-3.81 ± 0.42
13	P-PH-PC	DOTA (5%)	NA	23 ± 1 (n = 3)	0.15 ± 0.01 (n = 3)	-2.06 ± 0.73

* In mixed micelles with both PAEMA and PHEMA type unimers, the chelator was exclusively conjugated to the PAEMA. In micelles with only PHEMA type, the chelator was conjugated to this unimer. † The issue of capping the remaining free amines in PAEMA unimers is addressed in **section 3.3.2**. ** P: PEG, PA: PAEMA, PH: PHEMA, PM: PMMA, PC: PCMA.

3.3 Pilot radiolabeling experiments

Generally, radiolabeling with ^{64}Cu was done by incubating the chelator-conjugated micelles with the radioisotope followed by size-exclusion chromatography (SEC) on a Sephadex G25 (*fine*) packed column, onto which the micelles would be loaded and eluted by fully-automated equipment. Before incubation with micelles, the ^{64}Cu was dissolved in an NH_4OAc (pH 5.5, 0.1 M) buffer, forming copper acetate. This was stirred with the PMs for 2-3 hours at RT (DOTA) or 60-95 °C (CB-TE2A). Subsequent purification by size exclusion chromatography was done in an isotonic (NaCl, 150 mM) PIPES-buffer (10 mM) at pH = 7.0. PIPES does not chelate Cu^{2+} [352] and above pH 7, Cu^{2+} can precipitate as the hydroxide.

Under normal conditions, elution would result in two separate peaks (fig. 3.7). The first-eluted of these, termed **Peak 1**, contained the micelles. This was confirmed by 1) Visual inspection. That micelles were present in the most concentrated fractions could be observed as opalescence in the dispersion, 2) The fractions were measured by DLS showing micelles of

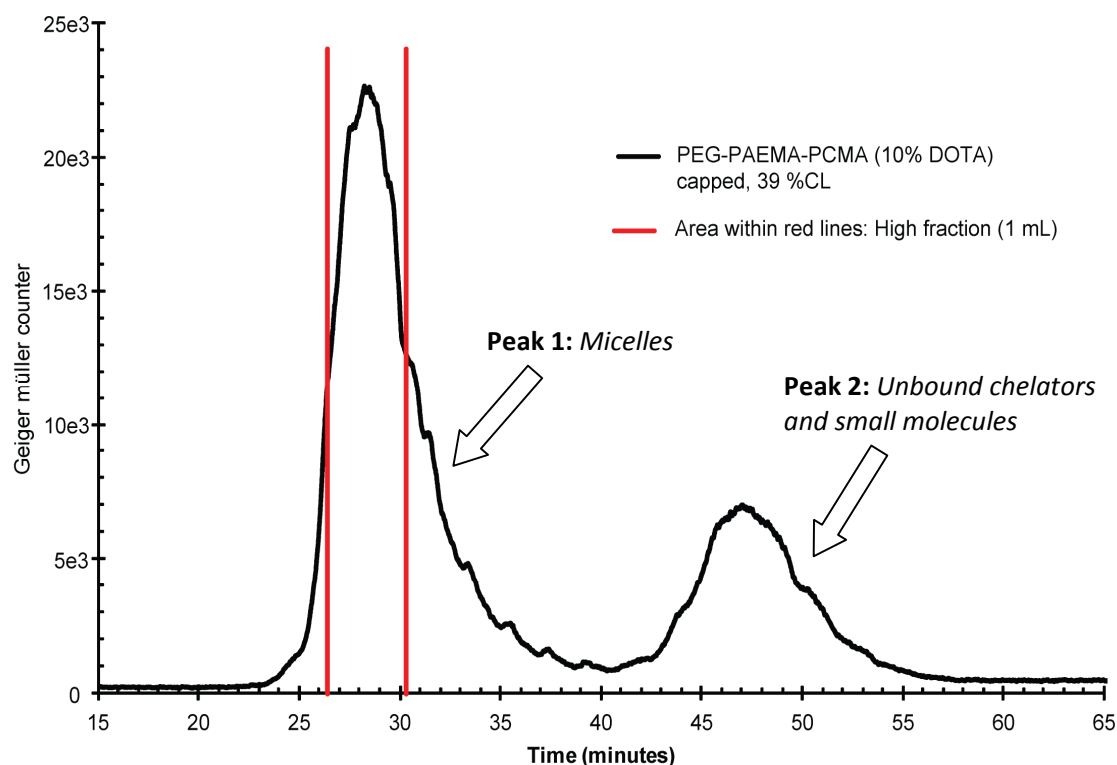


Figure 3.7 – Size exclusion chromatogram from purification of radiolabeled PMs. The y-axis shows arbitrary unites detected on a GM counter upon exiting the SEC column. **Peak 1** is present between apporx. 25 and 40 minutes, while **Peak 2** was collected between approx. 40 minutes and 58 minutes. Between the two red lines is shown the volume (1 mL) that was collected as the “high fraction” (see section 3.3.5 and table 3.6).

the correct size, as well as increasing count rate in the most concentrated fractions, **3**) Later on, micelle material concentration in the micelle containing peaks was determined by UV, where the characteristic UV spectrum of coumarin (or crosslinked coumarin, see **section 3.4**) could be observed (for DLS and UV data from the fractions, see **section 3.3.5**). When **Peak 1** was analyzed by Radio-TLC the activity did not elute on the silica plate, which is characteristic of nanoparticles. It should also be noted that un-chelated ^{64}Cu does not elute on TLC, but as it also does not elute from the SEC column, it could not be present in **Peak 1**. The second peak that eluted, **Peak 2**, contained small molecular contaminants and, significantly, a prominent peak for ^{64}Cu -EDTA or ^{64}Cu -DTPA, when these were added to scavenge unspecifically bound ^{64}Cu (see **section 3.3.3**). Depending on the amount of radioactivity used, other smaller peaks were also seen (selected Radio-TLCs are shown in **Supplementary Information V**). These were thought to be radiolysis products, as they increased in prominence when more activity was applied during labeling. An experiment into the radiolysis of the micelles along with relevant RadioTLC chromatograms can be seen in **Supplementary information VII**. Radiolysis was however, not found to affect the integrity of the collected labeled micelles. After radiolabeling, both size and zeta potential of otherwise stable micelles were identical to those of the same micelles before radiolabeling.

From the outset of radiolabeling experiments and onwards, more than 95% of the applied radioactivity was consistently accounted for after labeling. It could therefore be concluded that none of the active species in use (except free ^{64}Cu) adhered to any significant extent to parts of the SEC apparatus. In addition very little activity (usually less than 5%) stayed behind in the glass vial in which the micelles were labeled.

3.3.1 Initial experiments and unspecific binding of EDTA

Initially, radiolabeling was performed on PEG-PAEMA-PMMA micelles that were conjugated to DOTA (100%) and uncapped. Almost all the activity was found to elute in **Peak 2**. As this was well before the SEC elution was fully understood, **Peak 2** was then thought to contain the micelles. However, experiments with DOTA-chelated ^{64}Cu showed that such small molecular species eluted in exactly the same place (**Peak 2**). It was apparent that something was wrong with these early micelle formulations. In order to ascertain that what was eluting was not un-chelated ^{64}Cu , ^{64}Cu -acetate was prepared and applied to the SEC column. This species was found not to elute at all, although it could be eluted by running a chelator, such as DTPA, through the column. Analyses by Radio-TLC made it clear that **Peak 2** contained ^{64}Cu -EDTA (see **Supplementary Information V** for Radio-TLC chromatograms). As already mentioned (**section 3.2.6**), EDTA was initially used when purifying the crude unimers by dialysis, in order to thoroughly remove the copper impurities from the polymerization reactions. In spite of several changes of the medium to EDTA-free Milli-Q water after dialysis against an EDTA containing medium, it appeared that the EDTA stayed with the micelles. It was hypothesized that this could be due

to the formation of several salt bridges [353] between the carboxylic acids on the EDTA and the numerous free amines in the PAEMA-block of the micelles. DOTA was found to exhibit the same behavior (see section 3.3.2), as was CB-TE2A although to a more limited extent, perhaps due to the latter only having two carboxylic acid groups.

In order to continue research on the DOTA-coupled micelles, it was hypothesized, that if radiolabeling was done at a higher temperature (instead of at room temperature), the ⁶⁴Cu would shift from the EDTA to the DOTA in the micelles, because of the higher thermodynamic stability of DOTA. This was indeed found to be the case. When, DOTA(100%) PEG-PAEMA-PMMA micelles with EDTA contamination was stirred with ⁶⁴Cu-acetate at 95 °C for 2 hours, 24% of the activity was shifted to **Peak 1**, i.e. to the micelles.

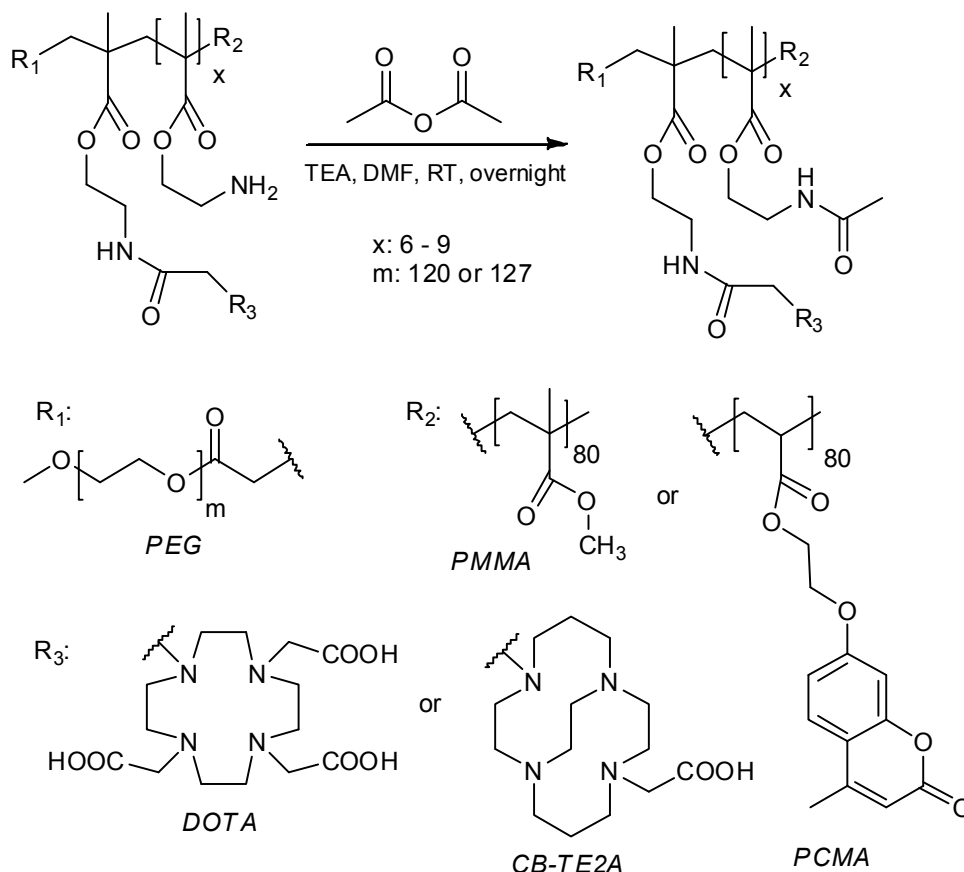
It was attempted to remove the EDTA carry-over. Ultrafiltration is a method in which hydrostatic pressure forces liquid through a semipermeable membrane. The pores in the membranes can be tuned to allow the passage of small molecular solutes but not nanoparticles. Such a system is available in the form of Amicon Ultra 4 centrifugal filters, where the pressure gradient is obtained by placing the device in a centrifuge. 1 mL of micelle dispersion was concentrated 5 times in this way and subsequently radiolabeling was attempted. Not much improvement was seen. After 1.5 hours at RT only an EDTA peak was observed on Radio-TLC, while after a further 3 hours at 95 °C, 16% activity was found to have shifted to **Peak 1**. Accordingly, this was not a suitable way of removing EDTA. It was tried to switch to a different type of dialysis tubing which was benzoylated (Sigma Aldrich, D 2272). This tubing is meant to exhibit smaller pore sizes, but it was thought that the lower polarity of the membrane would prevent adherence of EDTA, in case this was the reason why it was not removed during dialysis. It did not change anything significantly.

For the reasons specified above, EDTA was removed from the purification of the unimers. After this was done, EDTA was no longer observed during the radiolabeling experiments.

3.3.2 Unspecific binding of DOTA and capping

After EDTA had been eliminated from the formulation, it was attempted to label 100% DOTA micelles (PEG-PAEMA-PMMA) again. In the first attempt, micelles were incubated with ⁶⁴Cu-acetate for 2 hours at pH 5.5 (**procedure G**). This resulted in 58% activity in **Peak 1** and 35% in **Peak 2**, a great improvement. However, when analyzing **Peak 2** it was observed that the activity to a large extent eluted with an R_f that corresponded with ⁶⁴Cu-DOTA. In accordance with the observations for EDTA mentioned above, DOTA was thought to adhere to the micelles by the formation of salt bridges. The presence of DOTA indicated, as had the monitoring by MALDI-TOF, that during the DOTA conjugation to the unimer,

Scheme 3.5 - Capping of free amines on PAEMA micelles



small amounts of free DOTA were present after the reaction. When PEG-PAEMA-PMMA/PEG-PHEMA-PMMA (9:1, 10% DOTA) micelles were attempted labeled, DOTA carry-over was also observed. After 2 hours stirring at RT, about 25% was associated with micelles (peak at starting line at Radio-TLC), the rest appeared in a ^{64}Cu -DOTA peak.

Two strategies were devised for removing carry-over DOTA from the formulations. The first of these was dialyzing the reaction mixture after DOTA conjugation at pH \approx 4. Three fresh media (Milli-Q water) were added at pH 4, followed by three additions at neutral pH. According to the hypothesis of the formation of salt bridges, this would prevent DOTA carry-over by protonating the carboxylic acids on the DOTA chelator. This was indeed observed to remove DOTA. When these micelles were labeled, only 3% of total activity was seen to be associated with DOTA and when separated by SEC, 81% emerged in **Peak 1** and 10% in **Peak 2**.

Table 3.4 – Unspecific binding of $^{64}\text{Cu}^{2+}$ and scavenging. Notice that free ^{64}Cu does not elute, meaning that micelles that were not scavenged and were not chelator-conjugated did not give rise to a **Peak 2**.

Entry	Micelle	Incubation	Scavenger	Peak 1	Peak 2
1	PEG-PAEMA-PMMA	2 h, RT	None	8%	-
2	PEG-PHEMA-PMMA	4 h, RT	None	3%	-
3	PEG-PAEMA-PCMA	2 h, RT	None	20%	-
4	PEG-PAEMA-PCMA	4 h, 60 °C	None	30%	-
5	PEG-PAEMA-PCMA	2 h, RT	DTPA, 10 min	3%	87%
6	PEG-PAEMA-PMMA (100% DOTA), un-capped	2 h, RT	DTPA, 15 min	42%	49%
7	PEG-PAEMA-PMMA (100% DOTA), capped	2 h, RT	DTPA, 15 min	77%	9%
8	PEG-PAEMA-PCMA	2 h, RT	EDTA, 20 min	1%	92%
9	PEG-PHEMA-PCMA	3h, 80 °C	None	17%	-
9	PEG-PHEMA-PCMA	3h, 80 °C	EDTA, 20 min*	8%	87%

*Allowed to cool to room temperature while incubating for 20 min with EDTA.

The other strategy was to cap the free amines remaining after DOTA conjugation. In addition to removing the DOTA, this would have the added benefit of removing positive charges from the PMs, which are known to cause undesirable nanoparticles pharmacokinetics [354]. For this reason, capping was introduced in the preparation of chelator conjugated micelles. Initially, it was attempted to cap amine-exhibiting micelles in aqueous dispersion directly. This was done by adjusting the pH of the dispersion to 9.5 followed by addition of N-succinimidyl N-methylcarbamate. By freeze-drying the micelles and subjecting them to a Kaizer test [355] it was shown that the capping had worked and that no free amines were present. As it was deemed easier, capping was subsequently done immediately after DOTA conjugation, as a one-pot synthesis in DMF, by adding acetic anhydride (see **scheme 3.5** and **procedure C**). Capping almost completely abolished the presence of DOTA and provided good labeling results.

3.3.3 Unspecific binding of ^{64}Cu and DTPA/EDTA challenge

When radiolabeling PMs, some researchers have taken precautions against unspecific binding of ^{64}Cu , through end-process scavenging by addition of DTPA [11, 115, 330, 331] or EDTA [258, 356], while others have not [357]. Incubation time with DTPA/EDTA was 5-10 minutes. In our formulations, $^{64}\text{Cu}^{2+}$ could be non-specifically bound by **1**) association with the ether oxygens of the PEG layer or **2**) with the alcohols of the PHEMA block or **3**) with the amines on the PAEMA block. Importantly, this issue was addressed relatively late in the work meaning that all the preliminary investigations mentioned above, were *not* subjected to scavenging of any kind, meaning that micelle associated activity in **Peak 1** can be lower than it appears by 5-20%. All later formulations were scavenged by DTPA or EDTA.

The micelles were tested for non-specific binding (**table 3.4**). As can be seen, non-specific binding is a very relevant concern. It appears especially important with free amine containing unimers (entry **1, 3** and **4**). Addition of DTPA is seen to lower non-specific binding from a level of 20% to a level of 3%. It should be noted that all of the references cited above simply state that they add a scavenging chelator, not how much activity they expect to be non-specifically bound. In our method, 50 μmol scavenger (DTPA/EDTA) was added. For reference, 500 MBq of ^{64}Cu corresponds to 0.055 nmol. The specific activity of our ^{64}Cu (1 TBq/mmol) makes this number ~ 0.5 nmol). There was some evidence that high temperature increased unspecific labeling. Compare **entries 3** and **4** and **entries 2** and **9**.

When radiolabeling micelles with conjugated chelators, unspecific binding may not be as high as for micelles without conjugated chelators. When the former are incubated with ^{64}Cu for 2 hours (DOTA) or 3 hours (CB-TE2A, see below), much of the activity enters the chelators, thus diminishing the fraction available for unspecific binding. However, in subsequent experiments with scavenging, it was always observed that some activity was DTPA or EDTA associated. This indicated that either nonspecific binding always occurred, or that the scavengers retrieved activity from DOTA and CB-TE2A. In the case of CB-TE2A the latter seems unlikely though, due to great differences in thermodynamic stability. Nonspecific binding could arise due to a finite number of sites available on the micelles for nonspecific binding. In that case, the ratio of nonspecifically bound ^{64}Cu would decline as more activity was employed. In addition, other factors that would influence nonspecific ^{64}Cu -binding are other non-radioactive metal ion contaminants that may occupy such sites and/or components of the formulation, including added salts.

Initially, DTPA was employed as ^{64}Cu -scavenger. However, as the thermodynamic stability difference between DTPA [**358, 359**] and DOTA [**358, 360**] is only 1-2 orders of magnitude, it was decided to use EDTA [**359**] instead, where the difference is greater (about 4 orders of magnitude). Some indication that DTPA could extract activity from DOTA where observed. In addition, in the TLC Eluant system that was used as standard (H_2O -MeOH (1:1) w. 5% NH_4OAc), ^{64}Cu -EDTA eluted with an agreeable R_f of 0.73, while it proved difficult to find a system where ^{64}Cu -DTPA eluted.

It should be noted that when un-capped micelles are used, that is, micelles with free amines, it is possible that the chelators used as scavengers can adhere to the micelles themselves via salt-bridges. As EDTA only has six coordination sites, while DTPA as eight (3 amines and 5 carboxylic acids) it is possible that such an effect could be more pronounced for DTPA.

TABLE 3.5 – Labeling and aggregation of CB-TE2A PMs at elevated temperature.

Entry	Micelle	Scavenger	Incubation	Peak 1	Peak 2
1	PEG-PAEMA-PMMA (100% CB-TE2A), uncapped.	None	95 °C, pH 7	<i>Aggregation</i>	
2	PEG-PAEMA-PMMA (100% CB-TE2A), uncapped.	None	2h, 80 °C, pH 5.5.	82%	13%
3	PEG-PAEMA-PMMA/PEG-PHEMA-PMMA (10% CB-TE2A) uncapped.	None	95 °C, pH 5.5	<i>Aggregation</i>	
4	PEG-PAEMA-PMMA/PEG-PHEMA-PMMA (10% CB-TE2A) uncapped.	None	80 °C, pH 5.5	<i>Aggregation</i>	
5	PEG-PAEMA-PMMA/PEG-PHEMA-PMMA (10% CB-TE2A) uncapped.	None	80 °C, pH 7	<i>Aggregation</i>	
6	PEG-PAEMA-PMMA/PEG-PHEMA-PMMA (10% CB-TE2A) uncapped.	None	3h, 60 °C, pH 5.5.	45%	5%
7	PEG-PAEMA-PMMA/PEG-PHEMA-PMMA (10% CB-TE2A), uncapped	EDTA	3h, 60 °C, pH 5.5.	48%	48%

3.3.4 Labeling of CB-TE2A micelles and precipitation at elevated temperatures

The radiolabeling of CB-TE2A micelles shared many of the same experiences that were made in the labeling of DOTA micelles. However, a further aspect was added in that it is necessary to label CB-TE2A with ⁶⁴Cu at elevated temperature.

Initially, it was desired to follow a slightly modified (pH 7 instead of 8) published nature protocol [201] and label at 95 °C for 2 hours (an isotonic PIPES buffer was used). It had previously been observed that PEG-PAEMA-PMMA(DOTA) micelles were stable at such temperatures (see **section 3.3.1**). The first formulation that was tried was uncapped PEG-PAEMA-PMMA(CB-TE2A100%). Heating of this formulation consistently caused immediate precipitation of visible, copious aggregate. The concentration of micelle material during the attempted radiolabeling was 4-5 mg/mL. Halving this concentration still resulted in aggregation. Aggregation occurred regardless of heating speed. As DOTA-conjugated micelles had been previously heated to 95 °C without problems, it seemed that conjugation of CB-TE2A introduced instability at elevated temperature. It was speculated that aggregation could be caused by initial localized evaporation (to be deposited as condensate inside the lid of the vial) in the top of the dispersion. However, enabling slow homogenous heating (e.g. by raising it and covering in aluminum foil) did not solve the problem, nor did the use of a smaller vial with a smaller surface area. It appeared to be an intrinsic temperature-related instability in the micelles. Accordingly, it was

decided to lower the temperature of the labeling to 80 °C. At this temperature, the micelles could be stirred for > 3 h without visible aggregation. At the same time the buffer was changed to NH_4OAc (0.1 M, pH 5.5) – the same buffer used in DOTA labeling. Similar conditions were used by Seo *et al.* [39]. This resulted in good labeling as seen in **table 3.5 (entry 2)** (notice that some of these labelings were early experiments *without* scavenging).

When a PEG-PAEMA-PMMA/PEG-PHEMA-PMMA (10% CB-TE2A, uncapped) formulation was incubated at 95 °C, visible aggregation was observed again (**entry 3, table 3.5**). It was attempted to radiolabel this formulation at 80 °C, but precipitation was seen both at pH 7 (PIPES) and pH 5.5 (NH_4OAc) (**entry 4 and 5**). It seemed that PEG-PHEMA-PMMA introduced an increased tendency of aggregation at high temperature. It was attempted to incubate the formulation at 60 °C, which was observed to *not* cause aggregation. Incubation at 60 °C with ^{64}Cu for 3 hours gave a radiolabeling (**Peak 1**) at 45% (no scavenging), which is higher than the non-specific binding seen previously (**table 3.4**). This indicated that labeling was indeed taking place. Large amounts (~50%) of activity remained on the column in this experiment, characteristic of non-incorporated ^{64}Cu , indicating that full labeling did not take place under these conditions (**entry 6**). The same formulation was radiolabeled with EDTA scavenging giving 48% in **Peak 1**, with no activity stuck to the column (**entry 7**).

So far, the results discussed above have only concerned PMMA-type micelles. PCMA-type micelles were also conjugated with CB-TE2A and radiolabeled. PEG-PAEMA-PCMA was prepared with 10% CB-TE2A and capping. This formulation was observed to be entirely unstable at 60 °C, exhibiting rapid massive aggregation. At this point it was clear that capped PCMA-type micelles were unstable when heated even to 60 °C. For this reason the idea of radiolabeling CB-TE2A-conjugated PEG-PAEMA-PCMA micelles was abandoned. As it turned out however, CB-TE2A conjugated PEG-PHEMA-PCMA micelles fared well and were eventually tested in animals (**section 3.8**).

It quickly was apparent that certain unimer types were unstable and tended to aggregate when heated. In addition to the observation on CB-TE2A micelles, it was noted that capped PEG-PAEMA-PMMA/PEG-PHEMA-PMMA (10% DOTA) micelles aggregated at 60 °C, whereas uncapped identical micelles did not. In addition, such capped DOTA micelles aggregated a lot slower (after about an hour some aggregation was seen) than corresponding uncapped CB-TE2A micelles (massive aggregation after about 10 minutes) at even higher temperatures.

In conclusion, from the observations above, it seemed that thermostability of micelles is a general issue to be dealt with. It seemed that free amines in the B-region stabilized the micelles to heating, and that CB-TE2A made the micelles less stable than did DOTA.

3.3.5 Localization of the “high fractions”

For the animal studies to come, it was important only to use the most concentrated fractions eluted from the size-exclusion column. This was because the volume to be injected into mice is limited, with 0.2 mL per injection per mouse being the norm. In addition, it was desired to inject mice with a standardized amount of micelle material (0.2 mg), requiring a standard concentration of about 1 mg/mL (1 mg/mL * 0.2 mL = 0.2 mg). For this reason it was important to have plenty of activity in the used micelle fractions, so that the adequate dilutions could be made. The two fractions (1 mL in total) with the highest concentration of both activity and micelle material were termed the “high fractions” (fig. 3.7).

Micelle dispersion eluted from the column in fractions of 0.5 mL. The fractions making up **Peak 1** were collected and analyzed. **Peak 1** eluted over approx. 6 fractions (6 * 0.5 = 3 mL). Radioactivity in each fraction was measured, as well as count rate and size by DLS. The results are seen in **table 3.6**.

The results showed a few interesting things. First, the two high fractions were found to be **fraction 2** and **3** after the onset of **Peak 1**. These two fractions were very similar in concentrations and were profoundly more concentrated than the other fractions, usually containing 55-70% of the total activity present in Peak 1 (70% in **table 3.6**). Furthermore, the presence of micelles in **Peak 1** was verified both through size, where accurate measurements of about 30 nm was found. Micelle presence was also confirmed by the count rate, which correlated beautifully with the concentration of activity. It is thus reasonable to infer that when concerning the activity in **Peak 1**, activity and micelle material concentration can be assumed to be identical. Later UV results indicated that almost all micelle material eluted in **Peak 1**, see **section 3.5**.

TABLE 3.6 – Localization of the high fraction. Notice that the size measured in fraction 1 was an outlier, likely due to the low count rate.

Fraction	Time*	Activity	Count rate (keps)	Size	% of totals (activity/count rate)
1	24:52 – 26:25	1%	40.8	51.1	2% / 3%
2 (high)	26:25 – 28:25	17%	466.5	29.3	32% / 35%
3 (high)	28:25 – 30:20	20%	492	28.3	38% / 37%
4	30:20 – 32:25	9%	206.5	32.5	17% / 15%
5	32:15 – 34:15	4%	90.1	30.3	8% / 7%
6	34:15 – 36:05	2%	36.5	27.2	4% / 3%
Total	-	53%	1332.4	-	100% / 100%

* Time given as minutes after start of elution program

3.4 Cross-linking

Cross-linking of the PCMA micelles was done by UV irradiation. Normally, 1.1 mL micelle dispersion was irradiated at 2 W/cm² (320 < λ < 500 nm) in a 4 mL glass vial under intense stirring. The UV probe was placed about 1.5 cm from the water surface.

Initial experiments with crosslinking were carried out on very dilute dispersions, as was reported by Kumar *et al.* (submitted results). 16 μL PEG-PAEMA-PCMA micelle dispersion (5.6 mg/mL) was mixed with 2985 μL Milli-Q water in a quartz cuvette, for a concentration of 5.6*(16/3001) = 0.03 mg/mL. This mixture was irradiated without stirring giving the results shown in **figure 3.8**. The *degree of cross-linking* (%CL) was calculated by measuring the absorbance at 320 nm, $(A_{\text{before}} - A_{\text{after}})/A_{\text{before}} = \%CL$. In line with observation by Kumar *et al.* it was found that dilute dispersions could be cross-linked to a high degree in a relatively short time (80 %CL in 10 minutes).

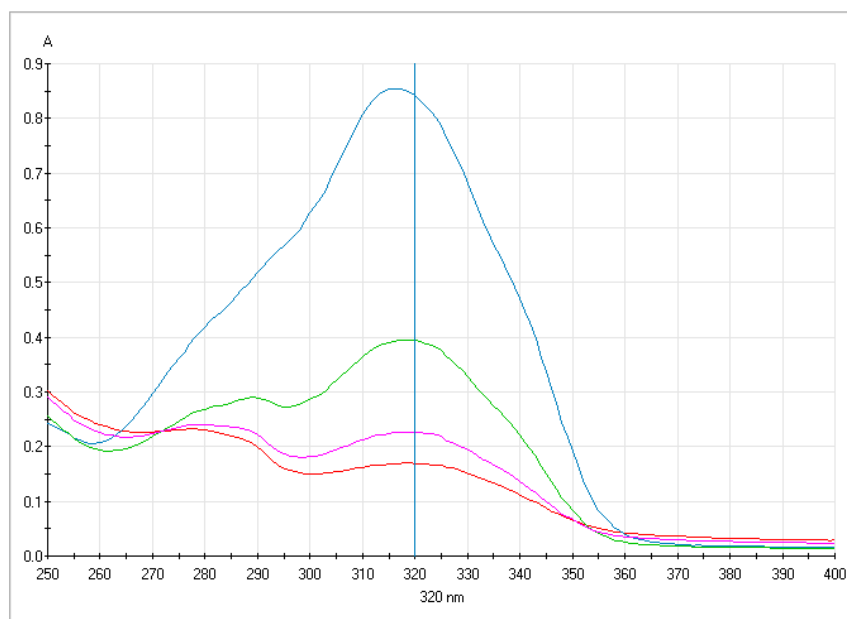


Figure 3.8 Cross-linking of a dilute micelle dispersion. A micelle dispersion of 0.03 mg/mL was crosslinked for 2 (green), 6 (pink) and 10 minutes (red). An absorption spectrum was recorded before (blue) and after the irradiations. %CL values were found to be 2 min: 53%, 6 min: 73%, 10 min: 80%.

Cross-linking of PEG-PAEMA-PCMA (10% DOTA, capped) micelles at higher concentration (~5 mg/mL) was attempted. In general, UV measurements were done in double and if the deviation between the two measurements was less than 5% the average value of the two was used. Micelle dispersions were diluted with Milli-Q water. The micelles were irradiated in “blocks” of 5 minutes continuous irradiation up to a total irradiation time of 15 minutes (**fig. 3.9**). It was clear that concentrated dispersions needed significantly longer irradiation times than dilute dispersion. 5 minutes irradiation resulted in a 36%CL while 10 minutes resulted in 44%. When irradiated for 15 minutes, *visible aggregation* was observed in the mixture. Size measurements were conducted after each irradiation block, giving: $t = 0$: 40 ± 5 nm (-4.3 mV), $t = 5$: 34 ± 1 nm (-1.4 mV), $t = 10$: 46 ± 5 nm (-3.0 mV). The increase in size at continued exposure to UV light was repeatedly observed. It seemed that irradiation caused slow aggregation culminating in visible precipitation of micelle material after about 15 minutes of irradiation at room temperature. As it had been found that increases in temperature could prompt the aggregation of micelles, especially capped micelles (**section 3.3.4**), it was hypothesized that local energy deposition

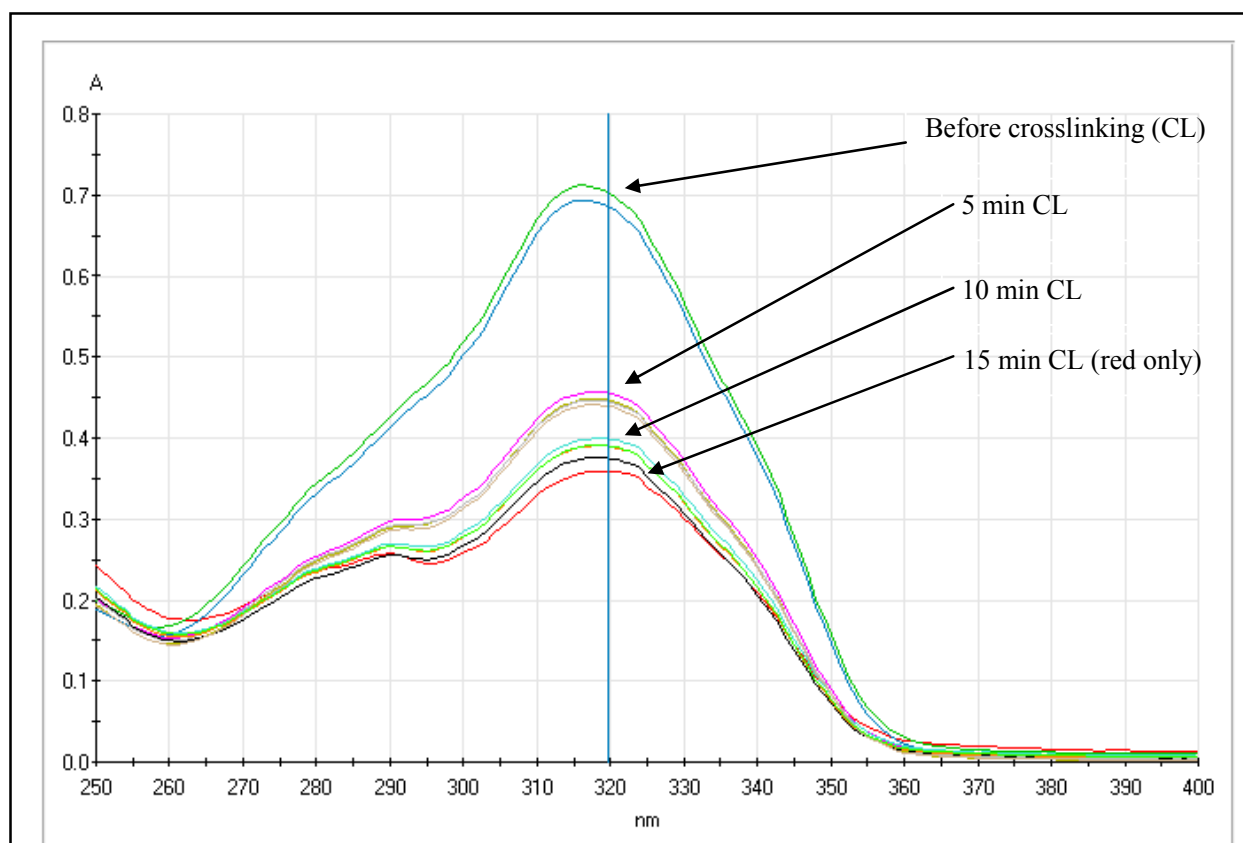


Figure 3.9 – Crosslinking of micelles at room temperature. Micelles were irradiated for 5, 10 and 15 minutes. Respectively resulting in 36%CL, 44%CL and *visible aggregation*.

TABLE 3.7 – Overview of crosslinking degrees. All depicted experiments were exposure of 1100 µL micelle dispersion at 5-7 °C. Data are given as: *size (PDI)*, *zeta pot.* n = 3 in all cases.

Type	Conc.	t = 0	t = 10	t = 20	t = 30
PEG-PAEMA-PCMA (10% DOTA, capped)	5.0 mg/mL	41±1 nm (0.12±0.01) -1.7±1.1mV 0% CL	40±4 nm (0.122±0.019) -6.14±0.58 mV 28% CL	38±2 nm (0.122±0.019) -9.26±0.45 mV 36% CL	48±3 nm (0.135±0.012) -8.55±0.40 mV 43% CL
PEG-PAEMA-PCMA (10% DOTA, capped)	4.8 mg/mL	39±5 nm (0.07±0.02) -4.3±0.5mV 0% CL	-	-	41±8 nm (0.092±0.038) -4.2±0.6mV 39% CL
PEG-PAEMA-PCMA /PEG-PHEMA-PCMA (10% CB-TE2A, capped)	*	25±2 nm (0.18±0.02) -3.4±0.7mV 0% CL	-	-	21±1 nm (0.24±0.02) -3.3±0.3mV 45% CL
PEG-PHEMA-PCMA (100% DOTA)	4.2 mg/mL	23±1 nm (0.15±0.01) -2.1±0.7mV 0% CL	-	-	18±1 nm (0.20±0.01) -2.3±0.4mV 42% CL
PEG-PHEMA-PCMA (100% CB-TE2A)	3.9 mg/mL	21±1 nm (0.17±0.02) -3.8±0.7mV 0% CL	-	-	21±1 nm (0.17±0.01) -3.5±0.3mV 45% CL

* Due to the presence of two different unimers, assessment of concentration was difficult, but is expected to be 4-5 mg/mL.

due to the irradiation could increase the temperature enough to cause precipitation.

CB-TE2A micelles (10%, PEG-PAEMA-PCMA, capped) were also cross-linked. Initially for 5 minutes at room temperature. This caused visible aggregation, underpinning the thermo-instability of CB-TE2A conjugated micelles when compared to DOTA micelles. As a result, it was attempted to cross-link the micelles at constant room temperature. The glass vial was placed in a water bath during irradiation. This solved the problem to some degree, although the CB-TE2A micelles still showed instability. 5 and 10 minutes of irradiation resulted in %CL of, respectively, 29% and 37%. However, there was also an increase in size, t = 0: 35±2 nm (-3.71 mV), t = 5: 53±5 nm (-5.71 mV), t = 10: 61±4 nm (-0.15 mV). This instability made CB-TE2A micelles unsuitable for UV-crosslinking at available conditions.

As it had been observed that temperature control was a crucial factor in preventing micelle aggregation, cross-linking at *decreased temperature* was tried. The glass vial was placed in an ice-bath, which was kept at 5-7 °C. Crosslinking at this temperature completely abrogated any problems of aggregation. Cross-linking results are seen in **table 3.7**.

PEG-PAEMA-PCMA (10% DOTA. capped) micelles were crosslinked. Exposure of 1100 µL micelle dispersion (ca. 5 mg/mL) to UV light for 30 minutes led to a general degree of crosslinking of $39 \pm 3 \%$ (n = 5). The degree of cross-linking obtained was relatively consistent. In **table 3.7**, top entry, is seen the development in %CL as the 30 min irradiation procedure progressed. %CL rose rapidly initially and then proceeded to a flatter curve. A reason for this can be speculated to be, besides the simple decrease in number of crosslinkable units, an increase in distance between non-crosslinked coumarin moieties. Thus, crosslinking becomes a compromise between achieving high %CL and low exposure to potentially damaging UV light. Generally, a %CL of about 40% was aimed for, as this should give a coherent micelle. There is the possibility that two coumarin moieties on the same unimer inter-crosslink. It has not been possible to find studies on the tendency for this to happen. However, at around 40%CL there should be a significant amount of crosslinking between individual unimers.

3.5 Quantification of micelle material in dispersion

The obvious method of quantifying micelle material was freeze-drying an aliquot of the dispersion and weighing the resulting dry substance. This method was ideal when large amounts of dispersion were available, as at least 5 mg of dry material should be weighed in order to prevent large inaccuracies. Often however, only small amounts were available. As coumarin absorbs UV radiation, a method based on this was investigated.

By accurately determining the concentration of micelle material by freeze-drying, a standard curve was made (fig. 3.10). This showed a good linear correlation with apparent intercept at (0,0) in relevant measurement ranges, showing a proportional relationship between concentration of micelles and absorbance by coumarin (as could be expected). This makes it possible to assess micelle material concentration through a one-point correlation. It is important to note that a given standard curve can only be used for one batch/length of PCMA block, as the number of coumarin moieties and their potential interactions in the micelle core are not accurately known. Therefore, when micelles from other syntheses, with other coumarin lengths (such as PEG-PHEMA-PCMA) were measured, the initial concentration was determined by freeze-drying after which an absorbance was measured. The concentration in diluted dispersions could then be determined based on the ratio with the absorbance of the original dispersion.

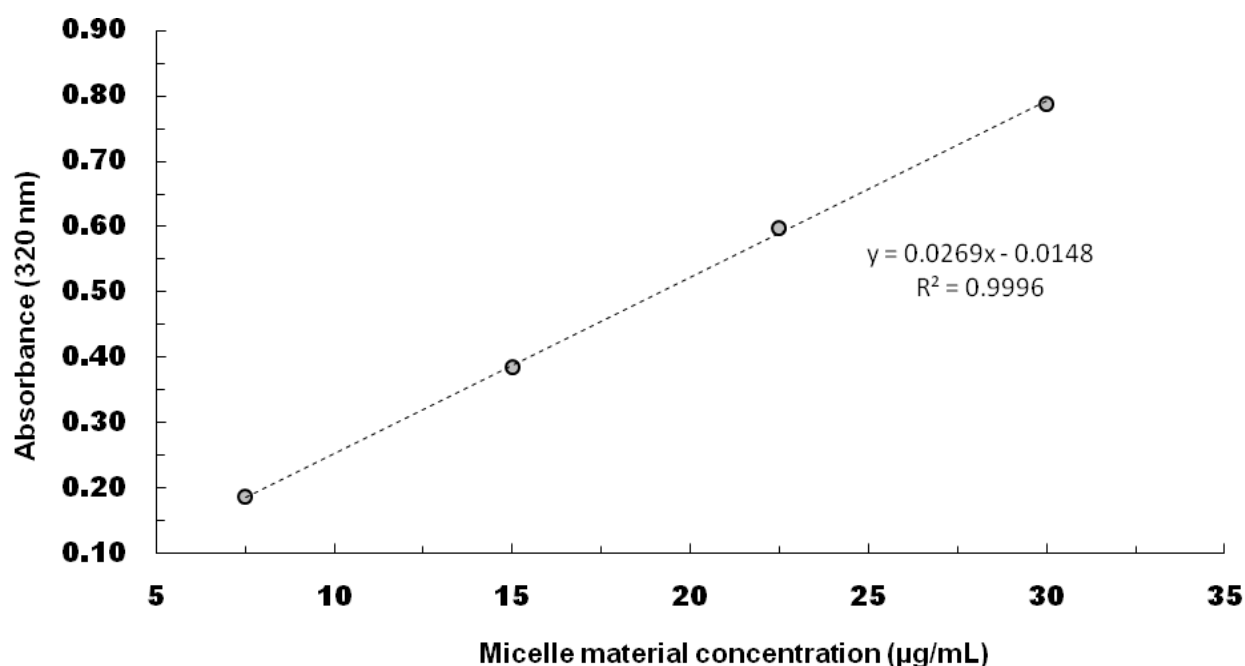


Figure 3.10 – Standard curve of absorbance of micelles in dispersion at 320 nm. If the intercept is set to (0,0), the equation becomes: $y = 0.0262x$ ($R^2 = 0.9989$).

TABLE 3.8 – Overview of selected radiolabeled formulations. 0.05 µmol scavenger was added. In case of a heated radiolabeling, the mixture was allowed to cool to RT during the scavenging period. All CB-TE2A micelles were heated to 80 °C for 3 hours unless otherwise noted. DOTA micelles were labeled for 2 hours at RT. A “high activity run” was conducted with activity > 350 MBq and some radiolysis could thus be expected – the products appearing in **peak 2**.

Entry	Micelle	Scavenger	Peak 1 (high)	Peak 2	Comments / CL
1	PEG-PAEMA-PMMA (100% DOTA) Un-capped	DTPA, 15 min	42% (-)*	49%	-
2	PEG-PAEMA-PMMA (100% DOTA) Capped	DTPA, 15 min	77% (-)*	9%	-
3	PEG-PAEMA-PMMA/PEG-PHEMA- PMMA (10% DOTA), capped	DTPA, 20 min	77% (44%)	17%	-
4	PEG-PAEMA-PMMA/PEG-PHEMA- PMMA (10% DOTA), uncapped, <i>pH</i> <i>4 dialysis</i>	DTPA, 30 min	45% (26%)	41%	-
5	PEG-PAEMA-PMMA/PEG-PHEMA- PMMA (10% CB-TE2A), uncapped, 3h at 60 °C.	EDTA, 20 min	48% (31%)	48%	-
6	PEG-PAEMA-PMMA/PEG-PHEMA- PMMA (10% DOTA), capped	EDTA, 20 min,	80% (49%)	11%	High-activity run
7	PEG-PAEMA-PMMA/PEG-PHEMA- PMMA (10% DOTA), capped	EDTA, 20 min,	64% (39%)	24%	High-activity run
8	PEG-PAEMA-PMMA/PEG-PHEMA- PMMA (10% DOTA), capped	EDTA, 20 min,	17% (10%)** <i>Used in-vivo</i>	62%	High-activity run %CL: 45% (RT)
9	PEG-PAEMA-PMMA/PEG-PHEMA- PMMA (10% DOTA), capped	EDTA, 20 min,	47% (26%)	38%	High-activity run %CL: 36% (RT)
10	PEG-PAEMA-PMMA/PEG-PHEMA- PMMA (10% DOTA), capped	EDTA, 20 min,	56% (31%) <i>Used in-vivo</i>	22%	High-activity run %CL: 39% (5-7 °C)
11	PEG-PAEMA-PMMA/PEG-PHEMA- PMMA (10% DOTA), capped	EDTA, 20 min,	69% (34%) <i>Used in-vivo</i>	12%	High-activity run
12	PEG-PAEMA-PMMA/PEG-PHEMA- PMMA (10% DOTA), capped	EDTA, 20 min,	44% (31%)	48%	High-activity run
13	PEG-PAEMA-PMMA/PEG-PHEMA- PMMA (10% DOTA), capped	EDTA, 20 min,	65% (42%)	18%	High-activity run
14	P-PH-PC /P-PA-PC (10% CB-TE2A)	EDTA, 20 min,	71% (46%)	22%	%CL: 45% (5-7 °C)
15	P-PH-PC (5% CB-TE2A)	EDTA, 20 min,	47% (30%) <i>Used in-vivo</i>	42%	%CL: 45% (5-7 °C) High-activity run
16	P-PH-PC (5% DOTA)	EDTA, 20 min,	60% (34%) <i>Used in-vivo</i>	23%	%CL: 42% (5-7 °C) High-activity run

* Not measured, **crosslinked at RT for 10 minutes – aggregation may prevent radiolabeling.

3.6 Compilation of labeling results at established conditions

In **table 3.8** is seen a compilation of selected radiolabeling micelles. The purpose is to show in which yield ranges labeling generally took place. As with most radiochemistry, variation was relatively large and generalizations were tough to make. All results are for capped micelles, except **entry 4**, and a scavenger was added in all cases. All formulations were labeled according to the standardized **procedures G** for DOTA micelles, and **H** for CB-TE2A micelles.

In the high-activity runs (350-600 MBq), to be seen as pilot experiments preparing for animal studies, size and charge of the high fraction were often measured after activity had decayed. In **entry 6 (table 3.8)** the micelles after labeling were: 27 ± 1 nm, -2.21 ± 0.57 mV (before labeling 26 ± 4 nm (-2.9 ± 1.0 mV)). Similar observations were routinely made and accordingly, it was concluded that high activity labeling at 500 MBq for 2 hours did not compromise micelle integrity (see **section 3.7** and **3.8**).

Comparing the first seven entries in **table 3.8**, it appears that there is a tendency for capped micelles to provide higher labeling efficiencies. This may be because uncapped amines cause higher unspecific binding, which is taken up by the scavenger and elutes in **Peak 2**. In addition, it seems that cross-linked micelles generally show lower, though still acceptable, labeling efficiencies. Especially **entry 8**, which was cross-linked at room temperature (44%CL), causing some aggregation (mentioned in **section 3.4**), with an increase in size to 46 nm, showed poor labeling. It may be that cross-linking, and in particular slight aggregation, restricts access to the chelators. Curiously, this exact formulation was tested *in-vivo* (**CL-1, section 3.7**) and showed impressive tumor accumulation.

3.7 Animal studies with PEG-PAEMA-PCMA micelles – CL versus NonCL

The culmination of the development work described in the previous sections of this chapter was animal studies. The two original frames for *in-vivo* investigation was 1) comparing the pharmacokinetics of crosslinked vs. non-crosslinked micelles, and 2) comparing the pharmacokinetics of DOTA vs. CB-TE2A conjugated micelles. However, as was described previously, CB-TE2A conjugated PEG-PAEMA-PCMA micelles suffered from gross thermoinstabilities, ruling out the use of such nanoparticles. Instead PEG-PHEMA-PCMA PMs would be used for CB-TE2A conjugation (**section 3.8**).

Therefore, focus was first on crosslinked (CL) vs. non-crosslinked (NonCL) micelles. PEG-PAEMA-PCMA (10% DOTA, capped) was the micelle type of choice, for reasons already explained. Three formulations were used. Their relevant data can be seen in **table 3.9**, along with their code designations (CL-1, CL-2, NonCL-2, CL-3 and NonCL-3).

While **Run 1** (CL-1) was meant as a pilot, **Run 2** (CL-2 and NonCL-2) and **Run 3** (CL-3 and NonCL-3) differed in the type of tumor xenografts the mice were carrying. In **Run 2**, small pieces of tumor were implanted, while in **Run 3** (as well as **Run 1**), individual cells were implanted.

The concentration of micelle materials (*mic. mat. conc.*) given in **table 3.9** was based on UV determination of the coumarin content as described in **section 3.5**. Through multiple analyses of the high fractions by UV, it had been established that slightly less than half (about 46%) of the applied micelle material eluted in the high fraction (1 mL). As the standard concentration in PEG-PAEMA-PCMA formulations was 5 mg/mL and 400 μ L (2 mg) was radiolabeled (**procedure G**), this meant that the concentration of micelle material in the high fraction was about 0.9 mg/mL. This value correlated

TABLE 3.9 – Physicochemical properties of PEG-PAEMA-PCMA (10% DOTA) *in-vivo* formulations. n equals 3 in all cases. The labeling efficiency is the activity in peak 1. The “high fraction” is shown in parenthesis.

	CL-1 (<i>pilot</i>)	CL-2	NonCL-2	CL-3	NonCL-3
Size (<i>nr. weighted</i>)	46 \pm 5 nm	41 \pm 8 nm	40 \pm 5 nm	43 \pm 4 nm	37 \pm 1 nm
PDI	0.12 \pm 0.02	0.09 \pm 0.04	0.07 \pm 0.02	0.11 \pm 0.02	0.12 \pm 0.01
Zeta-pot.	- 3.0 \pm 0.5 mV	- 4.2 \pm 0.6 mV	- 4.3 \pm 0.5 mV	- 6.0 \pm 1.2 mV	- 2.8 \pm 1.7 mV
Cross-linking	44%	39%	NA	38%	NA
Labeling efficiency	17% (10%)	56% (31%)	69% (34%)	67% (42%)	44% (31%)
Mic. mat. conc.	\sim 1.0 mg/mL	1.0 mg/mL	1.0 mg/mL	1.0 mg/mL	1.0 mg/mL

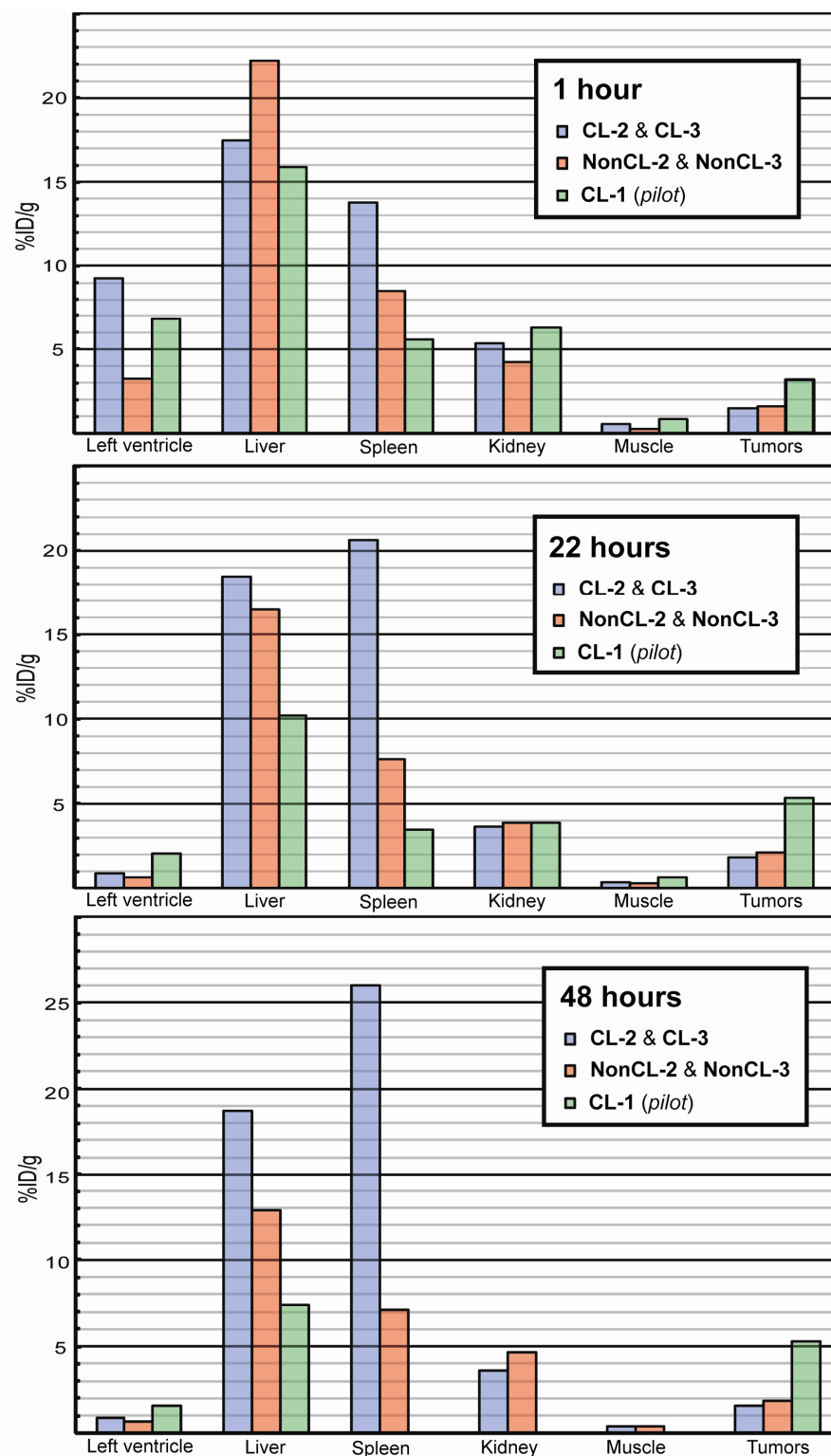


Figure 3.11 – Tissue accumulation of PEG-PAEMA-PCMA (10%DOTA) micelles, cross-linked (CL) and non cross-linked (non-CL). The figure shows accumulation at 1, 22 and 48 h. In the 48h figure, CT scans were not conducted for CL-1 (*pilot*) making it impossible to quantify spleen, kidney and muscle.

acceptably with the ratio of the high fraction to the entire micelle-associated activity and indicated that nearly all the micelle material emerged in the micelle peak, and consequently that radiolysis did not seem to be a major problem.

After radiolabeling, the contents of the high fraction were diluted with unlabeled (“cold” micelles) in PIPES/NaCl buffer to a micelle material concentration of about 1.0 mg/mL and 66-72 MBq/mL. In addition, the actual concentration of the high fraction was determined by UV measurement as soon as the activity had decayed. These calculations are shown in **table 3.10**. 200 µL of the resulting dispersion was injected into xenographted NMRI mice, resulting in an injection of about 0.2 mg polymer material (~8 mg/kg at an average mouse weight of 25 g). The injected activity was normally slightly above 10 MBq per mouse. A certain amount of nanoparticles is cleared by macrophages immediately upon injection [148, 150]. This is thought to be because of opsonization [149, 151]. For this reason, it is necessary to inject an appreciable amount of micelle material, as trace amounts would be cleared. For lipid nanoparticles (liposomes) the lower limit of dose-independent pharmacokinetics has been found to be about 2 µmol/kg (~2 mg/kg) [148]. In previous studies with polymeric micelles in mice have been used 3-5 mg/kg [11, 115] and 10 mg/kg [82, 142]. This suggests that 8 mg/kg is within the window of dose independent pharmacokinetics.

TABLE 3.10 – Dilution of formulations to 1 mg/mL for animal studies. H.F. is high fraction. The high fraction was diluted with “cold” micelles to a total volume of 1400 or 1600 µL.

	CL-1 (<i>pilot</i>)	CL-2	NonCL-2	CL-3	NonCL-3
Conc. main vial	4.8 mg/mL	4.8 mg/mL	4.8 mg/mL	5.0 mg/mL	5.0 mg/mL
Abs. main vial*	-	0.385 [†]	0.631	0.435 [†]	0.701
Activity in H.F.	37 MBq	160 MBq	194 MBq	200 MBq	145 MBq
Nr. of mice	4	6	6	6	6
Dilution to	No dilution	1400 µL	1400 µL	1600 µL	1600 µL
Diluted with		1.1 mg/mL	1.1 mg/mL	1.0 mg/mL	1.0 mg/mL
High/cold		665/735	621/779	(NA)	(NA)
Abs. H.F.**	Not done	0.064 (0.127)	0.097 (0.194)	0.090 (0.179)	0.133 (0.266)
Meas. conc. H.F		0.8 mg/mL	0.7 mg/mL	1.0 mg/mL	1.0 mg/mL
Final conc	~ 0.7 – 1.0 mg/mL	1.0 mg/mL	0.9 mg/mL	1.0 mg/mL	1.0 mg/mL,
Final activity	37 MBq	97 MBq	100 MBq	120 MBq	118 MBq

* 15 µL diluted to 3000 µL, ** Measured as 30 µL diluted to 3000 µL (in parenthesis) – corrected to 15 µL., *** The main micelle dispersion was diluted to 1.0 mg/mL with concentrated (x10) buffer and Milli-Q water and mixed with the high fraction. [†] Notice that absorbance for the CL formulation is lower, due to the crosslinking.

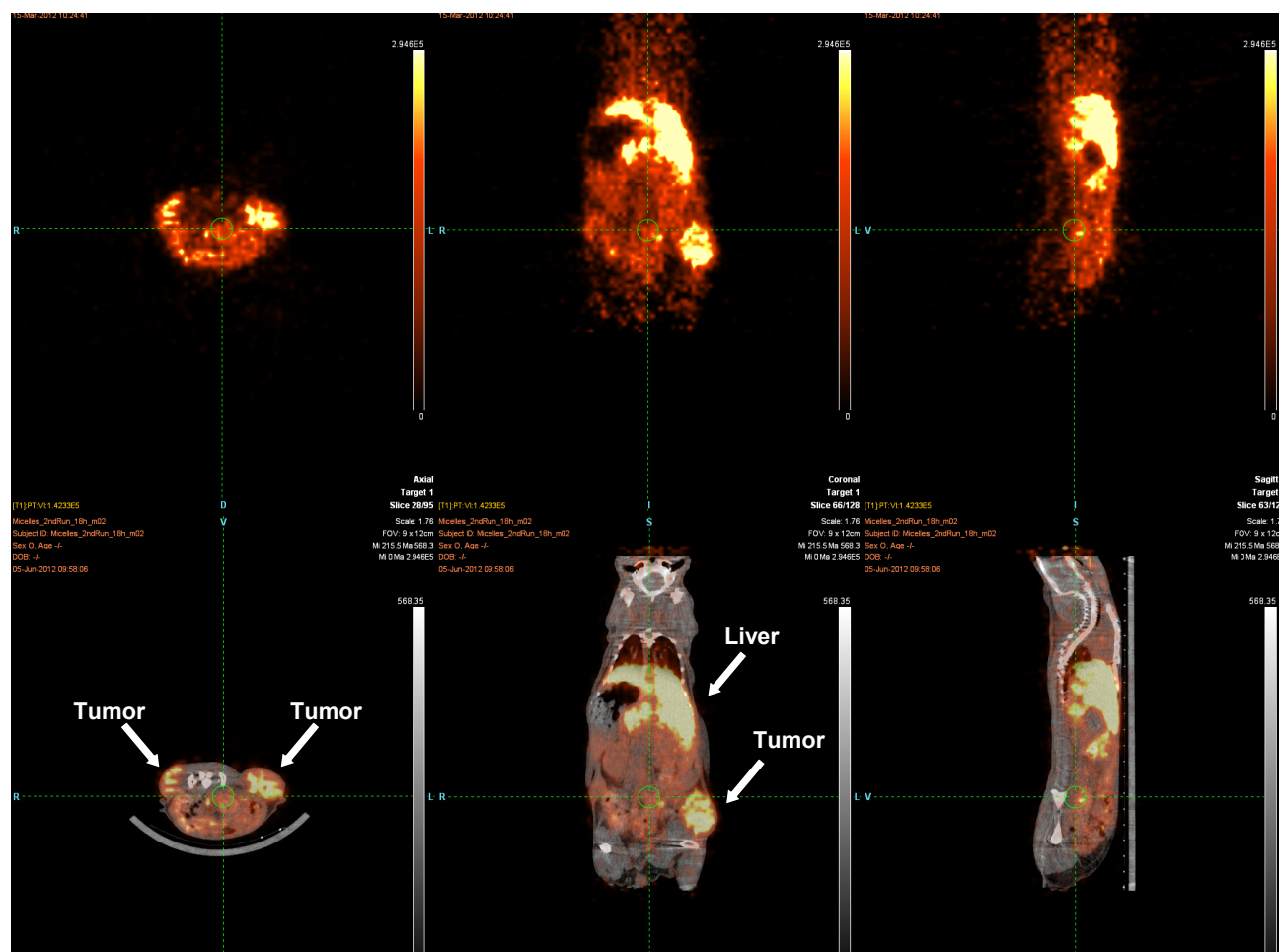


Figure 3.12 – PET images of accumulation by CL-1, crosslinked micelles at 22h after injection. The above panel is PET alone, while the lower panel is combined with a CT image. Significant accumulation is seen in liver and tumor.

The CL-1 formulation (*pilot*) was run first, generally showing promising results (**fig 3.11**). Liver uptake started out relatively high with lower splenic uptake. This is typical of smaller nanoparticles where elimination is primarily from macrophages through an initial opsonization step [149, 151]. The concentrations in these organs then proceeded to drop. Tumor uptake increased from 1h to 22h to 5.3 %ID/g. No further increase was seen at 48 h where tumor accumulation stayed at the same value (5.3 %ID/g). The concentration in the blood (*measured in the left ventricle of the heart*) started out at 6.8 %ID/g and dropped to 2.1 %ID/g (22h) and 1.58 %ID/g (48h). Compared with the PEG-PHEMA-PCMA micelles (**section 3.8**), these values are relatively low, and indicate fast clearance, both before 1h and from 1h to 22h. It seems that the initial clearance phase goes primarily to the liver. The blood values at 22h and 48h seem too low to be counted on completely, as cuproenzymes (*introduction*, **section 1.8**) could be responsible for some of this ^{64}Cu -activity.

The non-crosslinked formulations (NonCL-2 and NonCL-3) showed pharmacokinetics relatively consistent with what could intuitively be expected from non-crosslinked PMs of poor kinetic stability. The particles were cleared very rapidly from the blood stream with only 3.2 %ID/g present at 1h and less than 1 %ID/g at later time points. They exhibited higher initial liver and splenic uptake than CL-1 but then proceeded to follow expected developments. Tumor accumulation is poor and does not reach above 2 %ID/g (reached at 22h) which can be expected from particles of poor circulation time.

The other cross-linked formulations, CL-2 and CL-3 showed markedly different pharmacokinetics than CL-1 and were very different to what is expected from long-circulating, stabilized particles. The blood concentration starts out higher than the other two (9.3 %ID/g), but still relatively low. It is rapidly cleared to values below 1 %ID/g at subsequent measuring points. The clearance seems to occur in liver and spleen, with the spleen showing especially massive accumulation. Furthermore, the spleen accumulation increases throughout the scan. This indicates that mechanical filtration in the spleen could be a pathway of elimination suggesting that very large > 150-200 nm particles (aggregates) are present.

The results above, do not show inconclusively the effect of cross-linking of coumarin-core PMs on their pharmacokinetics. The main concerns are, first of all: Why did CL-1 not have PK comparable to CL-2/CL-3? There was especially one crucial factor making the two different – namely the temperature of crosslinking (RT for CL-1 and 5-7 °C for the other two) and the aggregation it seemed to cause. The second concern, related to the first, is why CL-2 and CL-3 exhibited such unexpected pharmacokinetics. These questions are discussed below.

3.7.1 What went wrong?

It appeared that formulations CL-2 and CL-3 were showing unexpected pharmacokinetics and that this could be related to size. Because of the frequently observed aggregation of capped PEG-PAEMA-PCMA micelles, the stability of cross-linked micelles was investigated. This had not been done previously, as cross-linking was usually done on small volumes (**procedure J**) the day before radiolabeling, and further, cross-linking was expected to *increase*, not decrease, micelle stability.

It was known through experience that non-crosslinked PEG-PAEMA-PCMA micelles, were stable upon prolonged storage (at least several months) at both room temperature and in the refrigerator. In addition, they did not change properties after radiolabeling (*see below*). **This strengthened the idea that NonCL-2 and NonCL-3 were showing genuine pharmacokinetics.** It had already been observed that aggregation occurred during cross-linking (**section 3.4**) and when the

high fractions for CL-2 and CL-3 were analyzed after they had decayed, a disturbing picture emerged. CL-2 had changed to 98 ± 12 nm (PDI: 0.32 ± 0.02) and -7.9 ± 0.3 mV, and CL-3 to 154 ± 6 nm (PDI: 0.21 ± 0.01) and -7.1 ± 0.6 mV. In comparison, NonCL-2 and NonCL-3 after radiolabeling were measured to be, respectively, 35 ± 3 nm (PDI: 0.19 ± 0.02), -2.6 ± 1.2 mV and 44 ± 3 nm (PDI: 0.13 ± 0.01), -3.8 ± 1.0 mV – that is, they did not show any significant change in properties.

In order to find out if this increase in size was related to radioactive degradation, stability tests were carried out on the cross-linked formulations. PEG-PAEMA-PCMA (10% DOTA, capped) were crosslinked at $5-7^{\circ}\text{C}$ for 30 minutes (36%) and incubated at 37° and 42°C overnight (22 h). This resulted in increases in size from around 40 nm to, respectively, 72 ± 7 nm (PDI: 0.24 ± 0.02), -9.1 ± 0.54 mV and 76 ± 7 nm (PDI: 0.31 ± 0.02), -9.8 ± 0.4 mV. Furthermore, similarly cross-linked micelles were stored in the refrigerator (5°C) for 12 days, resulting in a similar size increase to 77 ± 2 nm (PDI: 0.19 ± 0.02), -6.72 ± 1.4 mV.

In **conclusion**, the PEG-PAEMA-PCMA (10%DOTA, capped) micelles exhibited serious instability at any temperature after crosslinking, which could easily explain the pharmacokinetics observed. In addition to the size increase, it also seemed that a drop in zeta potential occurred. An intriguing question now seems to be why CL-1 showed intuitive PK and whether this formulation aggregated or not. Unfortunately the entire high fraction from this run was used *in-vivo* due to low labeling efficiency, preventing analysis. If it is assumed that aggregation did not occur after labeling, there must be structural differences between this and the other formulations. Such differences could have been caused by radiolabeling at RT instead of decreased temperature or by the slightly higher %CL of 45%. It seems that the former is more realistic as a difference in %CL of 5-6% should not be essential. The temperature might influence how cross-linking occur, inter-unimer or intra-unimer and how the micelle responds to the cross-linking in terms of three-dimensional changes. It would be interesting to investigate if this was the case, but unfortunately, time did not allow it.

3.8 Animal studies with PEG-PHEMA-PCMA micelles – CB-TE2A versus DOTA and the Effect of Crosslinking

After it had been realized that capped PEG-PAEMA-PCMA micelles were inherently unstable after crosslinking (section 3.7), and that they in addition could not be radiolabeled at increased temperature (section 3.3.4), it was decided to carry out the second part of the planned experiments using PEG-PHEMA-PCMA type micelles. Two separate studies were planned, 1) comparison of the PK of cross-linked CB-TE2A-PMs *versus* DOTA-PMs – hopefully shedding light on the difference in *in-vivo* stability of the two chelators that was discussed in section 1.9. The second part would be a comparison of the pharmacokinetics between crosslinked *versus* non crosslinked PEG-PHEMA-PCMA micelles. Both of these studies are addressed below. First, the preparation of the micelles is described, then the *in-vivo* results from each study are discussed.

3.8.1 Preparation of the micelles

PEG-PHEMA-PCMA unimers were synthesized and functionalized with DOTA and CB-TE2A, each at a 5% ratio (procedures C³ and E). The micelles were cross-linked for 30 minutes at 5-7 °C, which, due a slightly lower concentration of micelle material, resulted in slightly higher %CL values than previously (table 3.11). The micelles were radiolabeled by the standard procedures (G and H) with EDTA scavenging. The physicochemical properties of the used nanoparticles are given in table 3.11. Notice that when measuring these micelles, the number weighted sizes were generally found to fluctuate somewhat. For this reason, intensity weighted sizes are also given, as they were found to be stable and reliable.

TABLE 3.11 – Physicochemical properties of PEG-PHEMA-PCMA formulations. n = 3 in all cases, except zeta potential where n = 10. Notice that DOTA (NonCL) was not tested *in-vivo*. CB-TE2A (NonCL) were used below as a comparison with CB-TE2A (CL). These results are discussed in section 3.8.3.

	CB-TE2A (CL)	DOTA (CL)	CB-TE2A (Non-CL)	DOTA (NonCL)
Size (number)	21 ± 1 nm	18±1 nm	21 ± 1 nm	23 ± 1
Size (intensity)	45 ± 5 nm	47 ± 1 nm	45 ± 3 nm	44 ± 2 nm
PDI	0.17 ± 0.01	0.20 ± 0.01	0.17 ± 0.02	0.15 ± 0.01
Zeta-pot.	- 3.5 ± 0.3 mV	-2.3 ± 0.4 mV	- 3.8 ± 0.4 mV	-2.1 ± 0.7 mV
Cross-linking	45%	42%	NA	NA
Labeling efficiency*	47% (30%)	60% (34%)	40% (23%)	76% (50%)
Mic.mat. conc.	1.1 mg/mL	0.9 mg/mL	0.9 mg/mL	NA

* The labeling efficiency is the activity in peak 1. The “high fraction” is shown in parenthesis.

TABLE 3.12 – Dilution of formulations to 1 mg/mL for animal studies. H.F. is high fraction.

	CB-TE2A (CL)	DOTA (CL)	CB-TE2A (Non-CL)
Conc. main vial	3.9 mg/mL	4.2 mg/mL	3.9 mg/mL
Abs. main vial*	0.416	0.369	0.713 [†]
Activity in H.F.	141 MBq	178 MBq	102 MBq
Nr. of mice	8	8	5
Dilution to	2 mL	2 mL	1.4 mL
Diluted with	1.2 mg/mL	0.9 mg/mL	1.2 mg/mL
High/cold	779 μ L / 1121 μ L	725 μ L / 1175 μ L	928 μ L / 472 μ L
Abs. H.F.*	0.090	0.091	0.135 [†]
Meas. conc. H.F	1.0 mg/mL	0.9 mg/mL	0.7 mg/mL
Final conc	1.1 mg/mL	0.9 mg/mL	0.9 mg/mL
Final activity	115 MBq	100 MBq	85 MBq

* 30 μ L diluted to 3000 μ L, *** The main micelle dispersion was diluted to 1.0 mg/mL with concentrated (x10) buffer and Milli-Q water and mixed with the high fraction. [†] Notice that absorbance for the CL formulation is lower, due to the crosslinking. ⁺ Measured on nanodrop.

TABLE 3.13 – Tissue accumulation values based on PET and *ex-vivo* organ counting

	Time after intravenous administration							
	1 h		22 h		46 h		<i>Ex vivo organ counting</i>	
	CB-TE2A	DOTA	CB-TE2A	DOTA	CB-TE2A	DOTA	CB-TE2A	DOTA
blood	21.7 \pm 1.7	15.9 \pm 0.74	9.6 \pm 0.47	5.2 \pm 0.14	4.7 \pm 0.30	2.7 \pm 0.18	3.4 \pm 0.27	1.8 \pm 0.09
liver	8.2 \pm 0.6	7.1 \pm 0.25	7.8 \pm 0.36	6.8 \pm 0.21	7.0 \pm 0.40	5.5 \pm 0.14	4.7 \pm 0.09	3.7 \pm 0.26
spleen	7.6 \pm 0.4	5.5 \pm 0.43	5.8 \pm 0.26	3.7 \pm 0.22	5.6 \pm 0.30	3.2 \pm 0.14	6.0 \pm 0.43	3.4 \pm 0.22
kidney	6.2 \pm 0.4	5.5 \pm 0.35	3.7 \pm 0.18	3.2 \pm 0.15	2.6 \pm 0.10	2.6 \pm 0.14	1.9 \pm 0.14	2.6 \pm 0.15
muscle	1.0 \pm 0.11	1.0 \pm 0.22	0.8 \pm 0.06	0.6 \pm 0.01	0.8 \pm 0.1	0.6 \pm 0.05	0.3 \pm 0.04	0.3 \pm 0.04
tumors	1.9 \pm 0.10	1.9 \pm 0.10	4.0 \pm 0.35	3.8 \pm 0.13	4.9 \pm 0.40	3.6 \pm 0.11	4.0 \pm 0.28	3.4 \pm 0.19
heart	-	-	-	-	-	-	1.2 \pm 0.10	1.4 \pm 0.06
lung	-	-	-	-	-	-	2.1 \pm 0.13	2.0 \pm 0.17
intestine	-	-	-	-	-	-	1.1 \pm 0.07	1.7 \pm 0.12
pancreas	-	-	-	-	-	-	0.8 \pm 0.12	0.7 \pm 0.06
T/B	0.1 \pm 0.01	0.1 \pm 0.00	0.4 \pm 0.02	0.7 \pm 0.04	1.0 \pm 0.08	1.4 \pm 0.08	-	-
T/M	2.0 \pm 0.24	3.0 \pm 1.09	5.0 \pm 0.23	6.2 \pm 0.26	6.3 \pm 0.65	6.3 \pm 0.61	-	-
T/K	0.3 \pm 0.02	0.4 \pm 0.02	1.1 \pm 0.05	1.2 \pm 0.04	1.9 \pm 0.07	1.4 \pm 0.07	-	-
T/L	0.2 \pm 0.02	0.3 \pm 0.01	0.5 \pm 0.02	0.6 \pm 0.01	0.7 \pm 0.04	0.7 \pm 0.02	-	-
T/S	0.3 \pm 0.02	0.4 \pm 0.02	0.7 \pm 0.03	1.0 \pm 0.05	0.9 \pm 0.06	1.1 \pm 0.04	-	-

Values are represented as %ID/g, mean \pm SEM. For the PET scans, n = 6 in all cases, except tumors where n = 12. For the gamma counting, n = 4 in all cases, except tumors and kidneys where n = 8.

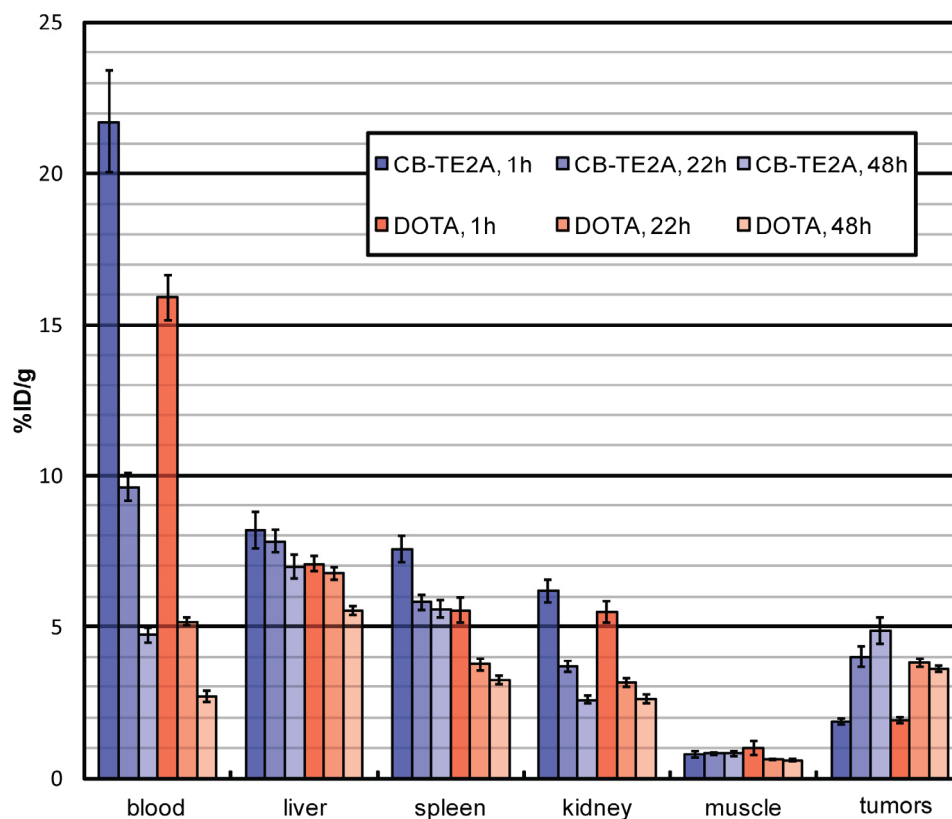


Figure 3.13 – In-vivo distribution of DOTA and CB-TE2A conjugated, crosslinked PEG-PHEMA-PCMA polymeric micelles labeled with ^{64}Cu .

As was done with the PEG-PAEMA-PCMA micelles, the high fraction was diluted with cold micelles to achieve an agreeable activity concentration (slightly above 10 MBq per 200 μL) and a micelle material concentration of about 1.0 mg/mL. **Table 3.12** shows how this dilution was carried out.

The micelles were injected into xenographted NMRI mice by Dr. Tina Binderup at the Panum Institute (Copenhagen, Denmark) (see **Supplementary information VI**).

3.8.2 Discussion of in-vivo results - CB-TE2A versus DOTA

Analysis of the images and *ex-vivo* gamma-counting of excised organs gave the results shown in **table 3.13**. *Region-of-interest* (ROI) values retrieved from the PET scan images are shown graphically in **figure 3.13**.

Starting with the blood values, it is apparent that the initial (1h) values for DOTA are lower than those of CB-TE2A. The difference was significant by t-test (unpaired, two-tailed, $t = 0.011$). The difference could be prompted by a fast initial renal clearance of DOTA micelles, but it seems unlikely that this should be different from the CB-TE2A micelles, as the sizes are similar and none are below the renal clearance threshold (~ 10 nm). If the clearance was due to rapid loss of $^{64}\text{Cu}^{2+}$ from the micelles, this activity would be expected to be present in either the bloodstream as carried by cuproenzymes or in the liver or kidneys (see **section 1.9 – chapter 1**). None of this seemed to occur. Accordingly, the difference *might* be statistically *insignificant* and caused by natural variation (6 mice were tested for each formulation). Assuming 2 mL (2 gram) blood in a mouse, the total activity (%ID) in the blood can be plotted as shown in **figure 3.14**. Nanoparticles are thought to follow a biphasic clearance profile [16, 259, 357], with a fast (usually lasting 1-3h) initial clearance (*distribution phase*) followed by a longer main clearance phase with about 10-40 h half-life, depending on the particle type. As our dataset does not include measurements before 1h, it is difficult to comment on the fast initial clearance. In **figure 3.14** it is seen that the half-life between the two first points is shorter than between the two later points. This suggests that the first clearance phase is not entirely over at 1h. In addition, by comparing the two curves for the DOTA micelles, it can be seen that for these micelles, the difference between early and late half-life is more pronounced than for the CB-TE2A micelles. This could indeed indicate that the first, fast clearance phase is longer and more pronounced for the DOTA micelles where only 19% of the injected dose appears to follow the second-phase, slow clearance profile (the backwards forecast of the “late points” trendline for the DOTA micelles). This number is 37% for the CB-TE2A micelles. In order to conclude that DOTA conjugated nanoparticles are cleared more rapidly, more solid data are needed. In addition, one would expect the cleared nanoparticles to emerge in liver and spleen and this is not seen. The lower blood concentration of the DOTA-micelles seems to affect the activity found in other tissues, thus making all of these (perhaps except tumor) slightly lower than the CB-TE2A micelles.

The apparent circulation half-lives of the PMs are 18-26 h for the DOTA micelles and 20-23 h for the CB-TE2A micelles. Such half-life values are generally longer than those observed for liposomes [41, 259], while similar values, and longer, are observed for PMs [3, 10, 16]. A general argument *against* long half-life, given that high tumor accumulation occurs within the first 10-20 hours, is that a fast clearance of activity from blood and muscle gives better contrast and thus improved imaging. It should be noted that *in-vivo* half-lives in larger animals, including humans, are commonly longer than in mice.

The relatively long half-lives may be a consequence of the low uptake in liver and especially spleen. Liposomes can accumulate in spleen about 3-4 times as much as observed here [210, 259]. Liver accumulation of liposomes is usually more modest and is generally observed to be similar to that observed here [38, 210] or slightly higher [259]. It can be hypothesized that the modest uptake in these organs, primarily macrophage-mediated, is because of smaller size. Especially in the spleen will larger particles be expected to accumulate more readily [157]. That little splenic accumulation is observed here, suggests that little aggregation of the PMs takes place (compare with **section 3.7**).

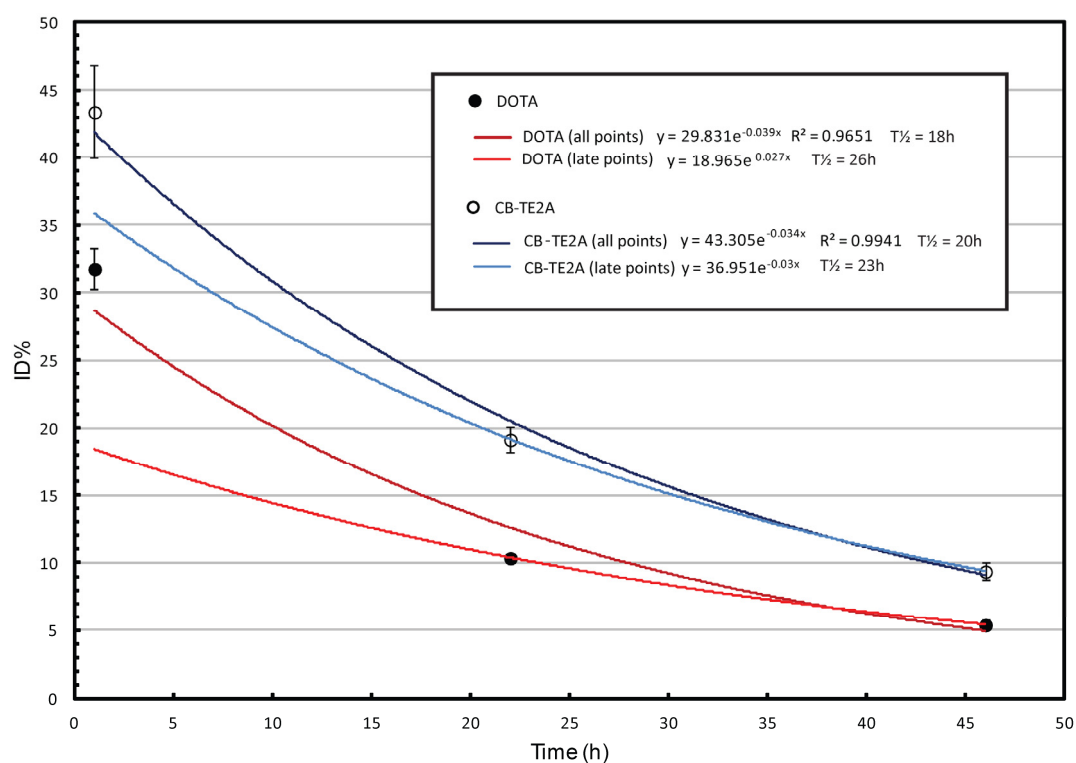


Figure 3.14 – Blood clearance data for DOTA and CB-TE2A conjugated micelles. The two darker shaded curves are exponential fits over all three points. The lighter shaded curves are exponential fits over the two later points. Equations, R^2 for the “all points” curves as well as calculated half-lives are shown. *2 gram blood per mouse is assumed.*

The kidney accumulation observed is similar or lower [16, 38] to what is usually observed for nanoparticles. It should be noted that kidney accumulation is in kidney tissue and should not be confused with accumulation in bladder and subsequent excretion through the urine. It should also be remembered that free Cu^{2+} has some tendency to accumulate in kidney tissue [38, 206, 361] as well as in the liver [38, 207]. Looking at figure 3.13 it seems indeed that liver and kidney accumulation for the DOTA-micelles is higher in comparison with the CB-TE2A micelles than is the splenic accumulations, where the ratios agree well with the difference in blood concentrations between the two micelle types. Thus could be a slight indicator that DOTA has a higher tendency to lose bound $^{64}\text{Cu}^{2+}$ in circulation.

Looking at tumor accumulation, a slightly different picture emerges. Contrary to the other organs, tumor values are very similar for the two micelle types at 1 and 22 hours. At 46 h however, CB-TE2A is higher than DOTA. The difference is significant on a t-test ($t = 0.0083$). In line with current theories on copper loss from DOTA [198, 199, 209], one could conclude that DOTA conjugated micelles do not show as long circulation due to copper-loss and therefore fail to

accumulate in tumor beyond 24 hours. In general however, as all other tissues exhibit lower values for DOTA than for CB-TE2A it seems reasonable that tumor should also do so. The tumor accumulation values observed here fit well with what is generally observed for long-circulating nanoparticles. Both poorer [3, 12] and better [10, 11, 16] values have been reported in the literature.

In order to better compare the two formulations, as well as assessing their potential and contrast as imaging agents, a series of tissue ratios were calculated. These are seen in **table 3.13**. The tumor-to-muscle (T/M) is what generally speaks about the potential as imaging agent. Values over 1.5 are thought to provide adequate contrast for tumor visualization [2]. Accordingly, these micelles can serve this purpose. The tumor-to-liver (T/L) and tumor-to-spleen (T/S) ratios are two other values that are often reported. They speak about the nanoparticles' tendency to accumulate in tumor as compared to the other usual (and unwanted) sites of accumulation. These values are (as already alluded to above) generally good for these PMs, with T/L ratios at 0.7 and T/S ratios about 1. Low liver and spleen uptake has been reported for PMs by other groups [16] although they reported higher tumor accumulation than we do. An interesting perspective on this study would be to investigate the causes of the fast initial clearance, as the particles themselves seem to have very good characteristics for preferential tumor accumulation.

In general, the dataset presented here does not provide a solid reason to believe that DOTA and CB-TE2A exhibit significant differences in stabilities *in-vivo*, and we conclude that both display similar stability.

3.8.3 Discussion of in-vivo results – The effect of crosslinking

The results obtained from the PEG-PHEMA-PCMA (CB-TE2A, NonCL) micelles are shown in **figure 3.15**. They are compared with the results already shown above for PEG-PHEMA-PCMA (CB-TE2A, CL). The results for the non-crosslinked CB-TE2A micelles arrived very late and were barely included in this thesis. For this reason, an experimental is not included, but for all practical purposes, it is similar to the experimental for the crosslinked PEG-PHEMA-PCMA micelles seen in **Supplementary Information VI**.

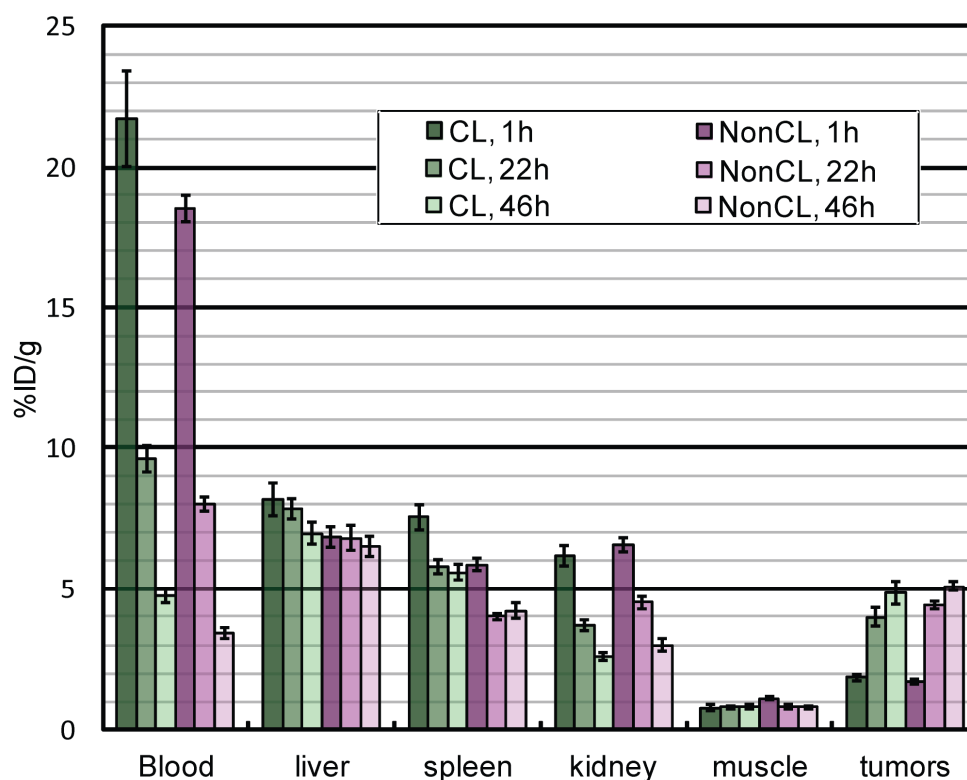


Figure 3.15. Comparison of *in-vivo* biodistribution of crosslinked (CL) versus non-crosslinked (NonCL) CB-TE2A conjugated micelles labeled with ^{64}Cu . These data are derived from region-of-interest (ROI) analysis of PET scans.

The most interesting aspect of this new set of data was that it appeared basically *identical* to that of the crosslinked CB-TE2A micelles. Taking into account that both micelle types display similar, relatively long (20-23 h) half-lives, it must be concluded that *the nonCL micelles exhibit good stability in circulation*. The tumor accumulation of the nonCL micelles is of the same magnitude as the CL. Blood, liver and spleen are slightly lower for the nonCL micelles, while kidney is slightly higher. These differences are negligible but could hint at a marginally higher renal clearance for the nonCL micelles. However, even if this was the case, it seems to have little practical influence on the performance of the micelles.

Crosslinked micelles have a problem, in that they are generally not easily biodegradable and can therefore accumulate in the body without any possibility of clearance. For this reason, stable micelles that are *not* crosslinked are generally interesting, as the unimers can dissociate from the micelles and be cleared individually.

The stability of these micelles can be related to the coumarin cores forming glassy cores with high kinetic stability. It is however, in stark contrast to the results presented in **section 3.7** (PEG-PAEMA-PCMA) where the nonCL micelles were

rapidly cleared and exhibited very poor tumor accumulation. It may be, that the short coumarin copolymer of the PEG-PHEMA-PCMA (18 repeats) may increase the stability when compared to the long copolymer of PEG-PAEMA-PCMA (80 repeats). The 120 monomer PEG chain may not be sufficient to stabilize a large hydrophobic core in the blood stream.

In the literature there are several reports of crosslinked and non-crosslinked polymeric micelles (*see introduction sections to this chapter*). However, only a few contain solid pharmacokinetic data obtained from radiolabeling. Many of the studies exhibit consistently low blood concentrations at all scanning times, while reporting substantial tumor accumulation as well as uptake in other organs. Hoang et al. used *non-crosslinked* micelles and reported high tumor uptake (9 %ID/g), though at the same time relatively high spleen (22 %ID/g) and liver (13 %ID/g) uptake and a long half-life 30 h [10]. Yang et al. used core-crosslinked micelles and reported a staggering 46 h half-life (clearance phase) with tumor uptake at 5-6 %ID/g after 48 hours [13]. From the same group, Zhao et. al. obtained even better tumor accumulation (~9 %ID/G). Judging from these results and the papers reviewed in the introduction to this chapter, polymeric micelle pharmacokinetics is at times a confusing field without good guidelines for what to expect from tumor accumulation or blood-stream stability when crosslinking micelles. Indeed, non-crosslinked micelles may deliver very good tumor accumulation and long half-lives.

Our results indicate that it may not be necessary to crosslink coumarin-core micelles. Stable, more easily cleared nanoparticles with good in-vivo properties can thus be obtained without UV treatment.

TABLE 3.14 – Comparison of micelle properties before and after radiolabeling.

<i>Before labeling</i>	CB-TE2A (CL)	DOTA (CL)	CB-TE2A (Non-CL)	DOTA (NonCL)*
Size (number)	21 ± 1 nm	18±1 nm	21 ± 1 nm	23 ± 1
Size (intensity)	45 ± 1 nm	47 ± 1 nm	45 ± 3 nm	44 ± 2 nm
PDI	0.17 ± 0.01	0.20 ± 0.01	0.17 ± 0.02	0.15 ± 0.01
Zeta-pot.	- 3.5 ± 0.3 mV	-2.3 ± 0.4 mV	- 3.8 ± 0.4 mV	-2.1 ± 0.7 mV
<i>After labeling</i>	CB-TE2A (CL)	DOTA (CL)	CB-TE2A (Non-CL)	DOTA (NonCL)*
Size (number)	29 ± 2 nm	34 ± 0.3 nm	35 ± 3	30 ± 2 nm
Size (intensity)	43 ± 2 nm	40 ± 1 nm	40 ± 1	41 ± 1 nm
PDI	0.08 ± 0.03	0.05 ± 0.00	0.03 ± 0.03	0.08 ± 0.01
Zeta-pot.	- 1.12 ± 0.59 mV	- 2.12 ± 1.32	**	- 1.50 ± 0.8 mV

* Not used *in-vivo* and radiolabeled at 10 MBq, not high (>500 MBq) activity. ** Too little was left for measuring the zeta potential.

3.8.4 Thermostability of PEG-PHEMA-PCMA micelles

As the thermostability of the crosslinked PEG-PAEMA-PCMA micelles had been found to be poor, the PEG-PHEMA-PCMA micelles were investigated for similar instabilities. As previously, this was done by allowing the high fraction to decay and analyzing it by DLS (**Table 3.14**). Generally, the formulation did not exhibit significant aggregation after labeling. However the high fractions were generally measured as having slightly narrower size distributions (lower PDI values) than before labeling (higher number weighted and lower intensity weighted sizes). There seems to be no good reason for this change, and it is attributed to uncertainties when using DLS (*when doing the stability tests mentioned below, PDIs were also narrower than had previously been observed, on the same particles*). It could be concluded that both CL and non-CL formulations were stable and that the *in-vivo* results obtained could be relied on as genuine.

In order to expand on the data from the high fractions, the effect of temperature on the micelles was investigated. Size was measured on crosslinked PMs after incubation at both 80 °C (*the temperature at which CB-TE2A micelles was labeled*) and 37 °C (*physiological pH*), after various amounts of time. The results are seen in **table 3.13**. It was observed that both micelle types were completely stable for 3 hours at 80 °C. In addition, the DOTA micelles were stable up until 61 h. the CB-TE2A micelles were stable after 4.5 h but after 61 h were found to having formed visible aggregation. This again underscores the lower thermostability of CB-TE2A micelles. At 37 °C the micelles were stable for up to 6 days. This shows that they are stable at physiological temperature for the circulation times reported here.

Table 3.13 - Stability data for PEG-PHEMA-PCMA micelles (CL and Non-CL). The times given are after incubation was begun. The sizes of the micelles before incubation (both before and after CL) are also given (repeated in on both the 37 °C and 80 °C columns). Size is given as *number weighted median / intensity weighted median (PDI)*.

37 °C			80 °C		
<i>Time</i>	DOTA (41% CL)	CB-TE2A (46% CL)	<i>Time</i>	DOTA (41% CL)	CB-TE2A (46% CL)
0 h	31 ± 5 / 41 ± 1	36 ± 3 / 40 ± 1	0 h	31 ± 5 / 41 ± 1	36 ± 3 / 40 ± 1
Before CL	(0.06 ± 0.03)	(0.04 ± 0.01)	Before CL	(0.06 ± 0.03)	(0.04 ± 0.01)
0 h	33 ± 3 / 41 ± 1	36 ± 2 / 40 ± 1	0 h	33 ± 3 / 41 ± 1	36 ± 2 / 40 ± 1
After CL	(0.06 ± 0.03)	(0.04 ± 0.01)	After CL	(0.06 ± 0.03)	(0.04 ± 0.01)
2.5 days	29 ± 3 / 40 ± 1 (0.09 ± 0.02)	34 ± 3 / 40 ± 1 (0.05 ± 0.01)	1.5 h	29 ± 1 / 41 ± 1 (0.08 ± 0.01)	29 ± 3 / 41 ± 1 (0.07 ± 0.01)
6 days	32 ± 3 / 40 ± 1 (0.06 ± 0.02)	38 ± 1 / 40 ± 1 (0.02 ± 0.01)	3 h	28 ± 2 / 40 ± 1 (0.09 ± 0.01)	34 ± 6 / 41 ± 1 (0.06 ± 0.03)
			4.5 h	<i>Not measured</i>	31 ± 5 / 43 ± 1 (0.08 ± 0.03)
			61 h	37 ± 3 / 40 ± 1 (0.04 ± 0.02)	1127 ± 1167 / 14056 ± 18695 (0.50 ± 0.12)

3.9 Concluding remarks

As has been laid out in the preceding sections, photo core-crosslinked triblock PMs with DOTA and CB-TE2A conjugated in the shell region were radiolabeled with ^{64}Cu and tested *in-vivo*. We have seen how manipulating the structural elements of the micelles can infer gross instabilities. This includes capping of the hydrophilic shell-region, CB-TE2A and crosslinking. This caused the micelles to aggregate when heated and, for the crosslinked PEG-PAEMA-PCMA micelles, even instability at room temperature. This prevented their use *in-vivo*.

On the other hand, PMs were prepared (PEG-PHEMA-PCMA) that were stable, even when heated to 80 °C for several hours. These micelles were successfully radiolabeled and investigated in a xenographted murine *in-vivo* model. They exhibited pharmacokinetics that were in accordance with what could be expected for small long-circulating nanoparticles with low interaction with the immune system, although the DOTA-conjugated particles did seem to display a fast initial clearance phase. Accumulation in RES organs was low and tumor accumulation good.

The nanoparticles presented here have importance in the understanding of the pharmacokinetics of PMs and their efficient radiolabeling. They may be a tool in the ongoing research to prepare better nanomedicines. For this reason it is important to know which chelators are superior. Our results indicated that the difference between DOTA and CB-TE2A *in-vivo* is probably insignificant. However, further results are needed in order to fully conclude which should be the chelator of choice.

On a different note, radiolabeled nanoparticles, especially liposomes, are currently being investigated as a pharmaceutical in their own right, useful in the imaging of cancer tumors. Nanoparticles have the major drawback that, besides tumor accumulation, they exhibit substantial liver and spleen accumulation. This raises the radioactive dose delivered to these organs. Nanoparticles that show low accumulation in secondary organs, such as the polymeric micelles presented here, might therefore have advantages in the imaging of tumors.

3.10 Experimental section

3.10.1 Materials and equipment

DOTA-NHS ester was purchased from CheMatech (F). CB-TE2A·2H₂O was purchased from Macrocyclics (USA). All solvents and chemicals were purchased from Sigma Aldrich in purum quality or better and were used without further purification. CuCl (99.995%) was washed with glacial acetic acid, followed by absolute ethanol and diethylether, dried and stored under argon. Solvents used for ATRP were purified by distillation over the drying agents indicated in parentheses, stored under molecular sieves (MeOH 3 Å and DMF 4 Å) and transferred under argon; MeOH (Mg(OMe)₂), DMF (CaH₂). CH₃O-PEG-OH (poly(ethylene glycol)monomethylether (M_n = 5000) was from Fluka. DMF for anhydrous syntheses was dried over 4 Å molecular sieves several times. Glassware was oven-dried overnight or heatgun-dried under a stream of dry argon prior to use. Reactions other than polymerizations were conducted in a nitrogen atmosphere. Polymers and micelles containing coumarin moieties were shielded from light whenever possible. Cellulose membrane dialysis tubing (12.400 cut-off) was purchased from Sigma Aldrich (DK). Sephadex G25 fine (GE Healthcare) was used for size-exclusion chromatography.

NMR-analyses were recorded in CDCl₃ on a Bruker Ultrashield 500 MHz or a 300 MHz Varian Mercury 300 BB. The residual solvent peak (CHCl₃) was used as reference. Photo core-crosslinking by UV irradiation was carried out on an Omnicure Series 1000 (Lumen Dynamics, Mississauga, Canada). FT-IR spectra were recorded by Perkin Elmer Spectrum 100 FT-IR Spectrometer. GPC measurements were carried out with a RID10A-SHIMADZU refractive index detector and Mixed-D GPC column from Polymer Laboratories with a flow rate of 0.5 mL/min at 25 °C, and DMF with 50 mM LiCl as eluent. UV-Vis spectra were recorded on Unicam Helios Uni 4923 spectrophotometer. Size and zeta potential were measured on ZetaPALS (Brookhaven, New York, USA). Size was repeated thrice for each measurement and is consistently reported as the number weighted median (lognormal distribution). Zeta potential was measured in a 10 mM HEPES disodium buffer, pH = 7.4.

⁶⁴Cu was produced on a GE PETtrace Cyclotron. Radio-TLC was performed on a Raytest MiniGita Star. Size-exclusion chromatography of the labeled micelles was carried out on an apparatus custom-built at our facility. The stationary phase was Sepharose G25 and PIPES/NaCl buffer (10mM:150mM), pH 7.0 was used as eluant.

3.10.2 Procedures

In the following each procedure is denoted by a letter. These letters are mentioned in the main text for easy reference. All procedures described here were carried out by the author. Procedures by collaborators (unimer synthesis and animal studies) are found in the **supplementary information – III and VI**, respectively.

All procedures were shielded from light if PCMA-type unimers were involved.

Procedure A – Purification of unimers by dialysis (typical procedure)

The crude unimer (190 mg) was dissolved in DMF (10 mL) by vigorous stirring for 30 minutes. Milli-Q water (20 mL) was added dropwise, turning the mixture opalescent and foamy. The mixture was transferred to a cellulose membrane dialysis tubing (MW cut off: 12.400 Da) and placed in 1 L Milli-Q water under slow stirring. The pH of the medium was checked and was always below pH 7. The mixture was dialyzed for three days, with a change of the medium to fresh Milli-Q water every day (two re-additions of medium). After dialysis the volume was about 25 mL. 10 mL was freeze-dried resulting in 49 mg dry substance. Yield after dialysis: $(49 \times 2.5)/190 = 64\%$. Yields were typically 60-80%.

Procedure B – Determination of CMC by the pyrene assay

Pyrene (12 mg, 59.3 μ mol) was dissolved in acetone (10 mL). 50 μ L of this solution was diluted in 10 mL acetone to 29.7 μ M. 34 μ L of this solution was placed in 4 mL glass vials and the acetone was allowed to evaporate in the hood over 4-5 hours, leaving 1 nmol pyrene in each vial. To each vial was added 2 mL micelle dispersion in concentrations of 0.05-1000 μ g/mL in 10 mM hepes with 150 mM NaCl, pH 7.4. The vials were incubated for one hour at 65 °C and then overnight (14 h) at 37 °C. Fluorescence was recorded on an Olis SLM 8000 fluorometer. Excitation spectra were collected at 25 °C using emission wavelength 390 nm and a 16 nm slit size. Excitation was scanned with 20 increments of 8 sec in the range of 325-345 nm with all slits set to 0.5 nm. All samples were taken out of the incubator at the same time and were kept at room temperature until analyzed (up to 5 hours). Throughout, the samples were protected from light. Intensity ratios (I338/I334) were calculated from the excitation spectra and plotted as a function of the polymer concentration.

Procedure C¹ – Conjugation of DOTA to PAEMA-type micelles (example procedure, 100% DOTA)

PEG-PAEMA-PMMA (45 mg, MW: 12.5 kDa, 3.6 μ mol) was dissolved in dry DMF (2 mL) by stirring for 30 min. DOTA-NHS ester (3 mg, 3.9 μ mol) was added as a solution in DMF (0.5 mL), along with TEA (15 μ L, 108 μ mol). The mixture was allowed to stir overnight. *If no capping was desired:* To the mixture was added 5 mL Milli-Q water dropwise and the mixture was dialyzed for three days according to **procedure F**. *If capping was desired:* Acetic anhydride (20 μ L, 216 μ mol)

was added, along with TEA (150 µL, 1.10 mmol). The mixture was stirred overnight after which 5 mL Milli-Q water was added dropwise and the mixture was dialyzed for three days according to **procedure F**.

Procedure C² – Conjugation of DOTA to PEG-PAEMA-PCMA (example procedure, 10% DOTA w. capping).

PEG-PAEMA-PCMA (35 mg, MW: 21 kDa, 1.7 µmol) was dissolved in dry DMF (1 mL) and TEA (21 µL, 0.13 mmol) in the main reaction vessel (MRV). DOTA-NHS ester (3 mg) was dissolved in DMF (2 mL) and 100 µL of this solution was added to the MRV (0.15 mg DOTA-NHS ester, 0.2 µmol). The resulting solution was stirred overnight at RT under a N₂ atmosphere. After 27 h, capping of the remaining free amines was carried out by adding acetic anhydride (12 µL, 0.13 mmol) and TEA (21 µL, 0.13 mmol). Stirred overnight at RT. After 29 h, Milli-Q water (5.9 mL) was added drop-wise under intense stirring. The resulting opalescent dispersion was dialyzed against Milli-Q water (1 L) for 3 days with daily changes of the medium. An aliquot of the dispersion was lyophilized for analysis. Negative Kaiser test confirmed completed capping. Final concentration 4.8-5.0 mg/mL.

Procedure C³ – Conjugation of DOTA to PEG-PHEMA-PCMA

PEG-PHEMA-PCMA (30 mg, MW: 11.8 kDa, 2.5 µmol) was dissolved in dry DMF (1 mL). DOTA-NHS ester (2.0 mg, 2.7 µmol) was added along with DMAP (2.0 mg, 16 µmol). The mixture was stirred overnight (19h) at RT under an N₂ atmosphere. Then 5 mL Milli-Q water was added dropwise and the mixture was dialyzed against Milli-Q water (1L) for three days with daily changes of the medium. Final concentration: 4.2 mg/mL. Size: 23 ± 1 nm (n = 3), Zeta-potential: -2.06 ± 0.42 mV (n = 10).

Procedure D – Conjugation of CB-TE2A (100%) to PAEMA-type PMs (w NHS, example procedure)

PEG-PAEMA-PMMA (56 mg, MW: 12.5 kDa, 4.5 µmol) was dissolved in dry DMF (2 mL) under nitrogen by stirring for 30 minutes in the *main-reaction vessel* (MRV). In a different vial (*vial 1*), 11 mg CB-TE2A·2H₂O (20 µmol) was dissolved in dry DMF (1.0 mL) with TEA (33 µL, 0.24 mmol) and NHS (6 mg, 50 µmol). In a different vial (*vial 2*), EDC.HCl (6.5 mg, 34 µmol) was dissolved in DMF (1 mL). 200 µL from vial 2 was added to vial 1 (EDC.HCl: 6.8 µmol). Vial 1 was shaken for a few seconds and then added to the MRV. The mixture was stirred overnight at room temperature. In case capping was desired, acetic anhydride was added in excess with TEA as described in **procedure C²**. If capping was not desired, micelles were prepared directly by dialysis as described in **procedure F**. *CB-TE2A was also conjugated in 10%. The same procedure as above was followed, with all reagents (except polymer and capping reagents) in a 10% molarity.*

Procedure E – Conjugation of CB-TE2A to PEG-PHEMA-PCMA (w DMAP)

In the main reaction vessel (MRV) was dissolved PEG-PHEMA-PCMA (30 mg, MW: 12.5 kDa, 2.4 µmol) and CB-TE2A·2H₂O (4.5 mg, 8.2 µmol) in dry DMF (1 mL). DMAP (17 mg) was dissolved in dry DMF (4 mL) and 40 µL of this solution was added to the MRV (DMAP: 0.17 mg, 1.4 µmol). EDC.HCl (4.0 mg) was dissolved in dry DMF (0.5 mL) and 69 µL of this solution was

added to the MRV (EDC.HCl: 0.55 mg, 2.9 μ mol). The mixture was stirred overnight (16h) at RT under a N₂ atmosphere. Then Milli-Q water (5 mL) was added dropwise and the mixture was dialyzed against Milli-Q water (1L) for three days with daily changes of the medium. Final concentration: 3.9 mg/mL. Size: 21 \pm 1 nm, Zeta-potential: -3.81 \pm 0.42 mV.

Procedure F¹ – Preparation of micelles by dialysis (from reaction mixture)

After chelator conjugation (and capping) was over, Milli-Q water was added directly to the reaction mixture. Milli-Q water was added dropwise in 1-3 times the volume of the present DMF. The mixture was then placed in a dialysis tube (cut-off: 12.4 kDa) and dialyzed against Milli-Q water (1 L) for three days at pH < 7. Each day the water was changed.

Procedure F² – Preparation of micelles by dialysis (preparation of mixed micelles (10% DOTA), example procedure)

PEG-PAEMA-PMMA (100% DOTA) (3.4 mg) and PEG-PHEMA-PMMA (29 mg) was dissolved in DMF (2 mL). The mixture was stirred for 60 minutes. Milli-Q water (4 mL) and the mixture was dialyzed as described in **procedure F¹**.

Procedure G – Radiolabeling of DOTA micelles (optimized standard procedure)

To a vial containing ⁶⁴CuCl was added 100 μ L NH₄OAc (0.1 M, pH 5.5) buffer. The mixture was stirred for 10 minutes at room temperature, forming ⁶⁴Cu-acetate. Then, 400 μ L micelle dispersion (4-5 mg/mL) was added. This mixture was stirred for 2 hours at room temperature, after which 1 mM EDTA-tri-potassium-dihydrate (0.05 μ mol, 50 μ L) was added. This gave a total volume of 550 μ L. After the addition of EDTA, the mixture was stirred for a further 20 minutes.

Procedure H – Radiolabeling of CB-TE2A micelles

To a vial containing ⁶⁴CuCl was added 100 μ L NH₄OAc (0.1 M, pH 5.5) buffer. The mixture was stirred for 10 minutes at room temperature, forming ⁶⁴Cu-acetate. Then, 400 μ L micelle dispersion (4-5 mg/mL) was added and the mixture was stirred for 3 hours at 80 °C, after which 50 μ L 1 mM EDTA-tri-potassium-dihydrate (0.05 μ mol) was added. This gave a total volume of 550 μ L. After addition of EDTA, the mixture was stirred for a further 20 minutes. During these 20 minutes, the mixture was allowed to cool to RT.

Procedure I – Purification of radiolabeled micelles by size-exclusion chromatography

The radiolabeled micelle dispersion (550 μ L) was applied to a size exclusion column charged with Sepharose G25 swelled in isotonic (150 mM NaCl) PIPES buffer (10 mM), pH 7.0. 500 μ L was applied to the column and the remaining 50 μ L was mixed with 500 μ L buffer (PIPES) and a further 500 μ L was applied (to avoid application of air). The PMs were eluted in a fully automated fashion with PIPES buffer, separating the nanoparticles from small-molecular contaminants.

Procedure J – Crosslinking (optimized procedure)

Micelle dispersion (1100 µL) was transferred to a 4 mL glass vial containing a magnet. The vial was placed in an ice/water bath, that was kept constantly at 5-7 °C and stirred vigorously. The dispersion was irradiated for 2x15 minutes at an intensity of 2 W/cm² and a wavelength of 320 < λ < 500 nm. The UV probe was placed about a centimeter from the water surface.

4. General conclusion & perspectives

Throughout the last two decades, interest in nanotechnology and nanomedicine has been high and increasing, both among the scientific community and the general populace. There has been a growing expectation that nanoparticles will revolutionize the field of medicine and be a powerful weapon in the fight against a range of human diseases, in particular cancer. However, 20 years after the invention of the PEG-coating, enabling long circulation, nanoparticles have, as of yet, failed to deliver. Several challenges have faced scientists working in the field. In liposomal chemotherapy, two important obstacles have been efficient drug loading and, upon reaching tumor tissue, site-specific release. Drug loading can for some drugs, notable doxorubicin, be solved by creating a pH-gradient across the liposomal membrane. This is employed in the only successful systemic anti-cancer drug, DOXIL. Efficient release however, continues to be a Holy Grail. This in spite of numerous attempts to take advantage of pathophysiological tumor characteristics such as lowered pH and over-expression of certain enzymes. In addition, the immune system remains the archenemy of the nanoparticle researcher. As we have seen throughout this thesis, both in the introduction and the reported research results, our body does not widely approve of being injected with little virion-like particles. For this reason, our particles are attacked by complement in the circulation and rapidly cleared in the macrophage dense tissues of the liver and spleen.

As nuclear tomographic imaging has reached a highly advanced state of accuracy, reliability and feasibility, radiolabeling has become an integrated part of nanoparticulate drug delivery. From the radiopharmacist/radiochemist's point of view, there are three major ways in which to contribute to the field of nanomedicine.

The **first** of these is to develop efficient labeling methodology for nanoparticles. Such methodology has to be fast, reliable, very stable *in-vivo* and to include isotopes with the right emissions and the right half-lives. *Fast*, because interesting isotopes decay rapidly, *reliable*, because the preparation of radiopharmaceuticals is usually a "one-shot" endeavour, *stable in-vivo*, because one has to be able to trust that the desired entity is being tracked. Desirable radioisotopes are few, since PET isotopes are currently preferred and half-lives should be long enough to permit scanning times of at least 8 hours. On the other hand, half-lives that are too long could cause unacceptable levels of dose to healthy organs. ^{18}F ($T_{1/2} = 110$ min) and ^{64}Cu ($T_{1/2} = 12.7$ h) are undergoing intense research in this field. New stars on the horizon may very well be ^{124}I ($T_{1/2} = 4.2$ days) and ^{89}Zr (3.3 days). These isotopes offer longer half-lives, and the possibility of tracking particles for very long periods, beyond 48-72 hours. Also, ^{61}Cu ($T_{1/2} = 3.4$ h) might be an interesting PET-isotope in the future. Efficient labeling methodology will aid the field in tracking newly developed particles and conveniently analyze their pharmacokinetics. Such research may lead to nanoparticles more adept at avoiding the immune system. A niche within the field of radiolabeling for research purposes is the idea of visualizing site-specific degradation of liposomes. By double-labeling

General conclusion and perspectives

liposomes with different isotopes, e.g. one attached to a lipid in the membrane and one dissolved in the aqueous core, it could be possible to visualize the separation of these two emitters at the site of degradation.

The **second** way is in the use of radiolabeled nanoparticles as radiopharmaceuticals. As nanoparticles accumulate in tumor tissue, it has long been envisaged that they could be used to visualize and diagnose cancer tumors. For the majority of systems, the contrast achievable with nanoparticle system is high enough for acceptable visualization of tumors. However, due to substantial uptake in secondary, healthy organs, the dose delivered to these organs is a general concern. Therefore, general advances in the efficient tumor-targeting and macrophage-avoiding properties of nanoparticles are beneficial to the use of radiolabeled nanoparticles in diagnostics. The **third** area and as of yet the most theoretic is the field of localized radiotherapy. By attaching tissue-destroying isotopes such as alpha and β^- emitters to nanoparticles they can accumulate in tumor tissue and kill cancer cells. For such an approach to be desirable however, greatly improved accumulation in tumors compared to healthy organs will probably be necessary. An amalgamation of radiolabeling for diagnostics and therapy has been suggested, termed *theranostics*. In this approach, nanoparticles are radiolabeled with both a diagnostic isotope, such as a PET-isotope, along with an isotope capable of causing heavy cell death. Alternatively labeling with a single isotope that fulfills both roles can be envisaged. ^{64}Cu has been suggested as such an isotope. Theranostics may become a heavily researched field in the near future.

In this thesis was presented research on the radiolabeling of nanoparticles. The results regarding labeling of liposomes with ^{18}F showed that this isotope is able to provide adequate contrast for tumor imaging during an 8 hour scan. This has a number of advantages as ^{18}F is generally easy to work with due to its short half-life. In addition it is cheap and widely available. For the patient it is also an advantage to only “be radioactive” for about 8 hours. On the other hand however, for scanning 8 hours, it is necessary to have a relatively high amount of radioactivity upon injection. This can prompt tissue-dose considerations. ^{18}F however, being an almost 100% positron emitter, generally gives a low tissue dose per positron emitted. There are currently no simple and perfectly reliable ways of labeling liposomes with ^{18}F . In the research presented here, liposomes were labeled with an ^{18}F -lipid probe, which to us seems the best current method. The presented research into labeling with phosphazene bases in organic solvents presents a desirable method of preparing highly lipophilic ^{18}F -probes. Future applications of ^{18}F -labeling of nanoparticles could include the automated synthesis of ^{18}F -labeled small molecules which can be incubated with pre-fabricated nanoparticles and quickly react with components of their architecture in aqueous medium. Such a method would have the added bonus of being able to radiolabeled commercial formulations off the shelf.

In addition to work on liposomes our efforts to radiolabeled polymeric micelles was presented. In our group, we had synthesized triblock copolymers with a functionalizable shell-region and a lipophilic core. Polymeric micelles are one of the new types of nanoparticles which have exhibited diminished uptake in liver and spleen, thus solving part of the problems

General conclusion and perspectives

alluded to above. An advantage of polymeric micelles, and a possible reason for their improved properties, is the possibility of preparing them in very small sizes. At the moment, nanoparticles of 20-50 nm are thought especially interesting. The micelles we prepared were within this range. In order to chemically stabilize the micelles in the blood stream, we prepared them with cores consisting of coumarin moieties. Coumarin is a molecule which can covalently inter-link through exposure to UV radiation. The objective of the research was to investigate the pharmacokinetics of such particles. For labeling them with ^{64}Cu , we conjugated them with chelators in the shell-region, where they were thought to be protected from interacting with blood stream components. The chelators chosen were DOTA and CB-TE2A. In the literature there is an on-going debate on the instability of DOTA *in-vivo*, especially with regard to transchelation. An instability which CB-TE2A has been shown not to possess. In order to optimally track nanoparticles *in-vivo* it is necessary to possess stable and reliable chelators. We set out to investigate this stability difference through an *in-vivo* PET study. Our results were inconclusive on the subject of which chelator is the most stable. The evidence obtained however, did not generally suggest that there was a clinically significant difference in stability between the two. DOTA is a widely used and available chelator, providing excellent images in the clinic. Based on our results, we believe that DOTA will be in use for a long time to come and that transchelation after uptake in cells has little or no clinical relevance, at least for nanoparticles.

In addition, we compared core-crosslinked micelles with non-crosslinked micelles of identical architecture. To our surprise, we found that the two exhibited identical pharmacokinetics, showing relatively long half-lives of about 20 hours, and achieving acceptable tumor accumulation. Crosslinked micelles have the general disadvantage of low biodegradability. This is a concern if such therapeutics are to be used in humans as imaging radiopharmaceuticals. Accumulation of non-degradable nanoparticles is undesirable. Therefore, non-crosslinked micelles with good *in-vivo* properties are interesting. Such micelles can be cleared unimers by unimer as they naturally dissociate. In addition, such micelle systems should, while achieving good tumor accumulation have limited blood half-life. This is in order to achieve appreciable contrast between tumor and blood and thus easier visualization.

Generally, polymeric micelles seem to have a future place in the field of nanoparticle based radiopharmaceuticals. Because of their superior *in-vivo* pharmacokinetics they can potentially deliver less dose to healthy tissues.

5. References

1. Belov VV, Bonab, AA, Fischman, AJ, et al., **Iodine-124 as a Label for Pharmacological PET Imaging.** *Mol Pharm*, (2011). 8(3): p. 736.
2. Phillips WT, **Delivery of gamma-imaging agents by liposomes.** *Adv Drug Del Rev*, (1999). 37(1-3): p. 13.
3. Fonge H, Huang, H, Scollard, D, et al., **Influence of formulation variables on the biodistribution of multifunctional block copolymer micelles.** *J control release*, (2012). 157(3): p. 366.
4. Gomme J, *Isotopteknik (in Danish)*. 1997, Gad.
5. Richardson VJ, Jeyasingh, K, Jewkes, RF, et al., **Properties og [TC-99M] technetium-labeled liposomes in normal and tumor-bearing rats.** *Biochem Soc Trans*, (1977). 5(1): p. 290.
6. Malvezzi M, Bertuccio, P, Levi, F, et al., **European cancer mortality predictions for the year 2012.** *Ann onco.*, (2012). 23(4): p. 1044.
7. Hwang KJ, **Modes of interaction of (In³⁺)-8-hydroxyquinoline with membrane bilayer.** *J Nucl Med*, (1978). 19(10): p. 1162.
8. Siegel R, Naishadham, D, and Jemal, A, **Cancer Statistics, 2012.** *CA-Cancer J Clin*, (2012). 62(1): p. 10.
9. Mauk MR and Gamble, RC, **Preparation of lipid vesicles containing high-levels of entrapped radioactive cations.** *Anal Biochem*, (1979). 94(2): p. 302.
10. Hoang B, Lee, H, Reilly, RM, et al., **Noninvasive monitoring of the fate of 111In-labeled block copolymer micelles by high resolution and high sensitivity microSPECT/CT imaging.** *Mol Pharm*, (2009). 6(2): p. 581.
11. Rossin R, Pan, DPJ, Qi, K, et al., **Cu-64-labeled folate-conjugated shell cross-linked nanoparticles for tumor imaging and radiotherapy: Synthesis, radiolabeling, and biologic evaluation.** *J Nucl Med*, (2005). 46(7): p. 1210.
12. Xiao YL, Hong, H, Javadi, A, et al., **Multifunctional unimolecular micelles for cancer-targeted drug delivery and positron emission tomography imaging.** *Biomaterials*, (2012). 33(11): p. 3071.
13. Yang Z, Zheng, SY, Harrison, WJ, et al., **Long-circulating near-infrared fluorescence core-cross-linked polymeric micelles: Synthesis, characterization, and dual nuclear/optical imaging.** *Biomacromolecules*, (2007). 8(11): p. 3422.
14. Hnatowich DJ, Friedman, B, Clancy, B, et al., **Labeling of preformed liposomes with Ga-67 and Tc-99m by chelation.** *J Nucl Med*, (1981). 22(9): p. 810.
15. Ehrlich P, **Aus Theorie und Praxis der Chemoterapie** *Folia Serologica*, (1911). 7: p. 697.
16. Zhao J, Song, SL, Zhong, M, et al., **Dual-Modal Tumor Imaging via Long-Circulating Biodegradable Core-Cross-Linked Polymeric Micelles.** *ACS Macro Lett*, (2011). 1(1): p. 150.
17. Arrowsmith M, Hadgraft, J, and Kellaway, IW, **The in vivo release of cortisone esters from liposomes and the intramuscular clearance of liposomes.** *Int J Pharm*, (1984). 20(3): p. 347.

5. References

18. Gabizon A, Huberty, J, Starubinger, M, et al., **An improved method for in vivo tracing and imaging of liposomes using a gallium 67-deferoxamine complex.** *J Liposome Res*, (1988). 1.
19. Gabizon AA, **Stealth liposomes and tumor targeting: One step further in the quest for the magic bullet.** *Clin Cancer Res*, (2001). 7(2): p. 223.
20. Love WG, Amos, N, Williams, BD, et al., **Effect of liposome surface-charge on the stability of technetium (Tc-99m) radiolabeled liposomes.** *J Microencapsulation*, (1989). 6(1): p. 105.
21. Bangham AD and Horne, RW, **Negative staining of phospholipids + their structural modification by-surface active agents as observed in electron microscope.** *J Mol Biol*, (1964). 8(5): p. 660.
22. Bangham AD, Standish, MM, and Watkins, JC, **Diffusion of univalent ions across lamellae of swollen phospholipids.** *J Mol Biol*, (1965). 13(1): p. 238.
23. Phillips WT, Rudolph, AS, Goins, B, et al., **A simple method for producing a Tc-99m-labeled liposome which is stable in-vivo.** *Nucl Med Biol*, (1992). 19(5): p. 539.
24. Gregoria.G, Wills, EJ, Swain, CP, et al., **Drug-carrier potential of liposomes in cancer chemotherapy.** *Lancet*, (1974). 1(7870): p. 1313.
25. Kim S, Turker, MS, Chi, EY, et al., **Preparation of multivesicular liposomes.** *Biochim Biophys Acta*, (1983). 728(3): p. 339.
26. Oku N, Namba, Y, Takeda, A, et al., **Tumor imaging with Tc-99m DTPA encapsulated in RES-avoiding liposomes.** *Nucl Med Biol*, (1993). 20(4): p. 407.
27. Oku N, Tokudome, Y, Tsukada, H, et al., **Real-time analysis of liposomal trafficking in tumor-bearing mice by use of positron emission tomography.** *Biochim Biophys Acta-Biomembr*, (1995). 1238(1): p. 86.
28. Dams ETM, Oyen, WJG, Boerman, OC, et al., **Tc-99m-PEG liposomes for the scintigraphic detection of infection and inflammation clinical evaluation.** *J Nucl Med*, (2000). 41(4): p. 622.
29. Oyen WJG, Boerman, OC, Storm, G, et al., **Detecting infection and inflammation with technetium-99m-labeled Stealth(R) liposomes.** *J Nucl Med*, (1996). 37(8): p. 1392.
30. Corvo ML, Boerman, OC, Oyen, WJG, et al., **Intravenous administration of superoxide dismutase entrapped in long circulating liposomes.** *Biochim Biophys Acta-Biomembr*, (1999). 1419(2): p. 325.
31. Laverman P, Dams, ETM, Oyen, WJG, et al., **A novel method to label liposomes with Tc-99m by the hydrazino nicotiny derivative.** *J Nucl Med*, (1999). 40(1): p. 192.
32. Bao A, Goins, B, Klipper, R, et al., **A novel liposome radiolabeling method using 99mTc-"SNS/S" complexes: in vitro and in vivo evaluation.** *J Pharm Sci*, (2003). 92(9): p. 1893.
33. Mougin-Degraef M, Jestin, E, Bruel, D, et al., **High-activity radio-iodine labeling of conventional and stealth liposomes.** *J Liposome Res*, (2006). 16(1): p. 91.
34. Mougin-Degraef M, Bourdeau, C, Jestin, E, et al., **Doubly radiolabeled liposomes for pretargeted radioimmunotherapy.** *Int J Pharm*, (2007). 344(1-2): p. 110.
35. Urakami T, Akai, S, Katayama, Y, et al., **Novel amphiphilic probes for [F-18]-radiolabeling preformed liposomes and determination of liposomal trafficking by positron emission tomography.** *J Med Chem*, (2007). 50(26): p. 6454.

5. References

36. Urakami T, Kawaguchi, AT, Akai, S, et al., **In vivo distribution of liposome-encapsulated hemoglobin determined by positron emission tomography.** *Artif Organs*, (2009). 33(2): p. 164.
37. Marik J, Tartis, MS, Zhang, H, et al., **Long-circulating liposomes radiolabeled with [18F]fluorodipalmitin ([18F]FDP).** *Nucl Med Biol*, (2007). 34(2): p. 165.
38. Seo JW, Zhang, H, Kukis, DL, et al., **A novel method to label preformed liposomes with Cu-64 for positron emission tomography (PET) imaging.** *Bioconjugate Chem*, (2008). 19(12): p. 2577.
39. Seo JW, Mahakian, LM, Kheirilomoom, A, et al., **Liposomal Cu-64 labeling method using bifunctional chelators: poly(ethylene glycol) spacer and chelator effects.** *Bioconjugate Chem*, (2010). 21(7): p. 1206.
40. Weiner N, Martin, F, and Riaz, M, **Liposomes as a drug delivery system.** *Drug Dev Ind Pharm*, (1989). 15(10): p. 1523.
41. Petersen AL, Binderup, T, Rasmussen, P, et al., **64Cu loaded liposomes as positron emission tomography imaging agents.** *Biomaterials*, (2011). 32(9): p. 2334.
42. Barenholz Y, Amselem, S, and Lichtenberg, D, **New method for preparation of phospholipid vesicles (liposomes) - french press.** *FEBS Lett*, (1979). 99(1): p. 210.
43. Maitani Y, Soeda, H, Wan, JP, et al., **Modified ethanol injection method for liposomes containing beta-sitosterol beta-D-glucoside.** *J Liposome Res*, (2001). 11(1): p. 115.
44. Pons M, Foradada, M, and Estelrich, J, **Liposomes obtained by the ethanol injection method.** *Int J Pharm*, (1993). 95(1-3): p. 51.
45. Batzri S and Korn, ED, **Single Bilayer Liposomes Prepared without Sonication.** *Biochim Biophys Acta*, (1973). 298(4): p. 1015.
46. Duzgunes N, **Preparation and quantitation of small unilamellar liposomes and large unilamellar reverse-phase evaporation liposomes.** *Liposomes, Pt A*, (2003). 367: p. 23.
47. Szoka F and Papahadjopoulos, D, **Procedure for preparation of liposomes with large internal aqueous space and high capture by reverse-phase evaporation.** *Proc Natl Acad Sci U S A*, (1978). 75(9): p. 4194.
48. Foged C, Nielsen, HM, and Frokjaer, S, **Liposomes for phospholipase A(2) triggered siRNA release: Preparation and in vitro test.** *Int J Pharm*, (2007). 331(2): p. 160.
49. Jukes TH, **The electrometric titration of lecithin and cephalin.** *J Biol Chem*, (1934). 107(3): p. 783.
50. Rao NM, **Cationic lipid-mediated nucleic acid delivery: beyond being cationic.** *Chem Phys Lipids*, (2010). 163(3): p. 245.
51. Kinnunen P, Alakoskela, JM, and Laggnier, P, **Phase behavior of liposomes.** *Liposomes, Pt A*, (2003). 367: p. 129.
52. Ulrich AS, **Biophysical aspects of using liposomes as delivery vehicles.** *Biosci Rep*, (2002). 22(2): p. 129.
53. Szoka F and Papahadjopoulos, D, **Comparative properties and methods of preparation of lipid vesicles (liposomes).** *Annu Rev Biophys Bioeng*, (1980). 9: p. 467.
54. Needham D, Anyarambhatla, G, Kong, G, et al., **A new temperature-sensitive liposome for use with mild hyperthermia: characterization and testing in a human tumor xenograft model.** *Cancer Res*, (2000). 60(5): p. 1197.

5. References

55. Lange Y, Swaisgood, MH, Ramos, BV, et al., **Plasma-membranes contain half the phospholipid and 90-percent of the cholesterol and sphingomyelin in cultured human-fibroblasts.** *J Biol Chem*, (1989). 264(7): p. 3786.
56. Ipsen JH, Karlstrom, G, Mouritsen, OG, et al., **Phase-equilibria in the phosphatidylcholine-cholesterol system.** *Biochim Biophys Acta*, (1987). 905(1): p. 162.
57. Maulik PR and Shipley, GG, **N-palmitoyl sphingomyelin bilayers: Structure and interactions with cholesterol and dipalmitoylphosphatidylcholine.** *Biochemistry (Mosc)*, (1996). 35(24): p. 8025.
58. McMullen TPW, Lewis, R, and McElhaney, RN, **Differential scanning calorimetric study of the effect of cholesterol on the thermotropic phase-behavior of a homologous series of linear saturated phosphatidylcholines.** *Biochemistry (Mosc)*, (1993). 32(2): p. 516.
59. Corvera E, Mouritsen, OG, Singer, MA, et al., **The permeability and the effect of acyl-chain length for phospholipid-bilayers containing cholesterol - theory and experiment.** *Biochim Biophys Acta*, (1992). 1107(2): p. 261.
60. Mouritsen OG and Zuckermann, MJ, **What's so special about cholesterol?** *Lipids*, (2004). 39(11): p. 1101.
61. Raffy S and Teissie, J, **Control of lipid membrane stability by cholesterol content.** *Biophys J*, (1999). 76(4): p. 2072.
62. Poste G, Bucana, C, Raz, A, et al., **Analysis of the fate of systemically administered liposomes and implications for their use in drug delivery.** *Cancer Res*, (1982). 42(4): p. 1412.
63. Scherphof GL, Dijkstra, J, Spanjer, HH, et al., **Uptake and intracellular processing of targeted and nontargeted liposomes by rat kupffer cells invivo and invitro.** *Ann NY Acad Sci*, (1985). 446: p. 368.
64. Allen TM, Hansen, C, Martin, F, et al., **Liposomes containing synthetic lipid derivatives of poly(ethylene glycol) show prolonged circulation half-lives invivo.** *Biochim Biophys Acta*, (1991). 1066(1): p. 29.
65. Klibanov AL, Maruyama, K, Torchilin, VP, et al., **Amphipathic polyethyleneglycols effectively prolong the circulation time of liposomes.** *FEBS Lett*, (1990). 268(1): p. 235.
66. Harrington KJ, Mohammadtaghi, S, Uster, PS, et al., **Effective targeting of solid tumors in patients with locally advanced cancers by radiolabeled pegylated liposomes.** *Clin Cancer Res*, (2001). 7(2): p. 243.
67. Moghimi SM, Hamad, I, Andresen, TL, et al., **Methylation of the phosphate oxygen moiety of phospholipid-methoxy(polyethylene glycol) conjugate prevents PEGylated liposome-mediated complement activation and anaphylatoxin production.** *FASEB J*, (2006). 20(14): p. 2591.
68. Kabanov AV, Chekhonin, VP, Alakhov, VY, et al., **The neuroleptic activity of haloperidol increases after its solubilization in surfactant micelles - micelles as microcontainers for drug targeting.** *FEBS Lett*, (1989). 258(2): p. 343.
69. Gong J, Chen, M, Zheng, Y, et al., **Polymeric micelles drug delivery system in oncology.** *J Control Release*, (2012). 159(3): p. 312.
70. Maibaum L, Dinner, AR, and Chandler, D, **Micelle formation and the hydrophobic effect.** *J Phys Chem B*, (2004). 108(21): p. 6778.

5. References

71. Li Z, Ma, J, Lee, NS, et al., **Dynamic cylindrical assembly of triblock copolymers by a hierarchical process of covalent and supramolecular interactions.** *JACS*, (2012). 133(5): p. 1228.
72. Zhang LF and Eisenberg, A, **Multiple morphologies of crew-cut aggregates of polystyrene-b-poly(acrylic acid) block-copolymers.** *Science*, (1995). 268(5218): p. 1728.
73. Oerlemans C, Bult, W, Bos, M, et al., **polymeric micelles in anticancer therapy: targeting, imaging and triggered release.** *Pharmaceutical Research*, (2010). 27(12): p. 2569.
74. Nishiyama N, Okazaki, S, Cabral, H, et al., **Novel cisplatin-incorporated polymeric micelles can eradicate solid tumors in mice.** *Cancer Res*, (2003). 63(24): p. 8977.
75. Stubbs M, McSheehy, PMJ, Griffiths, JR, et al., **Causes and consequences of tumour acidity and implications for treatment.** *Mol Med Today*, (2000). 6(1): p. 15.
76. Newell K, Franchi, A, Pouysségur, J, et al., **Studies with glycolysis-deficient cells suggest that production of lactic acid is not the only cause of tumor acidity.** *Proceedings of the National Academy of Sciences*, (1993). 90(3): p. 1127.
77. Lee ES, Na, K, and Bae, YH, **Polymeric micelle for tumor pH and folate-mediated targeting.** *J Controlled Release*, (2003). 91(1-2): p. 103.
78. Gao ZG, Lee, DH, Kim, DI, et al., **Doxorubicin loaded pH-sensitive micelle targeting acidic extracellular pH of human ovarian A2780 tumor in mice.** *J Drug Target*, (2005). 13(7): p. 391.
79. Lee ES, Shin, HJ, Na, K, et al., **Poly(L-histidine)-PEG block copolymer micelles and pH-induced destabilization.** *J Controlled Release*, (2003). 90(3): p. 363.
80. Leroux JC, Roux, E, Le Garrec, D, et al., **N-isopropylacrylamide copolymers for the preparation of pH-sensitive liposomes and polymeric micelles.** *J Controlled Release*, (2001). 72(1-3): p. 71.
81. Liu SY, Weaver, JVM, Tang, YQ, et al., **Synthesis of shell cross-linked micelles with pH-responsive cores using ABC triblock copolymers.** *Macromolecules*, (2002). 35(16): p. 6121.
82. Bae Y, Nishiyama, N, Fukushima, S, et al., **Preparation and biological characterization of polymeric micelle drug carriers with intracellular pH-triggered drug release property: Tumor permeability, controlled subcellular drug distribution, and enhanced in vivo antitumor efficacy.** *Bioconjugate Chem*, (2005). 16(1): p. 122.
83. Chung JE, Yokoyama, M, and Okano, T, **Inner core segment design for drug delivery control of thermo-responsive polymeric micelles.** *J Controlled Release*, (2000). 65(1-2): p. 93.
84. Lee HI, Wu, W, Oh, JK, et al., **Light-induced reversible formation of polymeric micelles.** *Angewandte Chemie-International Edition*, (2007). 46(14): p. 2453.
85. Van Butsele K, Sibret, P, Fustin, CA, et al., **Synthesis and pH-dependent micellization of diblock copolymer mixtures.** *J Colloid Interface Sci*, (2009). 329(2): p. 235.
86. Patil YB, Toti, US, Khadair, A, et al., **Single-step surface functionalization of polymeric nanoparticles for targeted drug delivery.** *Biomaterials*, (2009). 30(5): p. 859.
87. Kedar U, Phutane, P, Shidhaye, S, et al., **Advances in polymeric micelles for drug delivery and tumor targeting.** *Nanomed-Nanotechnol Biol Med*, (2010). 6(6): p. 714.

5. References

88. Wiradharma N, Zhang, Y, Venkataraman, S, et al., **Self-assembled polymer nanostructures for delivery of anticancer therapeutics**. *Nano Today*, (2009). 4(4): p. 302.
89. Wilhelm M, Zhao, CL, Wang, YC, et al., **Polymer micelle formation .3. poly(styrene-ethylene oxide) block copolymer micelle formation in water - a fluorescence probe study**. *Macromolecules*, (1991). 24(5): p. 1033.
90. Kwon GS and Okano, T, **Polymeric micelles as new drug carriers**. *Advanced Drug Delivery Reviews*, (1996). 21(2): p. 107.
91. Liu JB, Zeng, FQ, and Allen, C, **In vivo fate of unimers and micelles of a poly(ethylene glycol)-block-poly(caprolactone) copolymer in mice following intravenous administration**. *European Journal of Pharmaceutics and Biopharmaceutics*, (2007). 65(3): p. 309.
92. Jeong B, Bae, YH, and Kim, SW, **Biodegradable thermosensitive micelles of PEG-PLGA-PEG triblock copolymers**. *Colloids and Surfaces B-Biointerfaces*, (1999). 16(1-4): p. 185.
93. Toncheva V, Schacht, E, Ng, SY, et al., **Use of block copolymers of poly(ortho esters) and poly(ethylene glycol) micellar carriers as potential tumour targeting systems**. *Journal of Drug Targeting*, (2003). 11(6): p. 345.
94. Kubowicz S, Baussard, JF, Lutz, JF, et al., **Multicompartment micelles formed by self-assembly of linear ABC triblock copolymers in aqueous medium**. *Angewandte Chemie-International Edition*, (2005). 44(33): p. 5262.
95. Tang YQ, Liu, SY, Armes, SP, et al., **Solubilization and controlled release of a hydrophobic drug using novel micelle-forming ABC triblock copolymers**. *Biomacromolecules*, (2003). 4(6): p. 1636.
96. Bastakoti BP, Guragain, S, Yokoyama, Y, et al., **Incorporation and release behavior of amitriptylene in core-shell-corona type triblock copolymer micelles**. *Colloids and Surfaces B-Biointerfaces*, (2011). 88(2): p. 734.
97. Li YT, Lokitz, BS, and McCormick, CL, **RAFT synthesis of a thermally responsive ABC triblock copolymer incorporating N-acryloxysuccinimide for facile in situ formation of shell cross-linked micelles in aqueous media**. *Macromolecules*, (2006). 39(1): p. 81.
98. Zhu W, Li, YL, Liu, LX, et al., **Biamphiphilic triblock copolymer micelles as a multifunctional platform for anticancer drug delivery**. *Journal of Biomedical Materials Research Part A*, (2011). 96A(2): p. 330.
99. Endres TK, Beck-Broichsitter, M, Samsonova, O, et al., **Self-assembled biodegradable amphiphilic PEG-PCL-IPEI triblock copolymers at the borderline between micelles and nanoparticles designed for drug and gene delivery**. *Biomaterials*, (2011). 32(30): p. 7721.
100. Iijima M, Nagasaki, Y, Okada, T, et al., **Core-polymerized reactive micelles from heterotelechelic amphiphilic block copolymers**. *Macromolecules*, (1999). 32(4): p. 1140.
101. Rheingans O, Hugenberg, N, Harris, JR, et al., **Nanoparticles built of cross-linked heterotelechelic, amphiphilic poly(dimethylsiloxane)-b-poly(ethylene oxide) diblock copolymers**. *Macromolecules*, (2000). 33(13): p. 4780.
102. Kim JH, Emoto, K, Iijima, M, et al., **Core-stabilized polymeric micelle as potential drug carrier: Increased solubilization of taxol**. *Polymers for Advanced Technologies*, (1999). 10(11): p. 647.

5. References

103. Bontha S, Kabanov, AV, and Bronich, TK, **Polymer micelles with cross-linked ionic cores for delivery of anticancer drugs.** *Journal of Controlled Release*, (2006). 114(2): p. 163.
104. Jaturanpinyo M, Harada, A, Yuan, XF, et al., **Preparation of bionanoreactor based on core-shell structured polyion complex micelles entrapping trypsin in the core cross-linked with glutaraldehyde.** *Bioconjugate Chem*, (2004). 15(2): p. 344.
105. Thurmond KB, Huang, HY, Clark, CG, et al., **Shell cross-linked polymer micelles: stabilized assemblies with great versatility and potential.** *Colloids and Surfaces B-Biointerfaces*, (1999). 16(1-4): p. 45.
106. Kim Y, Pourgholami, MH, Morris, DL, et al., **Effect of Cross-Linking on the Performance of Micelles As Drug Delivery Carriers: A Cell Uptake Study.** *Biomacromolecules*, (2012). 13(3): p. 814.
107. Butun V, Lowe, AB, Billingham, NC, et al., **Synthesis of zwitterionic shell cross-linked micelles.** *J Am Chem Soc*, (1999). 121(17): p. 4288.
108. Shuai XT, Merdan, T, Schaper, AK, et al., **Core-cross-linked polymeric micelles as paclitaxel carriers.** *Bioconjugate Chem*, (2004). 15(3): p. 441.
109. Joralemon MJ, Smith, NL, Holowka, D, et al., **Antigen-decorated shell cross-linked nanoparticles: Synthesis, characterization, and antibody interactions.** *Bioconjugate Chem*, (2005). 16(5): p. 1246.
110. Nystroem AM and Wooley, KL, **Construction of thermoresponsive SCKs through tuning the crystalline melting point of the core domain.** *Soft Matter*, (2008). 4(4): p. 849.
111. Nystrom AM and Wooley, KL, **Thiol-functionalized shell crosslinked knedel-like (SCK) nanoparticles: a versatile entry for their conjugation with biomacromolecules.** *Tetrahedron*, (2008). 64(36): p. 8543.
112. Nystrom AM, Xu, Z, Xu, J, et al., **SCKs as nanoparticle carriers of doxorubicin: investigation of core composition on the loading, release and cytotoxicity profiles.** *Chemical Communications*, (2008)(30): p. 3579.
113. Shrestha R, Shen, Y, Pollack, KA, et al., **Dual Peptide Nucleic Acid- and Peptide-Functionalized Shell Cross-Linked Nanoparticles Designed to Target mRNA toward the Diagnosis and Treatment of Acute Lung Injury.** *Bioconjugate Chem*, (2012). 23(3): p. 574.
114. Sun G, Hagooley, A, Xu, J, et al., **Facile, efficient approach to accomplish tunable chemistries and variable biodistributions for shell cross-linked nanoparticles.** *Biomacromolecules*, (2008). 9(7): p. 1997.
115. Sun XK, Rossin, R, Turner, JL, et al., **An assessment of the effects of shell cross-linked nanoparticle size, core composition, and surface PEGylation on in vivo biodistribution.** *Biomacromolecules*, (2005). 6(5): p. 2541.
116. Turner JL, Becker, ML, Li, XX, et al., **PNA-directed solution- and surface-assembly of shell crosslinked (SCK) nanoparticle conjugates.** *Soft Matter*, (2005). 1(1): p. 69.
117. Zhang K, Fang, H, Wang, Z, et al., **Cationic shell-crosslinked knedel-like nanoparticles for highly efficient gene and oligonucleotide transfection of mammalian cells.** *Biomaterials*, (2009). 30(5): p. 968.
118. Li YT, Lokitz, BS, Armes, SP, et al., **Synthesis of reversible shell cross-linked micelles for controlled release of bioactive agents.** *Macromolecules*, (2006). 39(8): p. 2726.

5. References

119. Xu XW, Flores, JD, and McCormick, CL, **Reversible Imine Shell Cross-Linked Micelles from Aqueous RAFT-Synthesized Thermoresponsive Triblock Copolymers as Potential Nanocarriers for "pH-Triggered" Drug Release.** *Macromolecules*, (2011). 44(6): p. 1327.
120. Jiang JQ, Qi, B, Lepage, M, et al., **Polymer micelles stabilization on demand through reversible photo-cross-linking.** *Macromolecules*, (2007). 40(4): p. 790.
121. Gregoria.G and Ryman, BE, **Liposomes as carriers of enzymes or drugs - new approach to treatment of storage diseases.** *Biochem J*, (1971). 124(5): p. P58.
122. Moghimi SM and Szebeni, J, **Stealth liposomes and long circulating nanoparticles: critical issues in pharmacokinetics, opsonization and protein-binding properties.** *Prog Lipid Res*, (2003). 42(6): p. 463.
123. Gabizon A, Shmeeda, H, and Barenholz, Y, **Pharmacokinetics of pegylated liposomal doxorubicin - Review of animal and human studies.** *Clin Pharmacokinet*, (2003). 42(5): p. 419.
124. Barratt G and Legrand, P, **Comparison of the efficacy and pharmacology of formulations of amphotericin B used in treatment of leishmaniasis.** *Curr Opin Infect Dis*, (2005). 18(6): p. 527.
125. Matsumura Y and Maeda, H, **A new concept for macromolecular therapeutics in cancer-chemotherapy - mechanism of tumoritropic accumulation of proteins and the antitumor agent smancs.** *Cancer Res*, (1986). 46(12): p. 6387.
126. Maeda H, **The enhanced permeability and retention (EPR) effect in tumor vasculature: The key role of tumor-selective macromolecular drug targeting.** *Adv Enzyme Regul*, (2001). 41: p. 189.
127. Fang J, Nakamura, H, and Maeda, H, **The EPR effect: Unique features of tumor blood vessels for drug delivery, factors involved, and limitations and augmentation of the effect.** *Adv Drug Del Rev*, (2011). 63(3): p. 136.
128. Folkman J, **What is the evidence that tumors are angiogenesis dependent.** *J Natl Cancer Inst*, (1990). 82(1): p. 4.
129. Folkman J, **Angiogenesis in cancer, vascular, rheumatoid and other disease.** *Nat Med*, (1995). 1(1): p. 27.
130. Folkman J, Bach, M, Rowe, JW, et al., **Tumor angiogenesis - therapeutic implications.** *N Engl J Med*, (1971). 285(21): p. 1182.
131. Hobbs SK, Monsky, WL, Yuan, F, et al., **Regulation of transport pathways in tumor vessels: Role of tumor type and microenvironment.** *Proc Natl Acad Sci U S A*, (1998). 95(8): p. 4607.
132. Venturoli D and Rippe, B, **Ficoll and dextran vs. globular proteins as probes for testing glomerular permselectivity: effects of molecular size, shape, charge, and deformability.** *Am J Physiol-Renal Physiol*, (2005). 288(4): p. F605.
133. Torchilin VP, **Micellar nanocarriers: Pharmaceutical perspectives.** *Pharmaceutical Research*, (2007). 24(1): p. 1.
134. Konno T, Maeda, H, Iwai, K, et al., **Selective targeting of anti-cancer drug and simultaneous image-enhancement in solid tumors by arterially administered lipid contrast-medium.** *Cancer*, (1984). 54(11): p. 2367.
135. Kaasgaard T and Andresen, TL, **Liposomal cancer therapy: exploiting tumor characteristics.** *Expert Opinion on Drug Delivery*, (2010). 7(2): p. 225.

5. References

136. Minchinton AI and Tannock, IF, **Drug penetration in solid tumours**. *Nature Reviews Cancer*, (2006). 6(8): p. 583.
137. Heldin CH, Rubin, K, Pietras, K, et al., **High interstitial fluid pressure - An obstacle in cancer therapy**. *Nature Reviews Cancer*, (2004). 4(10): p. 806.
138. Baxter LT and Jain, RK, **Transport of fluid and macromolecules in tumors .1. role of interstitial pressure and convection**. *Microvasc Res*, (1989). 37(1): p. 77.
139. Vaupel P and Harrison, L, **Tumor hypoxia: causative factors, compensatory mechanisms, and cellular response**. *Oncologist*, (2004). 9 Suppl 5: p. 4.
140. Harrington KJ, Rowlinson-Busza, G, Syrigos, KN, et al., **Influence of tumour size on uptake of In-111-DTPA-labelled pegylated liposomes in a human tumour xenograft model**. *British Journal of Cancer*, (2000). 83(5): p. 684.
141. Waite CL and Roth, CM, **nanoscale drug delivery systems for enhanced drug penetration into solid tumors: current progress and opportunities**. *Critical Reviews in Biomedical Engineering*, (2012). 40(1): p. 21.
142. Cabral H, Matsumoto, Y, Mizuno, K, et al., **Accumulation of sub-100 nm polymeric micelles in poorly permeable tumours depends on size**. *Nat Nanotechnol*, (2011). 6(12): p. 815.
143. Dreher MR, Liu, WG, Michelich, CR, et al., **Tumor vascular permeability, accumulation, and penetration of macromolecular drug carriers**. *J Natl Cancer Inst*, (2006). 98(5): p. 335.
144. Jain RK and Stylianopoulos, T, **Delivering nanomedicine to solid tumors**. *Nature Reviews Clinical Oncology*, (2010). 7(11): p. 653.
145. Torchilin VP and Papisov, MI, **Why do polyethylene glycol-coated liposomes circulate so long?** *J Liposome Res*, (1994). 4(1): p. 725.
146. Szebeni J, Baranyi, L, Savay, S, et al., **The role of complement activation in hypersensitivity to pegylated liposomal doxorubicin (DOXIL (R))**. *J Liposome Res*, (2000). 10(4): p. 467.
147. Price ME, Cornelius, RM, and Brash, JL, **Protein adsorption to polyethylene glycol modified liposomes from fibrinogen solution and from plasma**. *Biochim Biophys Acta-Biomembr*, (2001). 1512(2): p. 191.
148. Utkhede DR and Tilcock, CP, **Effect of lipid dose on the biodistribution and blood pool clearance kinetics of PEG-modified technetium-labeled lipid vesicles**. *J Liposome Res*, (1998). 8(3): p. 381.
149. Laverman P, Carstens, MG, Boerman, OC, et al., **Factors affecting the accelerated blood clearance of polyethylene glycol-liposomes upon repeated injection**. *J Pharmacol Exp Ther*, (2001). 298(2): p. 607.
150. Laverman P, Brouwers, AH, Dams, ETM, et al., **Preclinical and clinical evidence for disappearance of long-circulating characteristics of polyethylene glycol liposomes at low lipid dose**. *J Pharmacol Exp Ther*, (2000). 293(3): p. 996.
151. Dams ETM, Laverman, P, Oyen, WJG, et al., **Accelerated blood clearance and altered biodistribution of repeated injections of sterically stabilized liposomes**. *J Pharmacol Exp Ther*, (2000). 292(3): p. 1071.
152. Gbadamosi JK, Hunter, AC, and Moghimi, SM, **PEGylation of microspheres generates a heterogeneous population of particles with differential surface characteristics and biological performance**. *FEBS Lett*, (2002). 532(3): p. 338.

5. References

153. Geneser F, *Histologi (in Danish)*. 4 ed. Vol. 1. 2004, Munksgaard.
154. Moghimi SM, Hunter, AC, and Murray, JC, **Long-circulating and target-specific nanoparticles: Theory to practice**. *Pharmacol Rev*, (2001). 53(2): p. 283.
155. Cesta MF, **Normal structure, function, and histology of the spleen**. *Toxicol Pathol*, (2006). 34(5): p. 455.
156. Personal communication with Prof. Moein Moghimi, The Nanomedicine Group (KU), July 2nd 2012.
157. Moghimi SM, Porter, CJH, Muir, IS, et al., **Non-phagocytic uptake of intravenously injected microspheres in rat spleen - influence of particle-size and hydrophilic coating**. *Biochem Biophys Res Commun*, (1991). 177(2): p. 861.
158. Choi HS, Liu, W, Misra, P, et al., **Renal clearance of quantum dots**. *Nat Biotechnol*, (2007). 25(10): p. 1165.
159. Davis ME, Chen, Z, and Shin, DM, **Nanoparticle therapeutics: an emerging treatment modality for cancer**. *Nature Reviews Drug Discovery*, (2008). 7(9): p. 771.
160. Fox ME, Szoka, FC, and Frechet, JMJ, **Soluble polymer carriers for the treatment of cancer: the importance of molecular architecture**. *Accounts of Chemical Research*, (2009). 42(8): p. 1141.
161. Moghimi SM, Hunter, AC, and Andresen, TL, **Factors controlling nanoparticle pharmacokinetics: an integrated analysis and perspective**. *Annu Rev Pharmacol Toxicol*, (2012). 52: p. 481.
162. Ishida T, Atobe, K, Wang, X, et al., **Accelerated blood clearance of PEGylated liposomes upon repeated injections: effect of doxorubicin-encapsulation and high-dose first injection**. *J Control Release*, (2006). 115(3): p. 251.
163. Ishida T, Harada, M, Wang, XY, et al., **Accelerated blood clearance of PEGylated liposomes following preceding liposome injection: effects of lipid dose and PEG surface-density and chain length of the first-dose liposomes**. *J Control Release*, (2005). 105(3): p. 305.
164. Ishida T and Kiwada, H, **Accelerated blood clearance (ABC) phenomenon upon repeated injection of PEGylated liposomes**. *Int J Pharm*, (2008). 354(1-2): p. 56.
165. Ishida T, Ichihara, M, Wang, X, et al., **Injection of PEGylated liposomes in rats elicits PEG-specific IgM, which is responsible for rapid elimination of a second dose of PEGylated liposomes**. *J Controlled Release*, (2006). 112(1): p. 15.
166. Kaminskas LM, McLeod, VM, Porter, CJH, et al., **Differences in Colloidal Structure of PEGylated Nanomaterials Dictate the Likelihood of Accelerated Blood Clearance**. *J Pharm Sci*, (2011). 100(11): p. 5069.
167. Volkert WA and Hoffman, TJ, **Therapeutic radiopharmaceuticals**. *Chem Rev*, (1999). 99(9): p. 2269.
168. Personal communication with Prof. Mikael Jensen (DTU Nutech), August 17th (2012).
169. Paulus MJ, Gleason, SS, Kennel, SJ, et al., **High resolution X-ray computed tomography: An emerging tool for small animal cancer research**. *Neoplasia*, (2000). 2(1-2): p. 62.
170. Rahmim A and Zaidi, H, **PET versus SPECT: strengths, limitations and challenges**. *Nucl Med Commun*, (2008). 29(3): p. 193.

5. References

171. Lubberink M and Herzog, H, **Quantitative imaging of I-124 and Y-86 with PET.** *Eur J Nucl Med Mol Imag*, (2011). 38: p. 10.
172. Severin GW, Engle, JW, Barnhart, TE, et al., **Zr-89 Radiochemistry for Positron Emission Tomography.** *Med Chem*, (2011). 7(5): p. 389.
173. Zhang Y, Hong, H, and Cai, W, **PET tracers based on Zirconium-89.** *Curr Radiopharm*, (2011). 4(2): p. 131.
174. Gambhir SS, **Molecular imaging of cancer with positron emission tomography.** *Nature Reviews Cancer*, (2002). 2(9): p. 683.
175. Willmann JK, van Bruggen, N, Dinkelborg, LM, et al., **Molecular imaging in drug development.** *Nature Reviews Drug Discovery*, (2008). 7(7): p. 591.
176. Alavi A and Basu, S, **Planar and SPECT imaging in the era of PET and PET-CT: can it survive the test of time?** *Eur J Nucl Med Mol Imag*, (2008). 35(8): p. 1554.
177. Pfeifer A, Knigge, U, Mortensen, J, et al., **Clinical PET of Neuroendocrine Tumors Using 64Cu-DOTATATE: First-in-Humans Study.** *J Nucl Med*, (2012).
178. Bateman TM, **Advantages and disadvantages of PET and SPECT in a busy clinical practice.** *J Nucl Cardiol*, (2012). 19(1): p. 3.
179. Keliher EJ, Yoo, J, Nahrendorf, M, et al., **Zr-89-Labeled Dextran Nanoparticles Allow in Vivo Macrophage Imaging.** *Bioconjugate Chem*, (2011). 22(12): p. 2383.
180. Kelloff G, Hoffman, JM, Johnson, B, et al., **Progress and promise of FDG-PET imaging for cancer patient management and oncologic drug development.** *Clin Cancer Res*, (2005). 11(8): p. 2785.
181. Coenen HH, Elsinga, PH, Iwata, R, et al., **Fluorine-18 radiopharmaceuticals beyond [F-18]FDG for use in oncology and neurosciences.** *Nucl Med Biol*. 37(7): p. 727.
182. Cai LS, Lu, SY, and Pike, VW, **Chemistry with [F-18]fluoride ion.** *Eur J Org Chem*, (2008)(17): p. 2853.
183. Hess E, Takacs, S, Scholten, B, et al., **Excitation function of the O-18(p,n)F-18 nuclear reaction from threshold up to 30 MeV.** *Radiochimica Acta*, (2001). 89(6): p. 357.
184. Zhan CG and Dixon, DA, **Hydration of the fluoride anion: Structures and absolute hydration free energy from first-principles electronic structure calculations.** *J Phys Chem A*, (2004). 108(11): p. 2020.
185. Vlasov VM, **Fluoride-ion as a nucleophile and a leaving group in aromatic nucleophilic-substitution reactions.** *J Fluorine Chem*, (1993). 61(3): p. 193.
186. Kemp DD and Gordon, MS, **Theoretical study of the solvation of fluorine and chlorine anions by water.** *J Phys Chem A*, (2005). 109(34): p. 7688.
187. Schlyer DJ, Bastos, MAV, Alexoff, D, et al., **Separation of [f-18] fluoride from [o-18]water using anion-exchange resin.** *Appl Radiat Isot*, (1990). 41(6): p. 531.
188. Mathiessen B, Jensen, ATI, and Zhuravlev, F, **Homogeneous Nucleophilic Radiofluorination and Fluorination with Phosphazene Hydrofluorides.** *Chem-Eur J*, (2011). 17(28): p. 7796.
189. Brodack JW, Kilbourn, MR, Welch, MJ, et al., **No-carrier-added 16-alpha fluorine-18 fluoroestradiol-17-beta the effect of reaction vessel on fluorine-18 resolubilization product yield and effective specific activity.** *Int J Appl Radiat Isot*, (1986). 37(3): p. 217.

5. References

190. Hamacher K, Coenen, HH, and Stocklin, G, **Efficient stereospecific synthesis of no-carrier-added 2-[f-18]-fluoro-2-deoxy-d-glucose using aminopolyether supported nucleophilic-substitution.** *J Nucl Med*, (1986). 27(2): p. 235.
191. Suehiro M, Vallabhajosula, S, Goldsmith, SJ, et al., **Investigation of the role of the base in the synthesis of [F-18]FLT.** *Appl Radiat Isot*, (2007). 65(12): p. 1350.
192. Cai WB, Wu, Y, Chen, K, et al., **In vitro and in vivo characterization of Cu-64-labeled Abegrin (TM) a humanized monoclonal antibody against integrin alpha(v)beta(3).** *Cancer Res*, (2006). 66(19): p. 9673.
193. Zhang Y, Hong, H, Engle, JW, et al., **Positron Emission Tomography Imaging of CD105 Expression with a Cu-64-Labeled Monoclonal Antibody: NOTA Is Superior to DOTA.** *PLoS One*. 6(12): p. 7.
194. Loudos G, Kagadis, GC, and Psimadas, D, **Current status and future perspectives of in vivo small animal imaging using radiolabeled nanoparticles.** *Eur J Radiol*, (2011). 78(2): p. 287.
195. Huang G, Khemtong, C, Bey, EA, et al., **Theranostic Polymeric Micelles for Cancer Imaging and Therapy**, in *Multifunctional Nanoparticles for Drug Delivery Applications*, D.J. Lockwood, Editor. 2012, Springer US. p. 257.
196. Kievit FM and Zhang, MQ, **Cancer Nanotheranostics: Improving Imaging and Therapy by Targeted Delivery Across Biological Barriers.** *Adv Mater*, (2011). 23(36): p. H217.
197. Obata A, Kasamatsu, S, McCarthy, DW, et al., **Production of therapeutic quantities of Cu-64 using a 12 MeV cyclotron.** *Nuclear Medicine and Biology*, (2003). 30(5): p. 535.
198. Anderson CJ and Ferdani, R, **Copper-64 Radiopharmaceuticals for PET Imaging of Cancer: Advances in Preclinical and Clinical Research.** *Cancer Biother Radiopharm*, (2009). 24(4): p. 379.
199. Bartholoma MD, **Recent developments in the design of bifunctional chelators for metal-based radiopharmaceuticals used in Positron Emission Tomography.** *Inorganica Chimica Acta*, (2012). 389: p. 36.
200. Cabbines.Dk and Margerum, DW, **Macrocyclic effect on stability of copper(ii) tetramine complexes.** *jacs*, (1969). 91(23): p. 6540.
201. Wadas TJ and Anderson, CJ, **Radiolabeling of TETA- and CB-TE2A-conjugated peptides with copper-64.** *Nature Protocols*, (2006). 1(6): p. 3062.
202. Jones-Wilson TM, Deal, KA, Anderson, CJ, et al., **The in vivo behavior of copper-64-labeled azamacrocyclic complexes.** *Nucl Med Biol*, (1998). 25(6): p. 523.
203. Kodama H and Fujisawa, C, **Copper metabolism and inherited copper transport disorders: molecular mechanisms, screening, and treatment.** *Metallomics*, (2009). 1(1): p. 42.
204. Liu NM, Lo, LSL, Askary, SH, et al., **Transcuprein is a macroglobulin regulated by copper and iron availability.** *J Nutr Biochem*, (2007). 18(9): p. 597.
205. Linder MC and HazeghAzam, M, **Copper biochemistry and molecular biology.** *American Journal of Clinical Nutrition*, (1996). 63(5): p. S797.
206. Tao TY and Gitlin, JD, **Hepatic copper metabolism: insights from genetic disease.** *Hepatology*, (2003). 37(6): p. 1241.

5. References

207. Di Bartolo NM, Sargeson, AM, Donlevy, TM, et al., **Synthesis of a new cage ligand, SarAr, and its complexation with selected transition metal ions for potential use in radioimaging.** *J Chem Soc-Dalton Trans*, (2001)(15): p. 2303.
208. Bass LA, Wang, M, Welch, MJ, et al., **In vivo transchelation of copper-64 from TETA-octreotide to superoxide dismutase in rat liver.** *Bioconjugate Chem*, (2000). 11(4): p. 527.
209. Boswell CA, Sun, XK, Niu, WJ, et al., **Comparative in vivo stability of copper-64-labeled cross-bridged and conventional tetraazamacrocyclic complexes.** *J Med Chem*, (2004). 47(6): p. 1465.
210. Petersen AL, Binderup, T, Rasmussen, P, et al., **(64)Cu loaded liposomes as positron emission tomography imaging agents.** *Biomaterials*, (2011). 32(9): p. 2334.
211. McQuade P, Miao, YB, Yoo, J, et al., **Imaging of melanoma using Cu-64- and Y-86-DOTA-ReCCMSH(Arg(11)), a cyclized peptide analogue of alpha-MSH.** *J Med Chem*, (2005). 48(8): p. 2985.
212. Rogers BE, Anderson, CJ, Connett, JM, et al., **Comparison of four bifunctional chelates for radiolabeling monoclonal antibodies with copper radioisotopes: Biodistribution and metabolism.** *Bioconjugate Chem*, (1996). 7(4): p. 511.
213. Wu Y, Zhang, XZ, Xiong, ZM, et al., **microPET imaging of glioma integrin alpha(V)beta(3) expression using Cu-64-labeled tetrameric RGD peptide.** *J Nucl Med*, (2005). 46(10): p. 1707.
214. Geue RJ, Hambley, TW, Harrowfield, JM, et al., **Metal-ion encapsulation - cobalt cages derived from polyamines, formaldehyde, and nitromethane.** *J Am Chem Soc*, (1984). 106(19): p. 5478.
215. Bottomley GA, Clark, IJ, Creaser, II, et al., **The synthesis and structure of encapsulating ligands - properties of bicyclic hexamines.** *Australian Journal of Chemistry*, (1994). 47(1): p. 143.
216. Smith SV, **Sarar technology for the application of Copper-64 in biology and materials science.** *Quarterly Journal of Nuclear Medicine and Molecular Imaging*, (2008). 52(2): p. 193.
217. Cai HC, Fissekis, J, and Conti, PS, **Synthesis of a novel bifunctional chelator AmBaSar based on sarcophagine for peptide conjugation and Cu-64 radiolabelling.** *Dalton Transactions*, (2009)(27): p. 5395.
218. Cai HC, Li, ZB, Huang, CW, et al., **An improved synthesis and biological evaluation of a new cage-like bifunctional chelator, 4-((8-amino-3,6,10,13,16,19-hexaazabicyclo[6.6.6]icosane-1-ylamino)methyl)benzoic acid, for Cu-64 radiopharmaceuticals.** *Nuclear Medicine and Biology*, (2010). 37(1): p. 57.
219. Voss SD, Smith, SV, DiBartolo, N, et al., **Positron emission tomography (PET) imaging of neuroblastoma and melanoma with Cu-64-SarAr immunoconjugates.** *Proc Natl Acad Sci U S A*, (2007). 104(44): p. 17489.
220. Wu AM, Yazaki, PJ, Tsai, SW, et al., **High-resolution microPET imaging of carcino-embryonic antigen-positive xenografts by using a copper-64-labeled engineered antibody fragment.** *Proc Natl Acad Sci U S A*, (2000). 97(15): p. 8495.
221. Wei L, Ye, Y, Wadas, TJ, et al., **Cu-64-Labeled CB-TE2A and diamsar-conjugated RGD peptide analogs for targeting angiogenesis: comparison of their biological activity.** *Nuclear Medicine and Biology*, (2009). 36(3): p. 277.

5. References

222. Cai HC, Li, ZB, Huang, CW, et al., **Evaluation of Copper-64 Labeled AmBaSar Conjugated Cyclic RGD Peptide for Improved MicroPET Imaging of Integrin $\alpha(v)\beta(3)$ Expression.** *Bioconjugate Chem.* 21(8): p. 1417.
223. Sprague JE, Kitaura, H, Zou, W, et al., **Noninvasive imaging of osteoclasts in parathyroid hormone-induced osteolysis using a Cu-64-labeled RGD peptide.** *J Nucl Med*, (2007). 48(2): p. 311.
224. Woodin KS, Heroux, KJ, Boswell, CA, et al., **Kinetic inertness and electrochemical behavior of copper(II) tetraazamacrocyclic complexes: Possible implications for in vivo stability.** *Eur J Inorg Chem*, (2005)(23): p. 4829.
225. Garrison JC, Rold, TL, Sieckman, GL, et al., **In vivo evaluation and small-animal PET/CT of a prostate cancer mouse model using Cu-64 bombesin analogs: Side-by-side comparison of the CB-TE2A and DOTA chelation systems.** *J Nucl Med*, (2007). 48(8): p. 1327.
226. Sprague JE, Peng, YJ, Sun, XK, et al., **Preparation and biological evaluation of copper-64-labeled Tyr(3) - Octreotate using a cross-bridged macrocyclic chelator.** *Clin Cancer Res*, (2004). 10(24): p. 8674.
227. Pool GL, French, ME, Edwards, RA, et al., **Use of Radiolabeled Hexadecyl Cholesteryl Ether as a Liposome Marker.** *Lipids*, (1982). 17(6): p. 448.
228. Laverman P, Boerman, OC, and Storm, G, **Radiolabeling of liposomes for scintigraphic imaging.** *Methods Enzymol*, (2003). 373: p. 234.
229. Ahkong QF and Tilcock, C, **Attachment of 99mTc to lipid vesicles containing the lipophilic chelate dipalmitoylphosphatidylethanolamine-DTTA.** *Int J Rad Appl Instrum B*, (1992). 19(8): p. 831.
230. Love WG, Amos, N, Kellaway, IW, et al., **Specific accumulation of technetium-99m radiolabeled, negative liposomes in the inflamed paws of rats with adjuvant induced arthritis - effect of liposome size.** *Ann Rheum Dis*, (1989). 48(2): p. 143.
231. Masson D, Jiang, XC, Lagrost, L, et al., **The role of plasma lipid transfer proteins in lipoprotein metabolism and atherogenesis.** *J Lipid Res*, (2009). 50: p. S201.
232. Nichols AV and Smith, L, **Effect of very low-density lipoproteins on lipid transfer in incubated serum.** *J Lipid Res*, (1965). 6(2): p. 206.
233. Dubravci.Mf and Nawar, WW, **Radiolysis of lipids - mode of cleavage in simple triglycerides.** *J Am Oil Chem Soc*, (1968). 45(10): p. 656.
234. Richardson VJ, Jeyasingh, K, Jewkes, RF, et al., **Possible tumor localization of tc-99m-labeled liposomes - effects of lipid-composition, charge, and liposome size.** *J Nucl Med*, (1978). 19(9): p. 1049.
235. Richardson VJ, Osborne, MP, Jeyasingh, K, et al., **Differential localization of (Tc-99m) technetium-labeled liposomes in normal and tumor-bearing lymph-nodes of rat.** *Br J Cancer*, (1978). 38(1): p. 177.
236. Richardson VJ, Ryman, BE, Jewkes, RF, et al., **Tc-99(m)-labelled liposomes preparation of radiopharmaceutical and its distribution in a hepatoma patient.** *Int J Nucl Med Biol*, (1978). 5(2-3): p. 118.
237. Love WG, Amos, N, Williams, BD, et al., **High-performance liquid-chromatographic analysis of liposome stability.** *J Microencapsulation*, (1990). 7(1): p. 105.
238. Düzgünes N, ed. *Liposomes (Volume 373)*. 2003, Elsevier, San Diego, CA. 241.

5. References

239. Goto R, Kubo, H, and Okada, S, **Liposomes prepared from synthetic amphiphiles .1. their technetium labeling and stability.** *Chem Pharm Bull (Tokyo)*, (1989). 37(5): p. 1351.
240. Espinola LG, Beaucaire, J, Gottschalk, A, et al., **Radiolabeled liposomes as metabolic and scanning tracers in mice .2. in-111 oxine compared with tc-99m dtpa, entrapped in multilamellar lipid vesicles.** *J Nucl Med*, (1979). 20(5): p. 434.
241. Neirinckx RD, Burke, JF, Harrison, RC, et al., **The retention mechanism of technetium-99m-hm-pao - intracellular reaction with glutathione.** *J Cereb Blood Flow Metab*, (1988). 8(6): p. S4.
242. Tilcock C, Yap, M, Szucs, M, et al., **Peg-coated lipid vesicles with encapsulated tc-99m as blood-pool agents for nuclear-medicine.** *Nucl Med Biol*, (1994). 21(2): p. 165.
243. King RC, Surfraz, MBU, Biagini, SCG, et al., **How do HYNIC-conjugated peptides bind technetium? Insights from LC-MS and stability studies.** *Dalton Trans*, (2007)(43): p. 4998.
244. Bao A, Goins, B, Klipper, R, et al., **Re-186-liposome labeling using Re-186-SNS/S complexes: In vitro stability, imaging, and biodistribution in rats.** *J Nucl Med*, (2003). 44(12): p. 1992.
245. Chang Y-J, Chang, C-H, Chang, T-J, et al., **Biodistribution, pharmacokinetics and microSPECT/CT imaging of Re-188-BMEDA-liposome in a C26 murine colon carcinoma solid tumor animal model.** *Anticancer Res*, (2007). 27(4B): p. 2217.
246. Chen L-C, Chang, C-H, Yu, C-Y, et al., **Biodistribution, pharmacokinetics and imaging of Re-188-BMEDA-labeled pegylated liposomes after intraperitoneal injection in a C26 colon carcinoma ascites mouse model.** *Nucl Med Biol*, (2007). 34(4): p. 415.
247. Bao A, Goins, B, Klipper, R, et al., **Direct 99mTc labeling of pegylated liposomal doxorubicin (Doxil) for pharmacokinetic and non-invasive imaging studies.** *J Pharmacol Exp Ther*, (2004). 308(2): p. 419.
248. Li S, Goins, B, Phillips, WT, et al., **Remote-loading labeling of liposomes with (99m)Tc-BMEDA and its stability evaluation: effects of lipid formulation and pH/chemical gradient.** *J Liposome Res*, (2011). 21(1): p. 17.
249. Li SH, Goins, B, Phillips, WT, et al., **Post-lumpectomy intracavitary retention and lymph node targeting of (99m)Tc-encapsulated liposomes in nude rats with breast cancer xenograft.** *Breast Cancer Res Treat*. 130(1): p. 97.
250. Wang SX, Bao, A, Herrera, SJ, et al., **Intraoperative Re-186-liposome radionuclide therapy in a head and neck squamous cell carcinoma xenograft positive surgical margin model.** *Clin Cancer Res*, (2008). 14(12): p. 3975.
251. Hwang KJ, Merriam, JE, Beaumier, PL, et al., **Encapsulation, with high-efficiency, of radioactive metal-ions in liposomes.** *Biochim Biophys Acta*, (1982). 716(1): p. 101.
252. Beaumier PL and Hwang, KJ, **An efficient method for loading in-111 into liposomes using acetylacetone.** *J Nucl Med*, (1982). 23(9): p. 810.
253. Ogihara I, Kojima, S, and Jay, M, **Differential uptake of gallium-67-labeled liposomes between tumors and inflammatory lesions in rats.** *J Nucl Med*, (1986). 27(8): p. 1300.
254. Ogihara I and Kojima, S, **Increased delivery of ga-67 to tumors using serum-stable liposomes.** *J Nucl Med*, (1988). 29(4): p. 516.

5. References

255. Laverman P, Carstens, MG, Boerman, OC, et al., **Factors affecting the accelerated blood clearance of polyethylene glycol-liposomes upon repeated injection.** *J Pharmacol Exp Ther*, (2001). 298(2): p. 607.
256. Harrington KJ, Rowlinson-Busza, G, Syrigos, KN, et al., **Pegylated liposomes have potential as vehicles for intratumoral and subcutaneous drug delivery.** *Clin Cancer Res*, (2000). 6(6): p. 2528.
257. Silindir M, Ozer, AY, and Erdogan, S, **The use and importance of liposomes in Positron Emission Tomography.** *Drug Deliv*. 19(1): p. 68.
258. Seo JW, Qin, S, Mahakian, LM, et al., **Positron emission tomography imaging of the stability of Cu-64 labeled dipalmitoyl and distearoyl lipids in liposomes.** *J Control Release*, (2011). 151(1): p. 28.
259. Petersen AL, Binderup, T, Jolck, RI, et al., **Positron emission tomography evaluation of somatostatin receptor targeted (64)Cu-TATE-liposomes in a human neuroendocrine carcinoma mouse model.** *J Control Release*, (2012). (in press).
260. Chacko AM and Divgi, CR, **Radiopharmaceutical Chemistry with Iodine-124: A Non-Standard Radiohalogen for Positron Emission Tomography.** *Med Chem*, (2011). 7(5): p. 395.
261. Hardy JG, Kellaway, IW, Rogers, J, et al., **The distribution and fate of i-131-labelled liposomes.** *J Pharm Pharmacol*, (1980). 32(5): p. 309.
262. Schroit AJ, **Synthesis and properties of a non-exchangeable radioiodinated phospholipid.** *Biochemistry (Mosc)*, (1982). 21(21): p. 5323.
263. Fraker PJ and Speck, JC, **Protein and cell-membrane iodinations with a sparingly soluble chloramide, 1,3,4,6-tetrachloro-3a,6a-diphenylglycoluril.** *Biochem Biophys Res Commun*, (1978). 80(4): p. 849.
264. Oku N, Tokudome, Y, Tsukada, H, et al., **In vivo trafficking of long-circulating liposomes in tumour-bearing mice determined by positron emission tomography.** *Biopharm Drug Dispos*, (1996). 17(5): p. 435.
265. www.avantilipids.com. *Preparation of liposomes - c. sizing of liposomes*. [cited 2012 March 16th].
266. Thistlethwaite AJ, Leeper, DB, Moylan, DJ, et al., **pH distribution in human-tumors.** *International Journal of Radiation Oncology Biology Physics*, (1985). 11(9): p. 1647.
267. Geisow MJ, Hart, PD, and Young, MR, **Temporal changes of lysosome and phagosome pH during phagolysosome formation in macrophages - studies by fluorescence spectroscopy.** *J Cell Biol*, (1981). 89(3): p. 645.
268. Augustinsson K, **Multiple forms of esterase in vertebrate bloodplasma.** *Ann NY Acad Sci*, (1961). 94(3): p. 844.
269. Wei BQQ, Mikkelsen, TS, McKinney, MK, et al., **A second fatty acid amide hydrolase with variable distribution among placental mammals.** *J Biol Chem*, (2006). 281(48): p. 36569.
270. Bell FP, **Lipid exchange and transfer between biological lipid protein structures.** *Prog Lipid Res*, (1978). 17(2): p. 207.
271. Tall AR, **Plasma-lipid transfer proteins.** *J Lipid Res*, (1986). 27(4): p. 361.
272. Tall AR, **Plasma cholesteryl ester transfer protein.** *J Lipid Res*, (1993). 34(8): p. 1255.

5. References

273. Anderson M, Paradis, C, and Omri, A, **Disposition of H-3-cholesteryl ether labeled liposomes following intravenous administration to mice: Comparison with an encapsulated C-14-inulin as aqueous phase marker.** *Drug Deliv*, (2003). 10(3): p. 193.
274. Kizelsztejn P, Ovadia, H, Garbuzenko, O, et al., **Pegylated nanoliposomes remote-loaded with the antioxidant tempamine ameliorate experimental autoimmune encephalomyelitis.** *J Neuroimmunol*, (2009). 213(1-2): p. 20.
275. Stein Y, Halperin, G, and Stein, O, **Biological stability of [3H]cholesteryl oleoyl ether in cultured fibroblasts and intact rat.** *FEBS Lett*, (1980). 111(1): p. 104.
276. Awasthi VD, Goins, B, Klipper, R, et al., **Dual radiolabeled liposomes: Biodistribution studies and localization of focal sites of infection in rats.** *Nucl Med Biol*, (1998). 25(2): p. 155.
277. Baumann WJ and Mangold, HK, **Reactions of aliphatic methanesulfonates .i. syntheses of long-chain glyceryl-(1) ethers.** *J Org Chem*, (1964). 29(10): p. 3055.
278. Schmid CR, Bryant, JD, Dowlatzedah, M, et al., **Synthesis of 2,3-o-isopropylidene-d-glyceraldehyde in high chemical and optical purity - observations on the development of a practical bulk process.** *J Org Chem*, (1991). 56(12): p. 4056.
279. Williamson A, **Theory of Aetherification.** *Philosophical Magazine*, (1850). 37: p. 350.
280. Middleton WJ, **New Fluorinating Reagents - Dialkylaminosulfur Fluorides.** *J Org Chem*, (1975). 40(5): p. 574.
281. Leroy J, Hebert, E, and Wakselman, C, **Maximum optical-rotation of 2-fluorooctane - survey of fluorinating reagents.** *J Org Chem*, (1979). 44(19): p. 3406.
282. Rozen S, Faust, Y, and Benyakov, H, **New method for fluorination of sterols.** *Tetrahedron Lett*, (1979)(20): p. 1823.
283. Zhao XQ, Zhuang, WP, Fang, DS, et al., **A highly efficient conversion of primary or secondary alcohols into fluorides with n-perfluorobutanesulfonyl fluoride-tetrabutylammonium triphenyldifluorosilicate.** *Synlett*, (2009)(5): p. 779.
284. Sripada PK, **A simple method for the synthesis of cholesteryl ethers.** *J Lipid Res*, (1986). 27(3): p. 352.
285. Deforge LE, Ruyan, MK, Schwendner, SW, et al., **Synthesis and evaluation of radioiodinated cholesteryl ethers as lipoprotein probes.** *Bioconjugate Chem*, (1991). 2(4): p. 254.
286. Bajaj A, Kondiah, P, and Bhattacharya, S, **Design, synthesis, and in vitro gene delivery efficacies of novel cholesterol-based gemini cationic lipids and their serum compatibility: A structure-activity investigation.** *J Med Chem*, (2007). 50(10): p. 2432.
287. Kim BK, Bae, YU, Doh, KO, et al., **The synthesis of cholesterol-based cationic lipids with trimethylamine head and the effect of spacer structures on transfection efficiency.** *Bioorg Med Chem Lett*. 21(12): p. 3734.
288. Cameron M, et al., **Novel cationic lipids with various head groups for oligonucleotide delivery.** International Patent, WO 2011/022460 A1, filed August 18, 2000, and issued February 24, 2011.
289. Marshall WM, et al., **Lipophilic polynucleotide conjugates.** International Patent, WO 2011/129672 A1, filed May 5, 2010, and issued November 11, 2010.

5. References

290. www.waters.com
291. Chen ZP, Wang, SP, Li, XM, et al., **A one-step automated high-radiochemical-yield synthesis of F-18-FECNT from mesylate precursor.** *Appl Radiat Isot*, (2008). 66(12): p. 1881.
292. Moon BS, Lee, TS, Lee, KC, et al., **Syntheses of F-18 labeled fluoroalkyltyrosine derivatives and their biological evaluation in rat bearing 9L tumor.** *Bioorg Med Chem Lett*, (2007). 17(1): p. 200.
293. Maisonia A, Maestrup, EG, Wiese, C, et al., **Synthesis, radiofluorination and pharmacological evaluation of a fluoromethyl spirocyclic PET tracer for central sigma(1) receptors and comparison with fluoroalkyl homologs.** *Bioorg Med Chem*, (2012). 20(1): p. 257.
294. Samnick S, Ametamey, S, Gold, MR, et al., **Synthesis and preliminary in vitro evaluation of a new memantine derivative 1-amino-3-[F-18]fluoromethyl-5-methyl-adamantane: A potential ligand for mapping the N-methyl-D-aspartate receptor complex.** *J Label Compd Radiopharm*, (1997). 39(3): p. 241.
295. Wang M, Gao, MZ, Miller, KD, et al., **Synthesis of [(11)C]PBR06 and [(18)F]PBR06 as agents for positron emission tomographic (PET) imaging of the translocator protein (TSPO).** *Steroids*, (2011). 76(12): p. 1331.
296. Dolle F, Hinnen, F, Damont, A, et al., **Radiosynthesis of [(18)F]PBR111, a selective radioligand for imaging the translocator protein (18 kDa) with PET.** *J Label Compd Radiopharm*, (2008). 51(13-14): p. 435.
297. Mancuso AJ, Huang, SL, and Swern, D, **Oxidation of long-chain and related alcohols to carbonyls by dimethyl-sulfoxide activated by oxalyl chloride.** *J Org Chem*, (1978). 43(12): p. 2480.
298. Omura K and Swern, D, **Oxidation of alcohols by activated dimethyl-sulfoxide - preparative, steric and mechanistic study.** *Tetrahedron*, (1978). 34(11): p. 1651.
299. Suehiro M, Burgman, P, Carlin, S, et al., **Radiosynthesis of [I-131]IAZGP via nucleophilic substitution and its biological evaluation as a hypoxia marker - is specific activity a factor influencing hypoxia-mapping ability of a hypoxia marker?** *Nucl Med Biol*, (2009). 36(5): p. 477.
300. Wester HJ, Schoultz, BW, Hultsch, C, et al., **Fast and repetitive in-capillary production of [(18)F]FDG.** *Eur J Nucl Med Mol Imag*, (2009). 36(4): p. 653.
301. Szebeni J, Muggia, F, Gabizon, A, et al., **Activation of complement by therapeutic liposomes and other lipid excipient-based therapeutic products: Prediction and prevention.** *Adv Drug Del Rev*, (2011). 63(12): p. 1020.
302. Gabizon A, Catane, R, Uziely, B, et al., **Prolonged circulation time and enhanced accumulation in malignant exudates of doxorubicin encapsulated in polyethylene-glycol coated liposomes.** *Cancer Res*, (1994). 54(4): p. 987.
303. de Kruffy B, Demel, RA, and van Deenen, LL, **The effect of cholesterol and epicholesterol incorporation on the permeability and on the phase transition of intact Acholeplasma laidlawii cell membranes and derived liposomes.** *Biochim Biophys Acta*, (1972). 255(1): p. 331.
304. Berger N, Sachse, A, Bender, J, et al., **Filter extrusion of liposomes using different devices: comparison of liposome size, encapsulation efficiency, and process characteristics.** *Int J Pharm*, (2001). 223(1-2): p. 55.

5. References

305. Oku N, **Delivery of contrast agents for positron emission tomography imaging by liposomes.** *Adv Drug Deliv Rev*, (1999). 37(1-3): p. 53.
306. Kamps JA, Koning, GA, Velinova, MJ, et al., **Uptake of long-circulating immunoliposomes, directed against colon adenocarcinoma cells, by liver metastases of colon cancer.** *Journal of drug targeting*, (2000). 8(4): p. 235.
307. Gabizon A, Goren, D, Horowitz, AT, et al., **Long-circulating liposomes for drug delivery in cancer therapy: A review of biodistribution studies in tumor-bearing animals.** *Adv Drug Del Rev*, (1997). 24(2-3): p. 337.
308. Poelstra KP, J. Beljaars, L., **Drug targeting to the diseased liver.** *J Controlled Release*, (2012). (in press).
309. van Nostrum CF, **Covalently cross-linked amphiphilic block copolymer micelles.** *Soft Matter*, (2011). 7(7): p. 3246.
310. Mishra B, Patel, BB, and Tiwari, S, **Colloidal nanocarriers: a review on formulation technology, types and applications toward targeted drug delivery.** *Nanomed-Nanotechnol Biol Med*, (2010). 6(1): p. 9.
311. Tegla CA, Cudrici, C, Patel, S, et al., **Membrane attack by complement: the assembly and biology of terminal complement complexes.** *Immunol Res*, (2011). 51(1): p. 45.
312. Paudyal B, Paudyal, P, Oriuchi, N, et al., **Positron emission tomography imaging and biodistribution of vascular endothelial growth factor with ⁶⁴Cu-labeled bevacizumab in colorectal cancer xenografts.** *Cancer science*, (2011). 102(1): p. 117.
313. Paudyal P, Paudyal, B, Hanaoka, H, et al., **Imaging and biodistribution of Her2/neu expression in non-small cell lung cancer xenografts with Cu-labeled trastuzumab PET.** *Cancer science*, (2010). 101(4): p. 1045.
314. Goins B, **Radiolabeled lipid nanoparticles for diagnostic imaging.** *Expert Opin Med Diagn*, (2008). 2: p. 853.
315. Schwesinger R and Schlemper, H, **Peralkylated polyaminophosphazenes - extremely strong, neutral nitrogen bases.** *Angewandte Chemie-International Edition in English*, (1987). 26(11): p. 1167.
316. Kwon GS, Yokoyama, M, Okano, T, et al., **Biodistribution of micelle-forming polymer drug conjugates.** *Pharmaceutical Research*, (1993). 10(7): p. 970.
317. Letchford K and Burt, HM, **Copolymer micelles and nanospheres with different in vitro stability demonstrate similar paclitaxel pharmacokinetics.** *Mol Pharm*, (2012). 9(2): p. 248.
318. Torchilin VP, **PEG-based micelles as carriers of contrast agents for different imaging modalities.** *Advanced Drug Delivery Reviews*, (2002). 54(2): p. 235.
319. Trubetskoy VS, FrankKamenetsky, MD, Whiteman, KR, et al., **Stable polymeric micelles: Lymphangiographic contrast media for gamma scintigraphy and magnetic resonance imaging.** *Acad Radiol*, (1996). 3(3): p. 232.
320. Tolmachev V, Wallberg, H, Andersson, K, et al., **The influence of Bz-DOTA and CHX-AaEuro(3)-DTPA on the biodistribution of ABD-fused anti-HER2 Affibody molecules: implications for In-114m-mediated targeting therapy.** *Eur J Nucl Med Mol Imaging*, (2009). 36(9): p. 1460.
321. Ekblad T, Orlova, A, Feldwisch, J, et al., **Positioning of Tc-99m-chelators influences radiolabeling, stability and biodistribution of Affibody molecules.** *Bioorg Med Chem Lett*, (2009). 19(14): p. 3912.

5. References

322. Sabbah EN, Kadouche, J, Ellison, D, et al., **In vitro and in vivo comparison of DTPA- and DOTA-conjugated antiferritin monoclonal antibody for imaging and therapy of pancreatic cancer.** *Nuclear Medicine and Biology*, (2007). 34(3): p. 293.
323. Fonge H, Lee, H, Reilly, RM, et al., **Multifunctional block copolymer micelles for the delivery of (111)in to egfr-positive breast cancer cells for targeted auger electron radiotherapy.** *Mol Pharm*, (2010). 7(1): p. 177.
324. Park YJ, Lee, JY, Chang, YS, et al., **Radioisotope carrying polyethylene oxide-polycaprolactone copolymer micelles for targetable bone imaging.** *Biomaterials*, (2002). 23(3): p. 873.
325. Letchford K and Burt, HM, **Copolymer micelles and nanospheres with different in vitro stability demonstrate similar paclitaxel pharmacokinetics.** *Mol Pharm*, (2011). 9(2): p. 248.
326. Sun G, Hagooley, A, Xu, J, et al., **Facile, efficient approach to accomplish tunable chemistries and variable biodistributions for shell cross-linked nanoparticles.** *Biomacromolecules*, (2008). 9(7): p. 1997.
327. Zeng D, Lee, NS, Liu, Y, et al., **⁶⁴Cu core-labeled nanoparticles with high specific activity via metal-free click chemistry.** *Acs Nano*, (2012). 6(6): p. 5209.
328. Pan DJ, Turner, JL, and Wooley, KL, **Shell cross-linked nanoparticles designed to target angiogenic blood vessels via alpha(v)beta(3) receptor-ligand interactions.** *Macromolecules*, (2004). 37(19): p. 7109.
329. Wooley KL, **From dendrimers to knedel-like structures.** *Chem-Eur J*, (1997). 3(9): p. 1397.
330. Pressly ED, Rossin, R, Hagooley, A, et al., **Structural effects on the biodistribution and positron emission tomography (PET) imaging of well-defined Cu-64-labeled nanoparticles comprised of amphiphilic block graft copolymers.** *Biomacromolecules*, (2007). 8(10): p. 3126.
331. Fukukawa KI, Rossin, R, Hagooley, A, et al., **Synthesis and characterization of core-shell star copolymers for in vivo PET imaging applications.** *Biomacromolecules*, (2008). 9(4): p. 1329.
332. Kadam VS, Nicol, E, and Gaillard, C, **Synthesis of flower-like poly(ethylene oxide) based macromolecular architectures by photo-cross-linking of block copolymers self-assemblies.** *Macromolecules*, (2011). 45(1): p. 410.
333. Buwalda SJ, Perez, LB, Teixeira, S, et al., **Self-assembly and photo-cross-linking of eight-armed peg-ptmc star block copolymers.** *Biomacromolecules*, (2011). 12(7): p. 2746.
334. Kim JS and Youk, JH, **Preparation of core cross-linked micelles using a photo-cross-linking agent.** *Polymer*, (2009). 50(10): p. 2204.
335. Jin Q, Liu, XS, Liu, GY, et al., **Fabrication of core or shell reversibly photo cross-linked micelles and nanogels from double responsive water-soluble block copolymers.** *Polymer*, (2010). 51(6): p. 1311.
336. Trenor SR, Shultz, AR, Love, BJ, et al., **Coumarins in polymers: from light harvesting to photo-cross-linkable tissue scaffolds.** *Chem Rev*, (2004). 104(6): p. 3059.
337. Anet R, **Photodimers of coumarin and related compounds.** *Can J Chem-Rev Can Chim*, (1962). 40(7): p. 1249.
338. Gnanaguru K, Ramasubbu, N, Venkatesan, K, et al., **A study on the photochemical dimerization of coumarins in the solid-state.** *Journal of Organic Chemistry*, (1985). 50(13): p. 2337.

5. References

339. Chen Y and Chou, CF, **Reversible photodimerization of coumarin derivatives dispersed in poly(vinyl acetate)**. *J Polym Sci Pol Chem*, (1995). 33(16): p. 2705.
340. Kaur G, Chang, SLY, Bell, TDM, et al., **Bioinspired core-crosslinked micelles from thymine-functionalized amphiphilic block copolymers: hydrogen bonding and photo-crosslinking study**. *J Polym Sci Pol Chem*, (2011). 49(19): p. 4121.
341. Yan LS, Yang, LX, He, HY, et al., **Photo-cross-linked mPEG-poly(gamma-cinnamyl-L-glutamate) micelles as stable drug carriers**. *Polym Chem*, (2012). 3(5): p. 1300.
342. Wang JS and Matyjaszewski, K, **Controlled living radical polymerization - atom-transfer radical polymerization in the presence of transition-metal complexes**. *J Am Chem Soc*, (1995). 117(20): p. 5614.
343. Kato M, Kamigaito, M, Sawamoto, M, et al., **Polymerization of methyl-methacrylate with the carbon-tetrachloride dichlorotris(triphenylphosphine)ruthenium(ii) methylaluminum bis(2,6-di-tert-butylphenoxide) initiating system - possibility of living radical polymerization**. *Macromolecules*, (1995). 28(5): p. 1721.
344. Matyjaszewski K and Xia, JH, **Atom transfer radical polymerization**. *Chem Rev*, (2001). 101(9): p. 2921.
345. Szwarc M, **Living polymers**. *Nature*, (1956). 178(4543): p. 1168.
346. Stevens M, *Polymer Chemistry - An introduction*. 3 ed. 1999.
347. Patten TE, Xia, JH, Abernathy, T, et al., **Polymers with very low polydispersities from atom transfer radical polymerization**. *Science*, (1996). 272(5263): p. 866.
348. Dufresne MH and Leroux, JC, **Study of the micellization behavior of different order amino block copolymers with heparin**. *Pharmaceutical Research*, (2004). 21(1): p. 160.
349. Obi M, Morino, S, and Ichimura, K, **Factors affecting photoalignment of liquid crystals induced by polymethacrylates with coumarin side chains**. *Chem Mat*, (1999). 11(3): p. 656.
350. Xia JH and Matyjaszewski, K, **Controlled/"living" radical polymerization. Atom transfer radical polymerization using multidentate amine ligands**. *Macromolecules*, (1997). 30(25): p. 7697.
351. Tsarevsky NV, Braunecker, WA, Brooks, SJ, et al., **Rational selection of initiating/catalytic systems for the copper-mediated atom transfer radical polymerization of basic monomers in protic media: ATRP of 4-vinylpyridine**. *Macromolecules*, (2006). 39(20): p. 6817.
352. Yu QY, Kandegedara, A, Xu, YP, et al., **Avoiding interferences from Good's buffers: A contiguous series of noncomplexing tertiary amine buffers covering the entire range of pH 3-11**. *Anal Biochem*, (1997). 253(1): p. 50.
353. Kumar S and Nussinov, R, **Close-range electrostatic interactions in proteins**. *Chembiochem*, (2002). 3(7): p. 604.
354. Chonn A, Cullis, PR, and Devine, DV, **The role of surface-charge in the activation of the classical and alternative pathways of complement by liposomes**. *J Immunol*, (1991). 146(12): p. 4234.
355. Kaiser E, Colescot, RL, Bossing, Cd, et al., **Color test for detection of free terminal amino groups in solid-phase synthesis of peptides**. *Anal Biochem*, (1970). 34(2): p. 595.

5. References

- 356. Wang Y, Liu, Y, Luehmann, H, et al., **Evaluating the pharmacokinetics and in vivo cancer targeting capability of au nanocages by positron emission tomography imaging.** *Acs Nano*, (2012). 6(7): p. 5880.
- 357. Dong H, Dube, N, Shu, JY, et al., **Long-circulating 15 nm micelles based on amphiphilic 3-helix peptide-peg conjugates.** *Acs Nano*, (2012). 6(6): p. 5320.
- 358. Anderegg G, Arnaud-Neu, F, Delgado, R, et al., **Critical evaluation of stability constants of metal complexes of complexones for biomedical and environmental applications (iupac technical report).** *Pure and Applied Chemistry*, (2005). 77(8): p. 1445.
- 359. Crouch AM, Khotseng, LE, Polhuis, M, et al., **Comparative study of cyclic voltammetry with potentiometric analysis for determining formation constants for polyaminocarboxylate-metal ion complexes.** *Analytica Chimica Acta*, (2001). 448(1-2): p. 231.
- 360. Chaves S, Delgado, R, and Dasilva, J, **The stability of the metal-complexes of cyclic tetra-aza tetraacetic acids.** *Talanta*, (1992). 39(3): p. 249.
- 361. Linder MC, **Biochemistry and molecular biology of copper in mammals**, in *Handbook of copper pharmacology and toxicology*, ed. E.J. Massaro. 2002. 3.

Preface

This thesis is the result of 3 years of graduate work carried out at the Hevesy Laboratory at DTU Nutech as well as in the CBIO (*Colloids & Biological Interfaces*) group at DTU Nanotech. In the project's first year, it was in collaboration with LiPlasome Pharma A/S but continued as a full DTU project from March 1st 2010 due to bankruptcy on the part of LiPlasome Pharma. The main supervisors on the project were Dr. Palle Rasmussen (Head of Program, DTU Nutech) and Dr. Thomas Andresen (Senior Scientist, DTU Nanotech).

During the project, an 8 months stay at the Hebrew University of Jerusalem (Israel) was included. The supervisors on this project were Prof. Yechezkel Barenholz and Dr. Eylon Yavin. This stay was conducted as a leave of absence and for this reason the results obtained are not described in this thesis.

The work is presented in three separate chapters. **Chapter 1** is a general introduction to the field of radiolabeling liposomes and polymeric micelles. **Chapter 2** describes work revolving around the ¹⁸F-radiolabeling of liposomes. **Chapter 3** is a description of work concerning the radiolabeling of polymeric micelles. A **general conclusion & perspectives** are given in the end.

Acknowledgements

I am grateful to a number of people that have helped, inspired and in other ways contributed to this project and my personal development. I would especially like to thank my supervisor **Dr. Palle Rasmussen** who has lead my education as a radiochemist and has been a constant support and motivator with an always open door. Special thanks also goes to my co-supervisor **Dr. Thomas Andresen** for being a great source of inspiration, for fruitful scientific discussions, and for setting up my stay in Israel. In addition, the two deserve my deep-felt gratitude for stepping in and taking over the project when the bankruptcy of LiPlasome Pharma would otherwise have ended it.

In addition, I would like to thank the following people;

Dr. Sorin Aburel & Lene Niebuhr for supplying ^{18}F target water rinses, for always being helpful and for keeping a great mood in the lab. **Dr. Dennis Elema, Cristine Sogaard** and **Anette Holst** for supplying ^{64}Cu and for never objecting to my erratic orderings of numerous vials, each containing minuscule amounts of radioactivity. A special thanks goes to Dennis Elema for his patience and his help in teaching me to send my own radioactive formulations to Panum. **Prof. Mikael Jensen** for his great knowledge and fruitful discussions on nuclear physics, PET technology and related subjects that at times have seemed like black magic. **Lasse Hauerberg** and **Henrik Prip** for possessing a practical prowess with which a PhD student may not always be endowed.

Of my fellow PhD students and post docs, special thanks goes to **Dr. Rasmus Jølck, Dr. Anncatrine Petersen, Dr. Simon Andersen, Dr. Thomas Etzerodt, Dr. Kristian Jensen, Dr. Jonas Henriksen, Evgeny Revunov** and **Lise Bjerg**. These individuals have all at some point stepped in and provided much-needed help and great discussions. A very special thanks goes to **Dr. Martin H. F. Pedersen**, who has made my PhD years immensely more enjoyable.

Of my collaborators, I would like to thank **Prof. Andreas Kjær** and **Dr. Tina Binderup** for carrying out our animal studies and for always invaluable input when interpreting the results, **Dr. Pramod Kumar** for synthesizing the unimers described in Chapter 3, and **Bente Mathiesen** for carrying out the bulk of the work in our joint paper. In particular, I would like to thank **Dr. Fedor Zhuravlev** for countless interesting discussions, scientific as well as private, for always being ready to help with chemical questions, and finally, for including me in the $[^{18}\text{F}]\text{HF}$ gas transfer project.

At last, I would like to thank my wife-to-be **Inés Areizaga**, who has somehow managed to accept and support me through my almost 4 years of relentless working hours, 8 months of absence and my infatuation with tiny radioactive particles.

Publications

Andreas T.I. Jensen, Tina Binderup, Thomas L. Andresen, Andreas Kjær, Palle H. Rasmussen.

“PET imaging of liposomes labeled with an [18F]-fluorocholesteryl ether probe prepared by automated radiosynthesis” Journal of Liposome Research, (**Epub ahead of print**). PubMed ID:22803638

Bente Mathiessen, **Andreas T.I. Jensen**, Fedor Zhuravlev.

“Homogeneous Nucleophilic Radiofluorination and Fluorination with Phosphazene Hydrofluorides” Chemistry – A European Journal, 2011. **17**(28): p. 7796-7805.

Andreas T.I. Jensen, Tina Binderup, Pramod Kumar, Andreas Kjær, Palle H. Rasmussen, Thomas L. Andresen.

“In-vivo comparison of DOTA and CB-TE2A through shell-region ⁶⁴Cu-labeling of core-crosslinked triblock polymeric micelles” Biomaterials (**Submitted**).

Andreas T.I. Jensen, Pramod Kumar, Tina Binderup, Andreas Kjær, Dennis Elema, Thomas L. Andresen, Palle H. Rasmussen.

“The effect of coumarin core-crosslinking on the pharmacokinetics of CB-TE2A conjugated triblock polymeric micelles” (**in preparation**)*.

* Results described in section 3.8.3.

List of abbreviations and acronyms

%CL	Degree of crosslinking
ABC	Accelerated blood clearance
ACN	Acetonitrile
ADME	Absorption distribution metabolism and excretion
ATRP	atom-transfer radical-polymerization
BFC	Bifunctional chelator
CE	Cholesteryl ether
CL	Crosslinked
CMC	Critical micelle concentration
DCM	Dichloromethane
DDS	Drug delivery system
DHG	1,2-di-hexadecyl-glycerol
DLS	Direct light scattering
DMF	Dimethylformamide
DMSO	Dimethylsulphoxide
DSC	Direct scanning calorimetry
DSPC	Di-stearoyl phosphatidylcholine
EC	Electron capture
ECM	Extracellular matrix
EPR	Enhanced permeation and retention
K222	Kryptofix-222
LE	Labeling efficiency
LUV	Large unilamellar vesicle
MLV	Multi-lamellar vesicle
NCA	no-carrier-added
NMRI	Naval Medical Research Institute
NonCL	Non-crosslinked
PAEMA	polyaminomethyl methacrylate
PCMA	polymethacryloyloxyethoxy-4-methylcoumarin
PEG	Polyethylene glycol
PEG	polyethylene glycol
PET	positron emission tomography
HEMA	polyhydroxyethyl methacrylate
PK	Pharmacokinetics

PM	Polymeric micelles
PMMA	polymethyl methacrylate
RCP	Radiochemical purity
RES	Reticuloendotheliam system
RT	Room temperature
SEC	Size-exclusion chromatography
SFC	Supel Flash Cartridge
SPECT	single-photon emission computed chromatography
SUV	Small unilamellar vesicle
T/M ratio	tumor-to-muscle ratio
THF	Tetrahydrofuran
T _m	membrane phase transition temperature
VEGF	Vascular endothelial growth factor

Abstract & Outline

Outline. This thesis is divided into three separate chapters that can be read independently. Chapter 1 is a general introduction, touching upon liposomes and polymeric micelles and radiolabeling with ^{18}F and ^{64}Cu . Chapter 2 and 3 address two separate research projects, each described below. A complete reference list is compiled in the end, immediately after the three chapters. This is followed by the supplementary information, divided into appropriate sections. Finally, the two first-authored manuscripts are attached as appendices.

Chapter 1. The field of nanoparticulate drug delivery has been hailed as a revolution in modern therapeutics, especially in chemotherapy. A major reason is the ability of nanoparticles to accumulate in tumor tissue. Liposomes are the classic nanoparticle, consisting of a lipid membrane with an aqueous core. Polymeric micelles are made from amphiphilic detergent-like copolymers, that self-assemble in water. Therapy with nanoparticles is hampered by often poor tumor accumulation, combined with massive uptake by macrophages in the liver and spleen. For this reason, visualizing nanoparticle pharmacokinetics *in-vivo* is a valuable tool in the on-going research. Such visualization can be done by labeling with radio isotopes. Isotopes that emit positrons (PET-isotopes) can be detected by PET (*positron emission tomography*) technology, an accurate technique that has gained popularity in recent years. PET-isotopes of interest include ^{18}F and ^{64}Cu . In addition to being a research tool, radiolabeled nanoparticles hold promise as a radiopharmaceutical in themselves, as a means of imaging tumor tissue, aiding in diagnosis and surgery.

Chapter 2. A method for labeling liposomes with ^{18}F (97% positron decay, $T_{1/2} = 110$ min) was investigated. ^{18}F is widely available, but is hampered by a short half-life only allowing up to 8 hours scans. ^{18}F must be covalently attached to components of the liposome. By binding to a lipid, it can be stably lodged in the membrane. A glycerolipid and a cholesteryl ether were synthesized with free primary alcohols and a series of their sulphonates (Ms, Ts, Tf) were prepared. [^{18}F]Radiofluorination of these substrates was performed on fully automated equipment using a classic Kryptofix222-mediated procedure in DMSO. Yields were poor, 3-17% depending on conditions. The [^{18}F]fluorinated probes were purified *in-situ* on SEP-Paks. The cholesteryl ether mesylate performed best. This substrate was radiolabeled and formulated in long-circulating liposomes by drying the probe and the lipids together, followed by hydration by magnetic stirring. The liposomes were extruded through 100 nm filter on fully automated equipment. Animal studies were done in tumor-bearing mice, and PET-scans were performed over 8 hours. Clear tumor uptake, as well as hepatic and splenic uptake, was observed, corresponding to expected liposomal pharmacokinetics. Tumor uptake was quantifiable (*tumor-to-muscle ratio* at 8 h: 2.20), showing that the maximum scan duration with ^{18}F is sufficient for visualizing tumor tissue. Because of the low [^{18}F]radiofluorination yields obtained, we investigated ways of labeling lipophilic substrates in nonpolar

solvents. This involved the transfer of [18]HF gas from a solution of concentrated sulphuric acid into a receiving vial containing the substrate in toluene. A phosphazene base was present to bind [18]HF and mediate fluorination. This procedure made it possible to fluorinate highly lipophilic substrates in 71% yields.

Chapter 3. Radiolabeling of polymeric micelles with ^{64}Cu (18% positron decay, $T_{1/2} = 12.7$ h) was investigated. ^{64}Cu allows longer scans (up to 48 hours), which mirrors the duration of nanoparticle pharmacokinetics. It is a metal and must be attached to polymeric micelles by covalently conjugated chelators. DOTA and CB-TE2A are two such chelators, but DOTA is widely believed to be unstable *in-vivo*. DOTA and CB-TE2A were conjugated to *triblock* polymeric micelles in the *shell*-region. Here, they were thought to be shielded by the outer PEG-layer. The micelles were crosslinked in their coumarin-containing cores by exposure to UV light. Subsequently, the micelles were labeled with ^{64}Cu , followed by removal of unspecifically bound ^{64}Cu by EDTA. Good labeling efficiency was achieved with both chelators (40-70%). Some of the prepared micelles were found to exhibit gross instabilities, especially with raised temperature, which prevented their *in-vivo* use. Other micelles were stable and were investigated in xenographted mice. These micelles were 20-45 nm. They showed good tumor uptake (4-5 %ID/g, 48h) and limited uptake in liver (5-7 %ID/g, 48h) and spleen (3-6 %ID/g, 48h). It was concluded that there did not seem to be a significant difference between DOTA and CB-TE2A *in-vivo*. In addition, crosslinked micelles (with ^{64}Cu bound to CB-TE2A) were compared with non-crosslinked micelles. To our surprise, we found that the non-crosslinked micelles exhibited good stability in circulation and obtained a biodistribution very similar to the crosslinked micelles.

Resumé (in Danish)

Kapitel 1. Brugen af nanopartikler til behandling har længe været anset som en revolution, der blot venter på at ske. De ses især som nyttige i kemoterapi mod cancer, da de har en evne til at akkumulere i tumorvæv. Den klassiske nanopartikel er liposomet, der er en fedtmembran, der omkranser en vandholdig kerne. Polymere miceller er en anden type nanopartikel, der består af sæbe-lignende polymerer, der samler sig til veldefinerede partikler i vand. Terapi med nanopartikler hæmmes ofte af lavt tumor-optag kombineret med højt optag i lever og milt. Derfor er det et nyttigt værktøj at kunne følge nanopartiklernes fordeling i organismen. En måde at opnå dette på er ved at mærke dem med radioaktive isotoper. Isotoper der udsender positroner (anti-elektroner) kan detekteres ved hjælp af PET (*positronemissions tomografi*), der er en præcis og relativt ny teknologi. Interessante PET-isotoper inkluderer ^{18}F og ^{64}Cu . Udover at være værktøj i forskningen, har radiomærkede nanopartikler desuden det potentiale at kunne bruges som et radiolægemiddel i sig selv, der kan visualisere tumorvæv og bistå i diagnose og kirurgi i kræftbehandlingen.

Kapitel 2. Vi undersøgte liposomers mærkning med ^{18}F . ^{18}F har en relativt kort halveringstid på 110 min, hvilket kun muliggør PET-scanninger på op til 8 timer. ^{18}F skal bindes kovalent til en bestanddel af liposomet. Ved at binde til et fedtmolekyle kan det indsættes stabilt i membranen. Et glycerolipid og en cholesterylether blev syntetiseret. De havde begge frie primære alkoholer, som blev omdannet til aktiverede sulfonater (Ms, Ts, Tf). Disse substrater blev [^{18}F]radiofluorerede i fuldt automatiseret udstyr ved en klassisk Kryptofix222-medieret procedure i DMSO. Udbyttet var ringe, 3-17% afhængig af reaktionsbetingelser. De [^{18}F]fluorerede prober blev oprenset *in-situ* på SEK-Paks. Mesylatet af cholesteryletheren viste sig at være bedst. Dette substrat blev radiomærket og formuleret i langtids-cirkulerende liposomer ved at tørre proben og lipider sammen, efterfulgt af hydrering ved magnetisk omrøring. Liposomerne blev ekstruderet gennem 100 nm filtre ved en fuldt automatiseret procedure. Undersøgelser i dyr, blev gjort i tumorbærende mus og PET-scanninger blev udført over 8 timer. Klart tumor-optag samt optag i lever og milt kunne ses, hvilket svarer til forventet farmakokinetik for liposomer. Tumoroptyget kunne kvantificeres og en *tumor-til-muskel ratio* på 2,20 fandtes efter 8 timer. Denne værdi giver kontrast nok til at kunne visualisere tumorvæv og viser at de ^{18}F -mærkede liposomer kan bruges til dette. På grund af de lave [^{18}F]radiofluoreringsudbytter der var opnået, undersøgte vi en metode til at radiomærke lipofile substrater i ikke-polære solventer. Dette involverede udvikling af [^{18}F]HF gas fra koncentreret svovlsyre hvorefter det blev ledt ned i en opløsning af substratet i toluen. En phosphazen-base var til stede, som bandt [^{18}F]HF og medierede fluoreringen. Ved denne metode blev udbytter på 71% opnået.

Kapitel 3. Radiomærkning af polymere miceller med ^{64}Cu undersøgt. ^{64}Cu muliggør længere scanningstider (op til 48 hours), i kraft af sin længere halverngstid (12,7 timer). 48 timer svarer godt til det vindue i hvilket nanopartikel-farmakokinetik normalt er interessant. Da ^{64}Cu er et metal skal det bindes til polymere miceller gennem en kovalent bundet chelator. DOTA og CB-TE2A er to sådanne chelatorer, men DOTA menes generelt at være ustabil *in-vivo*. DOTA og CB-TE2A blev begge bundet til triblock polymere miceller i *shell*-regionen, hvor de menes at være beskyttede af det omgivende PEG lag mod interaktion med substanser i blodet. Micellerne kunne krydsbundes idet de i kernen havde polymerer indeholdende coumarin. Coumarin-molekyler krydsbinder når de udsættes for UV-lys. Dernæst blev micellerne mærket med ^{64}Cu og uspecifikt bundet ^{64}Cu blev fjernet med EDTA. God mærkning blev opnået med begge chelatorer (40-70% af den samlede radioaktivitet). Nogle af de fremstillede miceller udviste dog alvorlig ustabilitet, især ved let øgede temperaturer. Dette forhindrede deres brug *in-vivo*. Derimod var andre typer miceller stabile og disse blev undersøgt i tumorbærende mus. Disse miceller havde en størrelsesfordeling mellem 20 og 45 nm. De udviste godt tumor-optag (4-5 %ID/g efter 48 timer) samt begrænset grad af det uønskede optag i lever (5-7 %ID/g) og milt (3-6 %ID/g). Vi konkluderede at vi ikke så nogen signifikant forskel på DOTA og CB-TE2A *in-vivo*. Derudover blev krydsbundne miceller (med ^{64}Cu bundet til CB-TE2A) testet overfor ikke-krydsbundne miceller. Til vores overraskelse fandt vi at de ikke-krydsbundne miceller udviste god stabilitet i blodbanen og faktisk havde samme *in-vivo* distribution som de krydsbundne.

Table of contents

CHAPTER 1 - Introduction to nanoparticulate systemic drug delivery and PET imaging	
1.1 Background	1
1.2 Liposomes	2
1.3 Polymeric micelles	5
1.4 <i>In-vivo</i> pharmacokinetics and accumulation of nanoparticles	9
1.5 Basic radiation theory	12
1.6 Spect & PET – Nuclear tomographic imaging	15
1.7 Important radioisotopes for SPECT and PET	17
1.8 Basic radiochemistry of ^{18}F	18
1.9 Basic radiochemistry and pharmacokinetics of ^{64}Cu and its chelators	20
1.10 Concluding remarks and rationale for nuclear imaging of nanoparticles	24
CHAPTER 2 - Preparation and <i>in-vivo</i> investigation of ^{18}F-labeled liposomes	
2.1 Background	25
2.1.1 Radiolabeling of liposomes with metal isotopes for SPECT-imaging	27
2.1.2 Radiolabeling of liposomes with metal isotopes for PET (^{64}Cu)	29
2.1.3 Radiolabeling by covalent binding (iodine)	30
2.1.4 Summing up radiolabeling methodology	31
2.1.5 Radiolabeling of liposomes with ^{18}F	32
2.1.6 Choice of lipid probe in membrane labeling	33
2.1.7 Double labeling of liposomes	34
2.1.8 Objective	34
2.2 Synthesis of lipophilic sulphonate substrates	35
2.2.1 Synthesis of a di-alkyl glycerol probe substrate	35
2.2.2 Synthesis of a cholesteryl ether probe precursor	39
2.3 Automated synthesis of an ^{18}F -labeled di-hexadecyl glyceride lipid	40
2.3.1 Preparation and drying of the reactor	41
2.3.2 Addition of the substrate	43
2.3.3 Choice of pseudohalide	45
2.3.4 Reaction conditions – Solvent, temperature and duration	46
2.3.5 Formation of impurities	46
2.4 Automated synthesis of an ^{18}F -labeled cholesteryl ether lipid	46
2.5 Purification of the radiolabel	49
2.6 Preparation of radioliposomes	52
2.7 Timeline of radioliposome preparation and locations of activity	55
2.8 <i>In-vivo</i> investigations	55
2.8.1 <i>In-vivo</i> investigation results	56
2.8.2 Discussion of <i>in-vivo</i> results	58
2.9 General discussion and concluding remarks	60
2.10 Fluorination of lipids in nonpolar solvents by [^{18}F]HF transfer to phosphazene bases	62
2.11 Experimental section	64
CHAPTER 3 - ^{64}Cu-labeling and <i>in-vivo</i> investigation of the pharmacokinetics of triblock polymer micelles	
3.1 Background	72
3.1.1 Radiolabeling of polymeric micelles with non-PET isotopes	75
3.1.2 Radiolabeling of polymeric micelles with PET isotopes	75
3.1.3 Photo core-crosslinking by coumarin	76

3.1.4 Objective	77
3.2 Synthesis and functionalization of unimers	78
3.2.1 Synthesis of macroinitiators and monomers	80
3.2.2 Synthesis of PEG-PAEMA-PCMA	80
3.2.3 Synthesis of PEG-PHEMA-PCMA	82
3.2.4 Synthesis of PEG-PHEMA-PMMA	84
3.2.5 Synthesis of PEG-PAEMA-PMMA	84
3.2.6 Purification of unimers by dialysis (procedure A)	84
3.2.7 Determination of CMC	85
3.2.8 Conjugation of chelators to unimers	86
3.2.9 Preparation of micelles (procedure F)	89
3.2.10 Nomenclature used for chelator conjugated micelles	89
3.2.11 Characterization of micelles	90
3.2.12 Formulation of micelles, sizes and zeta potentials	90
3.3 Pilot radiolabeling experiments	92
3.3.1 Initial experiments and unspecific binding of EDTA	93
3.3.2 Unspecific binding of DOTA and capping	94
3.3.3 Unspecific binding of ⁶⁴ Cu and EDTA/DTPA scavenging	96
3.3.4 Labeling of CB-TE2A micelles and precipitation at elevated temperatures	98
3.3.5 Localization of the "high fractions"	100
3.4 Crosslinking	101
3.5 Quantification of micelle material in dispersion	105
3.6 Compilation of labeling results at established conditions	107
3.7 Animal studies with PEG-PAEMA-PCMA micelles – CL versus nonCL	108
3.7.1 What went wrong?	112
3.8 Animal studies with PEG-PHEMA-PCMA micelles – CB-TE2A versus DOTA and the Effect of crosslinking	114
3.8.1 Preparation of the micelles	114
3.8.2 Discussion of <i>in-vivo</i> results – CB-TE2A versus DOTA	116
3.8.3 Discussion of <i>in-vivo</i> results – The effects of crosslinking	119
3.8.4 Thermostability of PEG-PHEMA-PCMA micelles	122
3.9 Concluding remarks	123
3.10 Experimental section	124
 4. GENERAL CONCLUSION & PERSPECTIVES	 129
 5. REFERENCES	 132

SUPPLEMENTARY INFORMATION

APPENDIX 1

"PET imaging of liposomes labeled with an [18F]-fluorocholesteryl ether probe prepared by automated radiosynthesis" (paper)

APPENDIX 2

"In-vivo comparison of DOTA and CB-TE2A through shell-region ⁶⁴Cu-labeling of core-crosslinked triblock polymeric micelles" (manuscript)

Supplementary Information

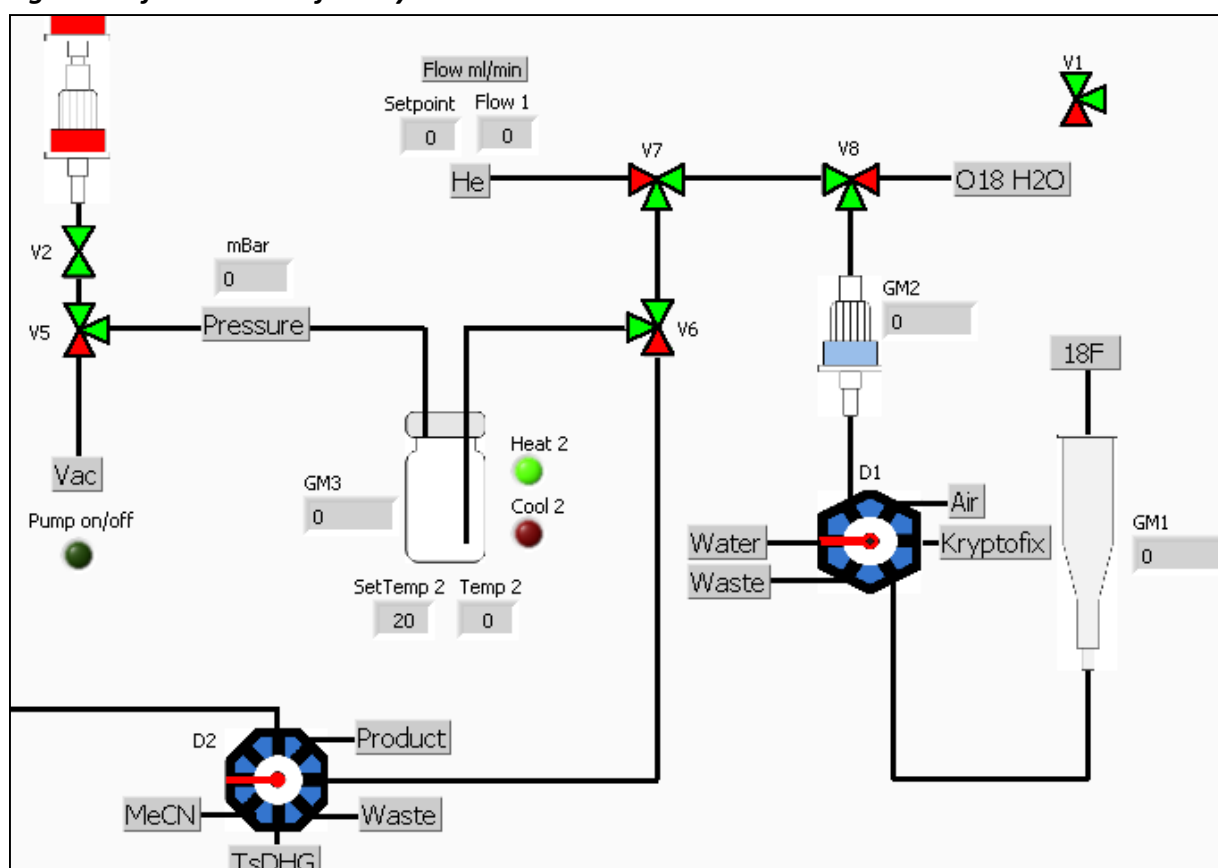
List of contents

I: A closer look at the synthesis robot	2
II: Identification of cholesteryl ether impurity A	4
III: Synthesis of PEG-PAEMA-PCMA and PEG-PHEMA-PCMA	7
IV: NMR spectra of selected unimers	11
V: Selected Radio-TLC chromatograms	14
VI: Animal studies experimentals	18
VII: A radiolysis study	21
VIII: [¹⁸F]HF transfer, phosphazene fluorination – experimental	26

Supplementary Information I – A closer look at the synthesis robot

Generally, the synthesis robot can be visualized by the figures already presented in the text as well as **figure A**, that is seen below. In the top left corner of **figure A** is seen two red SEP-PAKS (C18). These are the link that connect **figure A** with **Figure 2.5** in the main text. From application on the C18 SEP-PAKS the remaining process (purification) has been described in the main text.

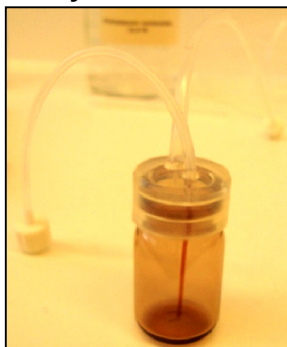
Figure A – first section of the synthesis robot



The graphic depiction of the workings of the synthesis robot shown here is part of the interface on the computer controlling the apparatus. The robot is explained using the labels shown on the figure (**given in parenthesis**). The ^{18}O -water containing the ^{18}F is placed in the container on the right (**18F**). The activity is monitored by **GM1**. **D1** is a syringe with a number of controllable

inlets and outlets. It takes up the fluoride and ejects it onto the blue QMA SEP-PAK at **GM2** (which monitors activity on the QMA). **D1** then takes up air and blows it through the QMA, ejecting the water *right* on valve **V8** into the waste **O18 H2O**. **D1** then takes up Kryptofix222 (**Kryptofix**) and passes it through the QMA, eluting the ^{18}F , this time *left* on **V8**, through **V7** and **V6**, into the **reactor** (photo shown below), placed at **GM3**. This step is followed by air.

Radiofluorination reactor



The solvents are then evaporated by applying a helium stream (**He**) through **V7** and **V6** as well as raising and lowering the temperature (**SetTemp2 / Temp2**). In addition, pressure can be controlled by applying vacuum (**Pressure & Vac**). The applied vacuum removes the evaporated solvents. Before the pump a cooling trap is placed, cooled with liquid nitrogen. **D2** is another syringe from which solutions can be added to the reactor. The acetonitrile for the azeotropic evaporations is added from here. The activity in the **reactor** can be monitored at **GM3**. After azeotropic evaporation, the substrate is added and the solvent is removed. Then is added the reaction solvent (usually DMSO) and the mixture is heated for reaction. After the reaction, the radiofluorinated probe is applied to the C18 SEP-PAKs and purified as described in the main text.

Supplementary Information II – Identification of cholesteryl ether impurity A

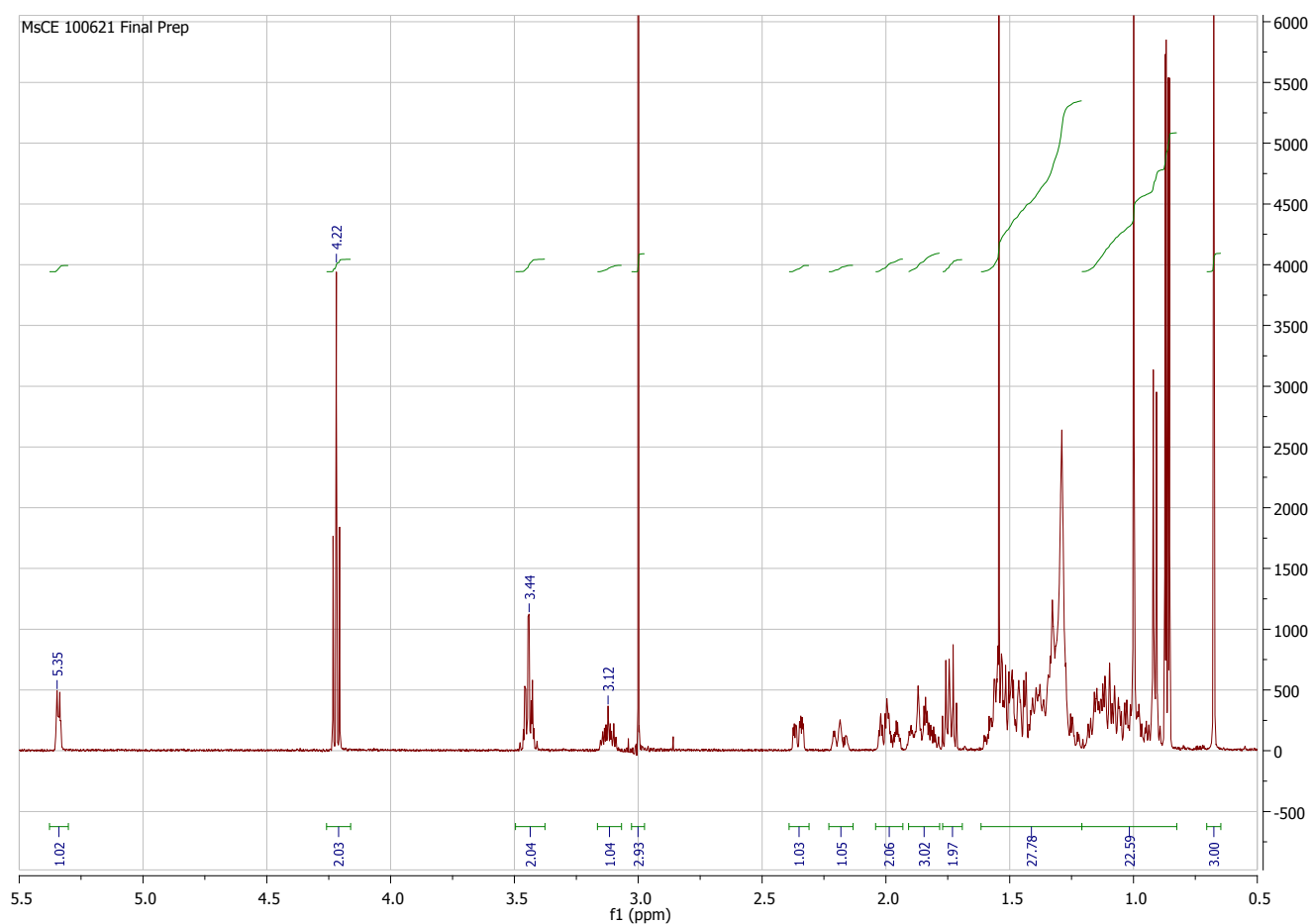
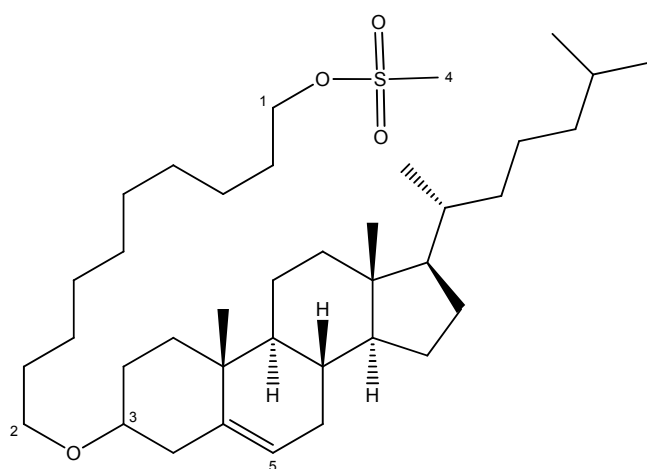


Figure A.1 – ^1H -NMR of cholesteryl ether mesylate (compound **15**)



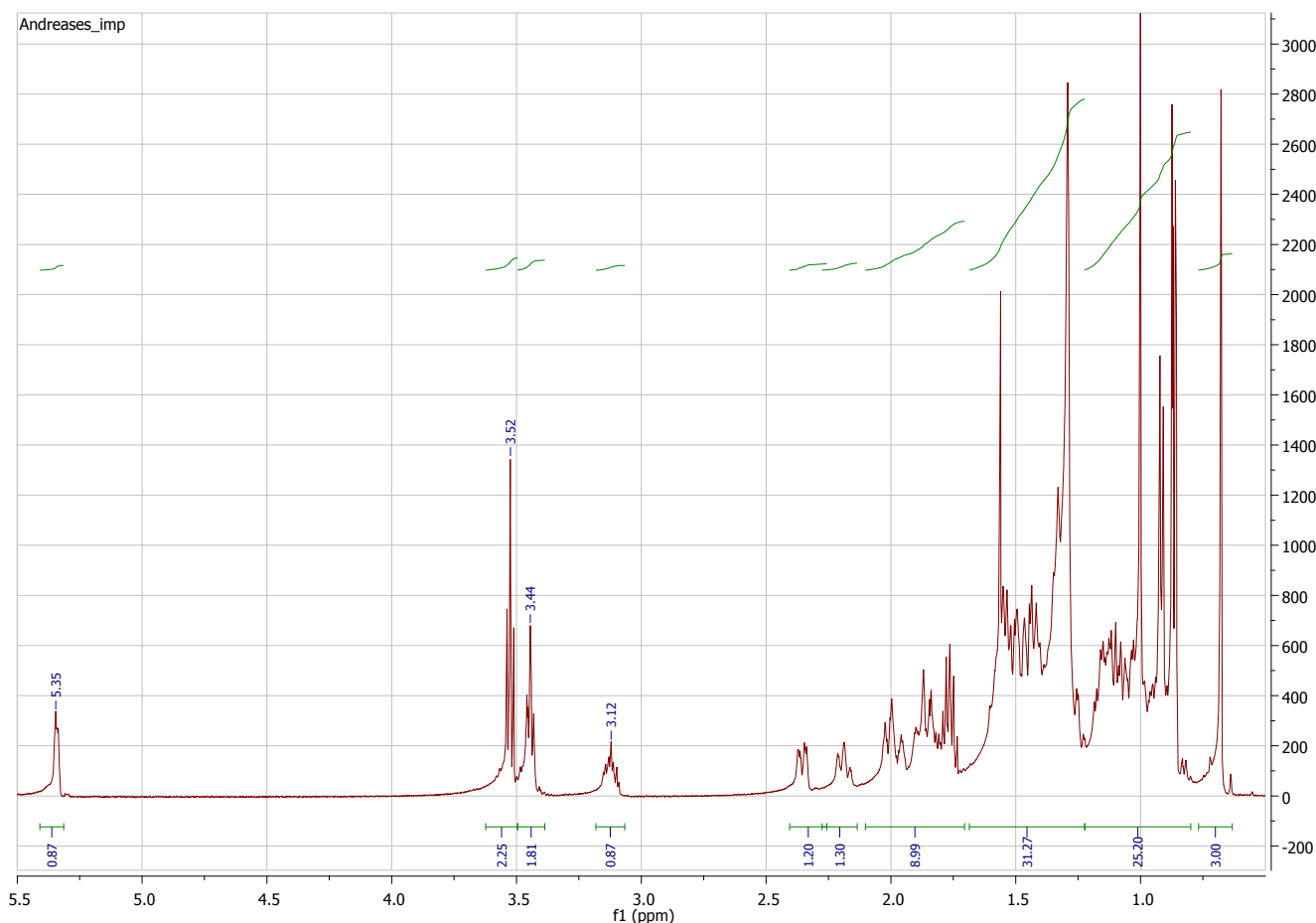


Figure A.2 – ^1H -NMR of cholesteryl ether impurity A.

Comments to spectra: The single proton at 5.35 are identical in both spectra. This is the proton of the unsaturated bond in the cholesterol moiety (**5**). Accordingly, this bond is not altered in impurity A. The peak at 3.44 – a 2-proton multiplet – also appear unaltered. This peak is assigned to the carbon sitting on the aliphatic decyl chain next to the cholesteryl ether oxygen (**2**). On the other side of this oxygen is a single proton multiplet appearing at 3.12 (**3**). This peak is also unaltered between the two compounds. In the spectra for the mesylate (**A.1**) the 2 proton peak for the carbon sitting next to the mesyl group appears at 4.22 (**1**). In the spectrum for impurity A, this peak seems to have moved to 3.52. This peak is a clear triplet ($J = 6.6$ Hz) in the mesylate spectrum. In the impurity A spectrum, it is still a triplet ($J = 6.8$), although some dissymmetry is seen in the peak. This is likely caused by the poor shimming of the impurity A spectrum. It is thus concluded that it is same peak, that has moved upfield, indicating that impurity A is formed by a reaction of the mesyl group. In the impurity A spectrum the characteristic 3-proton singlet at 3.00 is also gone, certifying that the mesyl group has been replaced. The fingerprint aliphatic region of the spectrum is not concluded to have changed. The appearance of the peaks, as well as their integrals are comparable. Thus, the cholesterol moiety does not appear to have been modified, although 1- or 2-proton peaks in the aliphatic region could go unnoticed.

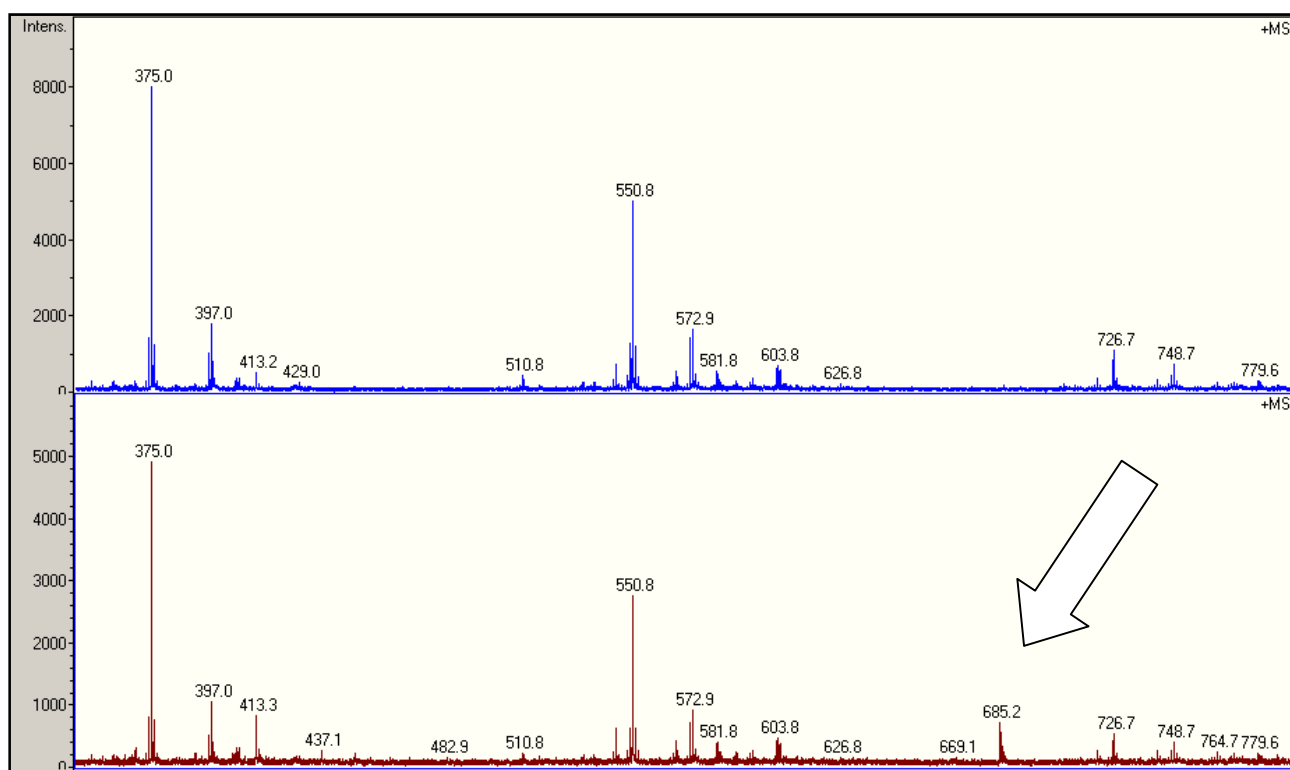


Figure A.3 – MALDI-TOF (Na-spiked) spectrum of DHB-matrix (*top*) and DHBmatrix + Impurity A (*bottom*). The peak for impurity A is seen at 685.2.

Supplementary Information III

– Synthesis of PEG-PAEMA-PCMA and PEG-PHEMA-PCMA

Synthesis of PEG-PAEMA-PCMA

- by Pramod Kumar, edited by Andreas Jensen.

Materials and measurements: 2-Aminoethyl methacrylate hydrochloride (AEMA.HCl) (90%), Bis(*tert*-butyl) dicarbonate (99%), triethylamine (TEA) (99.5%), 2-bromo-isobutyryl-bromide (98%), 2,2'-bipyridyl (bpy) (99%), PMDETA (99%), CuCl₂ (99.995%), trifluoroacetic acid (TFA) (99%) and all other solvents and chemicals were purchased from Sigma Aldrich and used as obtained. CuCl (99.995%) was washed with glacial acetic acid, followed by absolute ethanol and diethylether, dried and stored under argon. Solvents used for ATRP were purified by distillation over the drying agents indicated in parentheses, stored under molecular sieves (MeOH 3 Å and DMF 4 Å) and transferred under argon; MeOH (Mg(OMe)₂), DMF (CaH₂). CH₃O-PEG-OH (poly (ethylene glycol) monomethylether (M_n = 5000) was from Fluka. Argon atmosphere (99.9999%) used in the reactions was provided by AGA Denmark. NMR spectra were recorded by using 300 MHz Varian Mercury 300 BB spectrometer. FT-IR spectra were recorded by Perkin Elmer Spectrum 100 FT-IR Spectrometer. GPC measurements were carried out with a RID10A-SHIMADZU refractive index detector and Mixed-D GPC column from Polymer Laboratories with a flow rate of 0.5 mL/min at 25°C, and DMF with 50 mM LiCl as eluent. UV-Vis spectra were recorded on Unicam Helios Uni 4923 spectrophotometer

Synthesis of PEG₅₀₀₀Br: The macroinitiator was synthesized by using a slightly modified procedure from that reported in the literature.^[1] CH₃O-PEG-OH, M_n = 5000 (5 gram, 1 mmol) was dissolved in 60 mL of toluene. After azeotropic distillation of 10 mL of toluene under reduced pressure to remove traces of water, TEA (0.278 mL, 2 mmol) was added, and the solution was cooled to room temperature. 2-bromoisobutyryl bromide (0.185 mL, 1.5 mmol) was added drop wise to the mixture, and the reaction mixture was stirred at 40 °C for 2 days under a calcium chloride guard tube. The solution was filtered, and most of the toluene was removed by rotary evaporation prior to precipitation into 10 fold excess of cold ether. The crude polymer was dried under vacuum, dissolved in water at pH 8-9 and then extracted with DCM. The organic layers were collected and dried over anhydrous sodium sulfate. The removal of the solvent under reduced pressure afforded the purified macroinitiator in a yield of 5.1 g (99 %). ¹H-NMR (250 MHz, CDCl₃): δ = 3.63 (s, -CH₂CH₂O-), 1.91 (s, -C(CH₃)₂) ppm; FT-IR: ν = 2887, 1737, 1466, 1359, 1342, 1279, 1241, 1148, 1107, 1060, 963, 841 cm⁻¹.

Synthesis of 2-[N-(*tert*-Butoxycarbonyl)Amino]ethyl methacrylate (AEMA(Boc)): AEMA(Boc) was synthesized by a slightly modified procedure than reported.^[2] AEMA HCl (2.5 g, 15.15 mmol) was dissolved in 40 mL of dry DCM and cooled to 0 °C in an ice water bath. Anhydrous triethylamine (4.2 mL, 30.3 mmol) was added drop wise to the ice cold solution and stirred for 20 minutes. Bis(*tert*-butyl) dicarbonate (5.22 mL, 22.725 mmol) dissolved in 10 mL of dry DCM was slowly added to the reaction mixture, warmed to room temperature and stirred for 24 h under argon atmosphere. The organic layer was washed with water (2 × 25 mL), 1M HCl (2 × 25 mL), saturated aqueous sodium bicarbonate (2 × 25 mL) and with saturated brine solution (2 × 20 mL). The organic layer was dried over anhydrous sodium sulphate; this was followed by removal of the solvent under reduced pressure gave crystalline solid 3.3 g (95%). ¹H-NMR (250 MHz, CDCl₃): δ = 6.11 (1H, Vinylic H), 5.58 (1H, Vinylic H), 4.76 (broad (br), 1H, -NH), 4.20 (2H, -COOCH₂CH₂), 3.42 (2H, -COOCH₂CH₂), 1.94 (s, 3H, -CH₃), 1.44 (s, 9H, -C(CH₃)₃) ppm; FT-IR: ν = 3386, 2981, 1692, 1633, 1521, 1453, 1423, 1388, 1364, 1323, 1158, 1107, 1042, 998, 957, 915, 880, 853, 818, 777, 756, 653, 597 cm⁻¹.

7-(2-Methacryloyloxyethoxy)-4-methylcoumarin(CMA): was synthesized by the reported procedure^[3]

Synthesis of PEG-*b*-PAEMA(Boc)Cl: PEG-Br (1 gram, 0.19 mmol), AEMABoc (522 mg, 2.28 mmol), 2,2'-bipyridyl (62 mg, 0.40 mmol) and 5 mL MeOH were added to a 25 mL schlenk flask equipped with a magnetic stir bar. The flask was frozen in liquid nitrogen, and CuCl catalyst (21 mg, 0.21 mmol) was added. The reaction mixture was degassed with three freeze-pump-thaw cycles to remove the oxygen, and the polymerization was carried out at 40°C for 15 h under an argon atmosphere. The reaction was stopped by opening the flask to air. The reaction mixture was then passed through a silica gel column to remove the copper catalyst using MeOH as the solvent. On exposure to air, the dark brown reaction mixture turned blue, indicating the areal oxidation of the Cu(I) catalyst. After removing most of the MeOH by rotary evaporation, the polymer was precipitated into excess cold diethyl ether, isolated by filtration, and the precipitate dried under vacuum yielded 1.1 g (64%) of the diblock copolymer.

¹H-NMR (300 MHz, CDCl₃): δ = 5.50 (broad s, -NH), 4.0 (broad s, -OCH₂CH₂NH), 3.63 (s, -CH₂CH₂O), 3.37 (broad s, -OCH₂CH₂NH, -OCH₃), 1.82 (broad s, -CH₂ backbone), 1.43 (s, -C(CH₃)₃), 1.11-0.81 (m, -C(CH₃)₂, -CH₃ backbone) ppm; FT-IR: ν = 3387, 2892, 1716, 1520, 1466, 1391, 1361, 1342, 1279, 1241, 1150, 1112, 1060, 996, 965, 843 cm⁻¹.

Synthesis of PEG-*b*-PAEMA(Boc)-*b*-PCMA : PEG-*b*-PAEMA(Boc)-Cl (1g, 0.11 mmol), 7-(2-Methacryloyloxyethoxy)-4-methylcoumarin (CMA) (2.6 g, 9.02 mmol), CuCl₂ (12 mg, 0.088 mmol), PMDETA (0.068 mL, 0.33 mmol), and 10 mL of DMF, were added to a 25 mL schlenk flask equipped with a magnetic stir bar. The flask was frozen in liquid nitrogen, and CuCl catalyst (11 mg, 0.11 mmol) was added. The reaction mixture was degassed with three freeze-pump-thaw cycles to remove oxygen, and the polymerization was carried out at 80°C for 24 h under an argon

atmosphere. The reaction mixture was concentrated under vacuum, and the polymer was precipitated into excess of cold MeOH, filtered and dried; yield = 2 g (56%).

$^1\text{H-NMR}$ (300 MHz, CDCl_3): δ = 7.40-5.90 (coumarin **H**), 4.38-4.04 (-OCH₂CH₂O-coumarin), 4.02-3.86 (-OCH₂CH₂NH), 3.58 (s, -CH₂CH₂O), 3.39-3.25 (-OCH₂CH₂NH), 2.22 (s, -CH₃ of coumarin), 2.04-1.55 (-CH₂ backbones of PAEMA and PCMA blocks), 1.39 (s, -C(CH₃)₃), 1.15-0.77 (-CH₃ backbones of PAEMA and PCMA blocks) ppm.

Table. Molecular weights of PEG_n-*b*-PAEMA(Boc)_m-*b*-PCMA_p.

M_n [a]	M_w [a]	M_w/M_n [a]	M_n [b]	n [c]	m [c]	p [c]
22100	26800	1.21	30390	120	9	80

[a] Determined by GPC, [b] Determined by NMR, [c] Number of repeating units of PEG block (*n*), PAEMA(Boc) block (*m*) and PCMA block (*p*).

PEG-*b*-PAEMA-*b*-PCMA: PEG-*b*-PAEMA(Boc)-*b*-PCMA (500 mg, 0.016 mmol) was treated with 1:1 TFA:DCM mixture (8 mL) for 15 h at room temperature. After removing most of the solvent under rotary evaporation, the polymer was precipitated into excess cold diethyl ether, filtered and dried. The complete deprotection of *tert*-Butoxycarbonyl (Boc) was confirmed by the disappearance of Boc signal at 1.45 ppm in $^1\text{H-NMR}$ (300 MHz, CDCl_3).

Reference

- [1] S. Liu, J. V. M. Weaver, Y. Tang, N. C. Billingham, S. P. Armes, K. Tribe, *Macromolecules* **2002**, *35*, 6121.
- [2] M.-H. Dufresne, J.-C. Leroux, *Pharmaceutical Research* **2004**, *21*, 160.
- [3] M. Obi, S. Y. Morino, K. Ichimura, *Chemistry of Materials* **1999**, *11*, 656.

Synthesis of PEG-PHEMA-PCMA

- by Pramod Kumar, edited by Andreas Jensen

1. Synthesis of PEG₁₂₇-PHEMA₇-PCMA₁₈

The macroinitiator PEG-Br and diblock copolymer PEG-PHEMA-Cl were synthesised by the reported procedures.¹ The monomer 7-(2-Methacryloyloxyethoxy)-4-methylcoumarin (CMA) was synthesised by a procedure reported by M. Obi *et al*.²

The diblock copolymer PEG-PHEMA-Cl (1000 mg, 0.1 mmol), 7-(2-Methacryloyloxyethoxy)-4-methylcoumarin (CMA) (720 mg, 2.5 mmol), CuCl₂ (12 mg, 0.09 mmol), and PMDETA (146 µl, 0.7 mmol) were dissolved in DMF (10 mL) and frozen in liquid nitrogen. The catalyst CuCl (10 mg, 0.1 mmol) was then added and the reaction mixture was degassed three times by freeze-pump-thaw cycles and stirred under argon at 80°C for 24 hours. Most of the solvent was removed under vacuum; the polymer was then precipitated from methanol and dried under vacuum to give the pure amphiphilic triblock copolymer (yield = 0.8 g, 63%).

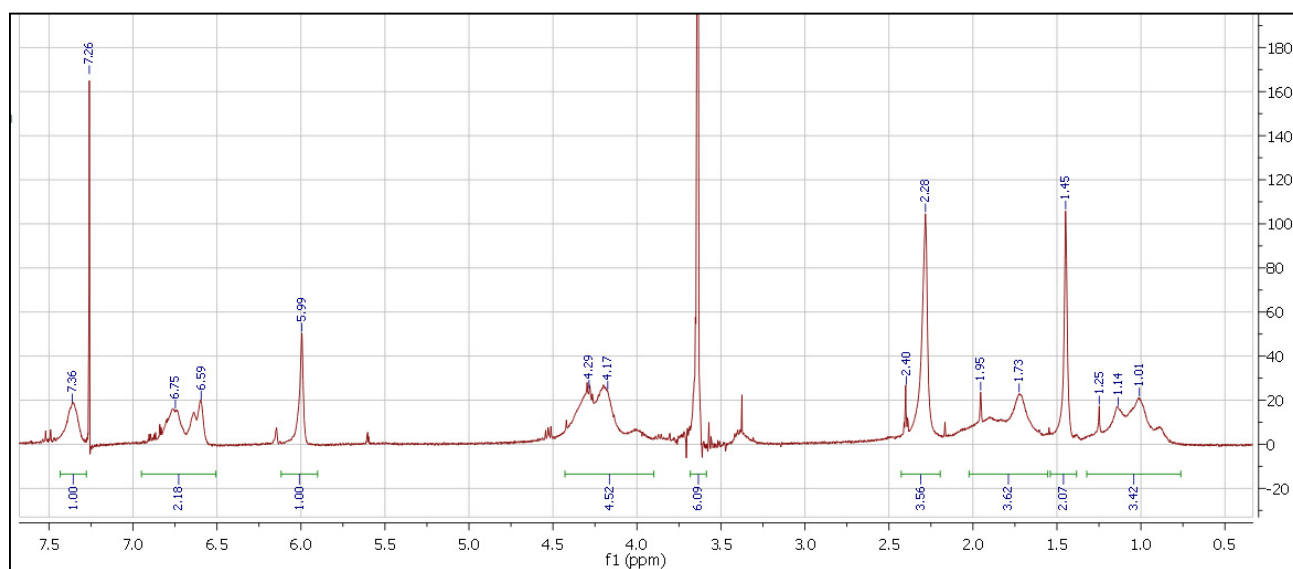
¹H-NMR (300 MHz, CDCl₃): δ = 7.38-6.00 (coumarin H), 4.60-3.73 (-OCH₂CH₂O-coumarin, -OCH₂CH₂OH), 3.65 (s, -CH₂CH₂O of PEG), 2.30 (s, -CH₃ of coumarin), 2.16-1.72 (-CH₂ backbones of PHEMA and PCMA blocks), 1.20-0.79 (-CH₃ backbones of PHEMA and PCMA blocks) ppm. FTIR (cm⁻¹): 3490, 2880, 1718, 1612, 1467, 1391, 1343, 1279, 1240, 1140, 1100, 963, 839, 750. Mn (from NMR) = 11814. From GPC: Mw = 12400, Mn = 9550, PD (Mw/Mn) = 1.3

The NMR spectrum for PEG-PHEMA-PCMA is shown below in Supplementary Information IV.

1. Pramod Kumar, E. K.; Almdal, K.; Andresen, T. L., Synthesis and characterization of ratiometric nanosensors for pH quantification: a mixed micelle approach. *Chemical Communications* 2012, 48 (39), 4776-4778.
2. Obi, M.; Morino, S. y.; Ichimura, K., Factors Affecting Photoalignment of Liquid Crystals Induced by Polymethacrylates with Coumarin Side Chains. *Chemistry of Materials* 1999, 11 (3), 656-664.

Supplementary Information IV – NMR spectra of selected unimers

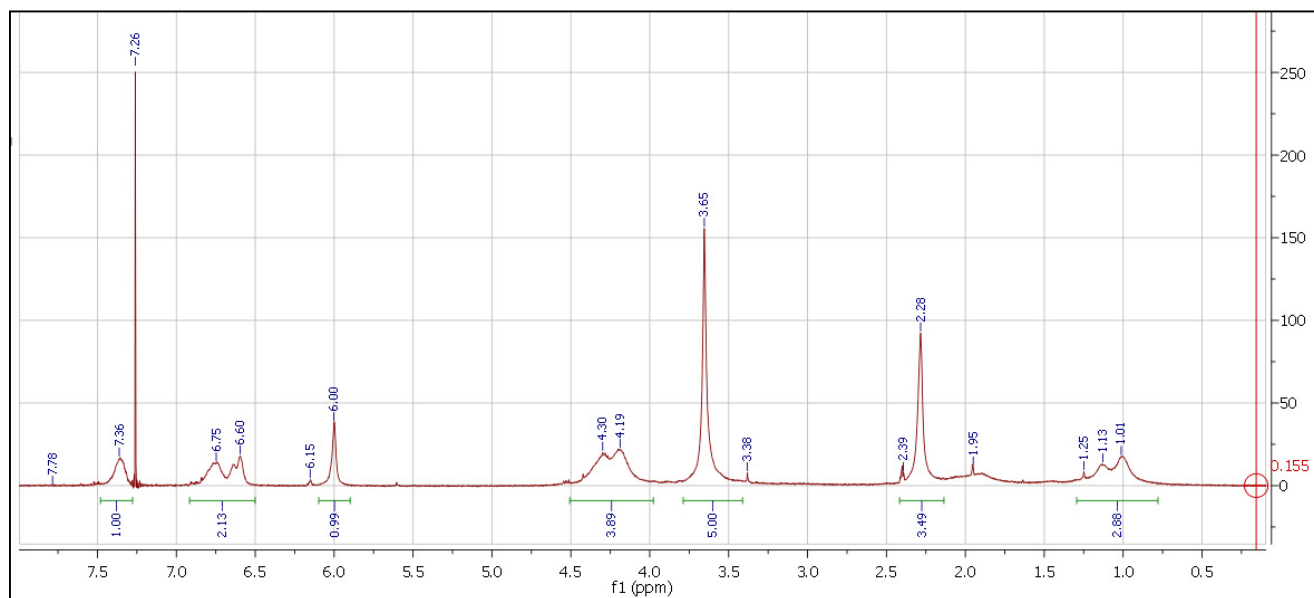
PEG-PAEMA(Boc)-PCMA (300 MHz, CDCl₃)



See below (PEG-PAEMA-PCMA spectrum) for explanation of peaks. The peak at 1.45 seen here is the tBb of the Boc (9 protons for each monomer). It can be calculated that the average number of PEG repeats in PEG5000 is on average 120 (based on H-NMR of PEG5000-Br, not shown here). Accordingly, the number of CMA monomers can be calculated based on the integrals of the PEG-peak (seen at 3.6-3.7) and the peak at 6.0, which represents the single proton sitting alpha to the carbonyl-group on the coumarin.

CMA: $120 * 1/(6/4) = 80$ (nr. of PEG monomers * integral of coumarin-peak/(integral of PEG/protons in PEG monomer)).

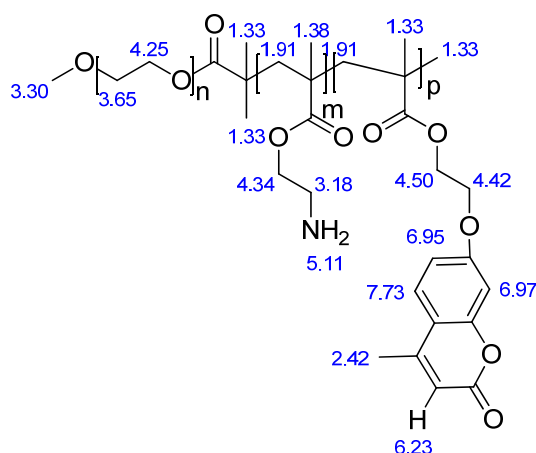
PEG-PAEMA-PCMA (300 MHz, CDCl₃)



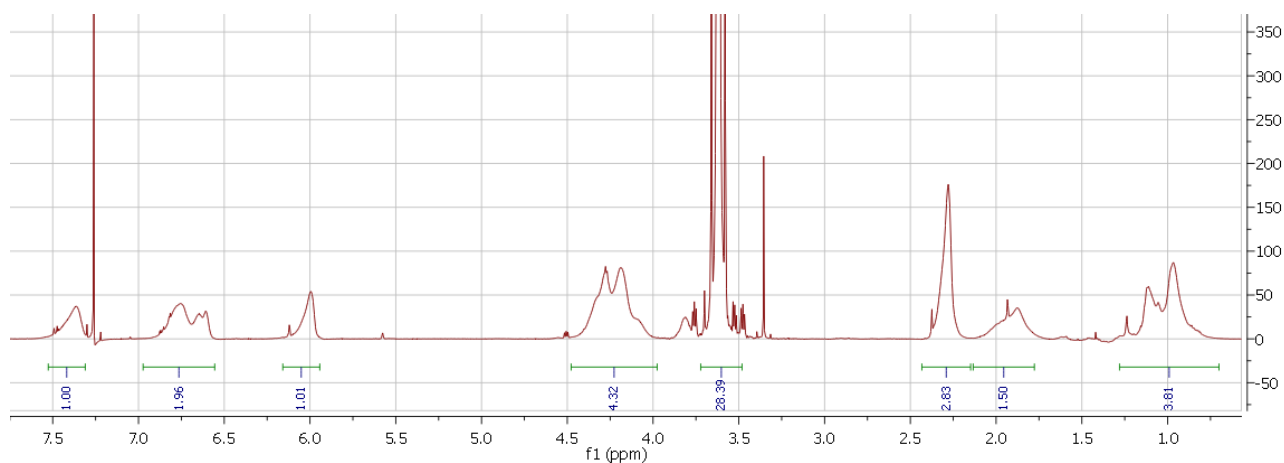
Above is shown a spectrum of PEG-PAEMA-PCMA with the Boc-groups removed by TFA-treatment. Note that the peak at 1.45 has disappeared. Also note that in this spectrum, the PEG-signal is lower compared to the coumarin signals, meaning that this batch of unimer has more coumarin repeats than the one shown above.

The major peak at 3.45 is the PEG-protons (4 protons per monomer). The integral of this peak is 5.00. The peak at 7.73 can be expected to be the aromatic proton, estimated to be at 7.73. Also the two protons estimated at 6.95-6.97 are seen in the spectrum at 6.60 and 6.75.

Finally, the remaining coumarin proton, estimated at 6.23, is seen at 6.00. The 4 protons linking coumarin to the backbone (est. 4.42-4.50) are seen in the interval 4.0-4.5, with an integral of 3.89. Due to the low amount of amine-monomers (AEMA), the 4 linking protons here are not identifiable in the spectrum. The large peak at 2.3 is the methyl group in the coumarin moiety. The other peaks seen upfield are backbone protons.



PEG-PHEMA-PCMA (500 MHz, CDCl₃)



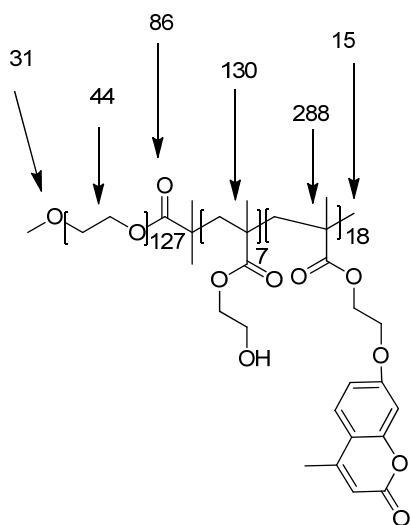
The peaks correspond with the general picture observed above for the PEG-PAEMA-PCMA spectrum.

The number of coumarin repeats can be calculated in the same manner:

$$\text{CMA: } 127 * 1/(28/4) = 18$$

By adding all components of the unimer, an MW based on NMR can be calculated:

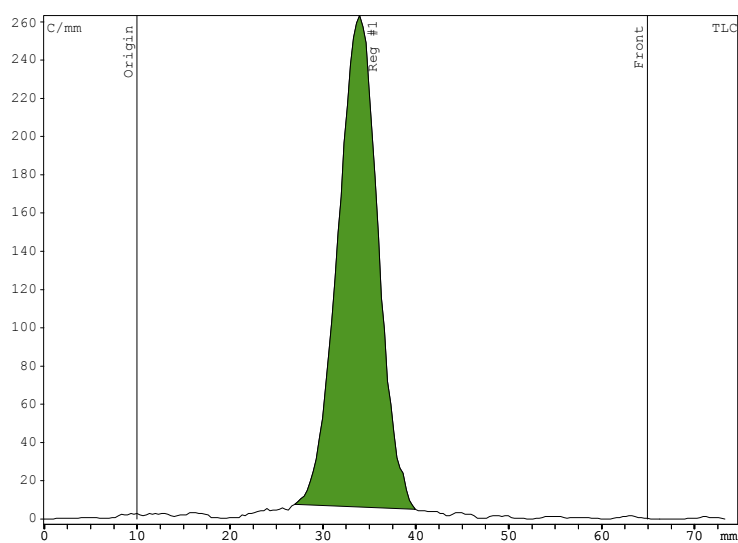
$$\text{MW} = 31 + 127 * 44 + 86 + 7 * 130 + 18 * 288 + 15 = 11814$$



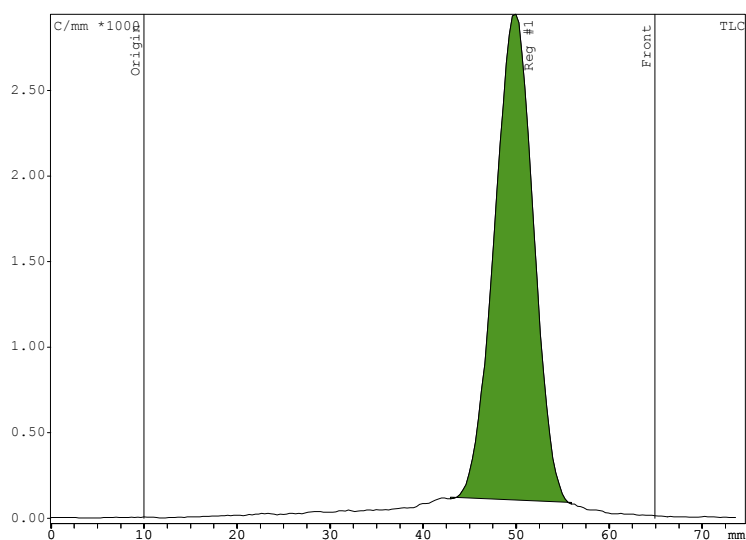
Supplementary Information V – Selected Radio-TLC chromatograms

All radio-TLC chromatograms shown here are eluted with 5% NH_4OAc in water-MeOH (1:1).

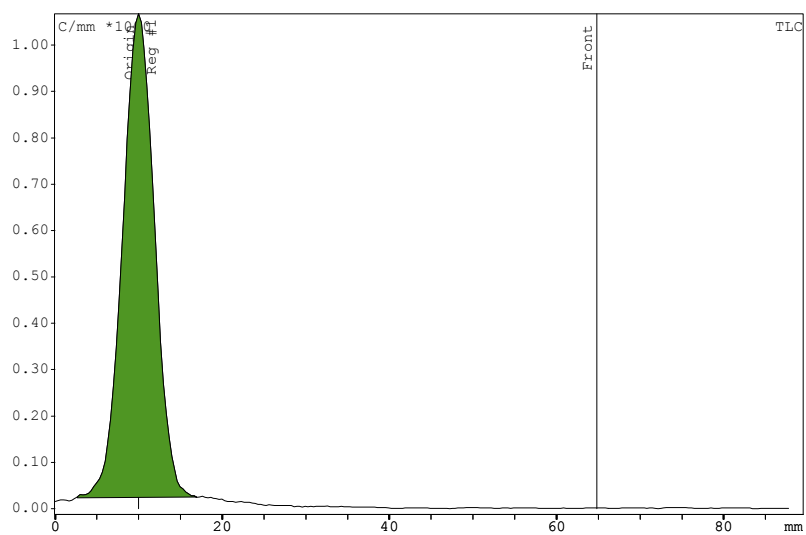
$\text{DOTA-}^{64}\text{Cu}$, $R_f = 0.42$



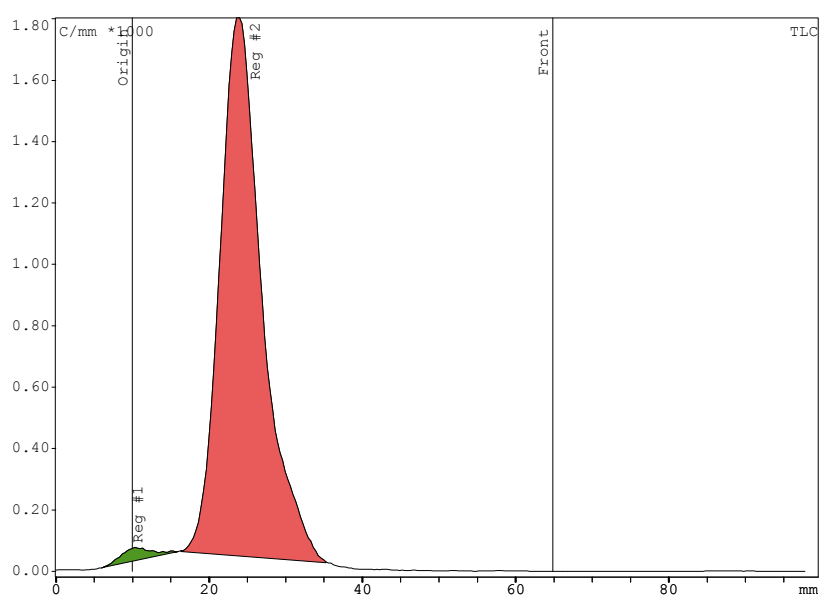
$\text{EDTA-}^{64}\text{Cu}$, $R_f = 0.72$



DTPA-⁶⁴Cu , $R_f = 0$

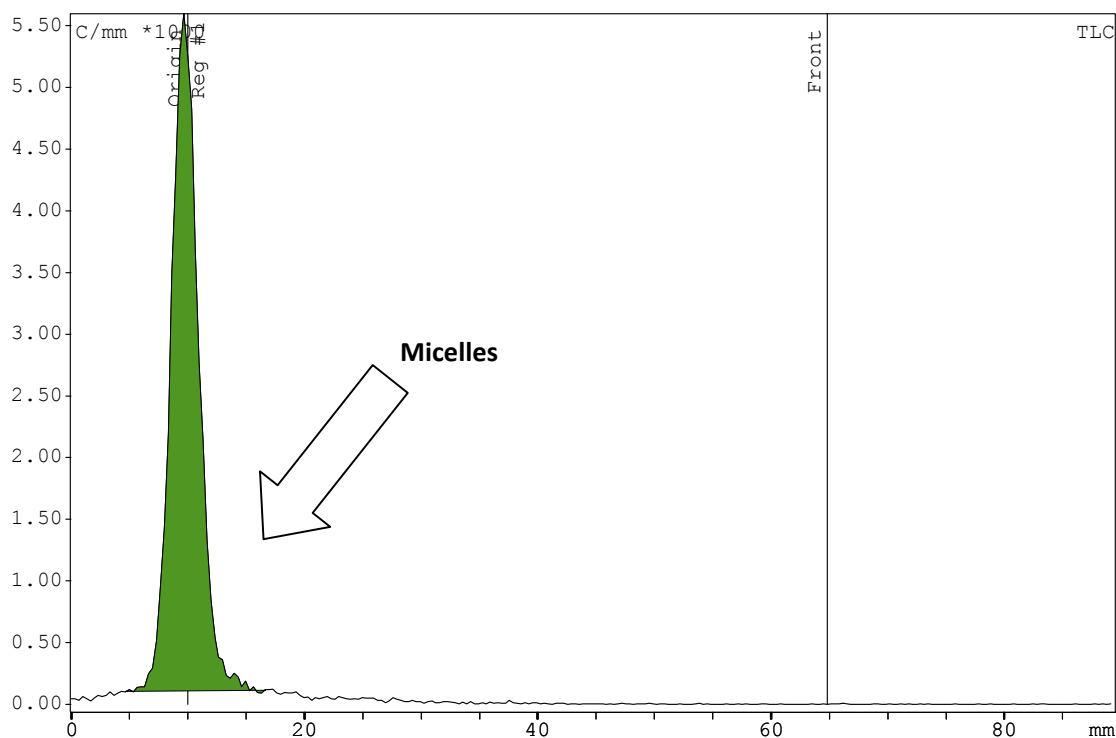


CB-TE2A-⁶⁴Cu , $R_f = 0.27$ (notice the trace of unchelated ⁶⁴Cu at the starting line)

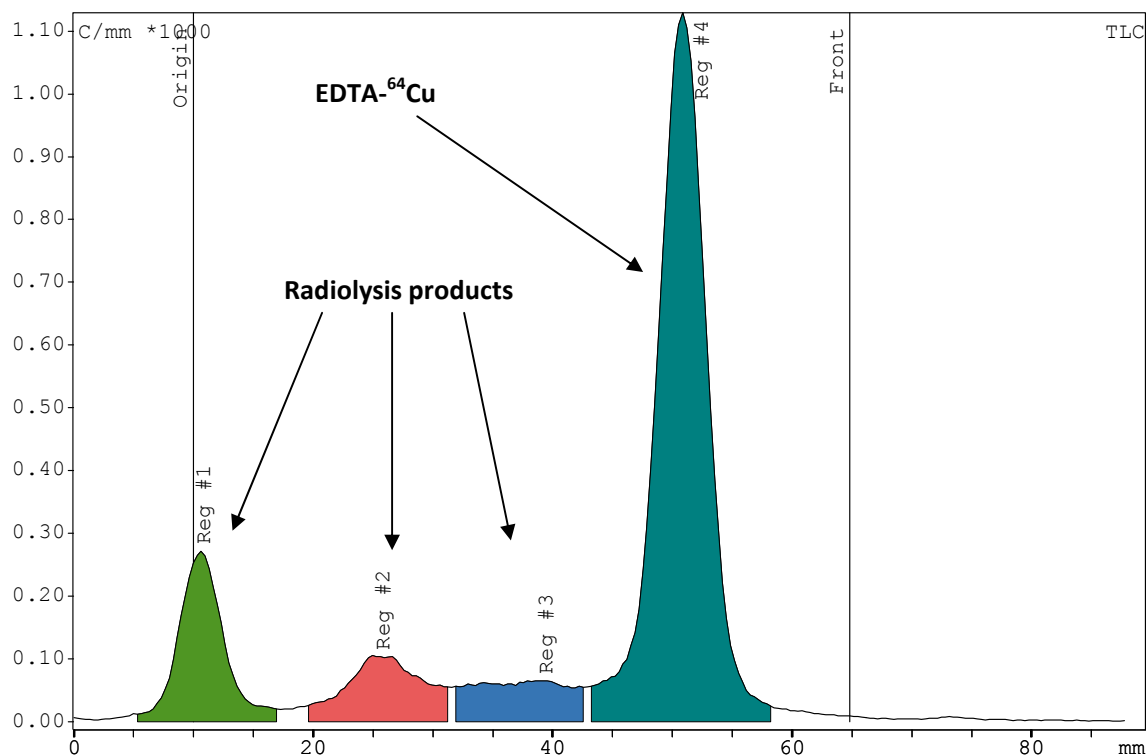


Below is seen typical analysis data from the “high fraction” and **Peak 2**. Data is from a high-activity labeling, where the micelles(PEG-PAEMA-PCMA, 10% DOTA, capped) were incubated with 618 MBq ^{64}Cu for 2.5 hours at room temperature. In the depicted experiment, **Peak 1** (54%) and **Peak 2** (26%) were normal. Notice the presence of radiolysis products.

*High fraction (most concentrated part of **peak 1**) – Micelles. It was clear from several experiments that micelles do not run on TLC. Notice that there are no radioactive contaminants in the high fraction, in particular, there is no ^{64}Cu bound to free chelators. This was always observed.*



Peak 2 – In the experiments where only little radioactivity was employed, the radiolysis products were not seen, only a prominent peak for the scavenging chelator (EDTA in this case). As a general rule however, a small peak at the starting line was always observed, regardless of radioactivity.



For an investigation into the radiolysis of the micelles, see **Supplementary Information VII**.

Supplementary Information VI – Animal studies experimentals

- By Tina Binderup

All tumor cell lines were purchased from ATCC-LGC Standards (LGC Standards AB, Borås, Sweden)

Animal studies with ^{18}F labeled liposomes (Chapter 2)

Human lung carcinoid (NCI-H727, 2 tumors, 1 mouse), small cell lung cancer (NCI-H69, 3 tumors, 2 mice) and glioblastoma (U87MG, 2 tumors, 1 mouse) tumor cells ($\sim 1 \times 10^7$ cells) were inoculated in the left and right flank of NMRI (Naval Medical Research Institute) nude mice ($n = 4$) and allowed to grow 2-4 weeks, depending on the growth rate of the tumors.

Prior to injection of the ^{18}F -labeled liposomes, mice were anaesthetized by intra-peritoneal injection of fluanisone/fentanyl citrate and midazolam (5 mg/0.625 mL/kg) and placed on a heated bed in the PET scanner (MicroPET Focus 120, Siemens Medical Solutions, Malvern, PA, USA), where the tracer was intravenously injected in a lateral tail vein. General anaesthesia was maintained using 1% sevofluran (Abbott Scandinavia AB, Solna, Sweden) mixed with 35% O_2 in N_2 . A dynamic scan was acquired from 0 to 20 min. post-injection with 19 frames for subsequent time-activity-curve generation. Two-and-a-half hour and 8h post-injection of the ^{18}F -liposomes, additional static PET emission scans were acquired. The acquisition time was 20 minutes for the 0 and 2.5h scans and 40 min. for the 8h scan to ensure proper signal-to-noise ratios. The pixel size was 0.866 x 0.866 x 0.796 mm and the resolution was 1.4 mm in the centre-field-of-view. PET data were reconstructed with the 2-dimensional ordered-subset expectation maximization (OSEM2D) reconstruction algorithm.

Computer tomography (CT) scans were acquired for anatomical localization of foci with a MicroCAT® II system (Siemens Medical solutions). CT settings were a tube voltage of 62 kVp, a tube current of 500 μ A, 360 rotation steps, an exposure time of 390 ms and a voxel size of 0.088 mm. PET and CT images were analyzed as fused images using the Inveon software (Siemens). ROIs were drawn around liver, kidney, spleen, muscle, tumors and the left-ventricle. Uptake in the left ventricle of the heart was taken as a measure of the blood concentration. Percent injected dose per gram (%ID/g) and tumor-to-muscle ratios were calculated.

The animal experiments were approved by the Animal Research Committee of the Danish Ministry of Justice.

Animal studies with ^{64}Cu labeled polymeric micelles (DOTA vs. CB-TE2A, PEG-PHEMA-PCMA micelles) (Chapter 3)

Seven weeks old female NMRI nude mice purchased from Taconic (Borup, Denmark) were inoculated in the right and left flank with 5×10^6 U87MG cells (LGC standards, Borås, Sweden) in a 1:1 mixture with matrixgel™ (BD Biosciences, Albertslund, Denmark). Tumors were allowed to grow for 2 weeks. The mice were divided in 2 groups; CB-TE2A (n = 6) and DOTA (n = 6). The animal experiments were approved by the Animal Research Committee of the Danish Ministry of Justice.

Either of the micelle formulations was intravenously injected in a lateral tail vein of anesthetized mice at an average dose of 7.8 ± 0.46 MBq (mean \pm SD) for the CB-TE2A micelles and 8.0 ± 0.84 MBq for the CB-DOTA-micelles at a volume of 200 μ L and a lipid concentration of XX. The PET/CT scans were acquired on a dedicated small animal system (MicroPET Focus 120 & MicroCAT® II, Siemens Medical Solutions, Malvern, PA, USA) at 1h, 22h and 46h post injection (p.i.) with PET acquisition times of 10, 15 & 30 min. respectively. PET data were reconstructed with the 2-dimensional ordered-subset expectation maximization (OSEM2D) reconstruction algorithm. PET and CT images were analyzed as fused images using the Inveon software (Siemens) where regions of interest (ROIs) were drawn around liver, kidney, spleen, muscle, tumors and the left-ventricle. Uptake in the left ventricle of the heart was taking as a measure of the blood concentration. CT settings were a tube voltage of 64 kVp, a tube current of 500

μA , 360 rotation steps, an exposure time of 440 ms and a voxel size of 0.092 mm. Immediately following the last PET scan 4 of the 6 mice in each group were euthanized and blood as well as organs of interest collected and counted in a gamma counter (Perkin Elmer Life Sciences).

The statistics were calculated using Excel 2010. Differences between the two chelator groups were analyzed using an unpaired, two-tailed t-test. Differences in the same animal at different times p.i was analyzed using a paired, two-tailed t-test. A p-value < 0.05 was considered significant. Error bars on tracer accumulation (%ID/g) is presented as standard error of the mean (S.E.M.).

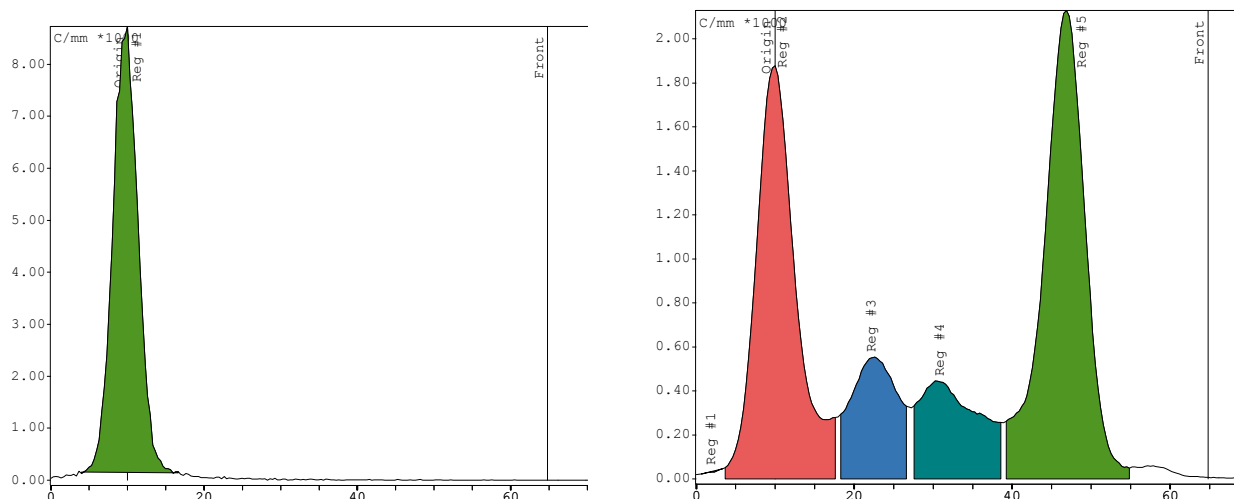
Supplementary Information VII – Radiolysis study

The susceptibility of the polymeric micelles towards radiolysis was studied. For this purpose, the micelles were incubated with an amount of radioactivity 5-6 times higher than normal and it was allowed to decay over an extended time. A procedure very similar to the standard labeling of DOTA-conjugated micelles was followed. 10% DOTA PEG-PAEMA-PMMA (capped) micelles were used.

To a vial containing **3.02 GBq** ^{64}Cu was added 100 μL NH_4OAc buffer (0.1 M, pH 5.5) and the mixture was stirred for 10 minutes. Then was added 400 μL micelle dispersion (ca. 5 mg micelle material per mL).

The mixture was stirred for 2 hours after which 100 μL was taken out. This was transferred to a 4 mL vial along with 10 μL EDTA solution (1 mM). This was stirred for 20 minutes and analyzed by Radio-TLC and size-exclusion chromatography. **Peak 1:** 78%, **Peak 2:** 8% (total activity accounted for: 92%). Radio-TLCs are shown below:

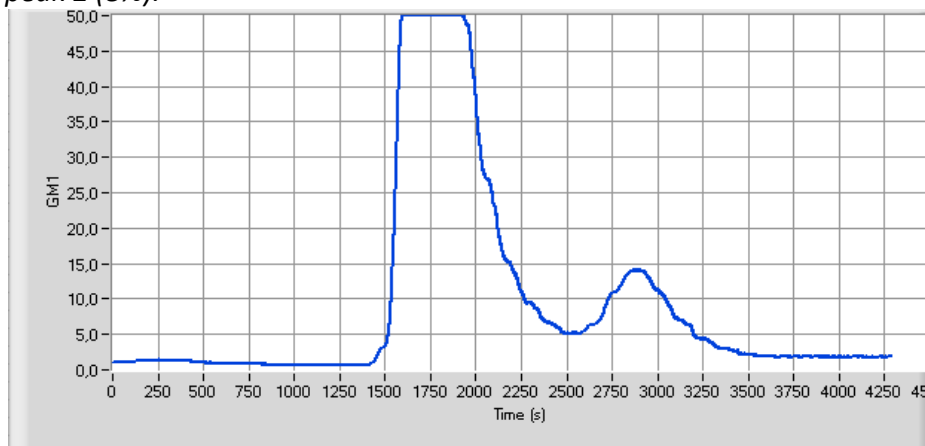
Radio-TLC chromatograms after 2.5 hours incubation. Peak 1 (left), Peak 2 (right)



In **Peak 1** (left figure) only a sharp peak for the micelles is seen. In **Peak 2** (right figure) a prominent EDTA peak (*green*) is seen along with an array of radiolysis products. It should be noted that the activity in **peak 2** was only 8%, signifying that the radiolysis products are not as abundant as their impressive appearance might suggest. As the activity was very high, the

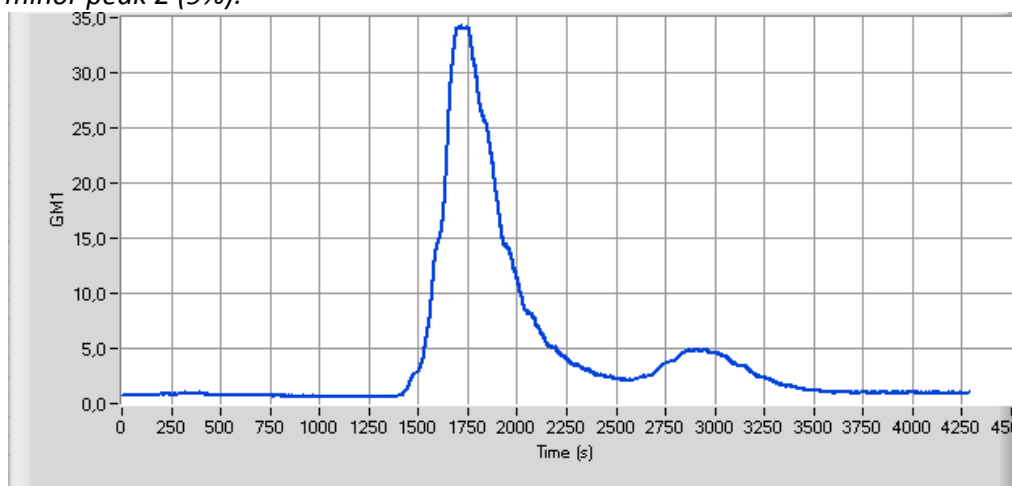
values from the GM counter on the size-exclusion apparatus were higher than the scale, giving the image shown below:

Size-exclusion chromatogram after 2.5 hours of incubation. Prominent peak 1 (78%) and minor peak 2 (8%).



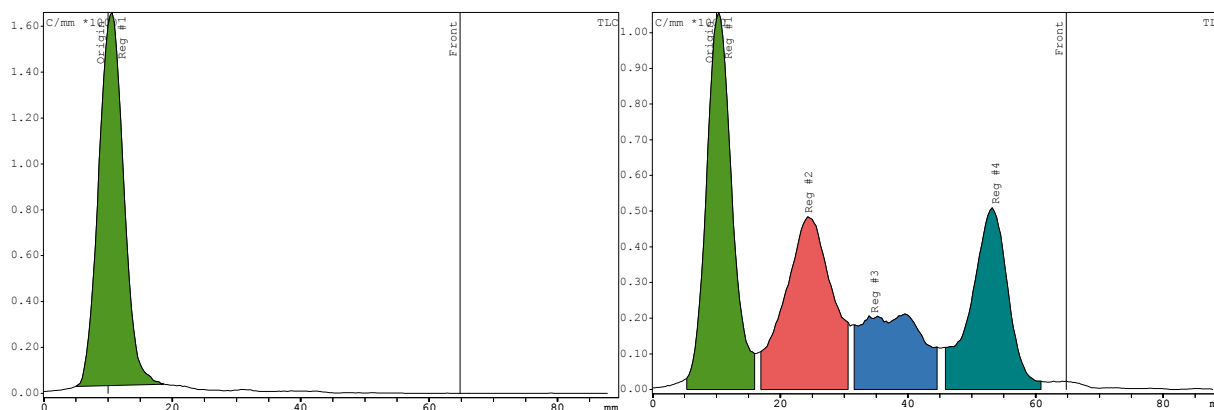
The main mixture was allowed to stir overnight and analyzed the next day (after about 20 hours), in the same way as was described above. The distribution between the two peaks was now: **Peak 1**: 47%, **Peak 2**, 9% and only 62% of the total activity was accounted for (6% was left behind in the glass vial after uptake to the size-exclusion column). This seemed to indicate that as the micelles are subjected to increased radiolysis, the degraded products tend to stick to the column and not elute. In addition, the **Peak 2/Peak1 ratio** had gone from 10% (2.5h) to 19% (20h). This indicates that hydrolysis products generally appear in **peak 2**. Now that the activity was at an acceptable level, the Geiger-müller counter on the size-exclusion apparatus could produce a proper image:

Size-exclusion chromatogram after 20 hours of incubation. Still a prominent peak 1 (47%) and minor peak 2 (9%).



As before the two peaks were analyzed by Radio-TLC. The results are seen below.

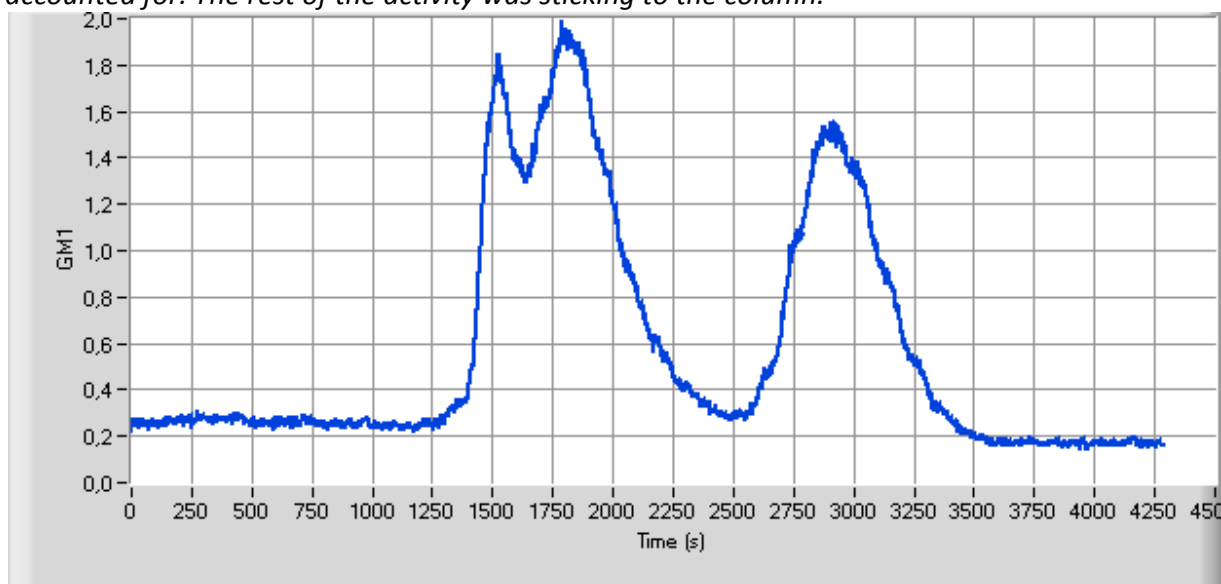
Radio-TLC chromatograms after 20 hours incubation. Peak 1 (left), Peak 2 (right)



It was clear that the amount of radiolysis product had increased. Notice that EDTA is still present (turquoise peak on the right).

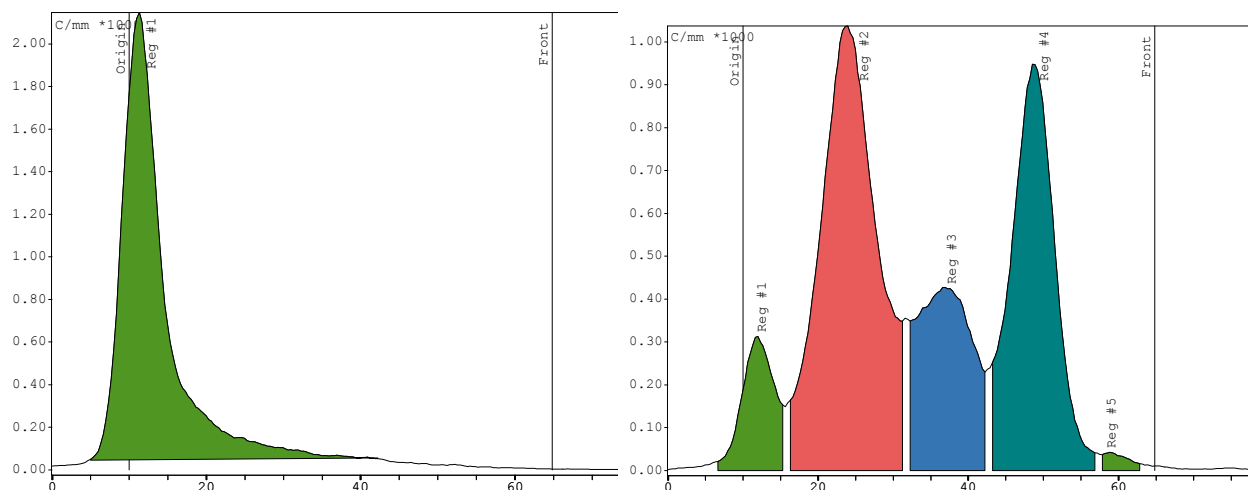
The mixture was allowed to incubate for a further night (total incubation, 2 days) and analyzed again. Below is seen the results from the size-exclusion chromatography.

*Size-exclusion chromatogram after 2 days of incubation. **Peak 1** is now split in two and makes up 22% of the total activity. **Peak 2** makes up 12%. With 8% left in the vial, only 42% was accounted for. The rest of the activity was sticking to the column.*



With a split **peak 1** it was now obvious that the micelles were in a compromised state. The **Peak 2/Peak1 ratio** had now risen to 56%. The peaks were again analyzed by Radio-TLC.

Radio-TLC chromatograms after 2 days of incubation. Peak 1 (left), Peak 2 (right)



It is seen now, that the micelle peak (left) starts to elute slightly, suggesting poor integrity of the particles. In the analysis of **peak 2** the radiolysis products are now seen to dominate the chromatogram, suggesting widespread degradation.

The micelles from this last outtake (2 days) were analyzed by DLS and were, rather surprisingly, found to have a size of about 40 nm (nr. weighted median), that is, no significant increase in size had taken place.

The remainder (200 μ L) of the main vial from which the outtakes had been done was allowed to decay and was also analyzed by DLS after several days had passed. These micelles were found to have aggregated heavily and were now about 800 nm (nr. weighted median).

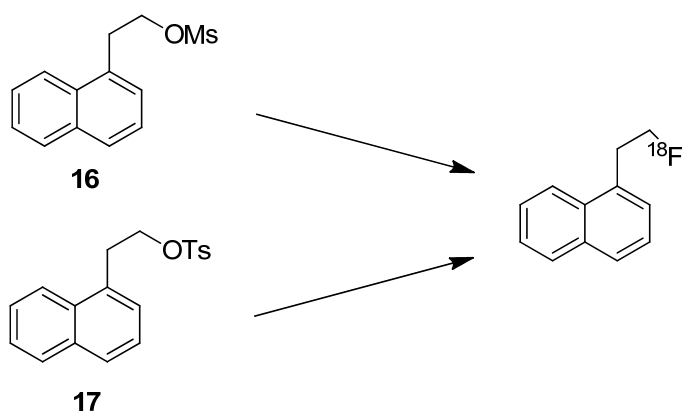
Conclusions: **1)** Even at very high activity (3 GBq) it takes a significant amount of time (>2.5 h) before noticeable radiolysis takes place, **2)** Radiolysis caused activity to stay on the column and radiolysis products appear in **peak 2** especially between the starting line and the EDTA-⁶⁴Cu peak. **3)** radiolysis products do not appear in **peak 1** and heavy radiolysis seems necessary in order to cause aggregation of the particles. **4)** It is concluded that the activity levels and incubation times used in the study should not induce significant radiolysis.

Supplementary Information VIII – [^{18}F]HF transfer, phosphazene fluorination - Experimental.

- By Fedor Zhuravlev, edited by Andreas Jensen

General procedure for [^{18}F]HF generation, transfer, and the synthesis of [^{18}F]P $_n^R$ HF

[^{18}F]fluoride (cyclotron target wash using [^{18}O]H $_2$ O, 15-1100MBq) was added to a reaction vial (polyethylene or glassy carbon) containing H $_2$ SO $_4$ (98%, the resulting acid/water ratio of 4-20, final volume 2.1-4.5mL). The reaction vial was heated for 30 min at 80°C in an ultrasound bath while irradiating at 35 kHz. [^{18}F]HF was carried by argon flow (300-400scc/min) to a receiving vial (glassy carbon) containing phosphazene base (30 μmol) in toluene at 0°C. The [^{18}F]HF transfer yield was 16-82% measured by the dose calibrator.



*General procedure – Radiofluorination of **16** and **17***

The content of the receiving vial ([^{18}F]P $_2^{\text{Et}}$ •HF in toluene) was transferred to a reaction vial (glassy carbon or a glass pressure tube) containing the substrate **16** or **17** (52 μmol). [^{18}F]fluorination was carried out at 120°C for 20 min. Radiochemical purity was determined by radioTLC. The [^{18}F]fluorinated product was purified using Silica Plus (Waters) cartridge.

Appendix 1

Andreas T.I. Jensen, Tina Binderup, Thomas L. Andresen, Andreas Kjær, Palle H. Rasmussen.

“PET imaging of liposomes labeled with an [18F]-fluorocholesteryl ether probe prepared by automated radiosynthesis” Journal of Liposome Research, (**Epub ahead of print**). PubMed ID:22803638

RESEARCH ARTICLE

PET imaging of liposomes labeled with an [^{18}F]-fluorocholesteryl ether probe prepared by automated radiosynthesis

Andreas Tue Ingemann Jensen,^{1,2} Tina Binderup,³ Thomas L. Andresen,² Andreas Kjær,³ and Palle H. Rasmussen¹

¹Hevesy Laboratory, DTU Nutech, Technical University of Denmark, Roskilde, Denmark, ²Department of Micro- and Nanotechnology, DTU Nanotech, Technical University of Denmark, Lyngby, Denmark, and ³Cluster for Molecular Imaging and Department of Clinical Physiology, Nuclear Medicine, and PET, Rigshospitalet, University of Copenhagen, Copenhagen, Denmark

Abstract

A novel [^{18}F]-labeled cholesteryl ether lipid probe was prepared by synthesis of the corresponding mesylate, which was [^{18}F]-fluorinated by a [^{18}F]KF, Kryptofix-222, K_2CO_3 procedure. Fluorination was done for 10 minutes at 165°C and took place with conversion between 3 and 17%, depending on conditions. Radiolabelling of the probe and subsequent *in situ* purification on SEP-Paks were done on a custom-built, fully automatic synthesis robot. Long-circulating liposomes were prepared by hydration (magnetic stirring) of a lipid film containing the radiolabeled probe, followed by fully automated extrusion through 100-nm filters. The [^{18}F]-labeled liposomes were injected into nude, tumor-bearing mice, and positron emission tomography (PET) scans were performed several times over 8 hours to investigate the *in vivo* biodistribution. Clear tumor accumulation, as well as hepatic and splenic uptake, was observed, corresponding to expected liposomal pharmacokinetics. The tumor accumulation 8 hours postinjection accounted for 2.25 ± 0.23 (mean \pm standard error of the mean) percent of injected dose per gram (%ID/g), and the tumor-to-muscle ratio reached 2.20 ± 0.24 after 8 hours, which is satisfactorily high for visualization of pathological lesions. Moreover, the blood concentration was still at a high level (13.9 ± 1.5 %ID/g) at the end of the 8-hour time frame. The present work demonstrates the methodology for automated preparation of radiolabeled liposomes, and shows that [^{18}F]-labeled liposomes could be suitable as a methodology for visualization of tumors and obtaining short-term pharmacokinetics *in vivo*.

Keywords: Liposomal trafficking, cancer diagnostics, nanomedicine, pharmacokinetics, radiolabeling

Introduction

Liposomes are nanosized particles consisting of one of more phospholipid bilayers encapsulating an aqueous core. Within this core, as well as in the lipid membrane itself, drugs can be contained. Liposomes were first described in 1964 by Bangham and Horne (1964) and have, in the past three decades, gained considerable interest as drug delivery systems.

In cancer therapy, liposomes accumulate passively in tumor tissue as a result of the enhanced permeability

and retention (EPR) effect (Matsumura and Maeda, 1986; Maeda, 2001). This accumulation is dependent on the ability of liposomes to circulate for longer periods of time (up to 24 hours) (Maeda, 2001). Early generations of liposomes were rapidly and extensively removed from the circulation by the macrophages of the reticuloendothelial system (RES) and were thus unable to accumulate in tumors (Poste et al., 1982; Scherphof et al., 1985). The advent of polyethylene glycol (PEG) coating provided liposomes with reduced RES clearance

Address for Correspondence: Palle H. Rasmussen, Hevesy Laboratory, DTU Nutech, Building 202, Frederiksborgvej 399, 4000 Roskilde, Denmark; Fax: +45 4677 5347; E-mail: pall@dtu.dk

(Received 01 February 2012; revised 11 April 2012; accepted 21 May 2012)

and allowed the liposomes to stay in the bloodstream long enough for accumulation to occur (Maeda, 2001; Allen et al., 1991; Klibanov et al., 1990). However, uptake in healthy tissue, such as liver and spleen, is still relatively high, in spite of PEGylation (Harrington et al., 2001). There is evidence that this effect is partly the result of the endogenous production of antibodies (Abs) against PEG lipids (Moghimani et al., 2006).

Increased tumor targeting of liposomes is still desirable, and active targeting strategies using Abs, peptides, and small ligands, such as folate, are being investigated for this purpose (Kaasgaard and Andresen, 2010). Radioimaging, such as single-photon emission computed tomography (SPECT) and positron emission tomography (PET), are useful tools in this process. They allow real-time monitoring of *in vivo* liposome trafficking and repeated measurements in the same animal in a noninvasive manner. SPECT studies have been carried out using γ -emitting isotopes. These isotopes were associated with liposomes by two main methods: 1) chelating ^{99m}Tc to the surface of the liposomes (Laverman et al., 1999; Tilcock et al., 1994) and 2) chelating various isotopes within the aqueous core using after-loading techniques, such as ^{111}In (Harrington et al., 2001; Corvo et al., 1999), ^{99m}Tc (Bao et al., 2003a; Phillips et al., 1992; Bao et al., 2004), ^{186}Re (Bao et al., 2003b), and ^{188}Re (Chang et al., 2010). In the labeling of liposomes, PET isotopes, such as ^{18}F and ^{64}Cu , have several advantages, compared to SPECT isotopes, such as ^{99m}Tc (Bao et al., 2004; Laverman et al., 1999; Li et al., 2011), ^{67}Ga (Gabizon et al., 1988), and ^{111}In (Corvo et al., 1999). PET is at least 10-fold more sensitive than SPECT, being in the range of 10^{-11} – 10^{-12} M (Gambhir, 2002; Willmann et al., 2008; Rahmim and Zaidi, 2008). Further, PET has a much better spatial resolution (Willmann et al., 2008; Alavi and Basu, 2008; Rahmim and Zaidi, 2008). These factors make small lesions easy to miss in SPECT (Alavi and Basu, 2008), and in the clinic, PET provides improved image quality over SPECT (Bateman, 2012). Further, with PET it is possible to quantify tracer uptake in target organs. Only two isotopes have been used for PET imaging of tumor targeting by liposomes so far, these being ^{64}Cu ($T_{1/2} = 12.7$ hours) (Seo et al., 2008, 2010, 2011; Petersen et al., 2011) and ^{18}F ($T_{1/2} = 110$ minutes) (Urakami et al., 2007, 2009; Oku et al., 1995, 1996; Marik et al., 2007). Although ^{64}Cu -labeling is attractive for the purpose of following the long-term pharmacokinetics of liposomes, ^{18}F -labeling is attractive also from a clinical perspective, because ^{18}F is much more readily available in nuclear medicine facilities worldwide than ^{64}Cu . Further, the shorter half-life of ^{18}F makes this isotope attractive from a dosimetry perspective. In addition, if the 8-hour time frame, where it is possible to make use of ^{18}F -labeled tracers, proves sufficient for visualization of the tumor accumulation, this will, again from a clinical perspective, be attractive, because a 1-day procedure will always be preferable for patients rather than a 2- (24-hour scan) or even 3-day procedure (48-hour scan).

In 1995, Oku et al. were the first to use ^{18}F with liposomes by passively encapsulating [^{18}F]fluorodeoxyglucose ([^{18}F]FDG) (Oku et al., 1995, 1996). Marik et al. developed [^{18}F]fluorodipalmitin as a lipid probe that was incorporated into the lipid membrane during hydration of the lipid film (Marik et al., 2007). To label preformed liposomes, Urakami et al. developed the SophT method (Urakami et al., 2007, 2009). In this method, incorporation of an amphiphilic [^{18}F]-labeled probe is achieved by incubation of the dried probe with a liposome dispersion around the phase-transition temperature of the lipids.

In the previous ^{18}F reports, only studies of up to 120 minutes after injection were performed. Further, the murine models used in these studies were only tumor bearing in two cases (Oku et al., 1995, 1996). Tumor accumulation was observed in both of these reports; however, PEGylated liposomes circulate for up to and beyond 48 hours, and tumor concentration of drug usually peaks between 24 and 48 hours after injection (Gabizon et al., 1997, 2003). This makes longer studies interesting. Because of the short half-life of ^{18}F , only studies of up to 8 hours are possible with this isotope (Phillips et al., 2009). However, some tumor accumulation does occur in the first 8 hours after injection and it is possible to evaluate clearance profile and biodistribution during this period (Gabizon et al., 1997). This indicates that an 8-hour window might be enough for assessing the *in vivo* performance of liposomes and provide imaging of tumors, both in animals and in humans, using ^{18}F PET imaging.

Cholesteryl ethers are known to be metabolically stable, not to transfer between liposomes and plasma lipoproteins, and to have a high affinity for the lipid membrane (Kizelsztejn et al., 2009; Pool et al., 1982; Stein et al., 1980). This makes them good markers for liposome trafficking (Figure 1).

In this report, we present our efforts to develop a fully automated synthesis and purification of the ^{18}F -labeled cholesteryl ether, 10-cholesteryloxy-1- ^{18}F fluoro-decanol (^{18}F CE), and its semiautomated incorporation into the membrane of 100-nm liposomes. Further, 8-hour PET studies of these liposomes in mice are presented.

Methods

Materials and methods

All reagents and solvents were purchased from Sigma-Aldrich Denmark A/S (Brøndby, Denmark). Solvents were purchased in purum quality or better and were not further purified. Solvents for anhydrous syntheses were dried over molecular sieves (Sigma-Aldrich) to water concentrations of <100 ppm (dimethylformamide; DMF) and <50 ppm (all others). Glassware was oven-dried overnight or heatgun-dried under a stream of dry argon before use. Reactions were conducted in an argon atmosphere. Chromatography was done using Merck silica purchased from VWR (Herlev, Denmark), flash chromatography in Silica gel 60 (0.040–0.063), and thin-layer chromatography (TLC) on Silica gel 60 F₂₅₄. All visualization was

done by ultraviolet light as well as KMnO_4 staining with heating. SEP-Paks (C18 Plus, Silica Plus, and QMA Light) were purchased from Waters (Milford, Massachusetts, USA). Chromacol 6-mL flat-bottomed fluorination vials and ^{18}O -enriched water were purchased from Rotem Industries Ltd. (Arava, Israel).

Nuclear magnetic resonance (NMR) analyses were recorded in CDCl_3 on a Bruker Ultrashield 500 MHz or

a Bruker/Spectrospin 250 MHz (Bruker BioSpin AG, Fällanden, Switzerland). The residual solvent peak (CHCl_3) was used as the reference peak in both ^1H - and ^{13}C -NMR spectra. Mass spectrometry (MS) was done on either an 1) Agilent 6410 Triple Quadrupole Electrospray Mass Spectrometer coupled to an Agilent 1200 high-performance liquid chromatography (HPLC) system (ESI/HPLC-MS; Agilent Technologies Inc., Santa Clara, California, USA) using a linear gradient of water/acetonitrile/trifluoroacetic acid (TFA) (A: 95/5/0.1 and B: 5/95/0.086) with a flow rate of 1 mL/min, 2) Bruker Esquire 4000 ion trap equipped with an electrospray ionization (ESI) interface; or 3) Bruker Daltonics REFLEX IV matrix-assisted laser desorption ionization/time of flight (MALDI-TOF) mass spectrometer.

^{18}F -fluoride anion was produced on a GE PETtrace Cyclotron (GE Healthcare, Chalfont St. Giles, UK). Radio-TLC was performed on a Raytest miniGita Star (Raytest GmbH, Straubenhardt, Germany).

Radiosynthesis, including purification, and extrusion were performed on two separate fully automated, LabView-operated systems, custom built in our group.

All tumor cell lines were purchased from ATCC-LGC Standards (LGC Standards AB, Borås, Sweden).

Nonradioactive syntheses

All syntheses were performed under anhydrous conditions and argon atmosphere, except for the preparation of compound 4.

10-O-TBDMS-1-decanol (compound 1)

1,10-decanediol (2.02 g, 11.6 mmol) was dissolved in DMF (35 mL). TBDMSCL (1.17 g, 3.90 mmol) was dissolved in



Figure 1. Cartoon of a PEGylated liposome incorporating radioactive lipophilic labels in the membrane. Figure not drawn to scale.

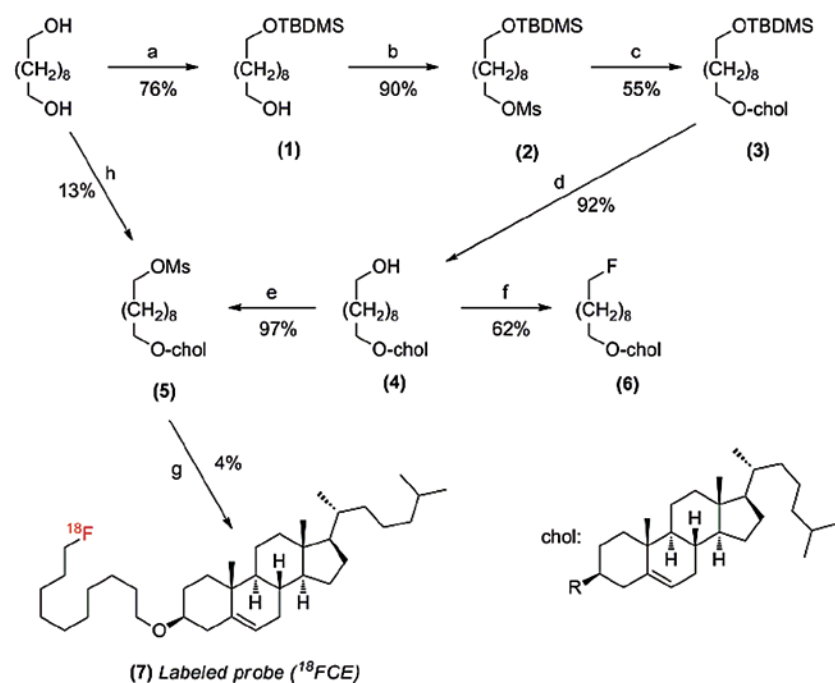


Figure 2. Synthesis of ^{18}F FCE and FCE. (A) TBDMSCL, imidazole, and DMF. (B) MsCl , pyridine, and DCM. (C) Cholesterol, NaH , and toluene/DMF. (D) TBAF and THF. (E) MsCl , pyridine, and DCM. (F) DAST and DCM. (G) $[^{18}\text{F}]\text{KF}$, Kryptofix-222, K_2CO_3 , and DMSO. (H) i. MsCl , pyridine, and DCM, ii. NaH , cholesterol, and THF/DMF.

DMF (10 mL) and added dropwise. Imidazole (530 mg, 7.78 mmol) was added in DMF (10 mL). The reaction was stirred for 20 hours at room temperature (RT). The mixture was partitioned between toluene (120 mL) and water (100 mL). The organic phase was washed with water (2 × 50 mL), and the solvent was removed *in vacuo*. Purification by column chromatography in heptane/EtOAc (80:20) gave 847 mg (76%) of compound 1 as a clear, colorless oil. $R_f = 0.31$ (heptane/EtOAc, 80:20). $^1\text{H-NMR}$ (500 MHz, CDCl_3): δ 3.65 (br.t., $J = 5.8$ Hz, 2H), 3.60 (t, $J = 6.8$ Hz, 2H), 1.55 (m, 4H), 1.38–1.30 (m, 13H), 0.91 (s, 9H), and 0.06 (s, 6H). $^{13}\text{C-NMR}$ (62.5 MHz, CDCl_3): 63.3, 63.1, 32.9, 32.9, 29.6, 29.6, 29.4, 26.0, 25.9, 25.8, 18.4, and –5.3. ESI- MS^+ (m/z):¹ found: 289.20 ($\text{M}+\text{H}^+$); calculated: $288.3 + 1.0 = 289.3$.

1-O-Ms-10-O-TBDMS-decane-diol (compound 2)

Compound 1 (759 mg, 2.76 mmol) was dissolved in DCM (30 mL). Pyridine was added (2.2 mL, 27.3 mmol). The flask was placed in an ice bath, and MsCl (650 μL , 8.40 mmol) was added. The reaction was stirred for 5 hours at RT. The mixture was partitioned between water (100 mL) and toluene (100 mL). The organic phase was washed with water (2 × 50 mL), and the solvent was removed *in vacuo*. Purification by column chromatography in toluene/EtOAc (95:5) gave 876 mg (90%) of compound 2 as a clear, colorless oil. $R_f = 0.42$ (toluene/EtOAc, 95:5). $^1\text{H-NMR}$ (250 MHz, CDCl_3): δ 4.22 (triplet, $J = 6.6$ Hz, 2H), 3.60 (t, $J = 6.5$ Hz, 2H), 3.00 (s, 3H), 1.74 (m, 2H), 1.5 (m, 2H), 1.43–1.29 (m, 12H), 0.90 (s, 9H), and 0.05 (s, 6H). $^{13}\text{C-NMR}$ (62.5 MHz, CDCl_3): 70.0, 63.2, 37.4, 32.8, 29.4, 29.27, 29.25, 29.1, 18.4, 25.9, 25.7, 25.4, 28.2, and –5.4. ESI- MS^+ (m/z):¹ found: 367.20 ($\text{M}+\text{H}^+$); calculated: $366.23 + 1.00 = 367.23$.

10-cholesteryloxy-1-O-TBDMS-decanol (compound 3)

Cholesterol (505 mg, 1.31 mmol) was dissolved in toluene (10 mL), and NaH (60%) in mineral oil (78 mg, 1.95 mmol) was added. The mixture was heated to 80°C, and after 1 hour, compound 2 (450 mg, 1.23 mmol) was added as a solution in toluene (1 mL). DMF (3 mL) was added. The mixture was stirred for 16 hours at 80°C. The reaction mixture was filtered, mixed with toluene (50 mL), and the organic phase was washed with brine (3 × 50 mL). The combined aqueous phases were extracted once with heptane (20 mL). The combined organic phases were dried over Na_2SO_4 , filtered, and the solvents were removed *in vacuo*. The crude product was purified by column chromatography in a gradient of heptane/toluene (9:1; 50 mL), followed by 1:1 (140 mL) and, finally, toluene (50 mL). The fractions containing only compound 3 were rotary evaporated yielding 444 mg (55%) of compound 3 as a clear, very viscous semisolid. $R_f = 0.5$ (heptane/toluene, 1:1). $^1\text{H-NMR}$ (500 MHz, CDCl_3): δ 5.36 (m, 1H), 3.61 (t, $J = 6.6$ Hz, 2H), 3.46 (m, 2H), 3.14 (m, 1H), 2.38 (m, 1H), 2.21 (m, 1H), 2.01 (m, 2H), 1.87 (m, 3H), 1.62–1.43 (m, 11H), 1.40–1.24 (m, 16H), 1.20–0.97 (m, 12H), 0.95–0.88 (m, 19H), 0.70 (s, 3H), and 0.07 (s, 6H). $^{13}\text{C-NMR}$ (125 MHz, CDCl_3): δ 141.2,

121.4, 79.0, 68.2, 63.3, 56.8, 56.2, 50.3, 42.4, 39.8, 39.5, 39.3, 37.3, 36.9, 36.2, 35.8, 32.9, 32.0, 31.9, 30.2, 29.57, 29.55, 29.49, 29.42, 28.5, 28.2, 28.0, 26.2, 26.0, 25.8, 24.3, 23.8, 22.8, 22.6, 21.1, 19.4, 18.7, 18.4, 11.9, and –5.3. m/z (MALDI-TOF, DHB-matrix— Na^+ -spiked, LP30%, 200 shots); found: 679.3 ($\text{M}+\text{Na}^+$); calculated: $656.59 + 22.99 = 679.58$.

10-cholesteryloxy-1-decanol (compound 4)

Compound 3 (722 mg, 1.10 mmol) was dissolved in tetrahydrofuran (THF; 25 mL). Tetrabutylammonium fluoride (TBAF) trihydrate (720 mg, 2.28 mmol) was added, and the mixture was stirred at RT for 6 hours. The mixture was concentrated under reduced pressure and partitioned between hexane (100 mL) and water (80 mL). The hexane phase was washed with water (2 × 60 mL), and the solvent was removed *in vacuo*. Purification by column chromatography in heptane/EtOAc (82:18) gave 582 mg (98%) of compound 4 as a white solid. The product was dissolved in boiling hexane and recrystallized at 0°C, with no change in yield. $R_f = 0.23$ (heptane/EtOAc, 85:15). $^1\text{H-NMR}$ (250 MHz, CDCl_3): δ 5.35 (m, 1H), 3.65 [doublet of triplets, $J = 6.1$ Hz (t), 5.2 Hz (d); 2H], 3.45 (t, $J = 6.8$ Hz 2H), 3.13 (m, 1H), 2.36 (m, 1H), 2.20 (m, 1H), 2.06–1.77 (m, 5H), 1.58–0.86 (m, 49H), and 0.69 (s, 3H). $^{13}\text{C-NMR}$ (125 MHz, CDCl_3): δ 141.2, 121.4, 79.0, 68.2, 63.1, 56.8, 56.2, 50.3, 42.4, 39.8, 39.5, 39.3, 37.3, 36.9, 36.2, 35.8, 32.8, 32.0, 31.9, 30.2, 29.52, 29.50, 29.47, 29.4, 28.5, 28.2, 28.0, 26.2, 25.7, 24.3, 23.8, 22.8, 22.6, 21.1, 19.4, 18.7, and 11.9. ESI- MS^+ (m/z):² found: 565.6 ($\text{M}+\text{Na}^+$); calculated: $542.9 + 22.99 = 565.9$.

10-cholesteryloxy-1-O-Ms-decanol (compound 5)

Compound 4 (199 mg, 0.366 mmol) was dissolved in DCM (15 mL) and pyridine (1.00 mL, 12.4 mmol). MsCl (100 μL , 1.29 mmol) was added, and the mixture was stirred for 5 hours at RT. The mixture was concentrated under reduced pressure and partitioned between toluene (50 mL) and water (50 mL). The organic phase was washed with water (2 × 50 mL), and the combined aqueous phases were extracted once with hexane (30 mL). The combined organic phases were dried over Na_2SO_4 , filtered, and the solvents were removed *in vacuo*. Purification by column chromatography in toluene/EtOAc (98:2) gave 221 mg (97%) of compound 5 as a white solid. $R_f = 0.40$ (toluene/EtOAc, 95:5). $^1\text{H-NMR}$ (500 MHz, CDCl_3): δ 5.36 (m, 1H), 4.24 (t, $J = 6.6$ Hz, 2H), 3.46 (m, 2H), 3.14 (m, 1H), 3.02 (s, 3H), 2.37 (m, 1H), 2.20 (m, 1H), 2.05–1.96 (m, 2H), 1.93–1.81 (m, 3H), 1.76 (m, 2H), 1.62–1.24 (m, 28H), and 1.20–0.88 (m, 22H). $^{13}\text{C-NMR}$ (125 MHz, CDCl_3): 141.2, 121.4, 79.0, 70.2, 68.1, 56.8, 56.2, 50.2, 42.3, 39.8, 39.5, 39.2, 37.4, 37.3, 36.9, 36.2, 35.8, 32.0, 31.9, 30.2, 29.4, 29.3, 29.1, 29.0, 28.5, 28.2, 28.0, 26.2, 25.4, 24.2, 23.8, 22.8, 22.6, 21.1, 19.4, 18.7, and 11.9. ESI- MS^+ (m/z):² found: 643.5 ($\text{M}+\text{Na}^+$), calculated: $620.48 + 22.99 = 643.47$.

10-cholesteryloxy-1-O-Ms-decanol (compound 5): alternative direct synthesis

1,10-decanediol (1.00 g, 5.74 mmol) was dissolved in DCM (50 mL) and pyridine (27 mL, 335 mmol). MsCl

(2.00 mL, 25.8 mmol) was added, and the mixture was stirred for 2.5 hours at RT. The solvents were removed *in vacuo*, and the resulting solids were redissolved in toluene/EtOAc (1:1). Solids that did not dissolve were discarded. The mixture was passed through 20 g of silica, and the solvents were removed *in vacuo*, giving 1.706 g (105%) of the crude dimesylate. In a different flask, NaH (60%) (206 mg, 5.15 mmol) was suspended in THF (5 mL) and placed in an ice bath. Cholesterol (1.79 g, 4.63 mmol) was added as a solution in THF (10 mL). The mixture was heated to 60°C for 30 minutes, allowing sodium cholesterolate to form. The crude dimesylate was dissolved in DMF (45 mL), and the cholesterolate was added by cannulation. The mixture was allowed to react at 65°C for 6.5 hours. Because this was insufficient time, it was allowed to stir at RT for 3 days, leading to completion. The mixture was partitioned between water (100 mL) and hexane (100 mL). The polar phase was washed with hexane (2 × 100 mL). The organic phases were combined, and the solvents were removed *in vacuo*, then purified by column chromatography in a gradient of neat toluene followed by toluene/EtOAc (98:2). The fractions containing only compound 5 were rotary evaporated, yielding 371 mg (13%) of compound 5 as a white solid. See above for characterization.

10-cholesteryloxy-1-fluoro-decane (compound 6)

Compound 4 (29 mg, 53.4 μmol) was dissolved in DCM (DCM; 2 mL) in a -78°C bath. [(Diethylamino)sulfur trifluoride] (DAST; 40 μL, 410 μmol) was added, and the mixture was allowed to attain RT. After 2 hours, 0.5 M of K₂CO₃ (2 mL) was added, and the mixture was partitioned between heptane (15 mL) and brine (15 mL). The organic phase was washed with brine (2 × 10 mL), dried over Na₂SO₄, and the solvents were removed *in vacuo*. Purification by flash chromatography in heptane/toluene (1:1) gave 18 mg (62%) of compound 6 as a white solid. *R*_f = 0.31 (heptane/toluene, 1:1). ¹H-NMR (500 MHz, CDCl₃): δ 5.36 (m, 1H), 4.44 [doublet of triplets, *J* = 50 Hz (d), 6.3 Hz (t); 2H], 3.45 (m, 2H), 3.13 (m, 1H), 2.36 (m, 1H), 2.20 (m, 1H), 2.00 (m, 2H), 1.86 (m, 3H), 1.69 (m, 2H), 1.62–0.82 (m, 47H), and 0.69 (s, 3H). ¹³C-NMR (125 MHz, CDCl₃) 141.2, 121.4, 83.59 (d, *J* = 162 Hz, 1C), 79.0, 68.1, 56.8, 56.2, 50.2, 42.3, 39.8, 39.5, 39.2, 37.3, 36.9, 36.2, 35.8, 32.0, 31.9, 30.4 (d, *J* = 19.1 Hz, 1C), 30.2, 29.46 (d, *J* = 4.5 Hz), 29.45, 29.2, 28.5, 28.2, 28.0, 26.2, 25.2, 24.3, 23.8, 22.8, 22.6, 21.1, 19.4, 18.7, and 11.9. *m/z* (MALDI-TOF, DHB matrix—Na⁺-spiked, LP28%, 200 shots); found: 567.5 (M+Na⁺); calculated: 544.50 + 22.99 = 567.49.

Automated radiochemical synthesis of 10-cholesteryloxy-1-fluoro-decane (compound 7)

[¹⁸F]fluoride was captured from ¹⁸O-enriched water on a QMA light Sep-Pak SPE cartridge preconditioned with K₂CO₃. The activity was eluted with 50% acetonitrile in water (0.6 mL) containing K₂CO₃ (7.0 mg, 50.8 μmol) and Kryptofix 222 (22.0 mg, 58.5 μmol). The eluate was transferred to a 6-mL Chromacol vial, and the

solvent was evaporated in 7 minutes through a series of increases in temperature under vacuum (≈60 mBar) and a helium stream (100 mL/min, followed by 200 mL/min). Residual water was removed by azeotropic evaporation with acetonitrile (3.0 × 0.3 mL). Compound 5 (2.5 mg, 4.0 μmol) was added in toluene (0.5 mL), and the solvent was evaporated. Dry dimethyl sulfoxide (DMSO) (1 mL) was added, and the mixture was allowed to react for 10 minutes at 165°C. After reaction, the mixture was passed through two C18 Sep-Pak Plus cartridges, previously treated with acetonitrile (15 mL) and water (15 mL). The reactor was washed three times with water (3, 4, and 5 mL). This water was led through the C18 Sep-Pak cartridges. The reactor was then washed three times with heptane (2 × 6 mL plus 1 × 7 mL). This was passed through the C18 cartridges and subsequently through three Silica Sep-Pak Plus cartridges, previously treated with heptane (20 mL), applying the lipid product to the Silica Sep-Pak cartridges. The product was eluted in heptane/EtOAc (97:3), giving compound 7 in a radiochemical purity (RCP) of >98% and a decay-corrected radiochemical yield (RCY) of 1.1%, identified against a cold reference compound (compound 6) by radio-TLC and KMnO₄ staining. *R*_f = 0.49 (toluene/heptane, 70:30).

The term conversion is used throughout this report to refer to the formation of the labeled probe at the end of the radiosynthesis, before isolation by chromatography. It was measured by running the fluorination reaction and extracting the DMSO reaction mixture, followed by a wash of the reaction vessel with 5 mL of chloroform. The activity in the DMSO and CHCl₃ extracts were measured and their ¹⁸FCE content was determined by radio-TLC. From this, a conversion degree was calculated.

Preparation of labeled liposomes

The eluent (4 mL) containing compound 7 was transferred to a 10-mL pear-shaped flask, and the solvent was removed in 5 minutes at 115°C under a slight vacuum and a stream of air. Lipids (7.5 mg of DSPC, 3.0 mg of cholesterol, and 2.7 mg of DSPE/PEG2000 in molar ratios of 0.52:0.43:0.05) were added in chloroform (0.5 mL) to dissolve compound 7. The resulting chloroform solution was transferred to a 4-mL vial containing a magnet and removed in 5 minutes at 70°C under a stream of argon. To transfer remaining lipids and activity, the 10-mL flask was rinsed with chloroform (0.5 mL), which was also transferred to the 4-mL vial and evaporated for 5 minutes under the same conditions. To remove residual chloroform, the vial was subjected to high vacuum and an argon stream for a further 5 minutes at 70°C. To the resulting lipid cake was added 0.7 mL of isotonic HEPES buffer at pH 7.4 (150 mM of NaCl and 10 mM of HEPES) and the lipids were hydrated by magnetic stirring at 1,200 rpm for 30 minutes at 60°C. Then, 0.5 mL of the lipid dispersion was extruded using an automated, custom-built extruder, where the multilammellar vesicles (MLVs) were passed through 100-nm polycarbonate filters 31 times.

MicroPET and MicroCT (computed tomography) imaging and data analysis

Human lung carcinoid (NCI-H727; 2 tumors, 1 mouse), small-cell lung cancer (NCI-H69; 3 tumors, 2 mice), and glioblastoma (U87MG; 2 tumors, 1 mouse) tumor cells ($\sim 1 \times 10^7$ cells) were inoculated in the left and right flank of Naval Medical Research Institute nude mice ($n = 4$) and allowed to grow 2–4 weeks, depending on the growth rate of the tumors.

Before injection of the ^{18}F -labeled liposomes, mice were anesthetized by intraperitoneal injection of fluani-sone/fentanyl citrate and midazolam (5 mg/0.625 mL/kg) and placed on a heated bed in the PET scanner (MicroPET Focus 120; Siemens Medical Solutions, Malvern, Pennsylvania, USA), where the tracer was intravenously (i.v.) injected in a lateral tail vein. General anesthesia was maintained using 1% sevofluran (Abbott Scandinavia AB, Solna, Sweden) mixed with 35% O_2 in N_2 . A dynamic scan was acquired from 0 to 20 minutes postinjection with 19 frames for subsequent time-activity-curve generation. After 2.5 and 8 hours postinjection of the ^{18}F -liposomes, additional static PET emission scans were acquired. The acquisition time was 20 minutes for the 0- and 2.5-hour scans and 40 minutes for the 8-hour scan to ensure proper signal-to-noise ratios. The pixel size was $0.866 \times 0.866 \times 0.796$ mm and the resolution was 1.4 mm in the center field of view. PET data were reconstructed with the two-dimensional ordered-subset expectation maximization reconstruction algorithm.

CT scans were acquired for anatomical localization of foci with a MicroCAT[®] II system (Siemens Medical Solutions). CT settings were a tube voltage of 62 kVp, a tube current of 500 μA , 360 rotation steps, an exposure

time of 390 ms, and a voxel size of 0.088 mm. PET and CT images were analyzed as fused images using the Inveon software (Siemens). Regions of interest (ROIs) were drawn around liver, kidney, spleen, muscle, tumors, and the left ventricle. Uptake in the left ventricle of the heart was taken as a measure of blood concentration. Percent injected dose per gram (%ID/g) and tumor-to-muscle (T/M) ratios were calculated.

Animal experiments were approved by the animal research committee of the Danish Ministry of Justice.

Results and discussion

Synthesis and liposome preparation

The cholesterol ether precursor was prepared by silyl ether (TBDMS) monoprotection of decanediol using the diol in excess (Figure 2). The obtained yield of 76% should be compared with the theoretical yield of 83% monoprotected alcohol (calculated in ROOT, assuming the same probability of reaction at all alcohols). The protection step was followed by mesylation of the remaining alcohol. The lipid chain was coupled to cholesterol using classic Williamson ether synthesis, conducted in toluene in the presence of DMF (Sripada, 1986). The TBDMS group was removed by TBAF, followed by recrystallization from hexane. The resulting primary alcohol was activated for nucleophilic fluorination by mesylation. The alternative direct synthesis (h) was employed as a less time-consuming way to reach the mesylate. Though the yield was poor (13% with respect to the cholesterol), the relatively cheap starting materials and low number of operations justified the method.

The substrate (compound 5) was not soluble in DMSO at RT, but dissolved at higher temperatures. It was possible

Table 1. Overview of conversions and RCYs at different conditions.

Conversions and RCYs						
Precursor (mg)	Kryptofix (mg)	K_2CO_3 (mg)	Reaction conditions	Conversion (%)	RCY (%)	Liposomes (%)
2.5	22.0	7.0	20 minutes at 165°C, 2 mL of DMSO	4.0	1.6	—
2.5	22.0	7.0	5 minutes at 165°C, 1 mL of DMSO	3.8	—	—
2.5	22.0	7.0	10 minutes at 165°C, 1 mL of DMSO	4.4	1.7 ± 0.2	—
2.5	22.0	7.0	20 minutes at 165°C, 1 mL of DMSO	3.1, 3.1	1.1	—
2.5	22.0	7.0	10 minutes at 165°C, 2 mL of DMSO	—	1.8	—
2.5	22.0	7.0	10 minutes at 165°C, 1 mL of DMSO ^a	—	2.8	0.79
2.5	22.0	7.0	10 minutes at 165°C, 1 mL of DMSO ^b	—	1.8	0.28
5.1	5.0	1.0	30 minutes at 120°C, 2 mL of DMSO, SB ratio: 1.1	3.64	—	—
35	22.0	7.0	30 minutes at 120 °C, 2 mL of DMSO, SB ratio: 1.1	17.3	—	—

In the two bottom rows, the >1 SB-ratio experiments are shown. Note the substantially higher conversion when adding 35 mg of substrate. The “liposomes” column denotes the decay-corrected RCY in the final liposomal formulation.

^aFull-scale ^{18}F -labeled liposome preparation carried out as a test. A particularly high RCY was obtained.

^bThe experiment where the liposomes were tested *in vivo*.

to prepare a supersaturated solution of compound 5 by heating in anhydrous DMSO, followed by cooling to RT. However, direct addition of this solution did not give any labeled product (compound 7). It is speculated that precipitation may have occurred during passage through the tubing to the reactor. Instead, after removing water from the reaction mixture by azeotropic distillation with acetonitrile, compound 5 was added as a solution in toluene. After evaporation of the toluene, DMSO was added and the mixture was heated for reaction to occur. The decay-corrected conversions of the reaction, as measured by radio-TLC directly from the reactor, are shown in Table 1.

The labeled cholesteryl ether, ^{18}FCE (compound 7), was purified by passing the reaction mixture (DMSO) through two serially connected C18 Sep-Pak Plus cartridges, onto which the lipophilic compound 7 was effectively retained. Remaining DMSO and most of the unreacted fluoride was removed by three successive washes of reactor and C18 Sep-Paks with water. No traces of compound 7 were detected in these eluates. The product was transferred to three silica Sep-Pak Plus cartridges by three successive washes of the reactor and the C18 and silica Sep-Paks with heptane. ^{18}FCE does not run on silica in heptane, allowing for an efficient trapping. Elution of compound 7 was then carried out by passing heptane/EtOAc (97:3) through the silica cartridges. The decay-corrected RCY after isolation was $1.7 \pm 0.2\%$ ($n = 3$), at the conditions employed in the preparation of radiolabeled liposomes for *in vivo* experiments, with an RCY of 1.8% obtained on the day of the *in vivo* experiments. In general, over half the ^{18}FCE was lost during purification. Experiments showed that it was primarily lost during passage of the silica. It could be reeluted with more polar eluants, such as acetonitrile.

The identity of the purified active product was confirmed by radio-TLC with compound 6 (FCE) as the reference and toluene as the mobile phase.

It has been reported that the ratio of the precursor to the base (K_2CO_3) is crucial to the degree of labeling in nucleophilic fluorination (Marik et al., 2007; Suehiro et al., 2007, 2009). If the substrate-to-base (SB) ratio is too low, yields will be greatly reduced as a result of an elimination side reaction. It is thought that this is a major factor contributing to the low yields reported here. Experiments were done with SB ratios above 1 (Table 1). It was found that it was possible to substantially increase the conversion (17.3% was obtained) by running the reaction with 35 mg of compound 5 in an SB ratio of 1.1. At these concentrations, however, significant amounts of by-products were formed. One of these by-products was difficult to remove by chromatography, and the presence of an unknown by-product is undesirable because it may affect the integrity of the liposomes. Therefore, it was opted to use a lower amount of mesylate (2.5 mg). At this substrate concentration, the above-mentioned by-product was only visible in a negligible amount on TLC (KMnO_4 staining). From the 1.1 SB-ratio experiment mentioned above, the impurity was isolated and

analyzed. The resulting H-NMR spectrum was compared with that of the mesylate (compound 5), and besides the disappearance of the mesyl methyl group, only the two protons next to the mesyl group were identified upfield (shift 4.25 \rightarrow 3.53). This suggests the substitution or other modifications of the mesyl group. The mass was measured on MALDI-TOF (Na-spiked) and found to be 685.3, suggesting a possible mass of $685.3 - \text{Na}^+ = 662.3$. It has, so far, not been possible to deduce the identity of the impurity. Because it was also observed in reactions run in acetonitrile, it seems unlikely that DMSO participates in the side reaction. A product of a similar R_f relative to the substrate was also observed in early experiments with a different mesylate. The presence of such impurities stresses the importance of a universal visualization and detection method. It is likely that a fully automated fluorination setup employing reaction vessels that allow concentrated reactions in small solvent volumes will be able to achieve high yields without high levels of impurities. It was attempted to employ an SB ratio >1 at lower substrate concentrations (see Table 1), but this did not increase the conversion in our system.

The eluant from the synthesis robot (4 mL) containing compound 7 was transferred to a 10-mL pear-shaped flask from which the eluant was evaporated, depositing compound 7 on the sides of the flask. The addition of the lipids in CHCl_3 effectively dissolved the deposited compound 7, and the subsequent transfer to a 4-mL vial, followed by a 0.5-mL CHCl_3 rinse, transferred $>95\%$ of the activity. In the 4-mL vial, the CHCl_3 was evaporated at 70°C . A stream of argon prevented the CHCl_3 from bumping and ensured fast evaporation. Hydration was done by magnetic stirring for 30 minutes. Extrusion of the MLVs could only be done using a single filter size, because filter change was impeded by the high radioactivity. Consequently, the MLVs were passed through a 100-nm filter 31 times. This gave liposomes with a mean diameter of 121 nm (number weighted; polydispersity index: 0.072).

The activity present in the finished radioliposomes was 156.1 MBq. An aliquot of the liposome suspension was dissolved in THF (giving a homogeneous, clear solution), subjected to radio-TLC, and found to have an RCP of $>98\%$.

Labeling of liposomes during preparation has its drawbacks, the main one being that liposomes and radioisotopes must be prepared at the same facility. Further, the liposomes are prepared during exposure to potentially large doses of radiation. This problem becomes more pressing in potential studies in larger animals or humans, where more activity is needed. We addressed this issue by employing 1) formation of a lipid film by evaporation from heated vials under vacuum and argon/air streams, 2) hydration of the lipid film by magnetic stirring, and 3) fully automated extrusion. By inserting the labeled probe into a preformed liposome, a major advantage would be that commercially available formulations could be readily labeled. This would require, however, that the labeling could be performed at a lower, ideally room, temperature (Goins, 2008), so as not

to cause leakage from the liposomes or to damage labile biomolecules, and that the labeling was stable *in vivo*.

The feasibility of using cholesteryl ethers derives from the ether bond being nonhydrolyzable, the probe being nonmetabolizable and the high lipophilicity preventing the probe from leaving the liposome. The main disadvantages of using the probe presented here is, first of all, the fact that it is not commercially available, making it necessary to synthesize it and the second being the relatively low yield obtained. As already discussed, however, this is not thought to derive from the nature of the probe.

Biodistribution

In vivo investigation was performed in tumor-bearing mice over a course of 8 hours. Selected data from the experiments are shown in Table 2 and Figure 3. In Figure 3A, the tumor accumulation is observed. In the muscle tissue, the activity stayed on a relatively stable and low level, although a slight drop was observed, which is in agreement with the decreased availability of the tracer resulting from clearance from the blood. In the tumors, %ID/g increased from 1.25 ± 0.13 (0 hours) to 2.25 ± 0.23 (8 hours) over the course of the measurement. This indicates that liposomes are accumulating in the tumor and that it is quantifiable within an 8-hour time frame (Figure 4). The accumulation is reflected in the T/M ratio, indicating that, despite the moderate accumulation in the tumors over the 8-hour time frame, the signal-to-noise ratio is good with a T/M ratio above 2 after 8 hours.

In Figure 3B, the tracer biodistribution for other relevant tissues is observed. In the spleen, accumulation of liposomes is relatively fast, with no significant difference in tracer uptake for the 2.5- and 8-hour scans. It is known that liposomes larger than 200 nm are caught in the red pulp tissue of the spleen (Moghimi et al., 2001). Therefore, some of what we are observing might be a relatively rapid removal of the larger liposomes. In absolute terms, this accounts for $3.53 \pm 0.43\%$ of the entire injected activity (ID%) at 8 hours (Table 2). Accumulation in the liver is also observed, however at a steadier pace. Hepatic accumulation at 8 hours accounts for 13.6 ± 1.2 %ID/g. The activity in the blood dropped, as could be expected from the hepatic and splenic elimination. The activity in the kidney stayed at a stable and

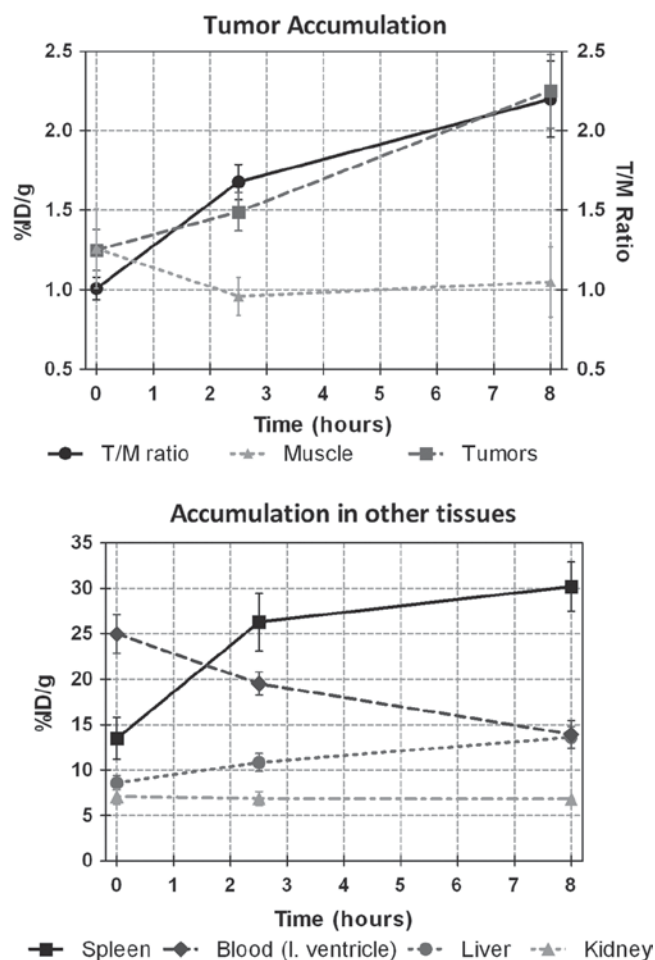


Figure 3. (A) Tumor accumulation. %ID/g is shown as averages for muscle and tumors in all mice (left y-axis). Average T/M ratio for the tumors is plotted on the right y-axis (values are decay corrected). All values were obtained by drawing ROIs around each tumor as well as the left upper thigh muscle of each mouse on fused PET/CT images 0, 2.5, and 8 hours postinjection of the tracer. A tissue density factor of 1 g/cm^3 was assumed in the calculation of %ID/g. Error bars are standard error of the mean values. (B) Accumulation in other relevant tissues. Average %ID/g for all mice, plotted for spleen, blood, liver, and kidney (values are decay corrected). All values were obtained by drawing ROIs around spleen, liver, left kidney, and left ventricle of the heart (for blood values) of each mouse on fused PET/CT images 0, 2.5, and 8 hours postinjection of the tracer. A tissue density factor of 1 g/cm^3 was assumed in the calculation of %ID/g. Error bars are standard error of the mean values.

Table 2. Biodistribution of ^{18}F CE liposomes at several time points after i.v. administration of the tracer.

	Biodistribution					
	0 hours		2.5 hours		8 hours	
	%ID	%ID/g	%ID	%ID/g	%ID	%ID/g
TB>Blood ($n = 4$)	0.39 ± 0.04	25.0 ± 2.20	0.37 ± 0.01	19.5 ± 1.30	0.19 ± 0.03	13.9 ± 1.50
Liver ($n = 4$)	10.0 ± 0.70	8.60 ± 0.79	13.5 ± 1.00	10.8 ± 1.00	15.6 ± 1.20	13.6 ± 1.20
Spleen ($n = 4$)	0.80 ± 0.06	13.5 ± 2.30	3.11 ± 0.27	26.3 ± 3.20	3.53 ± 0.43	30.2 ± 2.70
Kidney ($n = 4$)	1.93 ± 0.29	7.06 ± 0.81	1.84 ± 0.10	6.87 ± 0.73	1.83 ± 0.21	6.82 ± 0.48
Tumor ($n = 7$)	0.31 ± 0.09	1.25 ± 0.13	0.34 ± 0.08	1.49 ± 0.12	0.49 ± 0.11	2.25 ± 0.23
Muscle ($n = 4$)	0.04 ± 0.01	1.26 ± 0.25	0.06 ± 0.01	0.96 ± 0.14	0.07 ± 0.02	1.05 ± 0.22

Data were all acquired from drawing ROIs around the organs from fused PET/CT images. A tissue density factor of 1 g/cm^3 was assumed in the calculation of %ID/g. Blood values were acquired from regions drawn over the left ventricle of the heart and assuming a total blood volume of 2 mL in the calculation of %ID. Muscle values were acquired from regions drawn over the left upper thigh muscle of each mouse on fused PET/CT images 0, 2.5, and 8 hours postinjection of the tracer. Error values are given as standard error of the mean.

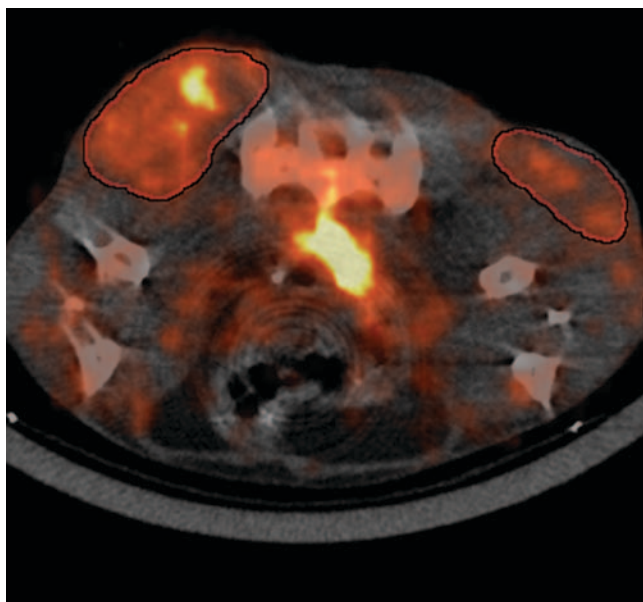


Figure 4. *In vivo* visualization of ^{18}FCE accumulation in xenografted tumors by coregistered microPET/CT. Tumors (NCI-H727) are marked by rings on the image of the tumor-bearing nude mouse (axial view). The PET/CT image was acquired 8 hours postinjection of ^{18}FCE .

relatively low level with no increase in accumulation over time, indicating that renal excretion is limited, as could also be expected with liposome-based tracers. Overall, the pharmacokinetic tendencies observed here correspond well with what is generally known about long-circulating, PEGylated liposomes (Figure 5) (Seo et al., 2008; Petersen et al., 2011; Oku, 1999; Kamps et al., 2000).

Although ^{64}Cu -labeled liposomes provide excellent pharmacokinetic data for long-term *in vivo* monitoring (Petersen et al., 2012), ^{18}F offers some conceivable advantages. The short half-life of ^{18}F makes only studies up to 8 hours feasible, but as we have shown here, this is enough to show tumor accumulation. With current liposome technology, tumor accumulation typically peaks between 24 and 48 hours (Gabizon et al., 1997, 2003). In the future, however, with, for example, improved targeting, it is conceivable that accumulation may be faster, warranting the use of shorter lived radioisotopes, where patient radiation dose will be smaller. Further, targeting methodology other than systemic targeting of tumors may have faster pharmacokinetics. This includes deliberate targeting of RES components (Poelstra et al., 2012). In addition, the lipid probe (compound 7) can be used with other lipidic nanosystems, such as polymeric micelles

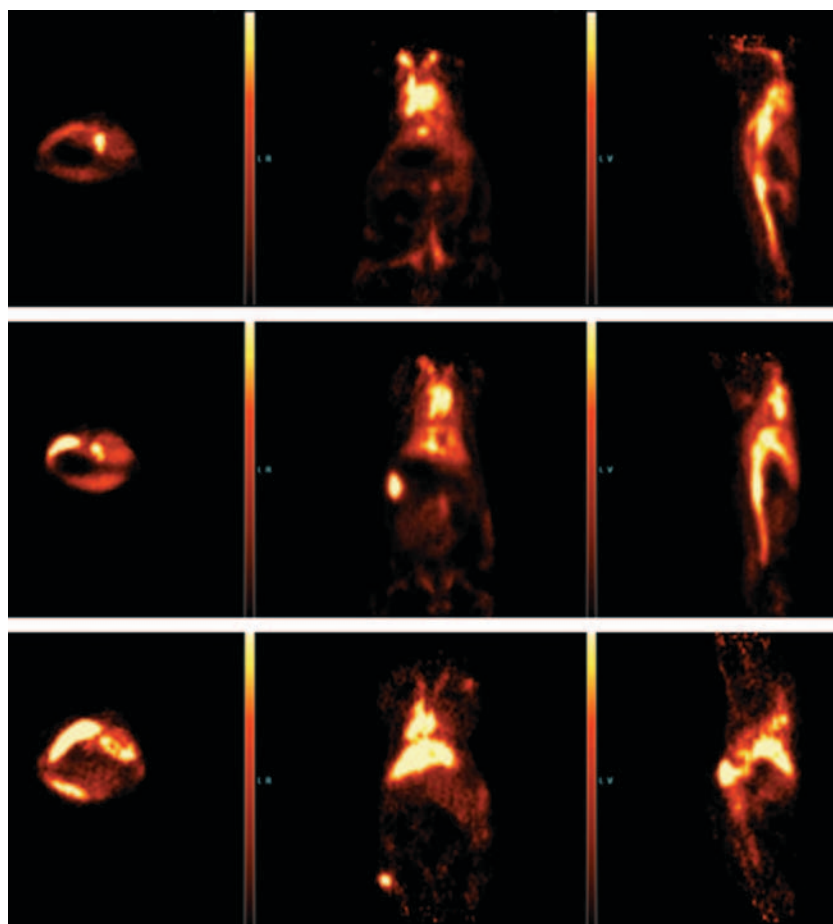


Figure 5. Representative PET images showing ^{18}FCE biodistribution at 0 (top panel), 2.5 (middle panel), and 8 hours (lower panel) postinjection of ^{18}FCE in the NCI-H727-bearing mouse. Accumulation in the spleen is evident from the axial view (left column), and heart and liver accumulation is evident from the coronal view (middle column), whereas accumulation in heart, liver, and vena cava is evident from the sagittal view (right column).

(van Nostrum, 2011) or solid lipid nanospheres (Mishra et al., 2010). As a general consideration, the short half-life of ^{18}F and the higher abundance of positron decays, as compared to ^{64}Cu , results in a lower radiation dose to the patient. Also, as a nonmetal, ^{18}F can be covalently linked to membrane lipids, providing a very stable linkage in a non-water-soluble probe. In the event of breakdown of the liposomes (e.g., by uptake and lysis in cells), this prevents the marker from entering the bloodstream and potentially accumulating in secondary locations or otherwise exhibiting behavior different to that of liposomes. Especially, ^{64}Cu suffers from substantial liver uptake resulting from copper metabolism in the liver, if the copper is released from the liposomes (Seo et al., 2010; Paudyal et al., 2010, 2011). It is also important to keep in mind, that ^{18}F is readily available to nuclear medicine facilities worldwide, whereas the access to, for example, ^{64}Cu is much more limited and therefore only available near highly specialized facilities. The cost of ^{64}Cu -labeled tracers is much higher than ^{18}F -labeled tracers and may limit clinical implementation.

Conclusion

A method for *in vivo* tracking of liposomes by a ^{18}F -labeled cholesteryl ether was developed. Labeled liposomes were injected into mice and tracked by PET for an 8-hour period. Clear tumor, as well as spleen and liver, accumulation was observed, showing that ^{18}F labeling of liposomes, despite the short half-life of ^{18}F , can be used for quantification of short-time tumor accumulation and biodistribution evaluation of liposomes, potentially paving the way for ^{18}F liposomes as a diagnostic tool.

Acknowledgments

The authors thank the staff at the Hevesy Laboratory for their fruitful discussions and for their daily assistance, in particular, Dr. Sorin Aburel, Dr. Martin F. Pedersen, Lene Niebuhr, and Professor Michael Jensen. Also, the authors thank Alex Givskov for carrying out the ROOT calculations used in this study. The authors thank the staff at the Hevesy Laboratory for providing [^{18}F]fluoride.

Declaration of interest

Financial support was kindly provided by the National Advanced Technology Foundation, the Danish Medical Research Council, Rigshospitalets Research Foundation, the Svend Andersen Foundation, the AP Møller Foundation, the Novo Nordisk Foundation, the Lundbeck Foundation, and the Danish Cancer Society.

References

- Alavi, A., Basu, S. (2008). Planar and SPECT imaging in the era of PET and PET-CT: can it survive the test of time? *Eur J Nucl Med Mol Imaging* 35:1554–1559.
- Allen, T. M., Hansen, C., Martin, F., Redemann, C., Yauyoung, A. (1991). Liposomes containing synthetic lipid derivatives of poly(ethylene glycol) show prolonged circulation half-lives in vivo. *Biochim Biophys Acta* 1066:29–36.
- Bangham, A. D., Horne, R. W. (1964). Negative staining of phospholipids and their structural modification by surface-active agents as observed in electron microscope. *J Mol Biol* 8:660–668.
- Bao, A., Goins, B., Klipper, R., Negrete, G., Mahindaratne, M., Phillips, W. T. (2003a). A novel liposome radiolabeling method using 99mTc-“SNS/S” complexes: in vitro and in vivo evaluation. *J Pharm Sci* 92:1893–1904.
- Bao, A., Goins, B., Klipper, R., Negrete, G., Phillips, W. T. (2003b). Re-186-liposome labeling using Re-186-SNS/S complexes: in vitro stability, imaging, and biodistribution in rats. *J Nucl Med* 44:1992–1999.
- Bao, A., Goins, B., Klipper, R., Negrete, G., Phillips, W. T. (2004). Direct 99mTc labeling of pegylated liposomal doxorubicin (Doxil) for pharmacokinetic and non-invasive imaging studies. *J Pharmacol Exp Ther* 308:419–425.
- Bateman, T. M. (2012). Advantages and disadvantages of PET and SPECT in a busy clinical practice. *J Nucl Cardiol* 19:3–8.
- Chang, Y. J., Chang, C. H., Yu, C. Y., Chang, T. J., Chen, L. C., Chen, M. H., et al. (2010). Therapeutic efficacy and microSPECT/CT imaging of Re-188-DXR-liposome in a C26 murine colon carcinoma solid tumor model. *Nucl Med Biol* 37:95–104.
- Corvo, M. L., Boerman, O. C., Oyen, W. J. G., Van Bloois, L., Cruz, M. E. M., Crommelin, D. J. A., et al. (1999). Intravenous administration of superoxide dismutase entrapped in long circulating liposomes. *Biochim Biophys Acta* 1419:325–334.
- Gabizon, A., Goren, D., Horowitz, A. T., Tzemach, D., Lossos, A., Siegal, T. (1997). Long-circulating liposomes for drug delivery in cancer therapy: a review of biodistribution studies in tumor-bearing animals. *Adv Drug Del Rev* 24:337–344.
- Gabizon, A., Huberty, J., Starubinger, M., Price, D. C., Papahadjopoulos, D. (1988). An improved method for in vivo tracing and imaging of liposomes using a gallium 67-deferoxamine complex. *J Liposome Res* 1:123–135.
- Gabizon, A., Shmeeda, H., Barenholz, Y. (2003). Pharmacokinetics of pegylated liposomal doxorubicin: review of animal and human studies. *Clin Pharmacokinet* 42:419–436.
- Gambhir, S. S. (2002). Molecular imaging of cancer with positron emission tomography. *Nat Rev Cancer* 2:683–693.
- Goins, B. (2008). Radiolabeled lipid nanoparticles for diagnostic imaging. *Expert Opin Med Diagn* 2:853–873.
- Harrington, K. J., Mohammadtaghi, S., Uster, P. S., Glass, D., Peters, A. M., Vile, R. G., et al. (2001). Effective targeting of solid tumors in patients with locally advanced cancers by radiolabeled pegylated liposomes. *Clin Cancer Res* 7:243–254.
- Kamps, J. A., Koning, G. A., Velinova, M. J., Morselt, H. W., Wilkens, M., Gorter, A., et al. (2000). Uptake of long-circulating immunoliposomes, directed against colon adenocarcinoma cells, by liver metastases of colon cancer. *J Drug Target* 8:235–245.
- Kaasgaard, T., Andresen, T. L. (2010). Liposomal cancer therapy: exploiting tumor characteristics. *Expert Opin Drug Deliv* 7:225–243.
- Kizelsztejn, P., Ovadia, H., Garbuzenko, O., Sigal, A., Barenholz, Y. (2009). Pegylated nanoliposomes remote-loaded with the antioxidant tempamine ameliorate experimental autoimmune encephalomyelitis. *J Neuroimmunol* 213:20–25.
- Klibanov, A. L., Maruyama, K., Torchilin, V. P., Huang, L. (1990). Amphipathic polyethyleneglycols effectively prolong the circulation time of liposomes. *FEBS Lett* 268:235–237.
- Laverman, P., Dams, E. T. M., Oyen, W. J. G., Storm, G., Koenders, E. B., Prevost, R., et al. (1999). A novel method to label liposomes with Tc-99m by the hydrazino nicotiny derivative. *J Nucl Med* 40:192–197.
- Li, S., Goins, B., Phillips, W. T., Bao, A. (2011). Remote-loading labeling of liposomes with (99m)Tc-BMEDA and its stability evaluation: effects of lipid formulation and pH/chemical gradient. *J Liposome Res* 21:17–27.

- Maeda, H. (2001). The enhanced permeability and retention (EPR) effect in tumor vasculature: the key role of tumor-selective macromolecular drug targeting. *Adv Enzyme Regul* 41:189–207.
- Marik, J., Tartis, M. S., Zhang, H., Fung, J. Y., Kheirloomoom, A., Sutcliffe, J. L., et al. (2007). Long-circulating liposomes radiolabeled with [¹⁸F]fluorodipalmitin ([¹⁸F]FDP). *Nucl Med Biol* 34:165–171.
- Matsumura, Y., Maeda, H. (1986). A new concept for macromolecular therapeutics in cancer chemotherapy: mechanism of tumorotropic accumulation of proteins and the antitumor agent smancs. *Cancer Res* 46:6387–6392.
- Mishra, B., Patel, B. B., Tiwari, S. (2010). Colloidal nanocarriers: a review on formulation technology, types, and applications toward targeted drug delivery. *Nanomedicine* 6:9–24.
- Moghimi, S. M., Hamad, I., Andresen, T. L., Jorgensen, K., Szebeni, J. (2006). Methylation of the phosphate oxygen moiety of phospholipid-methoxy(polyethylene glycol) conjugate prevents PEGylated liposome-mediated complement activation and anaphylatoxin production. *FASEB J* 20:2591–2593.
- Moghimi, S. M., Hunter, A. C., Murray, J. C. (2001). Long-circulating and target-specific nanoparticles: theory to practice. *Pharmacol Rev* 53:283–318.
- Oku, N. (1999). Delivery of contrast agents for positron emission tomography imaging by liposomes. *Adv Drug Deliv Rev* 37:53–61.
- Oku, N., Tokudome, Y., Tsukada, H., Kosugi, T., Namba, Y., Okada, S. (1996). In vivo trafficking of long-circulating liposomes in tumour-bearing mice determined by positron emission tomography. *Biopharm Drug Dispos* 17:435–441.
- Oku, N., Tokudome, Y., Tsukada, H., Okada, S. (1995). Real-time analysis of liposomal trafficking in tumor-bearing mice by use of positron emission tomography. *Biochim Biophys Acta* 1238:86–90.
- Paudyal, B., Paudyal, P., Oriuchi, N., Hanaoka, H., Tominaga, H., Endo, K. (2011). Positron emission tomography imaging and biodistribution of vascular endothelial growth factor with ⁶⁴Cu-labeled bevacizumab in colorectal cancer xenografts. *Cancer Sci* 102:117–121.
- Paudyal, P., Paudyal, B., Hanaoka, H., Oriuchi, N., Iida, Y., Yoshioka, H., et al. (2010). Imaging and biodistribution of Her2/neu expression in non-small cell lung cancer xenografts with Cu-labeled trastuzumab PET. *Cancer Sci*, 101:1045–1050.
- Petersen, A. L., Binderup, T., Jøelck, R. I., Rasmussen, P., Henriksen, J. R., Pfeifer, A. K., et al. (2012). Positron emission tomography evaluation of somatostatin receptor targeted (⁶⁴)Cu-TATE-liposomes in a human neuroendocrine carcinoma mouse model. *J Control Release* 160:254–263.
- Petersen, A. L., Binderup, T., Rasmussen, P., Henriksen, J. R., Elema, D. R., Kjaer, A., et al. (2011). ⁶⁴Cu loaded liposomes as positron emission tomography imaging agents. *Biomaterials* 32:2334–2341.
- Phillips, W. T., Goins, B. A., Bao, A. (2009). Radioactive liposomes. *Wiley Interdiscip Rev Nanomed Nanobiotechnol* 1:69–83.
- Phillips, W. T., Rudolph, A. S., Goins, B., Timmons, J. H., Klipper, R., Blumhardt, R. (1992). A simple method for producing a Tc-99m-labeled liposome which is stable in vivo. *Nucl Med Biol* 19:539–543, 545–547.
- Poelstra, K. P., Prakash, J., Beljaars, L. (2012). Drug targeting to the diseased liver. *J Control Release* 2012 Feb 17. [Epub ahead of print].
- Pool, G. L., French, M. E., Edwards, R. A., Huang, L., Lumb, R. H. (1982). Use of radiolabeled hexadecyl cholesteryl ether as a liposome marker. *Lipids* 17:448–452.
- Poste, G., Bucana, C., Raz, A., Bugelski, P., Kirsh, R., Fidler, I. J. (1982). Analysis of the fate of systemically administered liposomes and implications for their use in drug delivery. *Cancer Res* 42:1412–1422.
- Rahmim, A., Zaidi, H. (2008). PET versus SPECT: strengths, limitations, and challenges. *Nucl Med Commun* 29:193–207.
- Scherphof, G. L., Dijkstra, J., Spanjer, H. H., Derksen, J. T. P., Roerdink, F. H. (1985). Uptake and intracellular processing of targeted and nontargeted liposomes by rat Kupffer cells in vivo and in vitro. *Ann NY Acad Sci* 446:368–384.
- Seo, J. W., Mahakian, L. M., Kheirloomoom, A., Zhang, H., Meares, C. F., Ferdani, R., et al. (2010). Liposomal Cu-64 labeling method using bifunctional chelators: poly(ethylene glycol) spacer and chelator effects. *Bioconj Chem* 21:1206–1215.
- Seo, J. W., Qin, S., Mahakian, L. M., Watson, K. D., Kheirloomoom, A., Ferrara, K. W. (2011). Positron emission tomography imaging of the stability of Cu-64 labeled dipalmitoyl and distearoyl lipids in liposomes. *J Control Release* 151:28–34.
- Seo, J. W., Zhang, H., Kukis, D. L., Meares, C. F., Ferrara, K. W. (2008). A novel method to label preformed liposomes with (Cu)-C-64 for positron emission tomography (PET) imaging. *Bioconj Chem* 19:2577–2584.
- Sripada, P. K. (1986). A simple method for the synthesis of cholesteryl ethers. *J Lipid Res* 27:352–353.
- Stein, Y., Halperin, G., Stein, O. (1980). Biological stability of [³H]cholesteryl oleoyl ether in cultured fibroblasts and intact rat. *FEBS Lett* 111:104–106.
- Suehiro, M., Burgman, P., Carlin, S., Burke, S., Yang, G. B., Ouerfelli, O., et al. (2009). Radiosynthesis of [¹-¹³¹I]IAZGP via nucleophilic substitution and its biological evaluation as a hypoxia marker—is specific activity a factor influencing hypoxia-mapping ability of a hypoxia marker? *Nucl Med Biol* 36:477–487.
- Suehiro, M., Vallabhajosula, S., Goldsmith, S. J., Ballon, D. J. (2007). Investigation of the role of the base in the synthesis of [¹⁸-¹⁸F]FLT. *Appl Radiat Isot* 65:1350–1358.
- Tilcock, C., Ahkong, Q. F., Fisher, D. (1994). Tc-99m-labeling of lipid vesicles containing the lipophilic chelator PE-DTTA: effect of tin-to-chelate ratio, chelate content, and surface polymer on labeling efficiency and biodistribution behavior. *Nucl Med Biol* 21:89–96.
- Urakami, T., Akai, S., Katayama, Y., Harada, N., Tsukada, H., Oku, N. (2007). Novel amphiphilic probes for [¹⁸-¹⁸F]-radiolabeling preformed liposomes and determination of liposomal trafficking by positron emission tomography. *J Med Chem* 50:6454–6457.
- Urakami, T., Kawaguchi, A. T., Akai, S., Hatanaka, K., Koide, H., Shimizu, K., et al. (2009). In vivo distribution of liposome-encapsulated hemoglobin determined by positron emission tomography. *Artif Organs* 33:164–168.
- van Nostrum, C. F. (2011). Covalently cross-linked amphiphilic block copolymer micelles. *Soft Matter* 7:3246–3259.
- Willmann, J. K., van Bruggen, N., Dinkelborg, L. M., Gambhir, S. S. (2008). Molecular imaging in drug development. *Nat Rev Drug Discov* 7:591–607.

Appendix 2

Andreas T.I. Jensen, Tina Binderup, Pramod Kumar, Andreas Kjær, Palle H. Rasmussen, Thomas L. Andresen.

“In-vivo comparison of DOTA and CB-TE2A through shell-region ⁶⁴Cu-labeling of core-crosslinked triblock polymeric micelles” Biomaterials (**Submitted**).

In-vivo comparison of DOTA and CB-TE2A through shell-region ^{64}Cu -labeling of core-crosslinked triblock polymeric micelles

Andreas Tue Ingemann Jensen, Tina Binderup, Pramod Kumar, Andreas Kjær, Palle H. Rasmussen & Thomas L. Andresen.

Abstract

Copolymers of ABC-type (PEG-PHEMA-PMCA) architecture were prepared by atom transfer radical polymerization. The micelles were 29 ± 2 nm and possessed functionalizable primary alcohols in the shell-region. We compared the in-vivo stabilities of DOTA and CB-TE2A. The micelles were functionalized with DOTA and CB-TE2A in yields corresponding to 5% of each unimer carrying a chelator. The micelle cores were made from coumarin polymers, that were crosslinked by UV irradiation at 2 W/cm^2 for 30 minutes, giving degrees of crosslinking of 42-45%. The core-crosslinked micelles were labeled with ^{64}Cu at room temperature for 2 h (DOTA) or 80°C for 3 h (CB-TE2A), giving labeling efficiencies of 60-76% (DOTA) and 40-47% (CB-TE2A). The micelles were injected into tumor-bearing mice at a dose of 0.2 mg per mouse (8 mg/kg) and PET/CT scans were made at 1h, 22 and 46h. The micelles showed good blood stability ($T_{1/2}$: 20-26h) and tumor uptake. The blood concentrations for the DOTA micelles were significantly lower than for the CB-TE2A micelles, resulting in generally lower uptake in all organs except tumor. Tumor uptake was similar both types at 1h (1.9 %ID/g) and 22h (3.9% ID/g) but diverged at 46h with 3.6 %ID/g (DOTA) and 4.9 %ID/g (CB-TE2A). On the basis of our data, we conclude that the chelators have similar in-vivo stability.

1 Introduction

Polymeric micelles (PMs) are increasingly being investigated as a promising type of nanoparticle. PMs are dynamic systems in which long amphiphilic copolymers, known as *unimers*, self-assemble in water due to the hydrophobic effect. Polymeric micelles are characterized by a large degree of synthetic freedom when designing them. This means that they can achieve very small sizes (5-100 nm) and be modified in various ways.

Nanoparticles passively target tumor tissue through the EPR effect [1]. This makes them useful as drug delivery vehicles, as well as diagnostic radiopharmaceuticals when radiolabeled appropriately. However, poor tumor penetration often

hampers this accumulation [2] and causes nanoparticles to deposit in its periphery [3]. In order to reach all tumor cells, a chemotherapeutic should be capable of traveling up to 100 μm away from the vasculature and into the tumor tissue [2]. Contributing to poor penetration is the dense extracellular matrix (ECM) present in tumors [4]. Recent research has shown that nanoparticles smaller than 50 nm may exhibit superior tumor accumulation in poorly vascularized tumors [5, 6], possibly because of easier passage through the openings of the ECM [7]. For this reason, interest in small nanoparticles, such as PMs, is currently high [8].

In order to investigate and improve the properties of PMs, *in-vivo* visualization is a powerful tool. It can be achieved by positron emission tomography (PET). PET relies on the coincidence detection of anti-parallel photons emitted by annihilation of positron with electrons. Therefore, positron-emitting radioisotopes are used in PET. Compared with single photon emission computed tomography (SPECT), PET offers superior sensitivity and resolution [9-14]. Labeling of nanoparticles for PET imaging is a thriving field [8, 15-18]. Especially ^{64}Cu is a popular isotope as the window for PET scans of 48 hours it allows adequately mirrors the time in which nanoparticle pharmacokinetics takes place.

In order to attach ^{64}Cu to nanoparticles, a series of chelators are used. Traditionally, DOTA and TETA have been popular choices as they are widely available as bifunctional chelators and can be efficiently labeled at ambient temperature [19, 20]. However, the *in-vivo* stability of these chelators is widely questioned [21, 22]. This instability is thought to stem from poor kinetic stability, which may be entirely unrelated to the excellent thermodynamic stability of both chelators. ^{64}Cu has been shown to escape from DOTA through transchelation to superoxide dismutase in the liver [23-25]. In addition, after injection of ^{64}Cu bound to DOTA and TETA, ^{64}Cu was shown to appear in blood proteins [24] and ^{64}Cu bound to a DOTA-conjugated peptide caused more liver accumulation than a different radiolabel (^{86}Y) [26]. On the other hand, DOTA remains in widespread use, providing excellent clinical images [14].

CB-TE2A has been championed as providing both improved thermodynamic and kinetic stability over TETA and DOTA [27-29]. Labeling of CB-TE2A with $^{64}\text{Cu}^{2+}$ requires relatively harsh conditions, such as 1-2 h at 95 $^{\circ}\text{C}$ (pH = 8) for labeling yields of $\geq 95\%$ [19, 30] or 1 h at 85 $^{\circ}\text{C}$ (pH = 5.5) for labeling of 96% [31]. This is detrimental when labeling proteins, liposomes or other structures labile to high temperatures, but for thermostable structures, CB-TE2A provides a very sturdy chelate.

When conjugating chelators to nanoparticles, the location of the chelator may have some importance. When chelators are placed near the surface of liposomes, protected by the PEG-layer, lower liver and spleen accumulation occurred than when it was placed at the distal PEG-end [31]. Fonge et al. concluded that the chelator used for complexation has significant effects on nanoparticle pharmacokinetics, beyond that which can be explained by complexation stability [32]. They used chelators that were placed on the distal PEG-ends. Other research made on proteins has concluded that the position of chelators, as well is the chemical structure, may be important [33-35].

In the study at hand, we designed small (30-40 nm) shell-core-corona (ABC) triblock polymeric micelles exhibiting primary alcohols in the functionalizable shell-region. In order to compare the stability of DOTA and CB-TE2A, these two chelators were attached to the micelles. By conjugating in the shell-region, we envisaged that the chelators would be protected by the PEG-layer, negating any direct interaction of the chelators with blood stream components (**figure 1**). This was thought to emphasize the effect of the stability of the chelators on the observed pharmacokinetics and negate other effects. The micelle core was made from a 4-methylcoumarin polymer that was core-crosslinked by irradiation with UV light, ensuring stability *in-vivo* [36-40]. Several authors have reported ^{64}Cu -radiolabeling of PMs [8, 15, 41-44], but to the best of our knowledge, this is the first time a photo-core-crosslinked triblock PM has been labeled through CB-TE2A in the shell-region.

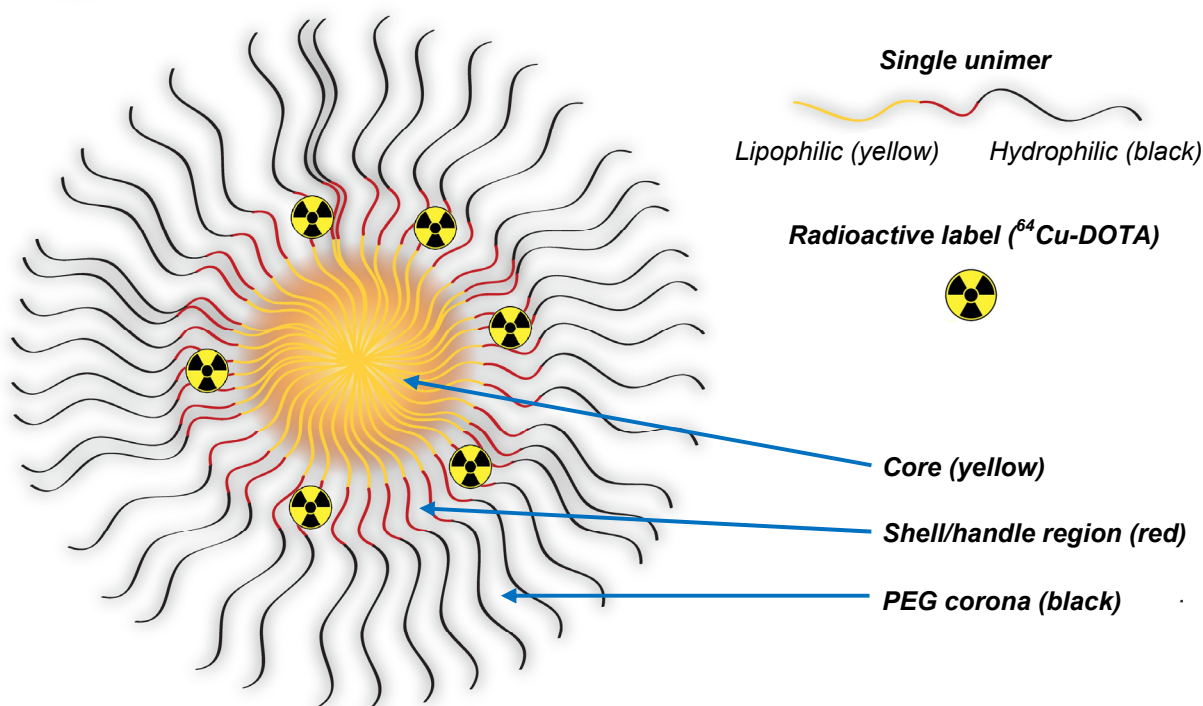


Figure 1. Cartoon of a radiolabeled ABC-type triblock polymeric micelle. The single unimer consists of a hydrophobic (*yellow*) block, a functionalizable handle-region (*red*) and a hydrophilic PEG-block (*black*). Polymeric micelles are formed by individual unimers in water. In the shell-region, a radiolabel is shown.

2 Materials and methods

2.1 Materials

DOTA-NHS ester was purchased from CheMatech (F). CB-TE2A·2H₂O was purchased from Macrocyclics (USA). All solvents and chemicals were purchased from Sigma Aldrich (DK). CuCl (99.995%) was washed with acetic acid followed by ethanol (99%) and diethylether, dried and stored under argon. Solvents used for ATRP were purified by distillation over Mg(OMe)₂ (MeOH) or CaH₂ (DMF), stored over mol. sieves (MeOH: 3 Å, DMF: 4 Å) and transferred under argon. CH₃-PEG₅₀₀₀ was from Fluka. DMF for anhydrous syntheses was dried over 4 Å molecular sieves several times. Glassware was oven-dried overnight or heatgun-dried under a stream of argon prior to use. Reactions other than polymerizations were conducted in a nitrogen atmosphere. Polymers and micelles containing coumarin moieties were shielded from light whenever possible. Cellulose membrane dialysis tubing (12.4 kDa cut-off) was from Sigma Aldrich (DK). Sephadex G25 fine (GE Healthcare) was used for size-exclusion chromatography.

NMR-analyses were recorded in CDCl₃ on 300 MHz Varian Mercury 300 BB and referenced to CHCl₃ (δ 7.26). Photo core-crosslinking by UV irradiation was done on an Omnicure Series 1000 (Lumen Dynamics, Mississauga, Canada). FT-IR spectra were recorded by Perkin Elmer Spectrum 100 FT-IR Spectrometer. GPC measurements were carried out with a RID10A-SHIMADZU refractive index detector and Mixed-D GPC column from Polymer Laboratories with a flow rate of 0.5 mL/min at 25 °C, and DMF with 50 mM LiCl as eluent. UV-Vis spectra were recorded on a Unicam Helios Uni 4923 spectrophotometer. Size and zeta potential were measured on a ZetaPALS (Brookhaven, New York, USA).

⁶⁴Cu was produced on a GE PETtrace Cyclotron. Radio-TLC was performed on a Raytest MiniGita Star. Size-exclusion chromatography of the labeled micelles was carried out on an apparatus custom-built at our facility.

2.2 Synthesis of PEG-PHEMA-PCMA

The macroinitiator PEG-Br and diblock copolymer PEG-PHEMA-Cl were synthesised as previously described [45]. The monomer 7-(2-methacryloyloxyethoxy)-4-methylcoumarin (CMA) was synthesised as previously described [46]. The diblock copolymer PEG-PHEMA-Cl (1000 mg, 0.1 mmol), 7-(2-Methacryloyloxyethoxy)-4-methylcoumarin (CMA) (720 mg, 2.5 mmol), CuCl₂ (12 mg, 0.09 mmol), and PMDETA (146 μ L, 0.7 mmol) were dissolved in DMF (10 mL) and frozen in liquid nitrogen. The catalyst CuCl (10 mg, 0.1 mmol) was added and the reaction mixture was degassed three times by freeze-pump-thaw cycles and stirred under argon at 80 °C for 24 hours. Most of the solvent was removed under vacuum. The polymer was then precipitated from methanol and dried under vacuum (yield = 0.8 g, 63%). Subsequently, the unimers were purified by dialysis (as described below) to yield the pure unimer. ¹H-NMR (300 MHz, CDCl₃): δ = 7.38-6.00 (coumarin H), 4.60-3.73 (-OCH₂CH₂O-coumarin, -OCH₂CH₂OH), 3.65 (s, -CH₂CH₂O of PEG), 2.30 (s, -CH₃ of coumarin), 2.16-1.72 (-CH₂ backbones of PHEMA and PCMA blocks), 1.20-0.79 (-CH₃ backbones of PHEMA and PCMA blocks) ppm. FTIR (cm⁻¹): 3490,

2880, 1718, 1612, 1467, 1391, 1343, 1279, 1240, 1140, 1100, 963, 839, 750. Mn (from NMR) = 11814. From GPC: Mw = 12400, Mn = 9550, PD (Mw/Mn) = 1.3.

2.3 Conjugation of DOTA

PEG-PHEMA-PCMA (30 mg, MW: 11.8 kDa, 2.5 μ mol) was dissolved in dry DMF (1 mL) under a nitrogen atmosphere. DOTA-NHS ester (2.0 mg, 2.7 μ mol) was added along with DMAP (2.0 mg, 16 μ mol). The mixture was stirred overnight (19h) at RT, followed by dialysis (*see below, section 2.5*).

2.4 Conjugation of CB-TE2A

In the main reaction vessel (MRV) was dissolved PEG-PHEMA-PCMA (30 mg, MW: 11.8 kDa, 2.5 μ mol) and CB-TE2A-2H₂O (4.5 mg, 8.2 μ mol) in dry DMF (1 mL). DMAP (17 mg) was dissolved in dry DMF (4 mL) and 40 μ L of this solution was added to the MRV (DMAP: 0.17 mg, 1.4 μ mol). EDC-HCl (4.0 mg) was dissolved in dry DMF (0.5 mL) and 69 μ L of this solution was added to the MRV (EDC.HCl: 0.55 mg, 2.9 μ mol). The mixture was stirred overnight (16h) at RT under a N₂ atmosphere, followed by dialysis (*see below, section 2.5*).

2.5 Formation of micelles

When chelator conjugation was over, Milli-Q water was added dropwise directly to the reaction mixture, until the ratio of DMF-water was 1:2. The mixture was placed in a dialysis tube (cut-off: 12.4 kDa) and dialyzed against Milli-Q water (1 L) for three days at pH < 7. Each day the water was changed. Conjugation yield was estimated by incubating the micelles (200 μ L, 1 equiv) with non-radioactive Cu²⁺, twice the maximum molarity of chelator present (2 equiv), spiked with ⁶⁴Cu. After incubation of 4h at 80 °C (CB-TE2A) or 3h at room temperature (DOTA) unincorporated copper was scavenged (30 min) by adding EDTA in excess (400 equiv). Conjugation yield was estimated as the ratio of the non-eluting peak (micelles) towards the EDTA-peak.

2.6 Characterization of micelles

The micelles were characterized by *direct light scattering* (DLS), providing hydrodynamic diameters and zeta-potential. Size was measured three times on the same sample. n = 3, unless otherwise stated. The number weighted (median) as well as the intensity weighted (median) sizes are reported (as specified), along with the PDI. Zeta-potentials were measured by running 20 runs of 10 scans on one sample (n = 10, unless otherwise specified).

2.7 Photo core-crosslinking of micelles

Micelle dispersion (1100 μ L) was transferred to a 4 mL glass vial containing a magnet. The vial was stirred vigorously and placed in an ice/water bath that was kept at 5-7 °C. The dispersion was irradiated for 2x15 minutes at an intensity of 2 W/cm² and a wavelength of 320 < λ < 500 nm. The UV probe was placed about a centimeter from the water surface. The

degree of crosslinking (%CL) was determined by measuring the drop in absorbance at 320 nm and calculating: $(A_{\text{before}} - A_{\text{after}}) / A_{\text{before}} = \%CL$. Crosslinking was verified by mixing 100 μL of both crosslinked and non-crosslinked dispersions with 1600 μL and measuring by DLS.

2.8 Determination of micelle material concentration

Determining the concentration of micelle material in dispersion was possible since coumarin absorbs UV light. There was a direct linear correlation between amount of micelle material (determined by freeze-drying and weighing an aliquot of dispersion) and UV absorbance at 320 nm, with intercept through (0,0). This made it possible to measure the absorbance of a micelle dispersion of known concentration and determining the concentration in diluted samples based on this value.

2.9 Radiolabeling with ^{64}Cu

To a vial containing $^{64}\text{CuCl}$ was added 100 μL NH_4OAc (0.1 M, pH 5.5) buffer. The mixture was stirred for 10 minutes at room temperature, forming ^{64}Cu -acetate. Then micelle dispersion (400 μL , ~ 4 mg/mL) was added. This mixture was stirred for 2 hours at room temperature (DOTA) or 3 hours at 80 $^{\circ}\text{C}$ (CB-TE2A). Then 1 mM EDTA-tri-potassium-dihydrate (0.05 μmol , 50 μL) was added and the mixture was stirred for a further 20 minutes, cooling to room temperature (CB-TE2A). The radiolabeled micelles were applied to a fully-automated size-exclusion column and eluted with an isotonic (150 mM NaCl) PIPES (10 mM) buffer, pH = 7.0. The activity eluted in two peaks, **Peak 1** (micelles) and **Peak 2** (small molecules, such as chelated ^{64}Cu).

2.10 Formulation of micelles for animal studies

From the size-exclusion chromatography (SEC) purification of the radiolabeled micelles, the *most concentrated fraction* (1 mL, ~ 1.0 mg/mL) from **Peak 1** was used. This was diluted with non-radiolabeled, identical micelles to give final concentrations of about 1.0 mg micelle material per mL and ~ 70 MBq/mL.

2.11 MicroPET/CT imaging

Seven weeks old female NMRI nude mice purchased from Taconic (Borup, Denmark) were inoculated in the right and left flank with 5×10^6 U87MG cells (LGC standards, Borås, Sweden) in a 1:1 mixture with matrixgel™ (BD Biosciences, Albertslund, Denmark). Tumors were grown for 2 weeks. The mice were divided into 2 groups; CB-TE2A ($n = 6$) and DOTA ($n = 6$). The animal experiments were approved by the Animal Research Committee of the Danish Ministry of Justice.

Either of the micelle formulations was intravenously injected in a lateral tail vein of anesthetized mice at an average dose of 7.8 ± 0.46 MBq (mean \pm SD) for the CB-TE2A micelles and 8.0 ± 0.84 MBq for the DOTA-micelles at a volume of 200 μL and a lipid concentration of ~ 1.0 mg/mL. The PET/CT scans were acquired on a dedicated small animal system (MicroPET Focus 120 & MicroCAT® II, Siemens Medical Solutions, Malvern, PA, USA) at 1h, 22h and 46h post injection (p.i.) with PET acquisition times of 10, 15 & 30 min, respectively. PET data were reconstructed with the 2-dimensional ordered-subset

expectation maximization (OSEM2D) reconstruction algorithm. PET and CT images were analyzed as fused images using the Inveon software (Siemens) where regions of interest (ROIs) were drawn around liver, kidney, spleen, muscle, tumors and the left-ventricle. Uptake in the left ventricle of the heart was taken as a measure of the blood concentration. CT settings were a tube voltage of 64 kVp, a tube current of 500 μ A, 360 rotation steps, an exposure time of 440 ms and a voxel size of 0.092 mm. Immediately following the last PET scan 4 of the 6 mice in each group were euthanized and blood as well as organs of interest collected and counted in a gamma counter (Perkin Elmer Life Sciences).

The statistics were calculated using Excel 2010. Differences were analyzed using an unpaired, two-tailed t-test. Differences in the same animal at different times p.i was analyzed using a paired, two-tailed t-test. A p-value < 0.05 was considered significant. Error bars on tracer accumulation (%ID/g) is presented as standard error of the mean (S.E.M.).

3 Results

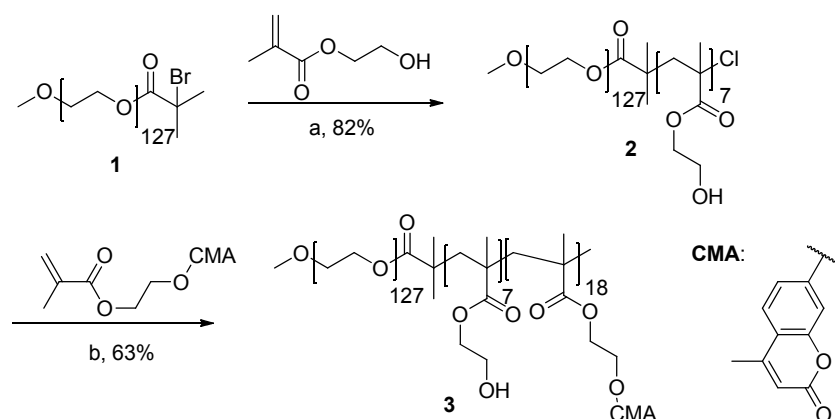


Figure 2. Synthesis of PEG-PHEMA-PCMA. *Reagents and conditions:* (a) CuCl/bpy, MeOH, 25 °C, 24h, (b) CuCl/PMDETA, CuCl₂, DMF, 80 °C, 24h.

3.1 Synthesis and chelator conjugation

After synthesis, the PEG-PHEMA-PCMA unimer was purified by dialysis, to remove small molecular contaminants and residual copper from the polymerization steps. Size after dialysis (nr. weighted): 29 ± 2 , PDI: 0.21 ± 0.02 , zeta: -4.1 ± 0.4 mV. (figure 2)

DOTA and CB-TE2A were conjugated to PEG-PHEMA-PCMA through ester bonds (**figure 3**). DOTA was conjugated by using the commercially available DOTA-NHS ester. DMAP was added in excess to function as both base and acyl transfer catalyst, in a variation of Steglich esterification. CB-TE2A, not being available as an activated ester, was conjugated through EDC-mediated coupling, in the presence of DMAP. EDC and CB-TE2A were present in about a 1:3 ratio. This would lead to predominant activation of one carboxylic acid on CB-TE2A, which in turn could lead to formation of an acid anhydride with a further CB-TE2A molecule. DMAP was added as catalyst. These conjugations were low yielding (*estimated yields*, DOTA: 4%, CB-TE2A: 5%), which fitted well with our desire to put relatively few chelators in the shell-region. A large number of chelators would occupy significant space and affect the micelles in possibly undesirable ways, while the increased copper-binding capacity was irrelevant. Accordingly, approx. 5% of the unimers in the micelles hold a chelator.

3.2 Micelle preparation and crosslinking

After chelator conjugation was carried out, micelles were formed by the dropwise addition of water directly to the reaction mixture. The mixture was subsequently dialyzed against ultra-purified water. The physicochemical properties of the prepared micelles are shown in **table 1**. The size distributions were between 21 (nr. weighted) and 45 (intensity weighted) nm, with slightly negative zeta potentials. Chelator conjugation was not generally observed to affect the size or the zeta potentials of the micelles. The micelle material concentration in the two formulation were 3.9 mg/mL (DOTA micelles) and 4.2 mg/mL (CB-TE2A micelles). Crosslinking was carried out by UV irradiation. It had been previously observed (*unpublished results*) that prolonged exposure to UV without temperature control could induce instability and aggregation in certain micelle types. For this reason, crosslinking was routinely done at lowered temperature (5-7 °C). In line with previous work, we observed that the rate of crosslinking dropped with exposure time [37]. As such, it becomes a compromise between achieving an appreciable degree of crosslinking and exposing the micelles to lengthy, potentially damaging, high intensity UV radiation. Crosslinking rate was also found to depend on the concentration of the dispersion. We assessed that 40-50% crosslinking was appropriate. This correlated with a total of 30 minutes of irradiation. Crosslinking degrees of 42% (DOTA) and 45% (CB-TE2A) were obtained (see **figure 4**). In order to test the stability of crosslinked vs. non-crosslinked micelles the dispersions were mixed with DMF in a 1:16 dispersion-DMF ratio. DMF is a non-selective solvent, capable of fully dissolving single unimers. The crosslinked micelles were found to be stable when mixed with DMF displaying intensity weighted sizes of

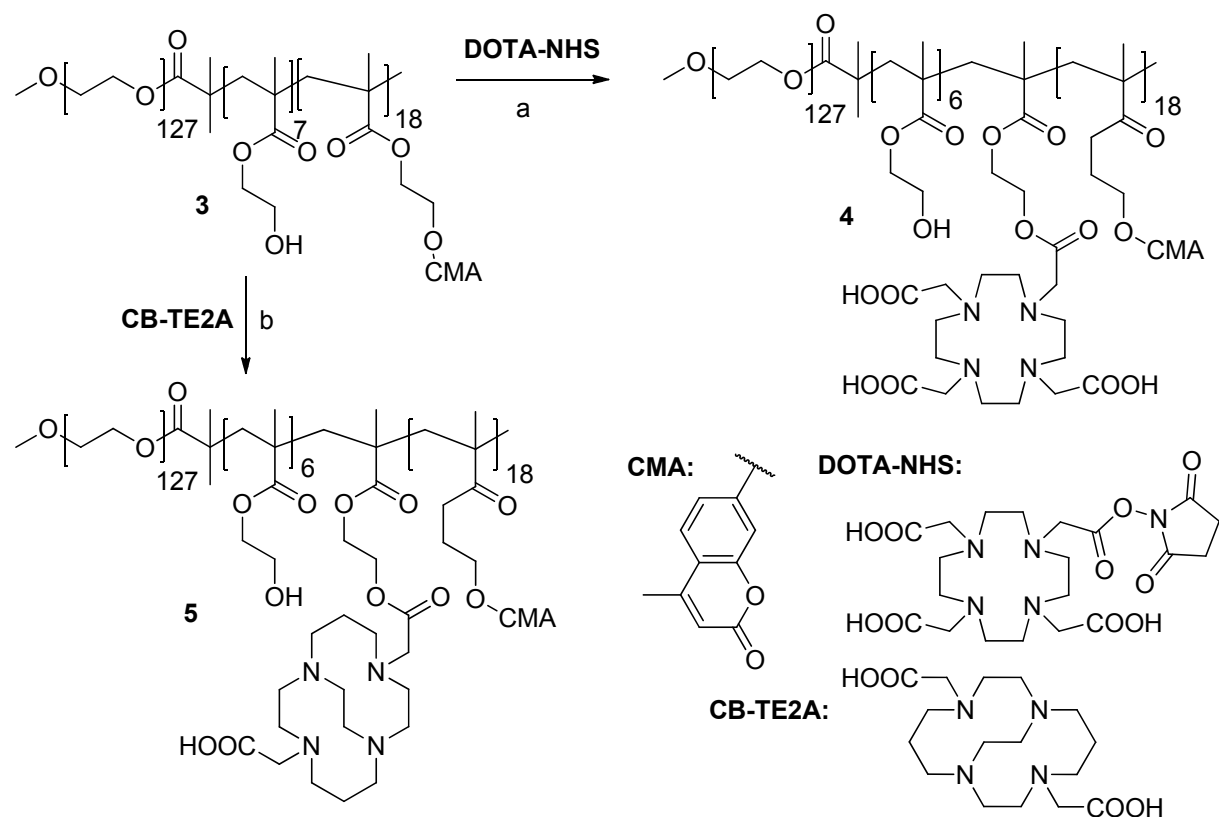


Figure 3. Conjugation of chelators to PEG-PHEMA-PCMA. *Reagents and conditions:* (a) DMAP, DMF, 19h, RT. (b) EDC.HCl, DMAP, DMF, 16h, RT.

3.3 Radiolabeling and formulation

Both crosslinked and non-crosslinked micelles were radiolabeled, in spite of only the crosslinked being used *in-vivo*. The micelles were radiolabeled by incubation with ^{64}Cu -acetate. The radiolabeling was problematic to monitor, so the incubation times (2h DOTA, 3h CB-TE2A) are arbitrary. Consistent, good labeling yields were observed. Initially it was attempted to label the CB-TE2A micelles at 95 °C, but this caused them to aggregate. 3h at 80 °C (pH 5.5) provided good labeling. Similar conditions were used by Seo et al. for labeling CB-TE2A [31]. After labeling, nonspecifically bound ^{64}Cu was removed by EDTA scavenging (50 μmol , 20 min incubation). When unmodified PEG-PHEMA-PCMA was incubated with ^{64}Cu for 3 h at 80 °C, 17% of the activity eluted in **peak 1**, nonspecifically bound to the micelles. Incubation with EDTA was found to lower this to 8%. When incubating chelator-conjugated micelles it can be assumed that far less is unspecifically bound, as most will displace into the chelators. We found that incubation at increased temperature generally augmented nonspecific labeling.

The radiolabeled micelles were purified by size-exclusion chromatography, resulting in two peaks. That **Peak 1** contained micelles was evident as the radioactivity concentration correlated with count rate on DLS as well as the intensity of the absorbance of coumarin units. **Peak 1** was routinely analyzed by radio-TLC showing a single peak that did not elute, which is characteristic of nanoparticles. Analysis of **Peak 2** by radio-TLC usually showed a prominent peak for ^{64}Cu -EDTA as well as minor radiolysis products. Radiolabeling efficiencies are seen in **table 1**. Generally, DOTA micelles were labeled with higher efficiencies than CB-TE2A micelles. The labeling efficiencies we obtained were generally high compared with the

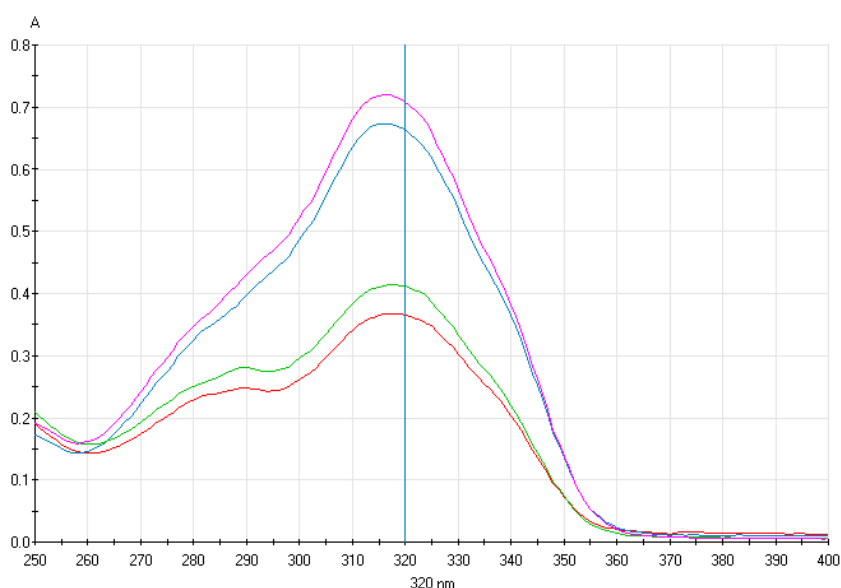


Figure 4. UV chromatograms of micelles before and after crosslinking. The absorbances recorded at 320 nm are given below.

— 0.664 CB-TE2A (t = 0) — 0.709 DOTA (t = 0)
 — 0.366 CB-TE2A (t = 30 min) — 0.412 DOTA (t = 30 min)

literature [41].

The most concentrated fraction (making up 1 mL) was collected. The concentration of radiolabeled micelles was slightly less than 1.0 mg/mL micelle material. For the final formulation for *in-vivo* studies, the radioactive micelles were diluted with a dispersion of non-radioactive micelles, also prepared in isotonic PIPES buffer and also having a concentration of about 1.0 mg/mL. When the radioactivity had decayed, the accurate concentrations of micelle material were determined by UV measurements. This resulted in the concentrations of the formulations used for *in-vivo* studies being 1.1 mg/mL (CB-TE2A micelles) and 0.9 mg/mL (DOTA micelles). With 200 μL injected into each mouse, this meant that the dose per mouse was 0.2 mg or about 8 mg/kg. A certain amount of nanoparticles is sequestered by macrophages immediately upon injection [47, 48]. For this reason, it is necessary to inject an appreciable amount of micelle material, as trace amounts

would be cleared. For lipid nanoparticles (liposomes) the lower limit of dose-independent pharmacokinetics has been found to be about 2 $\mu\text{mol/kg}$ ($\sim 2 \text{ mg/kg}$) [47]. In previous studies with polymeric micelles in mice have been used 3-5 mg/kg [41, 43] and 10 mg/kg [5, 49]. This suggests that 8 mg/kg is within the window of dose independent pharmacokinetics.

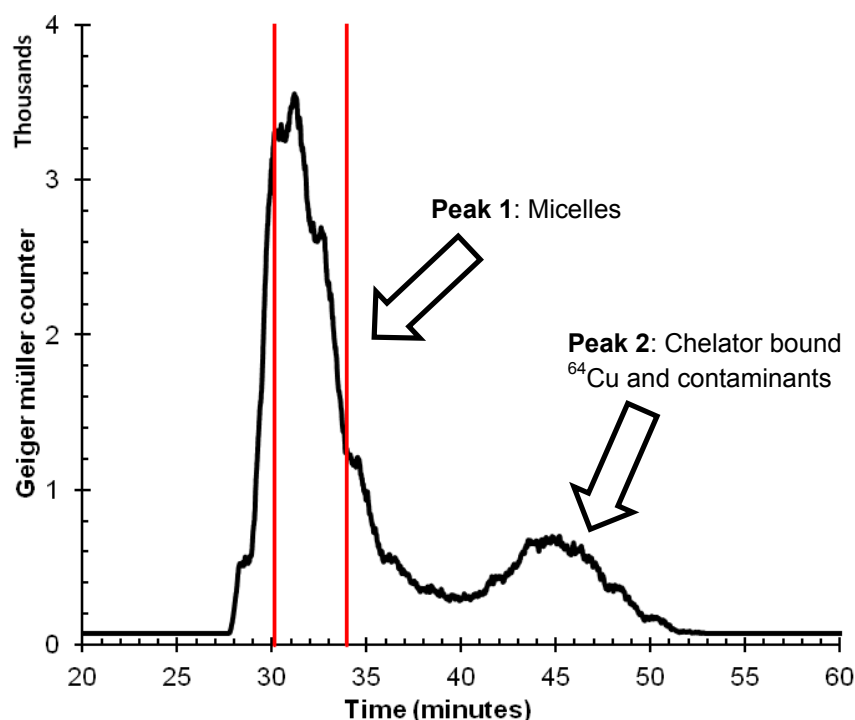


Figure 5. Size-exclusion (SEC) chromatogram of the purification of the radiolabeled micelles. **Peak 1:** Micelles. **Peak 2** Chelator (especially EDTA) bound ^{64}Cu and small-molecular contaminants. The elution time of the *most concentrated milliliter* is marked in red. The data shown are for DOTA (NonCL).

3.4 Stability of the micelles

The stability of the crosslinked micelles was investigated at 37 °C (physiological temperature) and 80 °C (radiolabeling temperature). At 37 °C both DOTA and CB-TE2A micelles were found to be stable for up to 6 days (no further measurements). No changes in size were seen. At 80 °C, the DOTA-micelles were stable up to 61 h (no further measurements). The CB-TE2A micelles were stable with no size changes up to 4.5 hours. After 61 h however, this micelle type had undergone heavy aggregation. This underscores our previous experience (unpublished results) that conjugation of CB-TE2A induced thermoinstabilities when compared with DOTA. We concluded that the micelles were stable under the conditions to which we exposed them during labeling and *in-vivo* studies.

3.5 In-vivo PET and biodistribution

Using positron emission tomography (PET) and computed tomography (CT) the tumor volume as well as the *in-vivo* biodistribution of the ^{64}Cu -labeled CB-TE2A and DOTA micelles were evaluated in mice bearing subcutaneously inoculated U87MG tumors on the right and left flank. The tumor volume was assessed on every CT scan and the tumor volume was $56.7 \pm 11.8 \text{ mm}^3$ ($n = 12$) and $56.8 \pm 10.6 \text{ mm}^3$ ($n = 12$) in the CB-TE2A and the DOTA groups respectively. Tumor uptake, organ distribution and plasma stability was evaluated over a 46 hour time-frame with PET/CT scans at 1h, 22h and 46h p.i. as well as radioactivity measurements at 48h p.i. using a gamma counter.

In agreement with the EPR effect and plasma stability of the two cross-bridged micelle formulations the tumor accumulation increased over time and was significantly higher at the 22h and 46h time-points compared to the 1h time-point for both groups ($p < 0.001$ in all cases). In addition, for the CB-TE2A micelles there was a significant increase in tumor accumulation from $4.0 \pm 0.35 \text{ \%ID/g}$ at 22h p.i. to $4.9 \pm 0.43 \text{ \%ID/g}$ at 46h p.i. ($p < 0.001$). In contrast, there was a significant decrease in tumor retention from $3.8 \pm 0.13 \text{ \%ID/g}$ at 22h p.i. of the DOTA micelles compared to $3.6 \pm 0.11 \text{ \%ID/g}$ at 46h p.i. ($p = 0.029$) (**Figure 6**). Between the two chelator groups there was as significantly higher tumor uptake at 46 hours p.i. in the CB-TE2A group compared to the DOTA group ($p = 0.0083$) whereas there was no significant difference between the two groups at 1h and 22h p.i. All organ values, as well as ex-vivo results from gamma counting of excised organs, and calculated organ ratios are shown in **table 2**.

Table 1 – Physicochemical properties of micelle formulations. $n = 3$ in all cases, except zeta potential ($n = 10$).

	CB-TE2A (CL)	DOTA (CL)	CB-TE2A (NonCL)	DOTA (NonCL)
Size (number)	$21 \pm 1 \text{ nm}$	$18 \pm 1 \text{ nm}$	$21 \pm 1 \text{ nm}$	23 ± 1
Size (intensity)	$45 \pm 5 \text{ nm}$	$47 \pm 1 \text{ nm}$	$45 \pm 3 \text{ nm}$	$44 \pm 2 \text{ nm}$
PDI	0.17 ± 0.01	0.20 ± 0.01	0.17 ± 0.02	0.15 ± 0.01
Zeta-pot.	$-3.5 \pm 0.3 \text{ mV}$	$-2.3 \pm 0.4 \text{ mV}$	$-3.8 \pm 0.4 \text{ mV}$	$-2.1 \pm 0.7 \text{ mV}$
Cross-linking	45%	42%	NA	NA
Labeling efficiency*	47% (30%)	60% (34%)	40% (23%)	76% (50%)
Mic.mat. conc.	1.1 mg/mL	0.9 mg/mL	NA	NA

* The labeling efficiency is the % of the total activity in **Peak 1**. The contents of the most concentrated milliliter is shown in parenthesis.

TABLE 2 – Tissue accumulation values based on PET and *ex-vivo* organ counting

	Time after intravenous administration							
	1 h		22 h		46 h		<i>Ex vivo organ counting</i>	
	CB-TE2A	DOTA	CB-TE2A	DOTA	CB-TE2A	DOTA	CB-TE2A	DOTA
blood	21.7 ± 1.7	15.9 ± 0.74	9.6 ± 0.47	5.2 ± 0.14	4.7 ± 0.30	2.7 ± 0.18	3.4 ± 0.27	1.8 ± 0.09
liver	8.2 ± 0.6	7.1 ± 0.25	7.8 ± 0.36	6.8 ± 0.21	7.0 ± 0.40	5.5 ± 0.14	4.7 ± 0.09	3.7 ± 0.26
spleen	7.6 ± 0.4	5.5 ± 0.43	5.8 ± 0.26	3.7 ± 0.22	5.6 ± 0.30	3.2 ± 0.14	6.0 ± 0.43	3.4 ± 0.22
kidney	6.2 ± 0.4	5.5 ± 0.35	3.7 ± 0.18	3.2 ± 0.15	2.6 ± 0.10	2.6 ± 0.14	1.9 ± 0.14	2.6 ± 0.15
muscle	1.0 ± 0.11	1.0 ± 0.22	0.8 ± 0.06	0.6 ± 0.01	0.8 ± 0.1	0.6 ± 0.05	0.3 ± 0.04	0.3 ± 0.04
tumors	1.9 ± 0.10	1.9 ± 0.10	4.0 ± 0.35	3.8 ± 0.13	4.9 ± 0.40	3.6 ± 0.11	4.0 ± 0.28	3.4 ± 0.19
T/B	0.1 ± 0.01	0.1 ± 0.00	0.4 ± 0.02	0.7 ± 0.04	1.0 ± 0.08	1.4 ± 0.08	-	-
T/M	2.0 ± 0.24	3.0 ± 1.09	5.0 ± 0.23	6.2 ± 0.26	6.3 ± 0.65	6.3 ± 0.61	-	-
T/K	0.3 ± 0.02	0.4 ± 0.02	1.1 ± 0.05	1.2 ± 0.04	1.9 ± 0.07	1.4 ± 0.07	-	-
T/L	0.2 ± 0.02	0.3 ± 0.01	0.5 ± 0.02	0.6 ± 0.01	0.7 ± 0.04	0.7 ± 0.02	-	-
T/S	0.3 ± 0.02	0.4 ± 0.02	0.7 ± 0.03	1.0 ± 0.05	0.9 ± 0.06	1.1 ± 0.04	-	-
S/B	0.35	0.35	0.60	0.71	1.2	1.2	-	-
L/B	0.38	0.45	0.81	1.3	1.5	2.0	-	-
K/B	0.29	0.35	0.39	0.62	0.55	0.96	-	-

Values are represented as %ID/g, mean ± SEM. For the PET scans, n = 6 in all cases, except tumors where n = 12. For the gamma counting, n = 4 in all cases, except tumors and kidneys where n = 8.

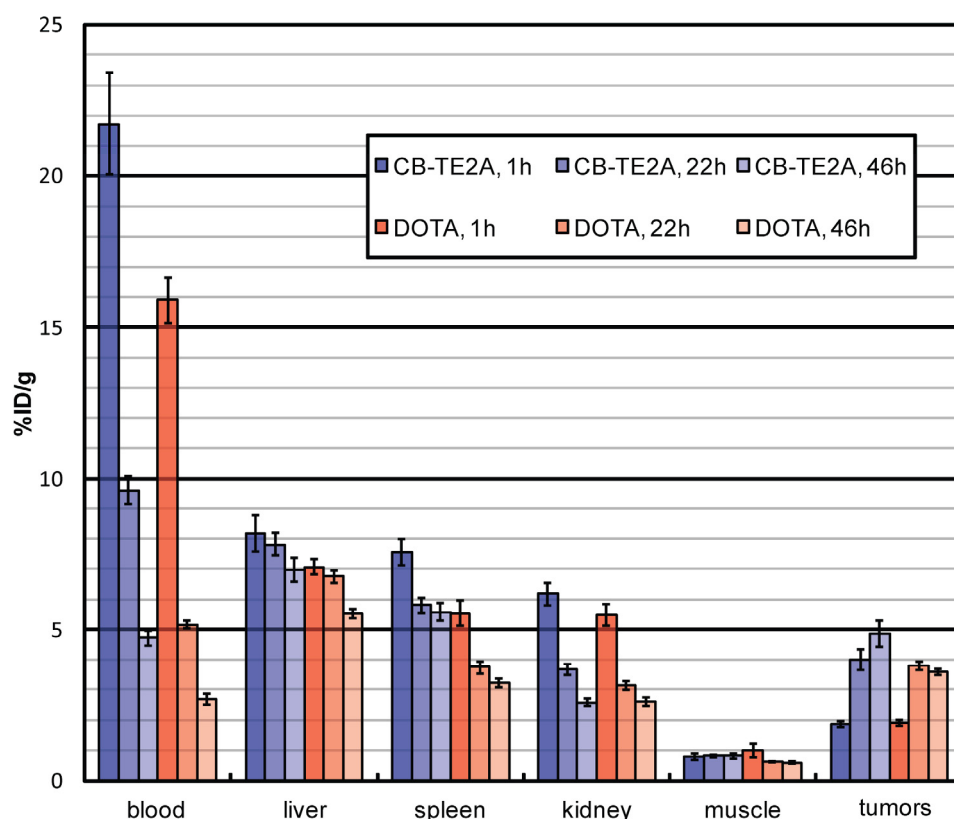


Figure 6. *In-vivo* distribution of DOTA and CB-TE2A conjugated micelles. PET scans were conducted after 1h, 22h and 46h. Organ accumulation was quantified by region-of-interest (ROI) image analysis. All values are \pm s.e.m. with $n = 6$, except for tumors where $n = 12$.

4 Discussion

It is apparent that the initial (1h) blood values for DOTA were lower than those of CB-TE2A. The difference was significant by t-test (unpaired, two-tailed, $t = 0.011$). The difference could be prompted by a fast initial renal clearance of DOTA micelles, but it seems unlikely that this should be different from the CB-TE2A micelles. The sizes are similar and none are below the renal clearance threshold (~ 10 nm). If the clearance was due to rapid loss of $^{64}\text{Cu}^{2+}$ from the micelles, this activity would be expected to rapidly (within one hour) accumulate in the liver and kidneys [50] or to appear in the blood (protein bound) [51-53]. Assuming 2 mL (2 gram) blood in a mouse, the total activity (%ID) in the blood can be plotted as shown in **figure 7**. Nanoparticles are thought to follow a biphasic clearance profile [8, 17, 54], with a fast (usually lasting 1-3h) initial clearance and distribution phase followed by a longer main clearance phase with about 10-30 h half-life, depending on the particle type. As our dataset does not include measurements before 1h, it is difficult to comment on the

fast initial clearance. In **figure 7** it is seen that the half-life between the two first points is shorter than between the two later points. This suggests that the first clearance phase is not entirely over at 1h. In addition, by comparing the two curves for the DOTA micelles, it can be seen that for these micelles, the difference between early and late half-life is more pronounced than for the CB-TE2A micelles. This could indeed indicate that the first, fast clearance phase is longer and more pronounced for the DOTA micelles where only 19% of the injected dose appears to follow the second-phase, slow clearance profile (the backwards forecast of the “late points” trendline for the DOTA micelles). This number is 37% for the CB-TE2A micelles. In order to conclude that DOTA conjugated nanoparticles are cleared more rapidly, more studies are needed. In addition, one would expect the cleared nanoparticles to emerge in liver and spleen and only modest accumulation is seen in these tissues. The lower blood concentration of the DOTA-micelles seems to affect the activity found in other tissues, thus making all of these (perhaps except tumor) slightly lower than the CB-TE2A micelles.

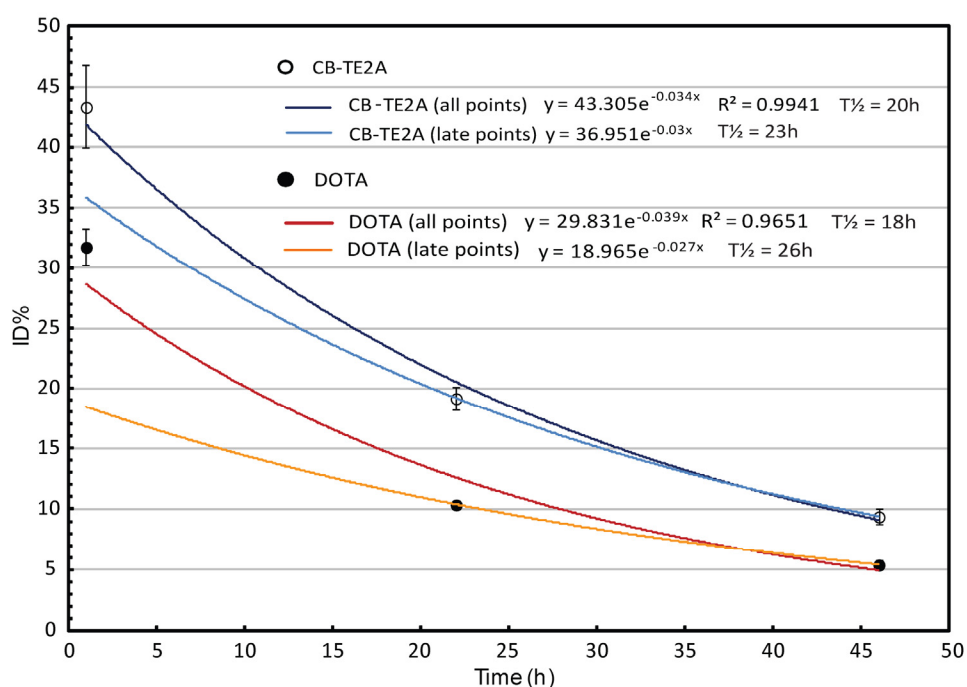


Figure 7. Blood clearance data for DOTA and CB-TE2A conjugated micelles. Values are given as ID%, assuming 2 gram blood per mouse. The two darker shaded curves are exponential fits over all three points. The lighter shaded curves are exponential fits over the two later points (22h and 46h). Equations, R² for the “all points” curves as well as calculated half-lives are shown.

The apparent circulation half-lives of the PMs are 18-26 h for the DOTA micelles and 20-23 h for the CB-TE2A micelles (**figure 7**). Such half-life values are generally longer than those observed for liposomes [17, 55], while similar values, and longer, are observed for PMs [32, 54, 56]. The relatively long half-lives may be a consequence of the low uptake in liver

and especially spleen. Liposomes can accumulate in spleen about 3-4 times as much as observed here [17, 57]. Liver accumulation of liposomes is usually more modest and is generally observed to be similar to that observed here [57, 58] or slightly higher [17]. Modest uptake in these organs, which is primarily macrophage-mediated, may be because of smaller size.

The kidney accumulation observed is similar or lower to what is usually observed for nanoparticles [54, 58]. Free Cu^{2+} has some tendency to accumulate in kidney tissue [53, 58, 59] as well as in the liver [50, 58]. From the biodistribution data it is seen that when the values are taken against blood concentration, liver and kidney accumulation are higher for the DOTA-micelles. Splenic accumulation is the same when taken against blood for the two types (organ-to-blood ratios are seen in **table 2**). Thus could be a slight indicator that DOTA has a higher tendency to lose bound $^{64}\text{Cu}^{2+}$ in circulation.

Looking at tumor accumulation, a different picture emerges. Contrary to the other organs, tumor values are very similar for the two micelle types at 1 and 22 hours. At 46 h however, CB-TE2A is higher than DOTA. The difference is significant on a t-test ($t = 0.0083$). In line with current theories on copper loss from DOTA [21, 22, 24], one could conclude that DOTA conjugated micelles do not show as long circulation due to copper-loss and therefore fail to accumulate in tumor beyond 24 hours. In general however, as all other tissues exhibit lower values for DOTA than for CB-TE2A it seems reasonable that tumor should also do so. The tumor accumulation values observed here fit well with what is generally observed for long-circulating nanoparticles. Both poorer [16, 32] and better [41, 54, 56] values have been reported in the literature.

In order to better compare the two formulations, as well as assessing their potential and contrast as imaging agents, a series of tissue ratios were calculated. These are seen in **table 2**. The tumor-to-muscle (T/M) is what generally speaks about the potential as imaging agent. Values over 1.5 are thought to provide adequate contrast for tumor visualization [60]. Accordingly, these micelles can serve this purpose. The tumor-to-liver (T/L) and tumor-to-spleen (T/S) ratios are two other values that are often reported. They speak about the nanoparticles' tendency to accumulate in tumor as compared to the other usual (and unwanted) sites of accumulation. These values are (as already alluded to above) generally good for these PMs, with T/L ratios at 0.7 and T/S ratios about 1. An interesting perspective on this study would be to investigate the causes of the fast initial clearance, as the particles themselves seem to have very good characteristics for preferential tumor accumulation.

In spite of the points made in the above, we feel that the dataset at hand does not provide substantial grounds for concluding that DOTA has significantly poorer *in-vivo* stability than CB-TE2A. DOTA is a very practical chelator, being widely available as a bifunctional chelator for easy conjugation and being easy to label at ambient temperature with short incubation times. Based on our data, we do not feel that DOTA should be discarded because of stability issues.

4 Conclusion

We prepared a triblock polymeric micelle systems, with DOTA and CB-TE2A conjugated to the shell-region. This system was photo-corecrosslinked by coumarin moieties in the core and radiolabeled with ^{64}Cu . The micelles displayed prolonged circulation in blood and good tumor accumulation with modest uptake in liver, spleen and other organs. We did not find substantial evidence on which to conclude that the proposed instability between DOTA and CB-TE2A affects their *in-vivo* performance.

5 Acknowledgements

The authors thank the staff at the Hevesy Laboratory (DTU Nutech) and CBIO (DTU Nanotech) for their fruitful discussions and daily assistance. In particular Dr. Dennis Elema, as well as Cristine Søgaaard and Anette Holst for providing ^{64}Cu .

6 Declaration of interests

The authors report no conflicts of interests.

7 References

1. Maeda H, **The enhanced permeability and retention (EPR) effect in tumor vasculature: The key role of tumor-selective macromolecular drug targeting.** *Adv Enzyme Regul*, (2001). 41: p. 189.
2. Minchinton AI and Tannock, IF, **Drug penetration in solid tumours.** *Nature Reviews Cancer*, (2006). 6(8): p. 583.
3. Fang J, Nakamura, H, and Maeda, H, **The EPR effect: Unique features of tumor blood vessels for drug delivery, factors involved, and limitations and augmentation of the effect.** *Adv Drug Del Rev*, (2011). 63(3): p. 136.
4. Waite CL and Roth, CM, **Nanoscale Drug Delivery Systems for Enhanced Drug Penetration into Solid Tumors: Current Progress and Opportunities.** *Critical Reviews in Biomedical Engineering*, (2012). 40(1): p. 21.
5. Cabral H, Matsumoto, Y, Mizuno, K, et al., **Accumulation of sub-100 nm polymeric micelles in poorly permeable tumours depends on size.** *Nat Nanotechnol*, (2011). 6(12): p. 815.
6. Dreher MR, Liu, WG, Michelich, CR, et al., **Tumor vascular permeability, accumulation, and penetration of macromolecular drug carriers.** *J Natl Cancer Inst*, (2006). 98(5): p. 335.
7. Jain RK and Stylianopoulos, T, **Delivering nanomedicine to solid tumors.** *Nature Reviews Clinical Oncology*, (2010). 7(11): p. 653.
8. Dong H, Dube, N, Shu, JY, et al., **Long-Circulating 15 nm Micelles Based on Amphiphilic 3-Helix Peptide-PEG Conjugates.** *Acs Nano*, (2012). 6(6): p. 5320.
9. Gambhir SS, **Molecular imaging of cancer with positron emission tomography.** *Nature Reviews Cancer*, (2002). 2(9): p. 683.
10. Willmann JK, van Bruggen, N, Dinkelborg, LM, et al., **Molecular imaging in drug development.** *Nature Reviews Drug Discovery*, (2008). 7(7): p. 591.
11. Rahmim A and Zaidi, H, **PET versus SPECT: strengths, limitations and challenges.** *Nucl Med Commun*, (2008). 29(3): p. 193.
12. Alavi A and Basu, S, **Planar and SPECT imaging in the era of PET and PET-CT: can it survive the test of time?** *Eur J Nucl Med Mol Imag*, (2008). 35(8): p. 1554.
13. Bateman TM, **Advantages and disadvantages of PET and SPECT in a busy clinical practice.** *J Nucl Cardiol*, (2012). 19(1): p. 3.
14. Pfeifer A, Knigge, U, Mortensen, J, et al., **Clinical PET of Neuroendocrine Tumors Using ⁶⁴Cu-DOTATATE: First-in-Humans Study.** *J Nucl Med*, (2012).
15. Zeng D, Lee, NS, Liu, Y, et al., **⁶⁴Cu Core-Labeled Nanoparticles with High Specific Activity via Metal-Free Click Chemistry.** *Acs Nano*, (2012). 6(6): p. 5209.
16. Xiao YL, Hong, H, Javadi, A, et al., **Multifunctional unimolecular micelles for cancer-targeted drug delivery and positron emission tomography imaging.** *Biomaterials*, (2012). 33(11): p. 3071.
17. Petersen AL, Binderup, T, Jolck, RI, et al., **Positron emission tomography evaluation of somatostatin receptor targeted (⁶⁴Cu-TATE-liposomes in a human neuroendocrine carcinoma mouse model.** *J Control Release*, (2012). (in press).
18. Jensen AT, Binderup, T, Andresen, TL, et al., **PET imaging of liposomes labeled with an [¹⁸F]-fluorocholesteryl ether probe prepared by automated radiosynthesis.** *J Liposome Res*.
19. Wadas TJ and Anderson, CJ, **Radiolabeling of TETA- and CB-TE2A-conjugated peptides with copper-64.** *Nature Protocols*, (2006). 1(6): p. 3062.
20. Jones-Wilson TM, Deal, KA, Anderson, CJ, et al., **The in vivo behavior of copper-64-labeled azamacrocyclic complexes.** *Nucl Med Biol*, (1998). 25(6): p. 523.

21. Anderson CJ and Ferdani, R, **Copper-64 Radiopharmaceuticals for PET Imaging of Cancer: Advances in Preclinical and Clinical Research.** *Cancer Biother Radiopharm*, (2009). 24(4): p. 379.
22. Bartholoma MD, **Recent developments in the design of bifunctional chelators for metal-based radiopharmaceuticals used in Positron Emission Tomography.** *Inorganica Chimica Acta*, (2012). 389: p. 36.
23. Bass LA, Wang, M, Welch, MJ, et al., **In vivo transchelation of copper-64 from TETA-octreotide to superoxide dismutase in rat liver.** *Bioconjugate Chem*, (2000). 11(4): p. 527.
24. Boswell CA, Sun, XK, Niu, WJ, et al., **Comparative in vivo stability of copper-64-labeled cross-bridged and conventional tetraazamacrocyclic complexes.** *J Med Chem*, (2004). 47(6): p. 1465.
25. Rogers BE, Anderson, CJ, Connett, JM, et al., **Comparison of four bifunctional chelates for radiolabeling monoclonal antibodies with copper radioisotopes: Biodistribution and metabolism.** *Bioconjugate Chem*, (1996). 7(4): p. 511.
26. McQuade P, Miao, YB, Yoo, J, et al., **Imaging of melanoma using Cu-64- and Y-86-DOTA-ReCCMSH(Arg(11)), a cyclized peptide analogue of alpha-MSH.** *J Med Chem*, (2005). 48(8): p. 2985.
27. Boswell CA, Regino, CAS, Baidoo, KE, et al., **Synthesis of a cross-bridged cyclam derivative for peptide conjugation and Cu-64 radiolabeling.** *Bioconjugate Chem*, (2008). 19(7): p. 1476.
28. Garrison JC, Rold, TL, Sieckman, GL, et al., **In vivo evaluation and small-animal PET/CT of a prostate cancer mouse model using Cu-64 bombesin analogs: Side-by-side comparison of the CB-TE2A and DOTA chelation systems.** *J Nucl Med*, (2007). 48(8): p. 1327.
29. Woodin KS, Heroux, KJ, Boswell, CA, et al., **Kinetic inertness and electrochemical behavior of copper(II) tetraazamacrocyclic complexes: Possible implications for in vivo stability.** *Eur J Inorg Chem*, (2005)(23): p. 4829.
30. Sprague JE, Kitaura, H, Zou, W, et al., **Noninvasive imaging of osteoclasts in parathyroid hormone-induced osteolysis using a Cu-64-labeled RGD peptide.** *J Nucl Med*, (2007). 48(2): p. 311.
31. Seo JW, Mahakian, LM, Kheirloomoom, A, et al., **Liposomal Cu-64 Labeling Method Using Bifunctional Chelators: Poly(ethylene glycol) Spacer and Chelator Effects.** *Bioconjugate Chem*, (2010). 21(7): p. 1206.
32. Fonge H, Huang, H, Scollard, D, et al., **Influence of formulation variables on the biodistribution of multifunctional block copolymer micelles.** *Journal of controlled release : official journal of the Controlled Release Society*, (2012). 157(3): p. 366.
33. Ekblad T, Orlova, A, Feldwisch, J, et al., **Positioning of Tc-99m-chelators influences radiolabeling, stability and biodistribution of Affibody molecules.** *Bioorg Med Chem Lett*, (2009). 19(14): p. 3912.
34. Sabbah EN, Kadouche, J, Ellison, D, et al., **In vitro and in vivo comparison of DTPA- and DOTA-conjugated antiferritin monoclonal antibody for imaging and therapy of pancreatic cancer.** *Nuclear Medicine and Biology*, (2007). 34(3): p. 293.
35. Tolmachev V, Wallberg, H, Andersson, K, et al., **The influence of Bz-DOTA and CHX-AaEuro(3)-DTPA on the biodistribution of ABD-fused anti-HER2 Affibody molecules: implications for In-114m-mediated targeting therapy.** *Eur J Nucl Med Mol Imaging*, (2009). 36(9): p. 1460.
36. Trenor SR, Shultz, AR, Love, BJ, et al., **Coumarins in polymers: from light harvesting to photo-cross-linkable tissue scaffolds.** *Chem Rev*, (2004). 104(6): p. 3059.
37. Jiang JQ, Qi, B, Lepage, M, et al., **Polymer micelles stabilization on demand through reversible photo-cross-linking.** *Macromolecules*, (2007). 40(4): p. 790.
38. Anet R, **PHOTODIMERS OF COUMARIN AND RELATED COMPOUNDS.** *Can J Chem-Rev Can Chim*, (1962). 40(7): p. 1249.
39. Chen Y and Chou, CF, **REVERSIBLE PHOTODIMERIZATION OF COUMARIN DERIVATIVES DISPERSED IN POLY(VINYL ACETATE).** *J Polym Sci Pol Chem*, (1995). 33(16): p. 2705.

40. Jin Q, Liu, XS, Liu, GY, et al., **Fabrication of core or shell reversibly photo cross-linked micelles and nanogels from double responsive water-soluble block copolymers**. *Polymer*, (2010). 51(6): p. 1311.
41. Rossin R, Pan, DPJ, Qi, K, et al., **Cu-64-labeled folate-conjugated shell cross-linked nanoparticles for tumor imaging and radiotherapy: Synthesis, radiolabeling, and biologic evaluation**. *J Nucl Med*, (2005). 46(7): p. 1210.
42. Sun G, Hagooly, A, Xu, J, et al., **Facile, efficient approach to accomplish tunable chemistries and variable biodistributions for shell cross-linked nanoparticles**. *Biomacromolecules*, (2008). 9(7): p. 1997.
43. Sun XK, Rossin, R, Turner, JL, et al., **An assessment of the effects of shell cross-linked nanoparticle size, core composition, and surface PEGylation on in vivo biodistribution**. *Biomacromolecules*, (2005). 6(5): p. 2541.
44. Pressly ED, Rossin, R, Hagooly, A, et al., **Structural effects on the biodistribution and positron emission tomography (PET) imaging of well-defined Cu-64-labeled nanoparticles comprised of amphiphilic block graft copolymers**. *Biomacromolecules*, (2007). 8(10): p. 3126.
45. Pramod Kumar EK, Almdal, K, and Andresen, TL, **Synthesis and characterization of ratiometric nanosensors for pH quantification: a mixed micelle approach**. *Chemical Communications*, (2012). 48(39): p. 4776.
46. Obi M, Morino, Sy, and Ichimura, K, **Factors Affecting Photoalignment of Liquid Crystals Induced by Polymethacrylates with Coumarin Side Chains**. *Chemistry of Materials*, (1999). 11(3): p. 656.
47. Utkhede DR and Tilcock, CP, **Effect of lipid dose on the biodistribution and blood pool clearance kinetics of PEG-modified technetium-labeled lipid vesicles**. *J Liposome Res*, (1998). 8(3): p. 381.
48. Laverman P, Brouwers, AH, Dams, ETM, et al., **Preclinical and clinical evidence for disappearance of long-circulating characteristics of polyethylene glycol liposomes at low lipid dose**. *J Pharmacol Exp Ther*, (2000). 293(3): p. 996.
49. Bae Y, Nishiyama, N, Fukushima, S, et al., **Preparation and biological characterization of polymeric micelle drug carriers with intracellular pH-triggered drug release property: Tumor permeability, controlled subcellular drug distribution, and enhanced in vivo antitumor efficacy**. *Bioconjugate Chem*, (2005). 16(1): p. 122.
50. Di Bartolo NM, Sargeson, AM, Donlevy, TM, et al., **Synthesis of a new cage ligand, SarAr, and its complexation with selected transition metal ions for potential use in radioimaging**. *J Chem Soc-Dalton Trans*, (2001)(15): p. 2303.
51. Linder MC and HazeghAzam, M, **Copper biochemistry and molecular biology**. *American Journal of Clinical Nutrition*, (1996). 63(5): p. S797.
52. Liu NM, Lo, LSL, Askary, SH, et al., **Transcuprein is a macroglobulin regulated by copper and iron availability**. *J Nutr Biochem*, (2007). 18(9): p. 597.
53. Tao TY and Gitlin, JD, **Hepatic copper metabolism: insights from genetic disease**. *Hepatology*, (2003). 37(6): p. 1241.
54. Zhao J, Song, SL, Zhong, M, et al., **Dual-Modal Tumor Imaging via Long-Circulating Biodegradable Core-Cross-Linked Polymeric Micelles**. *ACS Macro Lett*, (2011). 1(1): p. 150.
55. Petersen AL, Binderup, T, Rasmussen, P, et al., **64Cu loaded liposomes as positron emission tomography imaging agents**. *Biomaterials*, (2011). 32(9): p. 2334.
56. Hoang B, Lee, H, Reilly, RM, et al., **Noninvasive monitoring of the fate of 111In-labeled block copolymer micelles by high resolution and high sensitivity microSPECT/CT imaging**. *Mol Pharm*, (2009). 6(2): p. 581.
57. Petersen AL, Binderup, T, Rasmussen, P, et al., **(64)Cu loaded liposomes as positron emission tomography imaging agents**. *Biomaterials*, (2011). 32(9): p. 2334.

58. Seo JW, Zhang, H, Kukis, DL, et al., **A Novel Method to Label Preformed Liposomes with (CU)-C-64 for Positron Emission Tomography (PET) Imaging**. *Bioconjugate Chem*, (2008). 19(12): p. 2577.
59. Linder MC, *Biochemistry and molecular biology of copper in mammals. Handbook of copper pharmacology and toxicology*, ed. E.J. Massaro. 2002. 3.
60. Phillips WT, **Delivery of gamma-imaging agents by liposomes**. *Adv Drug Del Rev*, (1999). 37(1-3): p. 13.

DTU Nutech (Center for Nuclear Technologies) is Denmark's national competency center for nuclear technology. With roots in research in the peaceful use of nuclear power, DTU Nutech works with the applications of ionizing radiation and radioactive substances for the benefit of society. The Hevesy Laboratory develops radiotracers for the diagnosing of particularly cancer.

The center's expertise in radiation dosimetry is used both for radiation sterilization, for medical purposes and for dating. A third field of application is the studies and analysis of radioactive isotopes in the environment, in food and in materials. The center also monitors radioactive substances and radiation levels in the Danish environment, contributing to the national nuclear emergency.

DTU Nutech
Center for Nuclear Technologies
Technical University of Denmark

Frederiksborgvej 399
PO Box 49
4000 Roskilde
Denmark
Phone +45 4677 4677
Fax +45 4677 5688

<http://www.nutech.dtu.dk/>

ISBN 978-87-995321-3-1